Synthesis and Study of Carbametallaboranes Which Exhibit Facile Polytopal Rearrangements.

Gwenda O. Kyd

Thesis Presented for the Degree of
Doctor of Philosophy,
University of Edinburgh, 1993.

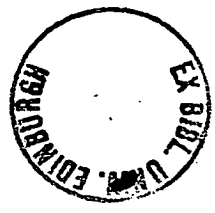

Declaration

Except where specific reference is made to other sources, the work presented in this thesis is the original work of the author. It has not been submitted in whole or in part, for any other degree. Certain of the results have been accepted for publication.

Gwenda Kyd.

This thesis is dedicated to my parents.

A set o' dull, conceited hashes
Confuse their brains in college-classes,
They gang in stirks, and come out asses,
Plain truth to speak;
An' syne they think to climb Parnassus
By dint o' Greek!

from *Epistle to J. Lapraik* by Robert Burns.

One of the symptoms of an approaching nervous breakdown is the belief that one's work is terribly important.

Bertrand Russell

Acknowledgements.

I would like to thank my supervisor Dr. Alan Welch for his enthusiasm and advice over the last four years. Further, I should like to thank Dr. Lesley Yellowlees for her supervision during the early part of this work.

I am particularly grateful to the departmental n.m.r. service, without whom this project would not have been possible, especially John Millar for tolerance beyond the call of duty.

The current and previous occupants of labs 290-293 all deserve a modicum of recognition for their contribution to this thesis. Special thanks go to Dr. Natalia Douek for her assistance in unravelling some of the mysteries of boron chemistry and for her support and encouragement in general. Jill Cowie and Tom McGrath also deserve thanks for putting up with me, especially during the last trying weeks! I would also like to thank Dr. Yvonne Roberts for donation of some diagrams and helpful discussions relating to polyhedral rearrangements. Finally, Dr. Henry Murdoch deserves a special mention, for everything!

I wish to acknowledge the S.E.R.C. and latterly the D.S.S. for financial support and the University of Edinburgh for use of facilities.

Abstract

Chapter 1 begins with a brief description of the terminology commonly associated with polyboron chemistry and some relevant synthetic routes. This is followed by a discussion of observed structural distortions in carbaborane and carbametallaborane complexes. To illustrate this the structures of mono- and diphenyl-substituted *closo*-carbaborane are described. This is followed by a survey of a selection of the known metalla-complexes containing phenyl-substituted carbaborane ligands. The chapter ends with a brief description of a few $\{ML_2\}$-carbametallaboranes.

Chapter 2 describes the synthesis and structural characterisation of the complex, 1-Ph-3,3-$(PMe_2Ph)_2$-3,1,2-$PtC_2B_9H_{10}$, **1**. Crucially, the plane through the metal fragment is rotated away from its predicted (on the basis of an E.H.M.O. calculation) orientation with respect to the ligated carbaborane ligand. **1** is thus considered to be ground-state destabilised, by virtue of phenyl substitution, and this may influence the observed facile isomerisation. At +55°C (328K) **1** undergoes a polytopal rearrangement to yield two 3,1,11-isomers **2** and **3**. In the former the (C-Ph) unit occupies position 11 while in **3** the (C-H) is situated at this location. The structures of these complexes have been determined by another group. This type of isomerisation is well known and several reported examples are discussed as well as the principal suggested mechanisms. The diphenyl substituted carbaborane complex, **4**, is then described. A crystal structure determination reveals this to be the 3,1,11-isomer 1,11-Ph_2-3,3-$(PMe_2Ph)_2$-3,1,11-$PtC_2B_9H_9$. In this case the 3,1,2-isomer is not isolated, and isomerisation occurs at, or below, room temperature. Increased steric demands of the carbaborane ligand are thought to facilitate this process.

In **Chapter 3** the spectroscopic characterisation of the two series of complexes, analogous to **1** and **4**, containing other phosphine/phosphite ligands, are described.

This shows that the behaviour of these species is largely independent of the electronic and steric properties of the phosphorus ligands. All the analogues of **1** undergo polytopal isomerisation at elevated temperature. Complexes with smaller phosphine ligands tend to form two 3,1,11-isomers, whereas complexes with larger phosphorus ligands tend to form a single isomer. Each analogue of **4** forms with a 3,1,11-framework, and, even for the complexes with the smallest metal fragment no 3,1,2-species is isolated. Finally, a preliminary study of the electrochemistry of each series of complexes is described.

Chapter 4 discusses the palladium analogues of **1** and **4**. A partial structure determination of the complex 1-Ph-3,3-$(PMe_2Ph)_2$-3,1,2-$PdC_2B_9H_{10}$, **16**, shows it to be less distorted than **1**. There is no evidence for the formation of a 3,1,11-isomer at elevated temperature. However, the study of this species is complicated by its ready conversion to another carbapalladaborane of unknown structure. The diphenyl species, **17**, is formed as the 3,1,11 -isomer. Next, the phenyl-carbaborane complexes which incorporate the {Pd(1,5-COD)} fragment are described. The monophenyl complex, **18**, is stable to isomerisation. A structure determination of the complex 1,2-Ph_2-3-(1,5-COD)-3,1,2-$PdC_2B_9H_9$, **19**, shows it to be the first example of an $\{ML_2\}$ complex with the $(C_2B_9H_9Ph_2)^{2-}$ ligand, in which the (C-Ph) units are adjacent on the metal-bonded face. The flexibility of the (1,5-COD) ligand is thought to enable the adoption of this polytopal arrangement, by tilting away from the cage-phenyl groups. **19** is subject to isomerisation at 110°C (383K). The platinum analogue of **18** is also stable to isomerisation. However, the analogue of **19** isomerises at room temperature. These results illustrate the previously noted enhanced stability of second-row transition metal carbaborane complexes to polytopal rearrangement, with respect to their third-row analogues.

Chapter 5 describes the experimental techniques employed in the synthesis, characterisation and structural analysis of the compounds discussed in chapters 2, 3

and 4. Supplementary crystallographic data are tabulated as well as the co-ordinates used in the E.H.M.O. calculations described in chapter 2.

Abbreviations.

COD cyclooctadiene

Cp cyclopentadiene

Cp^* pentamethylcyclopentadiene

Cy cyclohexyl

dppe diphenylphosphinoethane

Et ethyl

FAB fast-atom bombardment

i.r. infra-red

Me methyl

mes mesitylene

n.m.r. nuclear magnetic resonance

p-tol para-tolyl

p.p.m. parts per million

Ph phenyl

t.l.c. thin layer chromatography

Abbreviations for Specific Compounds.

1 1-Ph-3,3-$(PMe_2Ph)_2$-3,1,2-$PtC_2B_9H_{10}$

2 11-Ph-3,3-$(PMe_2Ph)_2$-3,1,11-$PtC_2B_9H_{10}$

3 1-Ph-3,3-$(PMe_2Ph)_2$-3,1,11-$PtC_2B_9H_{10}$

4 1,11-Ph_2-3,3-$(PMe_2Ph)_2$-3,1,11-$PtC_2B_9H_9$

5 1-Ph-3,3-$(P(OMe)_3)_2$-3,1,2-$PtC_2B_9H_{10}$

6 1,11-Ph_2-3,3-$(P(OMe)_3)_2$-3,1,11-$PtC_2B_9H_9$

7 1-Ph-3,3-$(PMe_3)_2$-3,1,2-$PtC_2B_9H_{10}$

8 1,11-Ph_2-3,3-$(PMe_3)_2$-3,1,11-$PtC_2B_9H_9$

9 1-Ph-3-(dppe)-3,1,2-$PtC_2B_9H_{10}$

10 1-Ph-3,3-$(PEt_3)_2$-3,1,2-$PtC_2B_9H_{10}$

11 1,11-Ph_2-3,3-$(PEt_3)_2$-3,1,11-$PtC_2B_9H_9$

12 1-Ph-3,3-$(PPh_3)_2$-3,1,2-$PtC_2B_9H_{10}$

13 1,11-Ph_2-3,3-$(PPh_3)_2$-3,1,11-$PtC_2B_9H_9$

14 1-Ph-3,3-$(P(p\text{-}tol)_3)_2$-3,1,2-$PtC_2B_9H_{10}$

15 1,11-Ph_2-3,3-$(P(p\text{-}tol)_3)_2$-3,1,11-$PtC_2B_9H_9$

16 1-Ph-3,3-$(PMe_2Ph)_2$-3,1,2-$PdC_2B_9H_{10}$

17 1,11-Ph_2-3,3-$(PMe_2Ph)_2$-3,1,11-$PdC_2B_9H_9$

18 1-Ph-3-(1,5-COD)-3,1,2-$PdC_2B_9H_{10}$

19 1,2-Ph_2-3-(1,5-COD)-3,1,2-$PdC_2B_9H_9$

20 1-Ph-3-(1,5-COD)-3,1,2-$PtC_2B_9H_{10}$

21 1,11-Ph_2-3-(1,5-COD)-3,1,11-$PtC_2B_9H_9$

22 1,11-Ph_2-3-(dppe)-3,1,11-$PtC_2B_9H_9$

Contents.

Chapter 1 Background.

1.1 Introduction.

Stock[1] first recognised the existence of boron hydrides, or boranes, in the early twentieth century. However, the predicted hydrocarbon chain-type structures of these species could not be satisfactorily explained in terms of the bonding theories accepted at that time. This was principally due to boron atoms having fewer valence electrons than valence orbitals. As the technique of X-ray crystallography developed it was established that boranes adopt novel structures. For example, the simplest borane, B_2H_6[2] (or diborane) has the structure shown in figure 1.1, containing two 3-centre 2-electron B-H-B bonds and no direct B-B linkage.

Figure 1.1

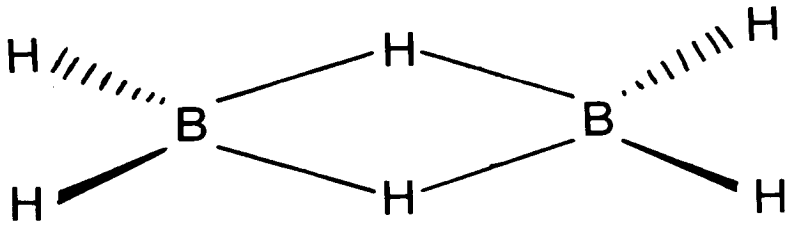

Higher boranes form regular polyhedra with {BH} fragments occupying each vertex. The bonding in these polyhedra is delocalised and this alleviates the formal electron deficiency. Rationalisation of these and related structures led to the development of electron counting rules which are outlined in section 1.2.

Formal replacement of a $\{BH\}^-$ vertex with a {CH} vertex gives rise to a series of more stable (with respect to air and moisture), neutral polyhedra; the carbaboranes. The existence of these was predicted on the basis of calculations[3] and many examples were duly synthesised. Initially the small carbaboranes *e.g.* $C_2B_3H_5$ and $C_2B_4H_6$[4] were reported and larger species, such as the *pseudo*-icosahedral

$C_2B_{10}H_{12}$[5], followed.

It was noted that the frontier molecular orbitals of the anionic carbaborane $[C_2B_9H_{11}]^{2-}$ are of a similar nature and energy to those of the cyclopentadienyl anion $[C_5H_5]^-$ (Cp^-)[6]. These orbitals are depicted in figure 1.2. The Cp^- ligand had been widely used in organometallic chemistry[7], so it seemed plausible that the $[C_2B_9H_{11}]^{2-}$ ion would act as a ligand to metal ions.

Figure 1.2

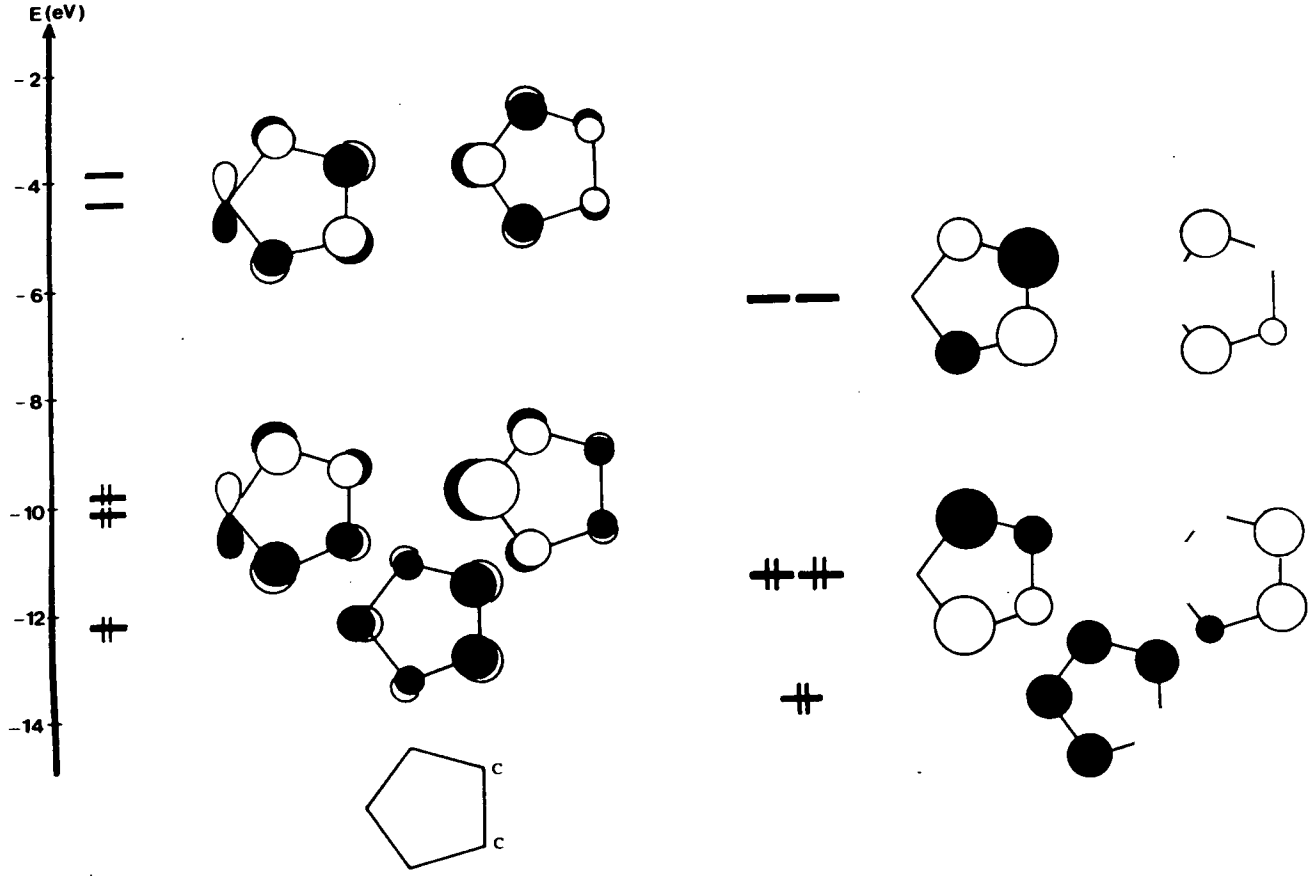

$[C_2B_9H_{11}]^{2-}$ $(C_5H_5)^-$

π M.O.s of $(C_2B_9H_{11})^{2-}$ and $(C_5H_5)^-$

Hawthorne[8] synthesised the first metal complex with a carbaborane ligand in 1965, the ferrocene analogue $[(C_2B_9H_{11})_2Fe]^{2-}$. In the years that followed a vast number of carbametallaboranes have been reported. These can be described in two complementary manners; as metal-ligand complexes or as heteroboranes containing a metal vertex. Both of these approaches are used in this thesis, where appropriate.

The development of borane and heteroborane chemistry has flourished in part due to the wide range of applications which these compounds have found. Substituted boranes have been used for the treatment of brain tumours, via the technique of boron-neutron capture therapy[9,10]. This relies on the behaviour of the ^{10}B isotope when it is exposed to thermal neutrons. Under these conditions the following occurs:

$$^{10}B + {}^{1}n \rightarrow \{^{11}B\} \rightarrow {}^{4}He + {}^{7}Li^{*} + 2.31Mev \rightarrow {}^{7}Li + \gamma + 0.48MeV.$$

When the ^{10}B nucleus and a neutron interact, they produce a metastable particle which then undergoes fission to produce energy, a Li nucleus and a He nucleus (α particle). The α particle travels the distance of a cell diameter (*circa* 10μm) eliminating any intervening matter. In this way, tumour cells can be destroyed. The boron containing complex currently favoured is $[B_{12}H_{11}SH]^{2-}$ (BSH), which is enriched with ^{10}B before introduction into the body. Much research[11,12] is being directed towards the search for boron complexes which bind more efficiently to the tumour cells or, indeed, become incorporated into the body of the tumour (rather than binding solely to the surface).

Carbaboranes have been used in the formation of polymers of high thermal stability[13], for example the siloxane polymer:

$$-[Si(Me)_2\text{-}CB_{10}H_{10}C\text{-}Si(Me)_2\text{-}O\text{-}Si(Me)_2\text{-}O\text{-}Si(Me)_2\text{-}O\text{-}]-$$

Carbametallaboranes containing a platinum group metal atom have proved to be

useful catalysts for alkene hydrogenation and isomerisation reactions[14-18]. The earliest reported examples were the hydrido-rhodium species 3,3-$(PPh_3)_2$-3-H-3,1,2-$RhC_2B_9H_{11}$ and the 3,1,11-analogue which were found to catalyse the isomerisation of hex-1-ene[14].

This chapter outlines the concepts utilised in the course of this work and describes some complexes of relevance which have appeared in the literature.

1.2 Rationalisation of the Structures of Boranes and Their Derivatives.

Polyhedral boranes and their derivatives can be classified in terms of their geometry. There are 4 main classes- "*closo*" (or closed) in which all faces are fully triangulated, "*nido*" (nest-like), which is the same basic geometry as *closo* but with one vacant vertex, "*arachno*" (web-like), which is *closo* with 2 vacant vertices and lastly "*hypho*" (network), which is 3 vertices short of a *closo*- structure[19].

As previously noted, the structures adopted by boranes and their derivatives present problems when trying to rationalise them in terms of the simple theories of bonding. The structures of the simple boranes can be satisfactorily described using the concept of 3-centre 2-electron bonding[2]. For example, diborane (B_2H_6) contains four 2-centre 2-electron BH bonds and two 3-centre 2-electron BHB bonds. However, this localised approach proves too complicated for the higher boranes. These are better discussed in terms of polyhedral skeletal electron pair (PSEP) theory[20]. This is based on the observation that the structures of polyhedra are dependent on the number of valence electrons which they contain.

A set of rules (Wade's rules[21]) was devised which allows prediction of the structure adopted by considering the number of skeletal electron pairs (SEP's). Considering firstly a {BH} vertex, it was assumed that the BH interaction involves an

sp hybrid orbital which points outwards from the polyhedral surface (exo-polyhedral). The other sp hybrid orbital points into the polyhedron and, hence, can become involved in cluster bonding. The remaining boron orbitals (2 p orbitals) are oriented such as to be available for bonding on the polyhedral surface. Therefore, a {BH} fragment has three orbitals available for cluster bonding. Of the three valence electrons possessed by a boron atom, one is used in a bonding interaction with the exo-polyhedral atom, leaving two to form cluster bonds. A {CH} (or {CPh}) vertex also presents 3 orbitals for cluster bonding but this time there are 3 available electrons. Cluster bonding electrons are also provided by bridging (or endo) H atoms and also by the overall charge of the molecule. Taking each vertex (and each extra atom or charge) in turn, the number of skeletal electrons can be calculated, and hence, the number of SEP's. This can then be compared with the number of vertices ({BH} and {CH}) (n) and the following relationships used to predict the structure.

No. of SEP's	Geometry
n + 1	*closo*
n + 2	*nido*
n + 3	*arachno*
n + 4	*hypho*

For example, the species $[C_2B_9H_{12}]^-$ contains the following:

```
9 {BH} vertices   = 9 x 2 skeletal electrons = 18
2 {CH} vertices   = 2 x 3 skeletal electrons =  6
1 endo-H atom     = 1 skeletal electron      =  1
1 negative charge = 1 skeletal electron      =  1

Total number of skeletal electrons      = 26 = 13SEP's
Number of vertices = 11
```

Therefore, there are (n + 2) SEP's and a *nido* structure would be predicted (and is observed[22]).

A transition metal fragment has 9 valence orbitals (rather than 4). When the fragment occupies a polyhedral vertex, six of these orbitals are involved in bonding to exo-polyhedral ligands (for a fragment with an octahedral geometry) or are non-bonding.

These orbitals are normally filled and hence, there are 12 electrons unavailable for cluster bonding. The number of electrons which are available (e) to occupy the 3 cluster bonding orbitals is calculated from the equation e = v + x - 12, where v is the number of valence electrons for the neutral metal atom and x is the number of electrons donated by the metal ligands.

For example, in the complex $[CpCoC_2B_9H_{11}]$

{CpCo}=9 + 5 - 12 = 2
9 x {BH} = 9 x 2 = 18
2 x {CH} = 2 x 3 = 6
Total skeletal electrons = 26 = 13SEP's = n + 1.

Hence, the observed [23] *closo-* structure would be predicted.

There are however, some exceptions to PSEP theory- for example the species B_8H_{12}. This has 10 SEP's (= n + 2) and therefore a *nido-* structure is predicted. However the observed structure is of the *arachno-* form[24]. This apparent anomaly has yet to be fully rationalised, *a priori*, although recent studies[24] have suggested that given the (*arachno*) structure it has, the neutral $[B_8H_{12}]$ is likely to be more stable than the PSEP-precise $[B_8H_{12}]^{2-}$.

1.3 Polyhedral Numbering.

For *closo-* carbaboranes, a carbon vertex is labelled as number 1 and numbering proceeds in a corkscrew fashion such that any other heteroatom has the lowest possible number. Carbon atoms are numbered in preference to metal atoms in carbametallaboranes. On moving from one pentagonal belt to another, a connectivity is crossed. In *nido-* species the atom opposite the open face is numbered 1 then numbering proceeds as above. Typical *closo-* and *nido-* numbering schemes are illustrated in figure 1.3.

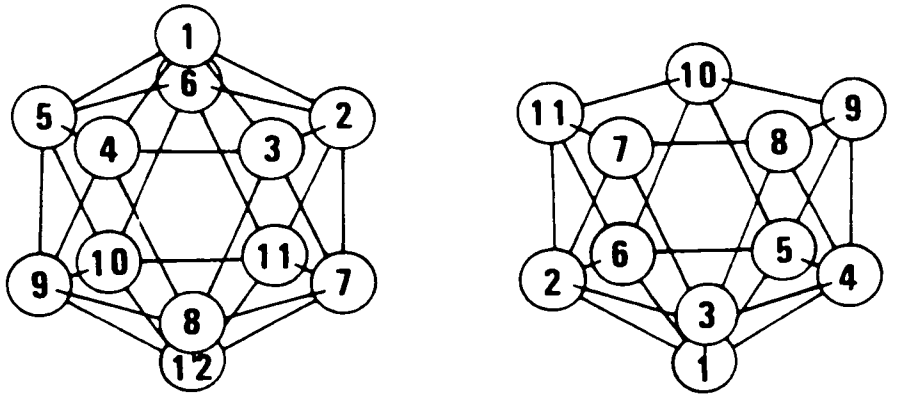

Figure 1.3

The presence of two carbon atoms in an icosahedral carbaborane gives rise to the possibility of three positional isomers. These are namely: 1,2-$C_2B_{10}H_{12}$ (colloquially ortho-carborane), 1,7-$C_2B_{10}H_{12}$ (meta-carborane) and 1,12-$C_2B_{10}H_{12}$ (para-carborane). The latter two are best synthesised by thermolysis of the former[25]. This type of isomerisation is discussed in chapter 2.

1.4 Distortions from Idealised Geometries.

When asymmetry is introduced into a polyhedral molecule, the structure adopted can be distorted from an idealised one. For example, the molecules $[B_{12}H_{12}]^{2-}$ and $C_2B_{10}H_{12}$ would be expected to have identical icosahedral structures (as they have the same number of vertices and SEP's). However, C-C connectivities are shorter than C-B connectivities which in turn are shorter than B-B ones and hence, the latter structure is slightly distorted compared with the former[26]. The introduction of a metal vertex can have a more pronounced effect on the structure. The distortions of relevance to the current work are detailed below. All of these are measured relative to a B_5 belt, which is assumed to be planar. For a species $L_xMC_2B_9H_9R^1R^2$ (L_xM= a transition metal fragment, R^1, R^2= H, alkyl, aryl) there are three notable distortions[27]:

1) A translational movement of the metal fragment away from the centre of the ligated face (see figure 1.4). This is defined as Δ and is positive if movement is towards the unique atom in this face.

2) A folding of the ligated (C_2B_3) face, normally about an axis through B4 and B7 (*closo* numbering). This gives rise to folding angles θ and ϕ, defined as the angles between the C1C2B4B7 plane and the B_5 plane and the angle between the B4B7B8 plane and the B_5 plane, respectively (see figure 1.4)

3) A movement of the C_2B_3 face with respect to the B_5 belt. This normally occurs in the same direction as Δ and therefore leads to a slight over-estimate of this value.

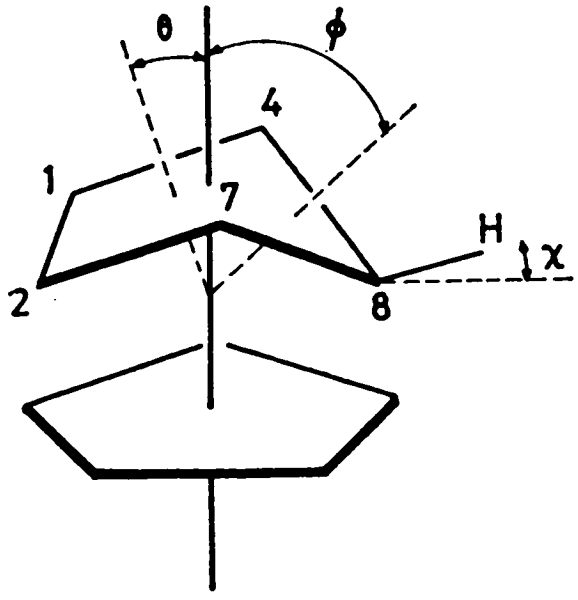

Figure 1.4

A comparison of these parameters for a variety of carbametallaboranes indicates that the degree of distortion depends on the nature of the metal fragment[27]. For d^6 and d^7 metal complexes the distortions are fairly small. However, for d^8 and d^9 complexes, larger distortions are observed.

This led to the suggestion that slippage occurs where there is the unfavourable >18 electron configuration, in order to reduce the electron density at the metal atom. Indeed the most extreme example of this type of distortion is observed in the main group metal species $[TlC_2B_9H_{11}]^-$. In this case, where the metal centre is relatively electron rich, a crystal structure determination[28] (of the $[PPh_3Me]^+$ salt) indicates that the Tl-cage interactions are virtually non-bonding (see figure 1.5). This species can be formally thought of as an ion-pair (Tl^+ $[C_2B_9H_{11}]^{2-}$).

Figure 1.5

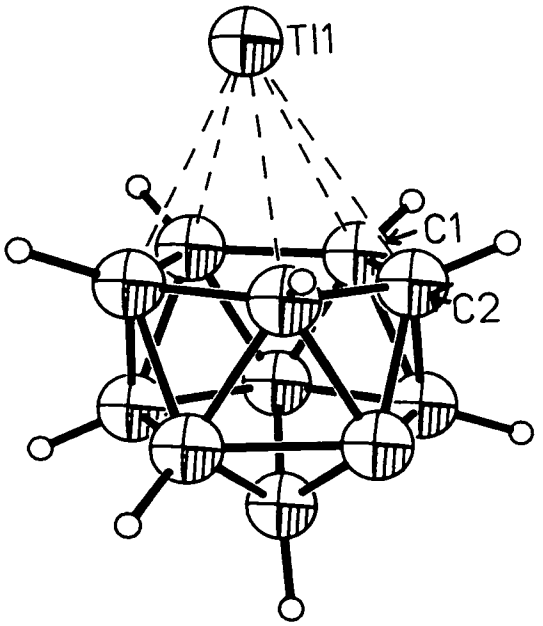

The thallium atom is readily replaced by a transition metal fragment and this leads to the synthetic utility of thallium carbaboranes as precursors to transition metal complexes (see section 1.5).

The formation of carbametallaboranes incorporating an $\{ML_2\}$ $(Pt(PH_3)_2)$ fragment has been considered via a series of E.H.M.O. calculations[27,29]. These assume a neutral metal fragment interacting with a neutral carbaborane ligand. The metal fragment has a mirror plane passing through the metal atom and the two phosphorus atoms, and the favoured orientation of this plane was determined relative to the ligated face. The frontier molecular orbitals of the metal fragment and those localised on 3 types of M-bonded carbaborane face (and a simple borane for comparison) are shown in figure 1.6. It was assumed that the orientation of the ML_2 fragment would be such as to maximise overlap of the metal fragment homo and the carbaborane lumo. At Δ = 0Å the primary metal ligand bonding effects originate from electron donation from the ligand $6a_1$ orbital to the hybrid (s-z) lumo of the metal fragment. The metal fragment homo is considered to be an (xz) hybrid orbital which back donates to one component of the $5e_1$ set. The metal (yz) orbital enters into a 4-electron destabilising interaction with the complementary (and filled) component of the $5e_1$ set (see figure 1.6).

Considering first a carbaborane with 2 carbon atoms adjacent on the ligated face (A), the lumo is concentrated on the 3 boron atoms and there is a mirror plane passing through the central boron atom and the C-C mid-point. The lumo is asymmetric about this mirror plane and therefore, it is predicted that the PtP_2 plane will lie perpendicular to the mirror plane and that there will be a large movement of the metal fragment towards the 3 boron atoms (+ve slippage).

When the facial carbon atoms are separated by a boron atom (B), the lumo is concentrated on the 2 carbon atoms and the 2 equivalent boron atoms, and there is a mirror plane passing through the unique boron atom and the mid-point of the B-B bond. In this case, the lumo is symmetric about the mirror plane and hence, the PtP_2 plane is predicted to lie parallel to the mirror plane with the fragment slipped away from the unique B atom (small -ve slippage).

Figure 1.6

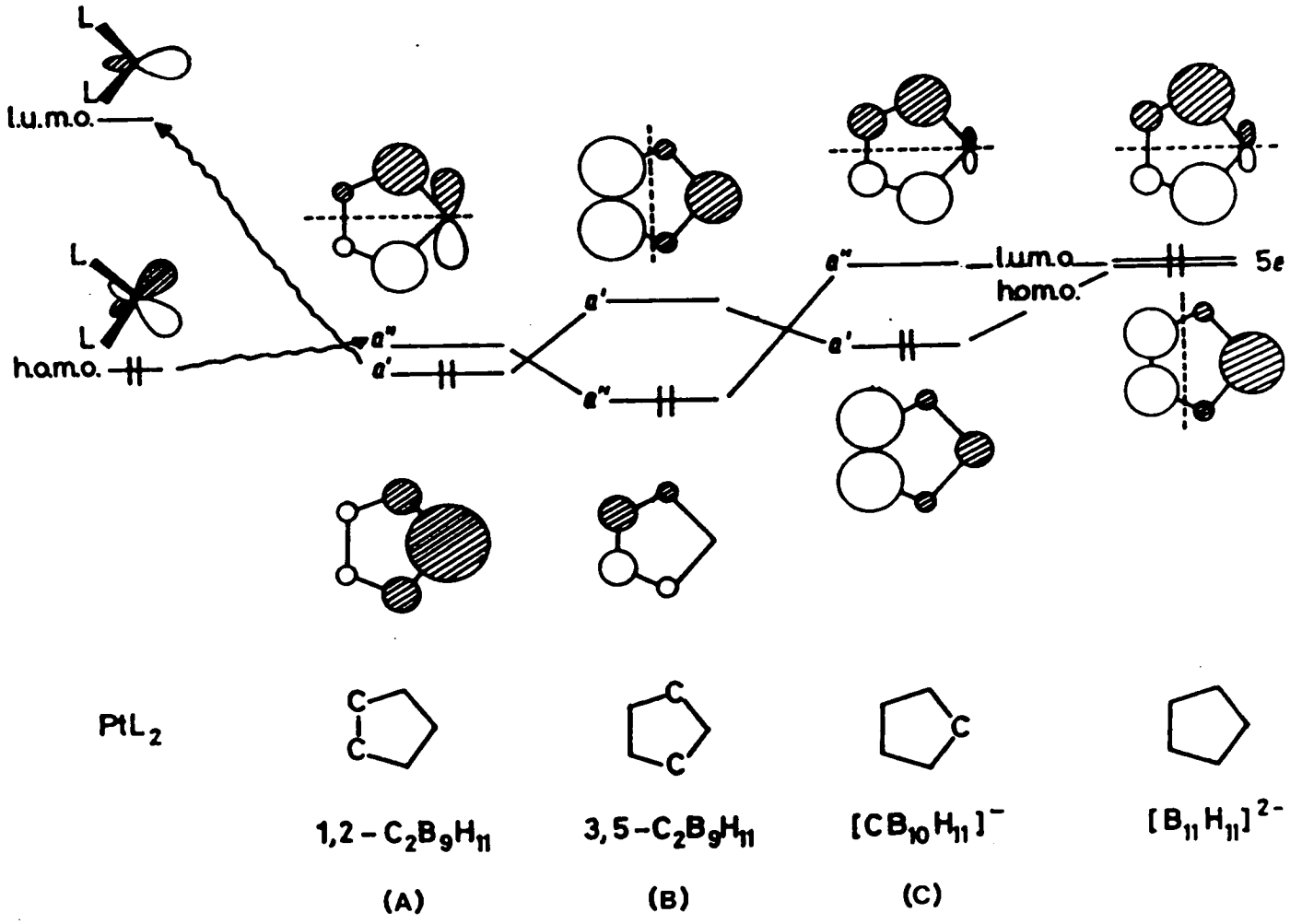

Schematic Representation of the Frontier Molecular Orbitals of an $\{ML_2\}$ Fragment and Ligating Carba(borane) Faces.

In the mono-carbon carbaborane (C) the lumo is concentrated on the two boron atoms remote from the carbon atom and there is a mirror plane which passes through this carbon atom and the mid-point of the remote B-B bond. As in A, the lumo is parallel to the mirror plane and, the PtP_2 plane is, therefore, predicted to lie perpendicular to this mirror plane and the fragment slipped away from the carbon atom (large -ve slippage). These predictions have been largely borne out experimentally and specific examples are discussed at the relevant points in the text.

1.5 Syntheses of Carbaboranes and Their Derivatives.

The simplest method of synthesis of carbaboranes is by insertion of an alkyne into an *arachno* borane. To form carbaboranes of the type utilised in this thesis requires alkyne insertion into a derivative of decaborane ($B_{10}H_{14}$), via the following reaction[30].

$$B_{10}H_{14} + R^1CCR^2 + MeCN \rightarrow B_{10}C(R^1)C(R^2)H_{10}$$

R= H, alkyl, aryl. MeCN can be substituted by SMe_2, PPh_3, *etc.*

Using substituted alkynes, a number of C-substituted carbaboranes can be formed[31]. The first stage of the reaction is the production of the decaborane adduct $B_{10}H_{12}(MeCN)_2$, followed by displacement of the co-ordinated MeCN by the alkyne.

Base hydrolysis of a carbaborane results in deboronation (removal of a {BH} vertex) to form a *nido-* species. The vertex which is removed is the one at which there is least electron density (one of those adjacent to both the relatively positive C atoms). This occurs via the following scheme[32].

$$C_2B_{10}H_{10}R^1R^2 + 5KOH \xrightarrow{EtOH} K_2[C_2B_9H_9R^1R^2] + B(OEt)_3 + H_2$$

The dipotassium salt is converted into the dithallium salt by reaction with Tl(OAc) in aqueous medium[33].

The carbaborane dianion is readily metallated by reaction of the dithallium salt with L_xMX_y (X = halide), in an organic solvent. A major driving force of this reaction is the precipitation of TlX and the product has the form $L_xMC_2B_9H_9R^1R^2$. The insolubility of the TlX means that separation of the generally soluble carbametallaborane is straightforward.

1.6 Characterisation of Carbaboranes and their Derivatives.

Characterisation of carbametallaboranes can be effected by a variety of spectroscopic and non-spectroscopic methods, but is best carried out using a combination of techniques.

The simplest non-spectroscopic method is microanalysis. This, alone, has been used to confirm the formation of some derivatised carbaboranes[34]. In theory the results can be very good, but ultimately can give no indication of the structure of a compound, only its gross composition.

Infra-red spectroscopy is of considerable utility in ascertaining the presence of boranes, due to the fact that the B-H (terminal) stretching absorption occurs in a region where no other commonly present function absorbs (in the range 2500 to 2660cm^{-1}[35]). This band is usually broad due to the presence of 2 isotopes of boron (19.8% ^{10}B, 80.2% ^{11}B). In addition, for asymmetric boranes, the frequency of the B-H stretch will vary with the connectivity of the boron atom. This does not usually manifest as the observation of multiple B-H bands but, instead, causes further broadening. In carbaboranes containing C-H bonds, a C-H stretching band may also be observed (commonly in the range 2900-3160cm^{-1}[35]).

FAB mass spectrometry can be used to confirm the presence of the target species, through the observation of a parent ion at the correct m/z value. However, the parent

ion is not always present[36], so while this technique can confirm the presence of a species, the absence of the parent ion does not necessarily suggest that the desired complex has not been formed.

Multinuclear n.m.r. spectroscopy can provide much structural information relating to carbametallaboranes. A set of rules for predicting the ^{11}B n.m.r. spectra of boranes and heteroboranes has been suggested[37]. In addition, *ab initio* chemical shift (IGLO) calculations using optimised geometries have been correlated with the observed n.m.r. spectra of some boranes and carbaboranes[147]. This has allowed alternative assignments of the peaks in the spectrum of B_8H_{12}. In the absence of these type of calculations, assignment of ^{11}B n.m.r. spectra is not usually possible unless the 2-D (^{11}B-^{11}B) COSY spectrum is considered. Boron resonances are intrinsically broad due to quadrupolar relaxation effects, and B-B coupling is not resolved. However, coupling to other nuclei can sometimes be observed. Of particular importance is ^{1}JB-H, which is typically within the range 80 to 160Hz.[38].

There is only one naturally occurring isotope of phosphorus (^{31}P) and this has a nuclear spin of 1/2, thus providing a valuable n.m.r. handle. Spectra are normally obtained broad-band proton decoupled, since ^{31}P-^1H couplings render the spectrum prohibitively complex. When resolved, the magnitude of coupling to other nuclei can provide an insight into the nature of the complex. For example, coupling to ^{195}Pt nuclei (33.8% natural abundance) varies depending on the nature of the geometry at the metal atom. Thus, the observed coupling involving a square planar Pt^{II} atom is larger than that involving an octahedral Pt^{IV} atom[39]. The magnitude of ^{195}Pt-^{31}P coupling depends principally on the degree of s-character in this bond[40]. Considering the orbital hybridisation at the metal atom, this is approximately 25% s-character in a square planar complex (dsp^2 hybridised) and 16.5% s-character in an octahedral complex (d^2sp^3 hybridised). When present, the magnitude of P-P coupling can provide information as to the geometrical relationship of the phosphorus nuclei.

For example, in square planar complexes, a *trans*-P-P coupling is larger than the corresponding *cis*-P-P coupling[41] (*e.g.* ^{2}JP-P is <5Hz.in *cis*-$PtCl_2(PEt_3)_2$ but approximately 90Hz. in *trans*-$PtCl_2(PEt_3)_2$).

Although all the above techniques can provide some data relating to the structure of the complex of interest, perhaps the ultimate analytical method is provided by X-ray crystallography. From an X-ray diffraction study a set of atomic co-ordinates are derived and thereby bond lengths, angles and torsions. This technique has the disadvantages of requiring single, diffraction-quality crystals and also that hydrogen atoms are often not located. Finally, it must be remembered that the structure obtained by this method is a solid-state structure and this may differ considerably from the structure in solution.

1.7 *Closo*- C-Phenyl Substituted Carbaboranes.

The carbaboranes utilised in this work bear one or two phenyl substituents on the cage carbon atoms. The X-ray crystal structures of the two parent species 1-$PhC_2B_{10}H_{11}$[42] and 1,2-$Ph_2C_2B_{10}H_{10}$[43] have been determined and these illustrate certain features which are of relevance to their metalla-derivatives.

1-$PhC_2B_{10}H_{11}$ was synthesised by the method of Reid[44], from decaborane and phenyl-acetylene. Crystals suitable for an X-ray diffraction study were obtained from a slowly cooled ethanolic solution. The structure solution indicated there were two crystallographically independent molecules in the lattice (denoted by A and B). Only in the latter could the position of the {CH} vertex be established. A schematic representation of a single molecule of B is shown in figure 1.7.

Figure 1.7

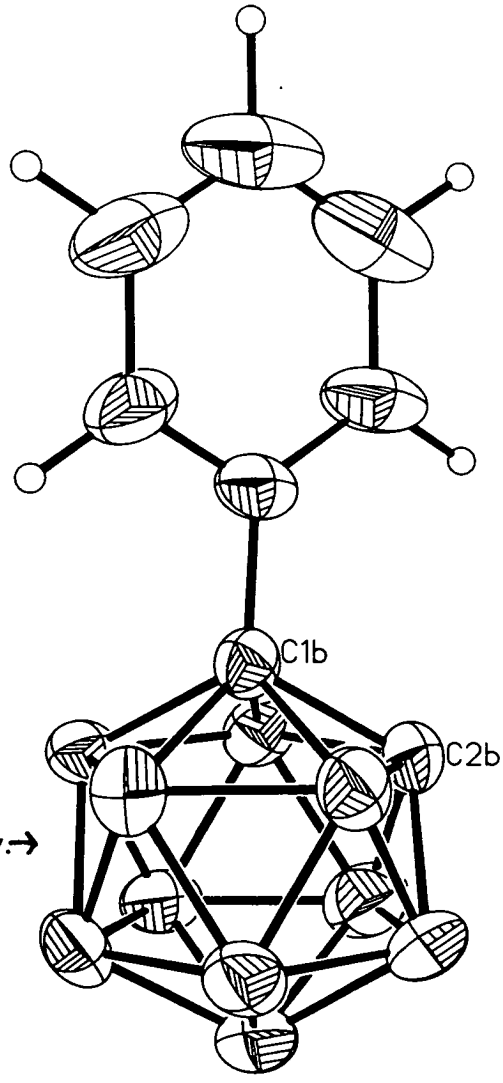

Hs removed for clarity.→

The C_{cage}-C_{cage} bond length of 1.646(8)Å is comparable with that observed[26] in the unsubstituted analogue (ortho-carborane) (= 1.653(49)Å). The C_{cage}-C_{phenyl} distance is 1.495(6)Å. The orientation of the phenyl substituent can be determined with respect to the C_{cage}-C_{cage} vector as the difference between the modulus of the torsion angles defined by C_{cage}-C_{cage}-$C_{1phenyl}$-$C_{2phenyl}$ and C_{cage}-C_{cage}-$C_{1phenyl}$-$C_{6phenyl}$ and 90°, where $C_{1phenyl}$ is the first atom in the phenyl ring. This value (θ_{phenyl}) is thus defined as being 0° when the phenyl group is perpendicular to the C_{cage}-C_{cage} bond. In 1-$PhC_2B_{10}H_{11}$ θ_{phenyl} is 68.8°.

1,2-$Ph_2C_2B_{10}H_{10}$ was synthesised by a modified version of the literature procedure[34]. Diffraction quality crystals were obtained by slow cooling of a methanolic solution. Structure solution indicated that there were two crystallographically independent molecules in the asymmetric fraction of the unit cell (again denoted by A and B). A schematic representation of a single molecule of B is shown in figure 1.8.

Figure 1.8

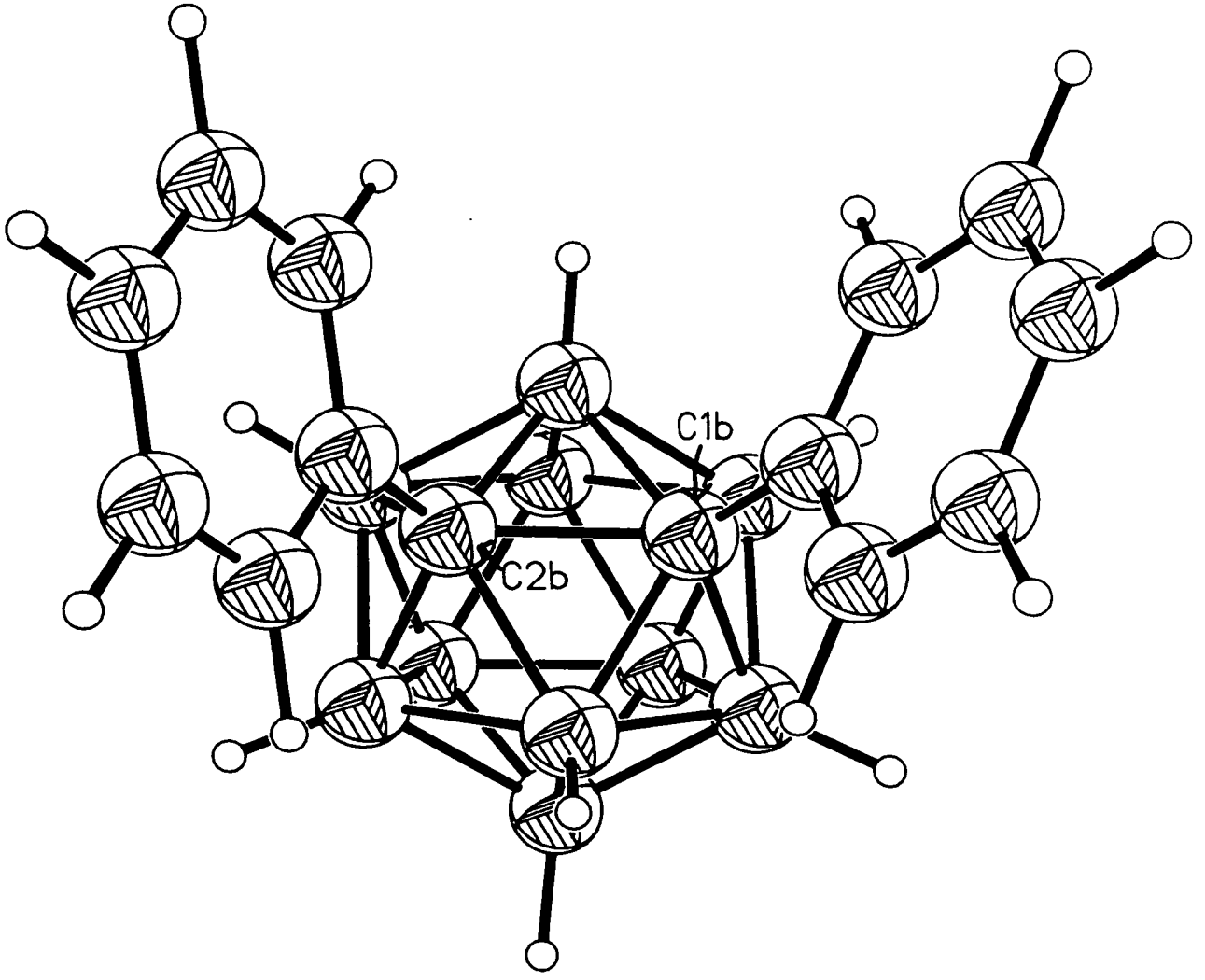

In molecule A the C_{cage}-C_{cage} distance is 1.733(4)Å while the C_{cage}-C_{phenyl} distances are 1.500(4) and 1.508(5)Å. The calculated values of θ_{phenyl} are 2.4° and 2.3°. In molecule B the C_{cage}-C_{cage} distance is 1.720(4)Å with C_{cage}-C_{phenyl} distances 1.494(4) and 1.508(4)Å. The values of θ_{phenyl} obtained were 9.2 and 8.0°. It was initially assumed that these low θ_{phenyl} values resulted from the mutual repulsion of the two phenyl groups and that this, in turn resulted in the longer C_{cage}-C_{cage} distances compared to those in 1-$PhC_2B_{10}H_{11}$ and ortho-carborane. However, the results of a series of E.H.M.O. calculations[43] indicated that there was an electronic contribution to the observed, longer distances.

Idealised models of $C_2B_{10}H_{12}$, 1-$PhC_2B_{10}H_{11}$ and 1,2-$Ph_2C_2B_{10}H_{10}$ were considered and the reduced overlap populations for the C_{cage}-C_{cage} and C_{cage}-C_{phenyl} (where appropriate) interactions were calculated. In addition, the effect on the overall energy of the molecule of rotating the phenyl substituent(s) was ascertained. Comparing the C_{cage}-C_{cage} interactions with that in ortho-carborane, this connectivity is weakened by introducing one or two phenyl substituents at θ_{phenyl}= 0° but strengthened at θ_{phenyl}= 90°. This is to some extent confirmed experimentally by a comparison of molecules A and B of 1,2-$Ph_2C_2B_{10}H_{10}$. In A, where the average θ_{phenyl}= 2.4°, the C_{cage}-C_{cage} distance is 0.013(6)Å longer than in B, which has an average θ_{phenyl} value of 8.6°. If the C_{cage}-C_{phenyl} distance is now considered this is predicted to be shortest for θ= 90° for both the phenyl-substituted molecules. This was believed to result from the most efficient conjugation between the phenyl and cage fragments occurring at this conformation.

For 1-Ph-$C_2B_{10}H_{11}$ a θ_{phenyl} value of 90° was calculated to minimise (by *circa* 0.2eV) the overall energy of the molecule. The deviation of the observed value of

θ_{phenyl}(= 68°) from the predicted value can be readily understood by considering intermolecular contacts. The phenyl rings of adjacent molecules are aligned (see figure 1.9) approximately 3.5Å apart, and as such can be considered to be interacting graphitically (this distance can be compared with twice the half thickness of a benzene ring[64]= 2 x 1.85Å[64]). It is assumed that the observed θ_{phenyl} value permits the most efficient stacking. An electron diffraction study of this compound is currently underway with the object of ascertaining if the predicted θ_{phenyl} value is observed in the absence of crystal packing forces.

Figure 1.9

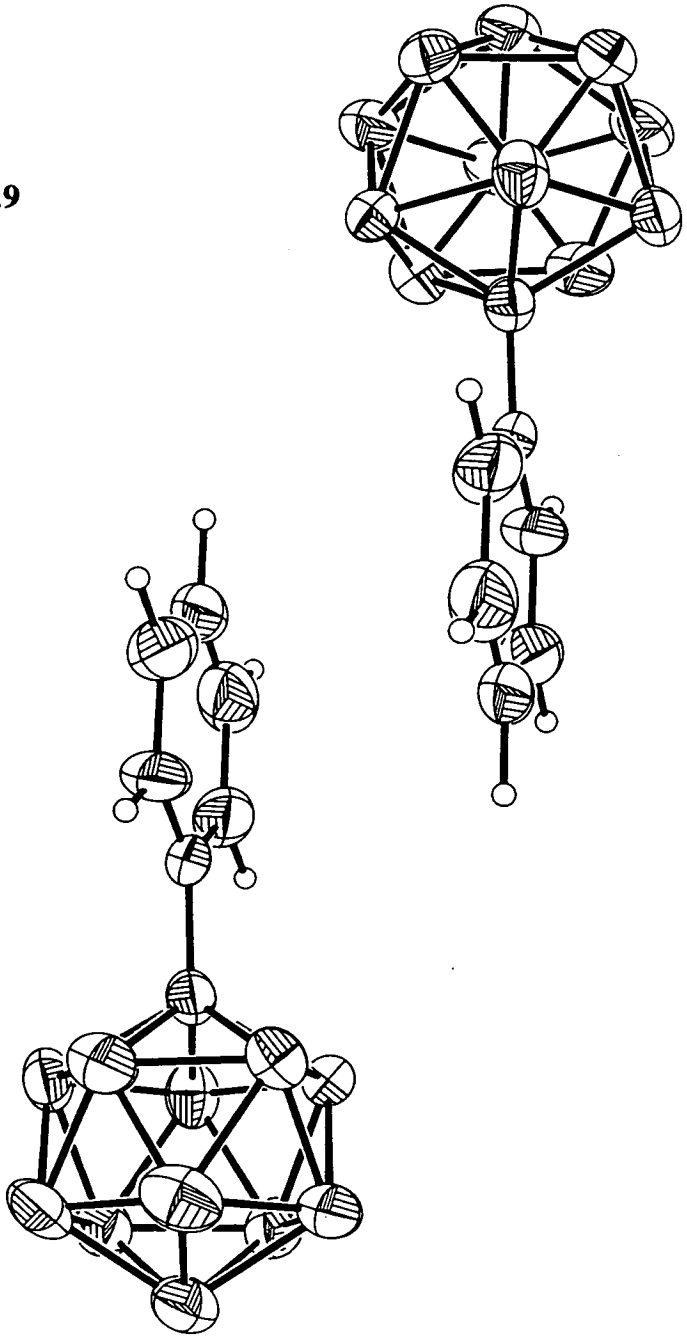

The rotation of the two phenyl rings in 1,2-$Ph_2C_2B_{10}H_{10}$, in a conrotatory manner, was considered. Rotation from θ_{phenyl}= 0° initially stabilises the molecule (in a similar manner to 1-$PhC_2B_{10}H_{11}$). At a θ_{phenyl} value of approximately 40° unfavourable contacts between H_{ortho} and C_{ortho} atoms are introduced and thereafter, further twisting rapidly destabilises the molecule. Thus, although at θ_{phenyl}= 90° there would be the most efficient C_{cage}-C_{cage} interaction, the steric constraints introduced by the two phenyl substituents, prevent the electronically preferred conformation being adopted. The experimentally observed values of θ_{phenyl} are close to 0°. The C_{cage}-C_{cage} connectivities are longer than those in ortho-carborane consistent with prediction (when θ_{phenyl} is close to 0°). Similarly, steric interactions between cage substituents in close proximity can also explain the deviation from θ_{phenyl}= 90° in the related complex 1-Me-2-Ph-$C_2B_{10}H_{10}$[45]. In this complex the value of θ_{phenyl}= 16.6° while the C_{cage}-C_{cage} connectivity is 1.696(5)Å.

The preceding discussion illustrates that, in substituted carbaboranes, the structures adopted often represent a compromise between the electronically favoured and the sterically allowed. Hence, while a single phenyl substituent can orient close to its electronically preferred conformation, the introduction of a second substituent (Me or Ph) in close proximity, prevents this, on steric grounds. Similar considerations are important when the structures of substituted carbametallaboranes are considered.

1.8 Carbametallaboranes Containing Phenyl-Substituted Carbaboranes.

A useful means of classifying carbametallaboranes is by the nature of the metal fragment, ML_n. Specifically, n refers to the number of co-ordination sites occupied by the metal (non-carbaborane) ligand(s). Hence, a complex containing either the fragment $\{Au(PPh_3)\}^+$ or $\{Hg(PPh_3)\}^{2+}$ can be described as an ML complex, one containing the fragment $\{Pt(PPh_3)_2\}^+$ or $\{Pd(1,5\text{-}COD)\}^{2+}$ can be designated an ML_2 complex and a compound incorporating the fragment $\{Ru(C_6H_6\}^{2+}$ or $\{Rh(C_5Me_5)\}^{2+}$ an ML_3 complex. The carbaborane ligand can act as a 6 (or 4) electron donor, occupying three (or two) metal co-ordination sites whence it is described as being π-bonded. Alternatively, it may form a single 2-centre 2-electron bond to the metal atom, in a σ (endo-) complex.

There are surprisingly few reported examples of metal complexes with phenyl carbaborane ligands, given the potential for the adoption of unusual structures, as a result of the steric requirements of the substituent(s). There are a few σ (exo) bonded metalla-complexes containing the $[1\text{-}PhC_2B_{10}H_{11}]^-$ ligand, for example $1\text{-}[(P(n\text{-}Pr)_3)_2PtCl]\text{-}2\text{-}Ph\text{-}1,2\text{-}(\sigma\text{-}C_2B_{10}H_{10})$[46]. However, the π complexes of $[1\text{-}Ph\text{-}C_2B_9H_{10}]^{2-}$ are of more relevance to the work described in this thesis. The earliest reported example of such a complex was the ML_3 species $1\text{-}Ph\text{-}3,3\text{-}(PPh_3)_2\text{-}3\text{-}H\text{-}3,1,2\text{-}IrC_2B_9H_{10}$[47]. No synthesis or structure determination was presented but an unexpectedly facile isomerisation was described. Heating in toluene at reflux temperature for 30 hours yielded a polytopal isomer with 84% conversion. An X-ray crystallographic study of this product revealed it to be the C-separated isomer $2,2\text{-}(PPh_3)_2\text{-}2\text{-}H\text{-}8\text{-}Ph\text{-}2,1,8\text{-}IrC_2B_9H_{10}$ (see figure 1.10).

Figure 1.10

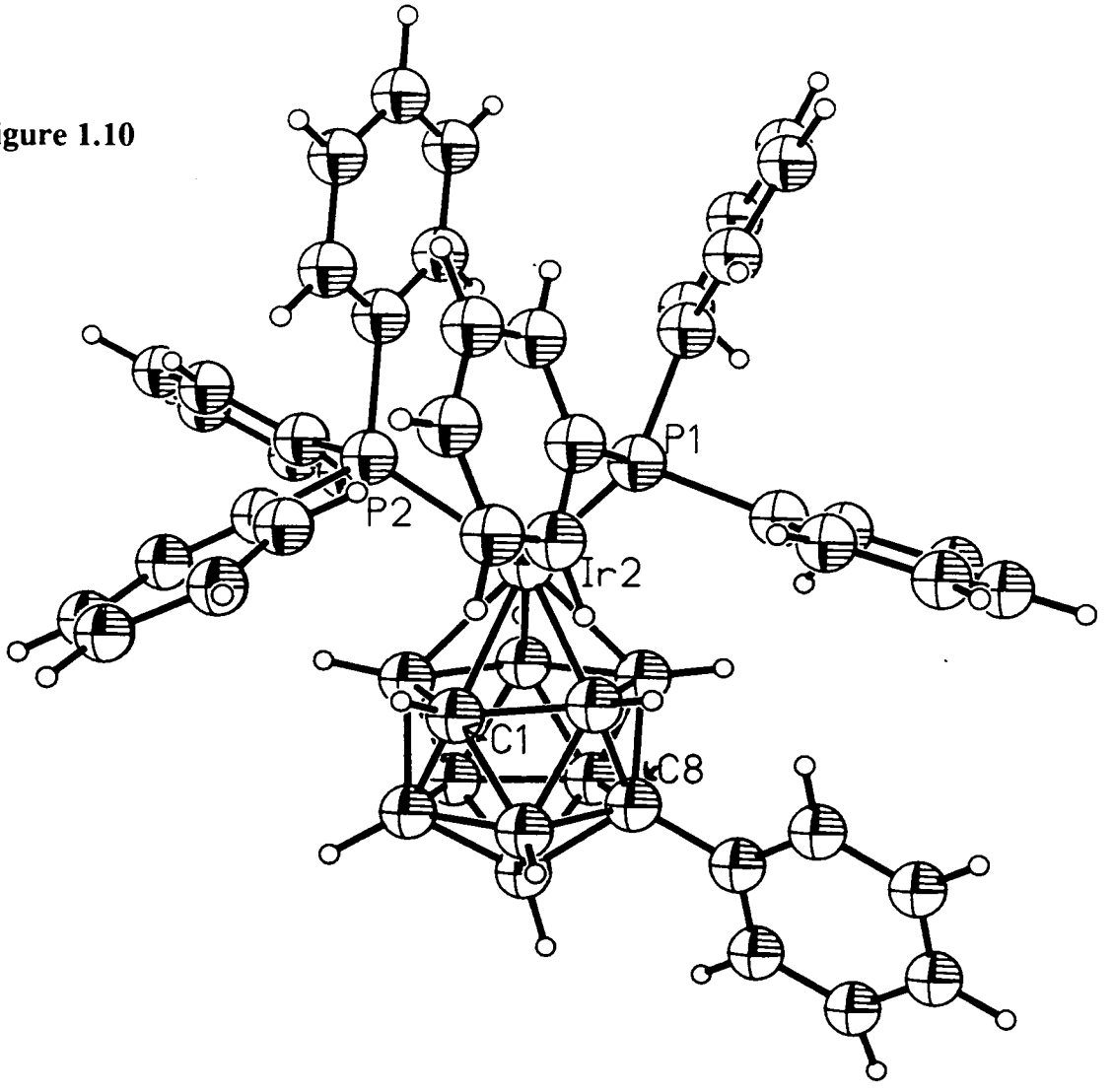

The carbon atom bearing the phenyl substituent is the one which migrates away from the metal fragment thereby alleviating the steric interaction between the phenyl ring and the metal fragment. This was considered to be the driving force of the reaction, on the basis that none of the other possible 2,1,8-isomer, in which the {CH} vertex has migrated, was detected. Similar behaviour was exhibited by the carbarhodaborane 1-Ph-2-Me-3,3-$(PPh_3)_2$-3-H-3,1,2-$RhC_2B_9H_9$[48]. Thermolysis of this species (THF, 65°C) yielded a single 2,1,8-isomer, in which it is the {CPh} vertex which has migrated to position 8. This type of behaviour is discussed fully in the main body of this thesis.

The other reported π-bonded complexes of this carbaborane ligand also incorporate an ML_3 fragment. Firstly, complexes with a $\{M(C_9H_7)\}$ vertex are considered[49, 63].

The carbacobaltaborane, 1-Ph-3-(η^5-C_9H_7)-3,1,2-$CoC_2B_9H_{10}$ was formed as the sole product of the reaction of the thallium carbaborane with $Co(acac)_3$ and LiC_9H_7 in THF. A crystal structure determination revealed that the icosahedral unit was virtually undistorted, with Δ= 0.035Å (as expected for a d^6 metal complex) (see figure 1.11).

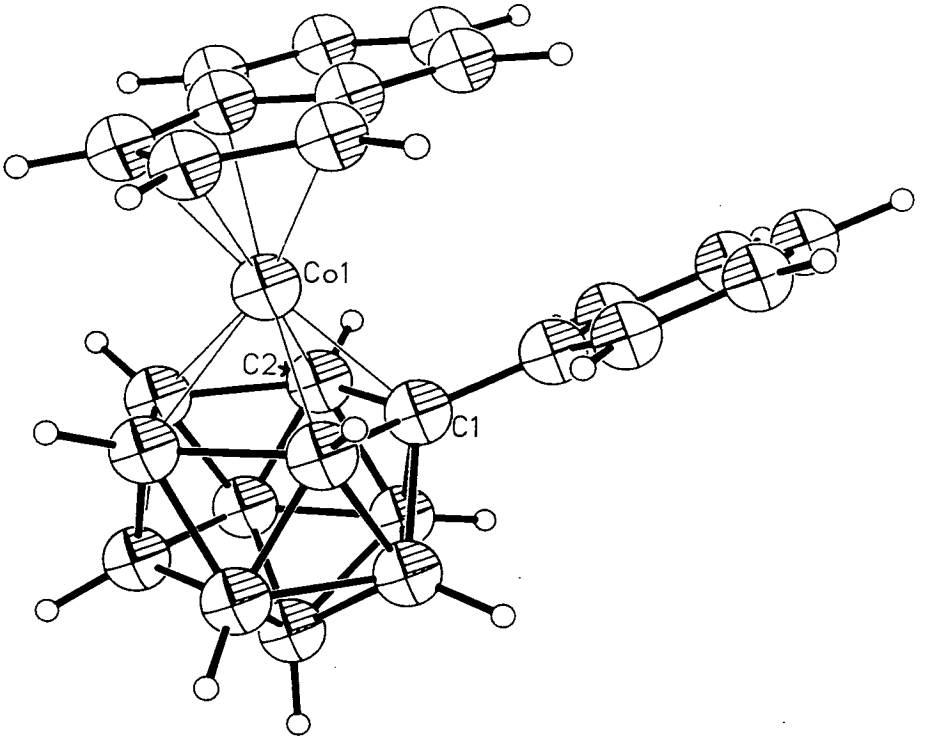

Figure 1.11

The observed value of θ_{phenyl} was close to 90°, corresponding to the predicted lowest energy conformation. However, the indenyl ligand was found to be distorted in comparison to the conformation adopted in the unsubstituted carbacobaltaborane[50], being twisted and tilted as to accommodate the proximal phenyl substituent.

The rhodium analogue was formed as one of the products of the reaction between $[(C_9H_7)RhCl_2]_2$ and the thallium carbaborane in CH_2Cl_2. The structure of the other major product of this reaction was not determined, however the available spectroscopic evidence suggests that it is of the form 7-Ph-9/11-(C_9H_6)Rh(C_9H_7))-7,8-$C_2B_9H_{10}$. In this case the cationic $[C_9H_6RhC_9H_7]^+$ is co-ordinated to a boron atom on the *nido* face via an indenyl-boron bond. This could involve either B(11) or B(9) which could not be distinguished.

A final example of an $\{ML_3\}$ complex incorporates the $\{Ru(\eta^6\text{-mesitylene})\}$ fragment (where the mesitylene ligand occupies 3 co-ordination sites) which can be denoted 1-Ph-3-(η_6-mes)-3,1,2-$RuC_2B_9H_{10}$[44]. A crystal structure determination of this complex revealed that it adopts a *closo-* geometry, as predicted on the basis of PSEP theory (13 SEP's for a 12 vertex species) and confirmed the 3,1,2-architecture. The metal fragment is not significantly slipped over the C_2B_3 face (Δ= 0.036Å) consistent with the prediction for a d_6 metal complex. The C_2B_3 face, the B_5 belt and the arene ring are all nearly co-planar indicating the undistorted nature of the complex. The value of θ_{phenyl} is 68°, significantly less than the predicted value of 90°. Inspection of a schematic representation of a single molecule (figure 1.12) indicates that this deviation may arise from the avoidance of an unfavourable interaction between the phenyl group and the arene ligand.

The C_{cage}-C_{cage} distance is 1.656(6)Å, identical to that in the related unsubstituted carbaruthenaborane 3-(η_6-(C_6Me_6))-3,1,2-$RuC_2B_9H_{11}$[51] (C_{cage}-C_{cage}= 1.657(10)Å).

Figure 1.12

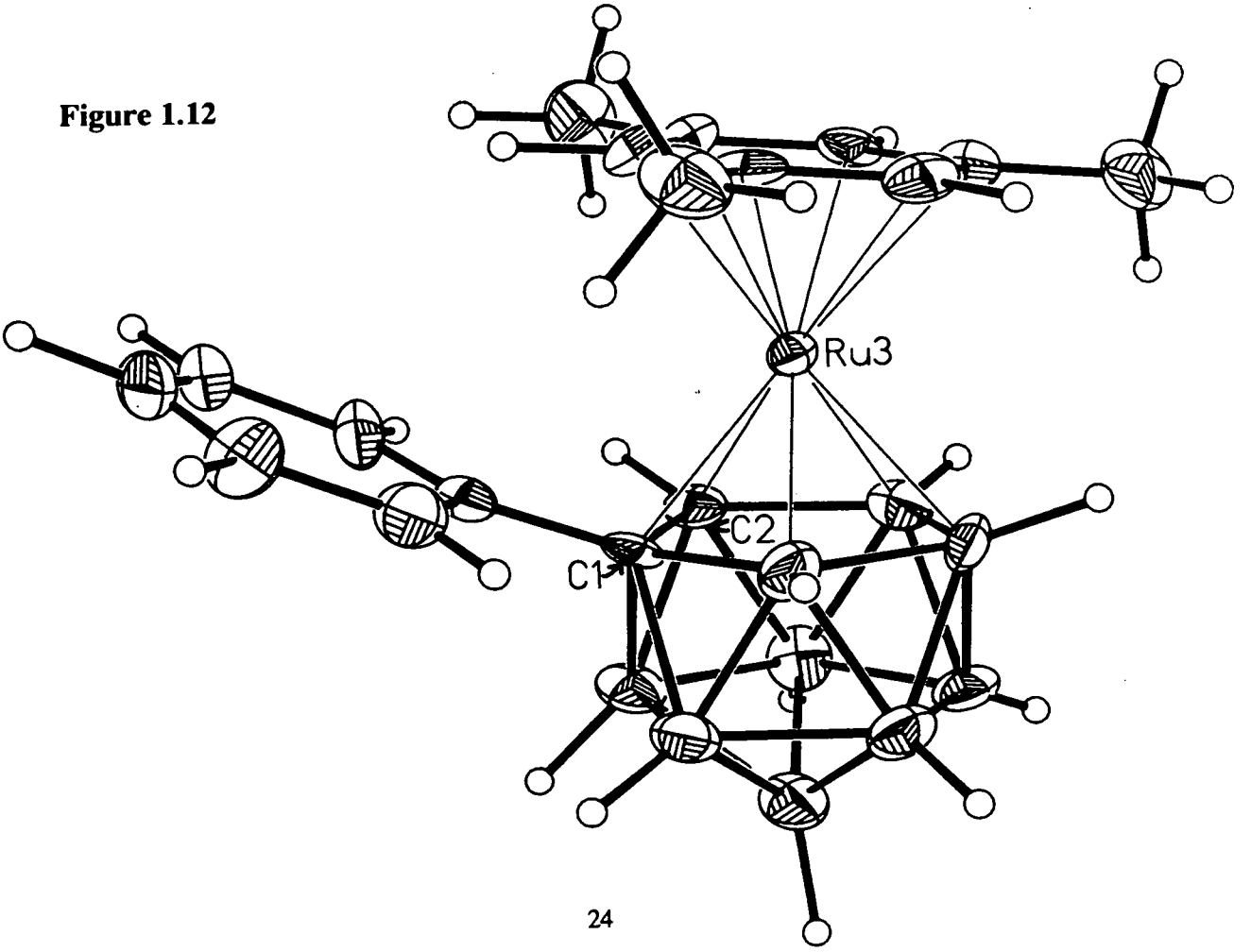

The metallation of the anion $[7,8\text{-}Ph_2C_2B_9H_9]^{2-}$ has been carried out solely by the author's co-workers. A selection of the resulting complexes is discussed below. However, the crystal structure of the mono-anionic ligand has also been determined[52] and is of relevance to this work. The structures of both the $[HNMe_3]^+$ and the $[Me_3NCH_2C_6H_5]^+$ salts were established and found to be practically identical. Both contain an open C_2B_3 face with an *endo*- proton on the central facial boron atom. An *endo* bond is one which points towards the vacant vertex in a *nido* carbaborane. The C_{cage}-C_{cage} distance is 1.590(5)Å in the former salt and 1.602(3) in the latter, both of which are significantly shorter than that in the parent *closo*-carbaborane. The values of θ_{phenyl} are 5.6 and 10.0° in the $[HNMe_3]^+$ salt and 17.9 and 20.0° in the $[Me_3NCH_2C_6H_5]^+$ salt. This indicates that the 2 {CPh} vertices can approach within reasonably short distances and suggests that there is an electronic contribution to the long C_{cage}-C_{cage} connectivity in $1,2\text{-}Ph_2C_2B_{10}H_{10}$ at low θ_{phenyl} values. As well as a shortening of the C_{cage}-C_{cage} connectivity on going from a *closo*- to a *nido*- carbaborane there is also lengthening of the facial B-B bonds and a shortening of facial B-C bonds (where facial refers to atoms on the open face of a *nido*- polyhedron), as a capping $\{BH\}^{2+}$ is replaced by an *endo* $\{H\}^+$. The variation in bond distances can be traced to different degrees of depopulation of π m.o.'s of *nido* $[C_2B_9H_{11}]^{2-}$ by the zero electron 3 orbital $\{BH\}^{2+}$ vertex and the zero electron 1 orbital $\{H\}^+$ unit. The deviation from the lowest energy orientation by virtue of conrotatory twisting of the two phenyl rings is within the limits of crystal packing forces.

Similar structural features are exhibited in the ML complex, $7,8\text{-}Ph_2\text{-}10\text{-}endo\text{-}(HgPPh_3)\text{-}7,8\text{-}nido\text{-}C_2B_9H_9$[49], formed from the reaction of $[Ph_3PHgCl_2]_2$ and $Tl_2[C_2B_9H_9Ph_2]$. An X-ray diffraction study indicated that, as expected for a species containing a d^{10} metal centre, the metal fragment is slipped away from the centre of the ligated face (see figure 1.13).

There is one relatively strong metal-boron bond (to B(10)) of 2.178(8)Å while the interactions with the other two facial boron atoms are virtually non-bonding (Hg-B(9)= 2.535(8) and Hg-B(11)= 2.616(7)Å). The observed structure is similar to that of the unsubstituted analogue[53] although the slippage of the metal fragment is more pronounced. The C_{cage}-C_{cage} distance of 1.589(9)Å is shorter than that in the parent *closo-* carbaborane but slightly longer than that in the unsubstituted $\{PPh_3Hg\}^{2+}$ analogue. The variations in bond distances when replacing a {BH} vertex with $\{PPh_3Hg\}^{2+}$ are similar to those observed when replacing a $\{BH\}^{2+}$ with an $\{H\}^{+}$. The values of θ_{phenyl} are 28° and 31° (conrotatory twist) and this causes the observed shortening of the C_{cage}-C_{cage} connectivity.

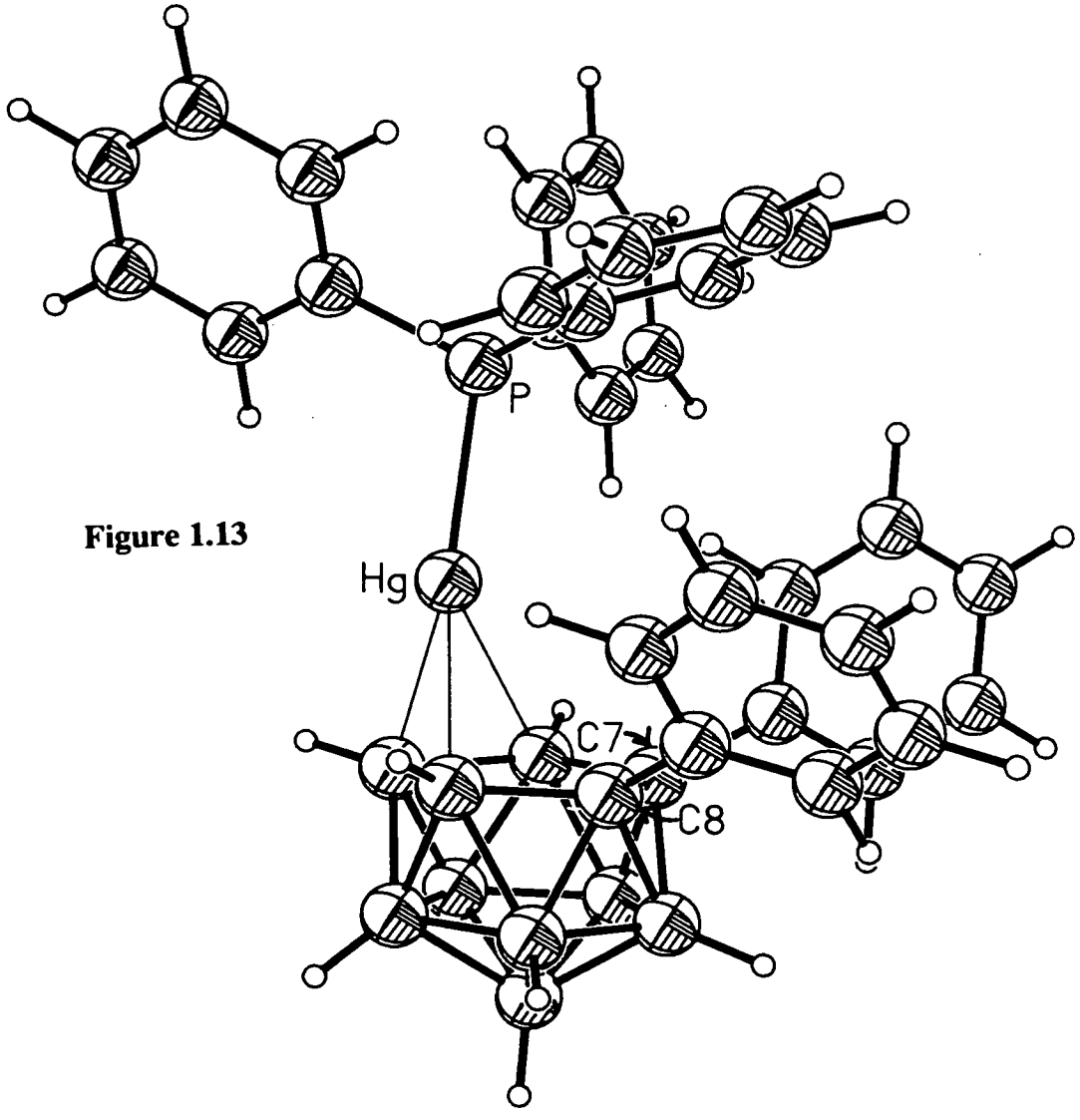

Figure 1.13

The earliest example[54] of an ML_3 complex contained the $\{RhCp^*\}^{2+}$ (Cp^*= C_5Me_5) fragment and was prepared by the reaction of $[RhCl_2Cp^*]_2$ with the carbaborane dianion. X-ray diffraction quality crystals were obtained by slow diffusion of n-hexane into a solution of the product in CH_2Cl_2. The structure solution identified the presence of 2 independent, but similar, molecules per asymmetric unit (designated A and B). A schematic representation of a single molecule of A is shown in figure 1.14.

This reveals the highly distorted nature of the complex. The C_{cage}-C_{cage} distance is virtually non-bonding (2.51(3)Å) and as a result the boron atom (B(6)) is pulled out of the plane of the other B atoms (B(5), B(9), B(11), B(12)). Although the B(6)-M distance (= 2.92(2)Å in A and 2.91(3)Å in B) is too long for the interaction to be described as bonding, it is shorter than that observed in true *closo*- complexes.

Figure 1.14

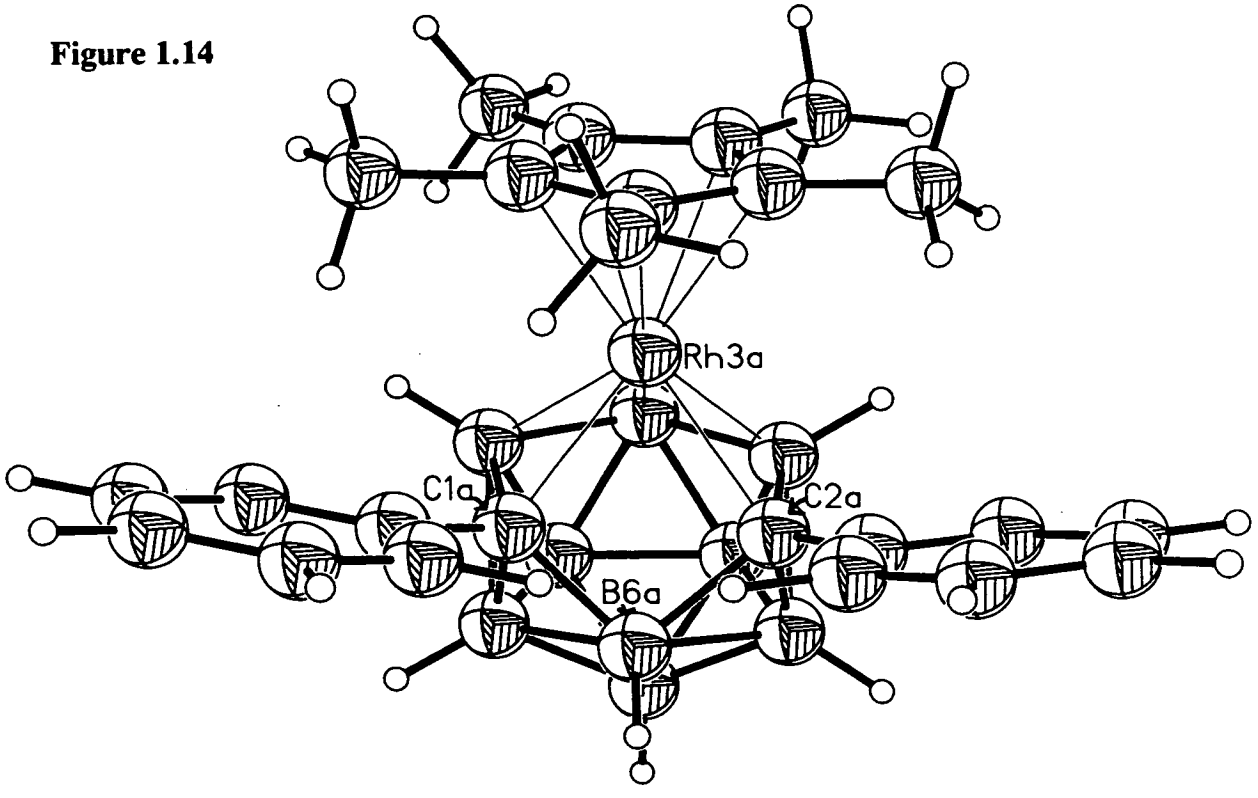

These distortions allow the phenyl substituents to adopt conformations close to the predicted orientation (θ_{phenyl}= 79° in A, 86° in B). This can be rationalised by considering the interaction of the C-phenyl groups with the Cp^* ligand. The metal fragment is virtually unslipped and so lies close to the centre of the ligated face. Thus, at θ= 0° there would be an unfavourable steric interaction of the phenyl groups with the planar Cp^* group. This can be alleviated by a rotation of the 2 phenyl groups by *circa* 90°, but this in turn leads to mutual congestion between the two phenyl rings and hence to a major lengthening of the C_{cage}-C_{cage} distance. Similar distortions were found in the related {C_6H_6Ru} and {(p-cym)Ru} complexes[55] (C_{cage}-C_{cage}= 2.49 and 2.45Å, respectively and θ_{phenyl}= 61 and 66/44°, respectively. These complexes have electron counts of *closo-* icosahedra but partially open structures. These can be considered as tending towards what is termed *hyper-closo* geometry, as observed in the complex $PtW(CO)_2(PEt_3)_2(\eta^6C_2B_9H_8(CH_2C_6H_4Me)Me_2$[56] (see figure 1.15).

Figure 1.15

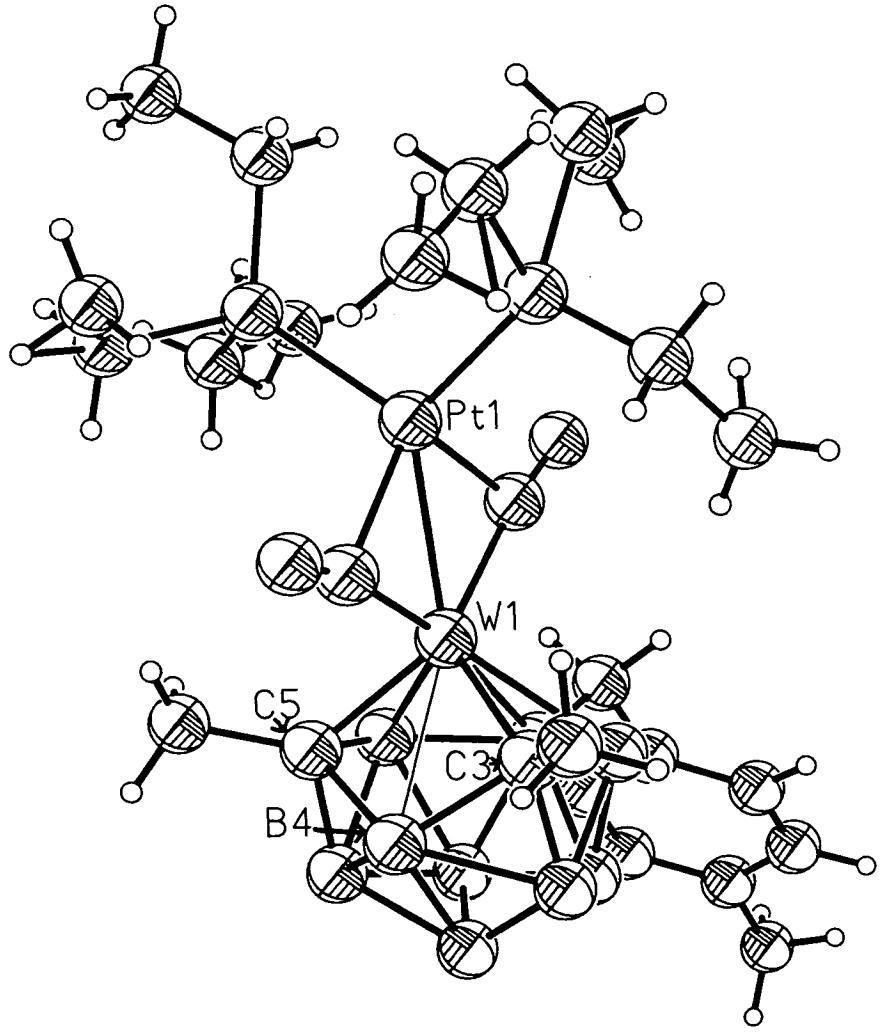

In this case, there is a formal bond between B(4) and the tungsten atom, and the complex possesses n SEP's and n vertices. Using this formalisation, these species can be considered more electron deficient than their *closo-* analogues and this is manifested in a shift of the ^{11}B n.m.r. resonances to higher frequency in *hyper-closo* complexes[56]. Similarly, the average ^{11}B chemical shift in the {$RhCp^*$} complex described above is substantially to high frequency of that in the unsubstituted analogue[54]. It could be that this is wholly or partly due to the electronic effect of 2 electron-withdrawing substituents rather than the concomitant change in structure (towards *hyper-closo*). However, the observation that the ^{11}B chemical shifts in 1,2-$Ph_2C_2B_{10}H_{10}$ are only slightly more positive than those for ortho-carborane suggests that the electron-withdrawing effect of the substituents has a relatively minor effect.

In contrast to the complexes containing the $[C_2B_9H_9Ph_2]^{2-}$ ligand, the related species incorporating the {Ru(p-cym)} fragment, 3-((p-cym)Ru)-1-Ph-2-Me-3,1,2-$RuC_2B_9H_9$[55] exhibits a virtually undistorted structure with a C_{cage}-C_{cage} distance of 1.70Å and a θ_{phenyl} value of 55°. This demonstrates the differing steric requirements of a methyl substituent with respect to a phenyl one.

The reaction of $Rh(PPh_3)_3Cl$ with $[HNEt_3][C_2B_9H_{10}Ph_2]$ gives rise to 2 carbametallaboranes. The n.m.r. data for both of these suggest *nido-* structures, but only the structure of the red product has been determined[57]. A schematic representation of a single molecule of this species, *exo*-μ^2-($Rh(PPh_3)_2$)-7,8-Ph_2-7,8-*nido*-7,8-$C_2B_9H_9$, is shown in figure 1.16. It exhibits what is termed an *exo-nido* structure, in which the metal fragment is co-ordinated to a B_2 edge, rather than occupying the twelfth icosahedral vertex.

Figure 1.16

Hs removed for clarity.

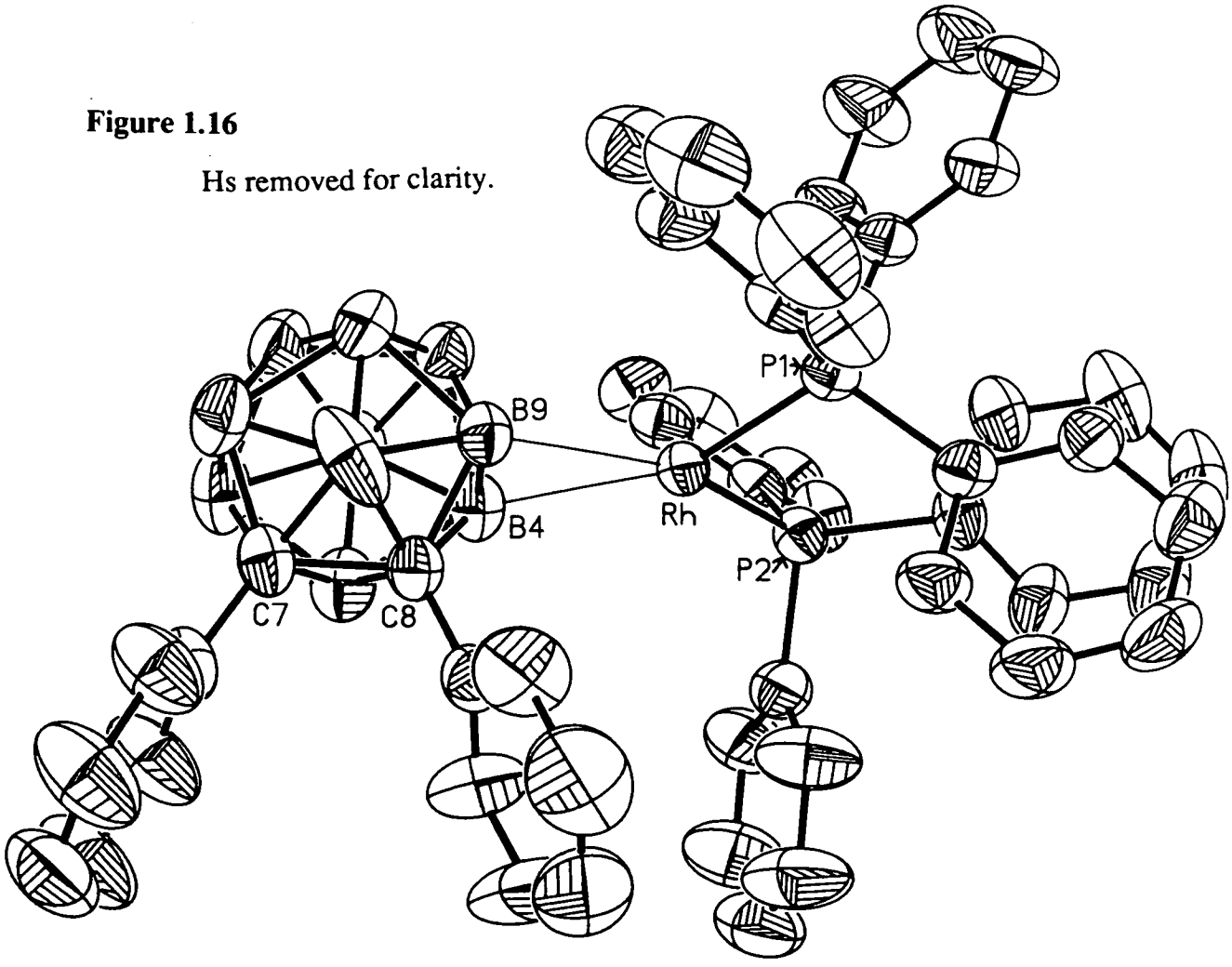

Bonding to the metal fragment is via two 3-centre 2-electron B-H-Rh bonds (to B(4) and B(9)). The metal centre adopts square planar geometry, consistent with a Rh^{I} description. The values of θ_{phenyl} are 3.38 and 9.85°, with rotation being in a conrotatory manner. The reaction of the ruthenium analogue $Ru(PPh_3)_3Cl_2$ with the carbaborane dianion also gives rise to two species[55]. The crystal structure of one of these has been determined and the molecule shown to be *exo*-η^3-5,6,10-{$Ru(PPh_3)_2Cl$}-7,8-Ph_2-*nido*-$C_2B_9B_9$. In this case the metal fragment is co-ordinated to the carbaborane via three Ru-H-B bonds, reflecting the preference of a Ru^{II} centre to adopt an octahedral geometry. Similarly to the Rh species, the second product appears, from spectroscopic data, to be a second *exo-nido* tautomer.

The unsubstituted analogue of the Rh species[15] has been found to catalyse processes such as alkene hydrogenation, hydrosilylation of ketones and deuterium exchange of terminal {BH} in boranes and heteroboranes. It is believed to be the *exo-nido-* tautomer rather than the *closo-* form which acts as the catalyst precursor. This is in keeping with the behaviour of Rh^{I} species which readily undergo oxidative addition reactions. In fact, the conversion of the *exo-nido-* tautomer to the *closo-* one can be considered as an oxidative addition in which the facial H atom adds to the metal centre. At the same time the nature of the interaction between the carbaborane and the metal fragment changes, the metal centre being co-ordinated in a π manner to $[C_2B_9H_{11}]^{2-}$ in the *closo*-species, occupying three co-ordination sites as opposed to two in the *exo-nido* tautomer. The metal atom undergoes concomitant oxidation from Rh^{I} to Rh^{III} and as expected adopts a nearly octahedral geometry. The *exo-nido* and *closo-* tautomers exist in equilibrium by an oxidative addition-reductive elimination cycle. It has been noted that the position of this equilibrium is affected by the nature of any *exo* polyhedral ligands (on the C atoms). For example, if the carbaborane is unsubstituted *e.g.* $(H)(PPh_3)_2Rh(C_2B_9H_{11})$, the *closo* Rh^{III} tautomer predominates, however when there are two methyl substituents[58], both tautomers can be observed. When there are two phenyl substituents, only the *exo-nido* isomer is present. This suggests that the diphenylcarbarhodaborane may be a more effective catalyst than its unsubstituted analogue.

From the preceding discussion it is apparent that the introduction of C-phenyl substituents can result in unexpected structural modifications in carbametallaborane derivatives. The nature of these can be described as:

a) polytopal rearrangement

b) severe elongation of the C_{cage}-C_{cage} connectivity (polyhedral deformation).

c) vertex extrusion (formation of an *exo-nido* complex rather than a *closo-* one).

1.9 $\{ML_2\}$ Complexes of Carbaboranes.

Although there have been several reported examples of carbametallaboranes in which there is phenyl substitution at the cage carbon vertices, there are few which involve an $\{ML_2\}$ fragment, and these are limited to the *exo-nido* species. There are no examples of stable, *closo-* complexes incorporating an $\{ML_2\}$ fragment and a Ph-substituted carbaborane. However, there are many examples of *closo-* $\{ML_2\}$ complexes involving other carbaborane ligands. A few relevant examples, in which the carbaborane ligand is the unsubstituted $[C_2B_9H_{11}]^{2-}$, are described below.

The "classic" example of an $\{ML_2\}$ fragment is $\{PtP_2\}$, where P is a phosphine ligand. There are a few reported examples of carbaplatinaboranes incorporating this fragment. A single molecule of one such complex, 3,3-$(PEt_3)_2$-3,1,2-$PtC_2B_9H_{11}$[27], is depicted in figure 1.17.

Figure 1.17

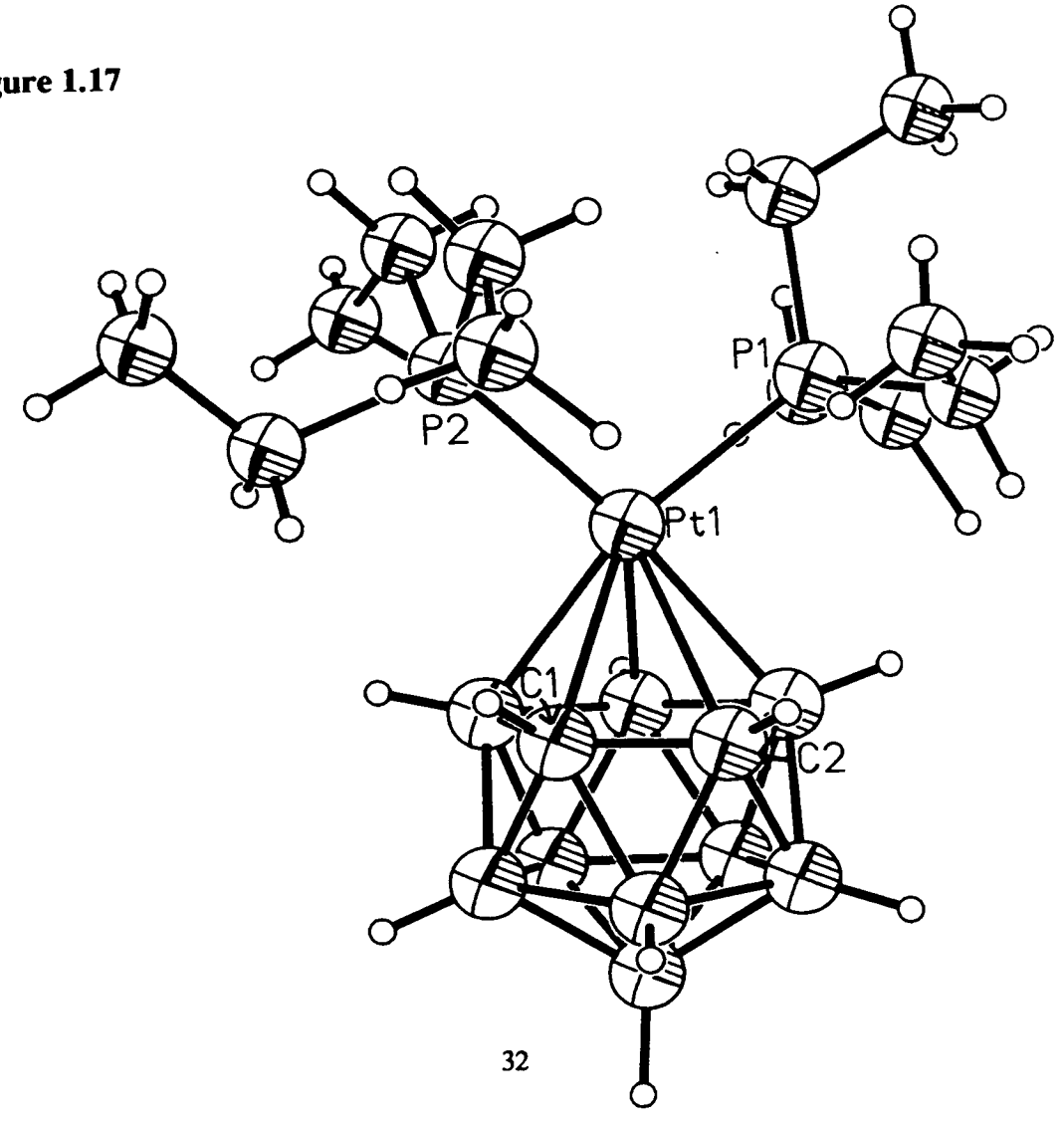

The plane through the metal fragment lies close to the predicted orientation perpendicular to the cage mirror plane. The observed deviation (13.9°) is believed to be such as to minimise intramolecular contacts. A slippage of the metal fragment towards B(8) of 0.42Å is observed. A complex[59] incorporating the bidentate phosphorus ligand, dppe, has also been described. This complex adopts a structure practically indistinguishable from that described above.

The structure of the related $\{PdP_2\}$ complex, 3,3-$(PMe_3)_2$-3,1,2-$PdC_2B_9H_{11}$ is less distorted[60], with a slippage parameter of only 0.26Å. This can be rationalised by considering the bonding between the metal atom and the carbaborane ligand. The $[carbaborane]^{2-}$ moiety is regarded as being a 6 electron donor and for a d^8 metal atom the dominant bonding interaction involves a metal (xz) hybrid orbital and the cage $5e^1$ (a'') orbital. The filled metal (yz) orbital enters into a 4 electron antibonding interaction with the cage $5e^1$ (a') orbitals.

This latter interaction can be reduced via d-p hybridisation of the metal-based orbitals. This directs metal d_{xy} electron density away from the cage. It is this effect which may be responsible for the reduced distortion of Pd complexes with respect to Pt ones; the d-p promotion energy in an electro-neutral Pd atom is lower than that for a Pt atom in the same environment[61].

The idea that d-p hybridisation leads to a less distorted structure was further justified by consideration of the structure of [K[18-crown-6]][3,3-$(PPh_3)_2$-3,1,2-$RhC_2B_9H_{11}$][62]. This adopts a *closo-* structure (Δ= 0.05Å), which can be ascribed to the smaller d-p promotion energy for Rh^I with respect to Pd^{II}. The ML_2 fragment lies close to its predicted perpendicular orientation with respect to the cage mirror plane.

The unfavourable 4 electron interaction can also be reduced by the introduction of π-acceptor ligands on the metal atom. This suggestion is justified by comparison of the observed structure of the complex containing the {Pd(tmen)} (tmen= $[Me_2N(CH_2)_2NMe_2]$)[60] (see figure 1.18). This was found to be more distorted than the $\{PdP_2\}$ analogue, with a slippage parameter of 0.52Å, consistent with (tmen) acting as a less efficient π acceptor ligand than a phosphine does.

Figure 1.18

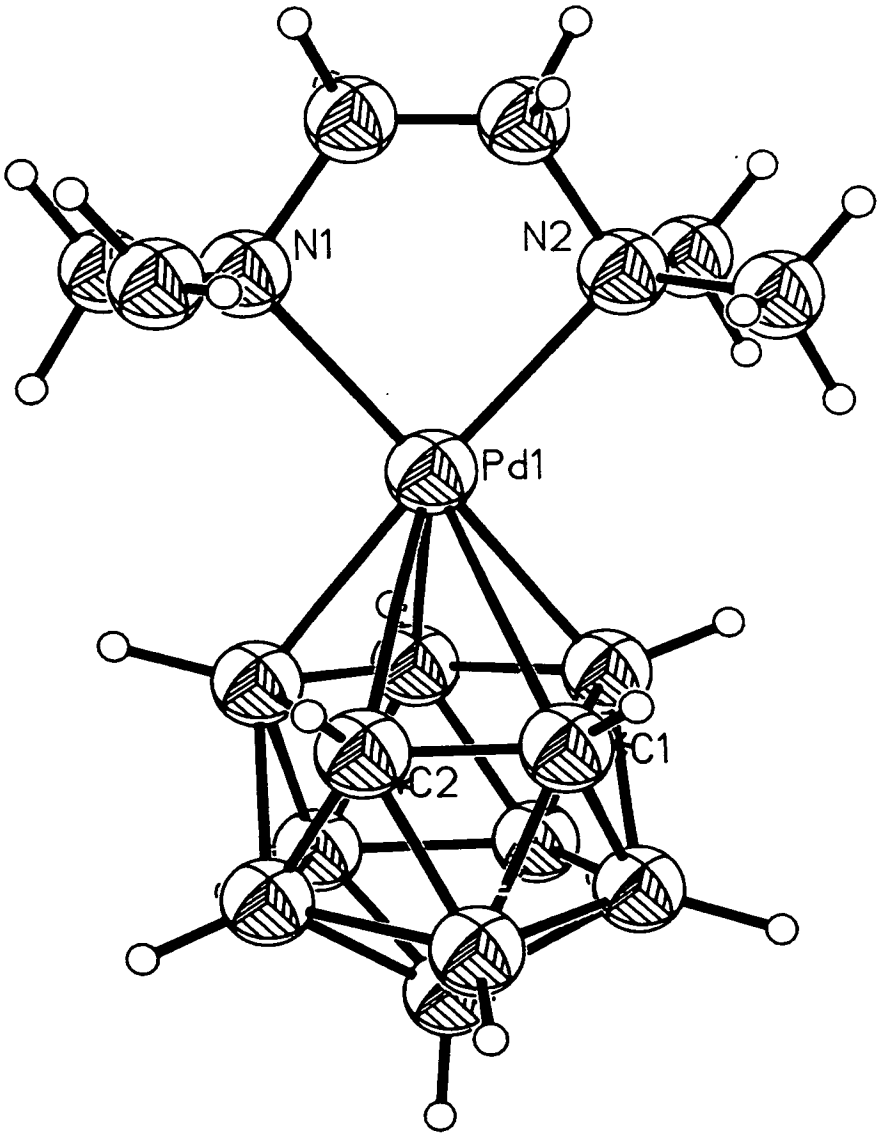

A final example of an $\{ML_2\}$-carbaborane complex is afforded by 3-(1,5-COD)-3,1,2-$PdC_2B_9H_{11}$[63]. A representation of a single molecule is depicted in figure 1.19. This species shows a modest slip distortion (= 0.24Å) and a C_{cage}-C_{cage} distance of 1.495(4)Å.

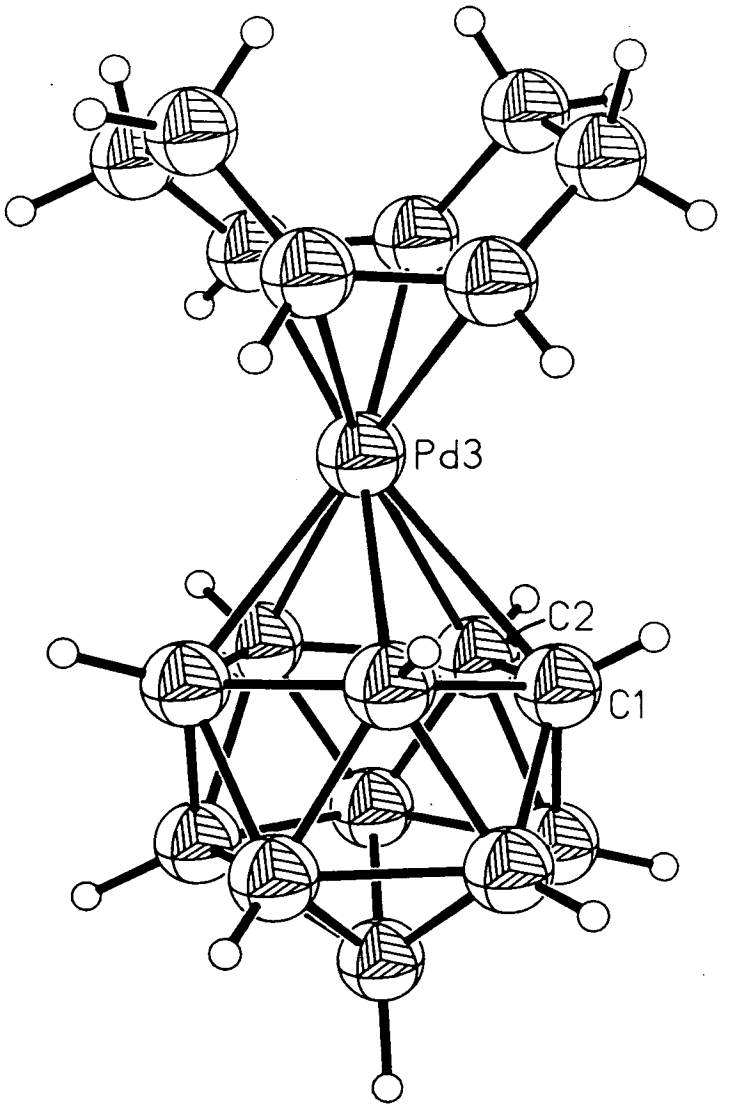

Figure1.19

Despite the diversity of $\{ML_2\}$ fragments for which carbametallaboranes have been structurally characterised, there is little observed deviation in the orientation of the ML_2 plane from that predicted from E.H.M.O. calculations. However, substitution of a bulky group on the cage ligated face may result in structural modification.

1.10 Aims and Scope of Work.

The initial aim of the studies presented in this thesis was to investigate the structural deformations caused by the introduction of C-Ph substituents in $\{ML_2\}$ carbametallaborane complexes. Of particular interest was the orientation of the $\{ML_2\}$ fragment with respect to the ligated carbaborane.

In the course of these studies, one of the structural modifications exhibited was found to be the migration of a {CZ} (Z= H, Ph) vertex over the polyhedral surface. The steric and electronic influences contributing to the relative ease of these processes provided the basis for much subsequent work. Such isomerisations have been the subject of much interest (and controversy) particularly relating to the mechanism(s) involved. However, in contrast to the isomerisations of *closo*-carbaboranes and some carbametallaboranes, which require extreme conditions, the species described exhibit a depression of the rearrangement temperatures, and this renders these processes more conducive to study.

Chapter 2

Phenyl-carbaborane Complexes Incorporating the {Pt(PMe$_2$Ph)} Fragment.

2.1 Introduction.

This chapter describes the synthesis, characterisation and single crystal X-ray diffraction study of two new C-phenyl substituted carbaborane complexes which incorporate the platinum bis-phosphine fragment $\{(PMe_2Ph)_2Pt\}^{2+}$.

The first of these is the 3,1,2-platina-monophenylcarbaborane complex, **1**. At elevated temperature this is found to undergo a skeletal rearrangement, yielding two isomeric carbaplatinaboranes, **2** and **3**. These have been independently synthesised and their structures determined by Mingos *et al*[66]. They provide the first examples of 2 isomeric 3,1,11-carbametallaboranes which are formed from a common precursor. The only other examples[47,48] of the rearrangement of asymmetrically substituted carbametallaboranes were both reported by Hawthorne *et al.* Both of these yielded only a single isomer. Some other reported isomerisations and the principal mechanistic proposals are discussed.

Finally, the platinum-bisphosphine complex of C,C-diphenylcarbaborane is described. In this case, the target 3,1,2-carbaplatinaborane is not observed and the major isolatable room temperature product is the rearranged 3,1,11-isomer, **4**.

2.2 Formation and Characterisation of the $\{(PMe_2Ph)_2Pt\}$ Complex of (C-Ph) Substituted Carbaborane.

When cis-$PtCl_2(PMe_2Ph)_2$ is stirred with $Tl_2C_2B_9H_{10}Ph$ in CH_2Cl_2, a bright orange soluble product, **1**, is produced, along with insoluble TlCl. Separation and purification are effected by columm chromatography (alumina/CH_2Cl_2), to yield an orange-red crystalline solid.

Micro-analysis figures are consistent with the formulation $B_9C_{24}H_{37}P_2Pt$ (molecular weight 679.9). The product was characterised by infra-red spectroscopy; FAB mass spectrometry; ^{11}B, ^{31}P (and ^1H) n.m.r. spectroscopies (see section 2.4) and the solid state structure was determined by a single crystal X-ray diffraction study.

The solution i.r. spectrum of **1** (CH_2Cl_2) shows a broad B-H stretching band centred on 2530cm^{-1} as well as a band attributable to the co-ordinated PMe_2Ph moiety, at 1490cm^{-1}. The principal peaks in the FAB mass spectrum of **1** are given in table 2.1, along with their assignments. These are based on a molecular ion of formula $[(PMe_2Ph)_2PtC_2B_9H_{10}Ph]^+$, m/z = 680.

Table 2.1 Principal Peaks in FAB Mass Spectrum of 1 and their Assignments.

m/z	Assignment
680	$[(PMe_2Ph)_2PtC_2B_9H_{10}Ph]^+$
471	$[(PMe_2Ph)_2Pt]^+$
456	$[(PMe_2Ph)(PMePh)Pt]^+$
441	$[(PMePh)_2Pt]^+$
424	$[(PPh)(PMePh)Pt]^+$
409	$[(PPh)_2Pt]^+$
394	$[(PMe_2Ph)(PMe_2)Pt]^+$
379	$[(PMe_2Ph)(PMe)Pt]^+$ or $[(PMe_2)(PMePh)Pt]^+$
364	$[(PMePh)(PMe)Pt]^+$
333	$[(PMe_2Ph)Pt]^+$
318	$[(PMePh)Pt]^+$
138	$[PMe_2Ph]^+$
123	$[PMePh]^+$

2.3 Crystal Structure of 1.

Crystals suitable for a single crystal X-ray diffraction study were obtained by the slow diffusion of n-hexane into a solution of **1** in CH_2Cl_2, at -30°C (243K). From this solution formed red, single crystals.

Data were collected on an Enraf-Nonius CAD-4 diffractometer, using graphite monochromated Mo K_α X-radiation. Full details of data collection and refinement are given in chapter 5. The unit cell and orientation matrix for data collection were established by least squares refinement of the setting angles of 25 strong, high angle reflections. Only data for which $F>2\sigma$ were retained for structure solution and refinement, in the range $1<\theta<23$. The structure was solved by Patterson (metal atom) and difference Fourier (all other non-H atoms) methods (SHELX76[67]). An empirical absorption correction was applied to the data set (DIFABS[68]). The positions of the cage carbon atoms were identified by a combination of their refined isotropic thermal parameters (when all cage skeletal atoms were refined as boron atoms) and internuclear distances. Cage hydrogen atoms were positionally refined from sites located from a ΔF map, and all other hydrogen atoms were set in idealised positions, dependent on the nature of the bound carbon atom.

The structure solution indicates that **1** forms neutral, monomeric crystals with no crystallographically imposed symmetry. Selected bond distances and bond angles are given in tables 2.2 and 2.3, respectively. A perspective view of a single molecule is shown in figure 2.1.

Figure 2.1 **Perspective View of 1.**

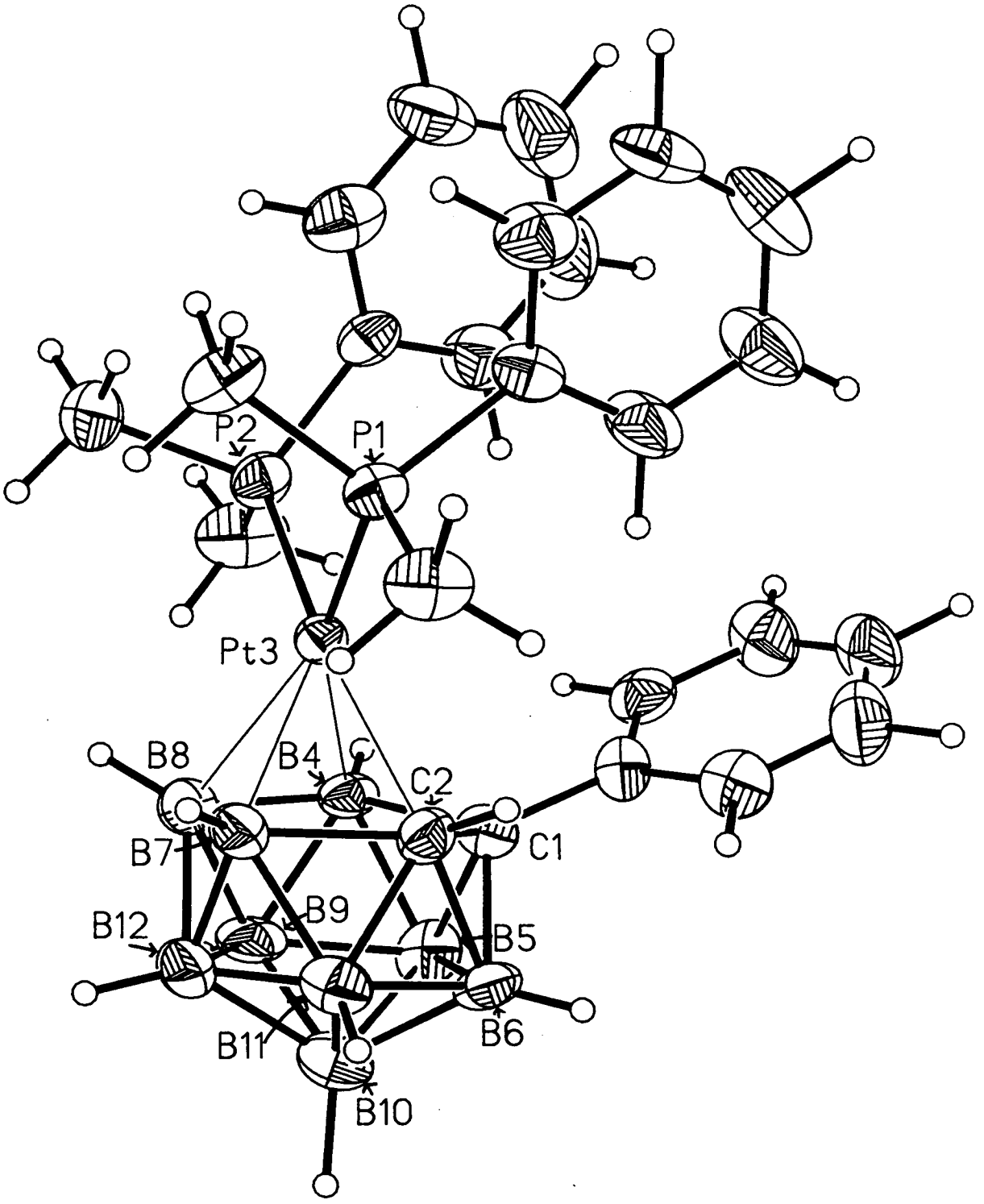

Table 2.2 Selected Bond Lengths in 1, Å, with Standard Deviations.

Pt(3) - C(1)	2.596(10)	B(9) -B(12)	1.776(19)
Pt(3) - C(2)	2.326(10)	B(10) -B(11)	1.776(18)
Pt(3) - B(4)	2.313(12)	B(10) -B(12)	1.786(19)
Pt(3) - B(7)	2.257(12)	B(11) -B(12)	1.752(18)
Pt(3) - B(8)	2.239(12)	C(101)-C(102)	1.424(14)
Pt(3) - P(1)	2.288(3)	C(101)-C(106)	1.360(14)
Pt(3) - P(2)	2.250(3)	C(102)-C(103)	1.393(17)
C(1) - C(2)	1.594(14)	C(103)-C(104)	1.348(19)
C(1) - B(4)	1.707(15)	C(104)-C(105)	1.347(19)
C(1) - B(5)	1.680(16)	C(105)-C(106)	1.398(16)
C(1) - B(6)	1.674(16)	P(1) -C(111)	1.824(10)
C(1) -C(101)	1.511(14)	P(1) -C(121)	1.830(11)
C(2) - B(6)	1.787(16)	P(1) -C(131)	1.822(12)
C(2) - B(7)	1.752(16)	C(111)-C(112)	1.383(15)
C(2) -B(11)	1.684(16)	C(111)-C(116)	1.367(15)
B(4) - B(5)	1.808(17)	C(112)-C(113)	1.379(17)
B(4) - B(8)	1.829(16)	C(113)-C(114)	1.379(18)
B(4) - B(9)	1.778(18)	C(114)-C(115)	1.344(17)
B(5) - B(6)	1.745(18)	C(115)-C(116)	1.388(16)
B(5) - B(9)	1.755(18)	P(2) -C(211)	1.829(10)
B(5) -B(10)	1.759(18)	P(2) -C(221)	1.805(12)
B(6) -B(10)	1.731(18)	P(2) -C(231)	1.821(12)
B(6) -B(11)	1.760(18)	C(211)-C(216)	1.391(16)
B(7) - B(8)	1.795(17)	C(211)-C(212)	1.364(15)
B(7) -B(11)	1.734(18)	C(216)-C(215)	1.393(19)
B(7) -B(12)	1.748(18)	C(215)-C(214)	1.417(22)
B(8) - B(9)	1.756(18)	C(214)-C(213)	1.345(21)
B(8) -B(12)	1.758(18)	C(213)-C(212)	1.376(18)
B(9) -B(10)	1.807(18)		

Table 2.3 Selected Bond Angles in 1, °, with Standard Deviations.

C(1) -Pt(3) - C(2)	37.3(3)	B(5) -B(10) - B(6)	60.0(7)
C(1) -Pt(3) - B(4)	40.2(4)	B(5) -B(10) - B(9)	58.9(7)
C(2) -Pt(3) - B(7)	44.9(4)	B(6) -B(10) -B(11)	60.2(7)
B(4) -Pt(3) - B(8)	47.4(4)	B(9) -B(10) -B(12)	59.2(7)
B(7) -Pt(3) - B(8)	47.1(4)	B(11) -B(10) -B(12)	58.9(7)
P(1) -Pt(3) - P(2)	95.05(9)	C(2) -B(11) - B(6)	62.5(7)
Pt(3) - C(1) - C(2)	62.1(5)	C(2) -B(11) - B(7)	61.6(7)
Pt(3) - C(1) - B(4)	60.9(5)	B(6) -B(11) -B(10)	58.6(7)
Pt(3) - C(1) -C(101)	106.4(6)	B(7) -B(11) -B(12)	60.2(7)
C(2) - C(1) - B(6)	66.3(7)	B(10) -B(11) -B(12)	60.8(7)
C(2) - C(1) -C(101)	120.0(8)	B(7) -B(12) - B(8)	61.6(7)
B(4) - C(1) - B(5)	64.5(7)	B(7) -B(12) -B(11)	59.4(7)
B(4) - C(1) -C(101)	120.9(8)	B(8) -B(12) - B(9)	59.6(7)
B(5) - C(1) - B(6)	62.7(7)	B(9) -B(12) -B(10)	61.0(7)
B(5) - C(1) -C(101)	121.3(8)	B(10) -B(12) -B(11)	60.2(7)
B(6) - C(1) -C(101)	117.7(8)	C(1) -C(101)-C(102)	119.2(9)
Pt(3) - C(2) - C(1)	80.6(5)	C(1) -C(101)-C(106)	123.0(9)
Pt(3) - C(2) - B(7)	65.5(5)	C(102)-C(101)-C(106)	117.7(9)
C(1) - C(2) - B(6)	59.0(6)	C(101)-C(102)-C(103)	118.9(10)
B(6) - C(2) -B(11)	60.8(7)	C(102)-C(103)-C(104)	120.9(12)
B(7) - C(2) -B(11)	60.6(7)	C(103)-C(104)-C(105)	121.2(13)
Pt(3) - B(4) - C(1)	78.9(5)	C(104)-C(105)-C(106)	119.4(12)
Pt(3) - B(4) - B(8)	64.2(5)	C(101)-C(106)-C(105)	121.8(10)
C(1) - B(4) - B(5)	57.0(6)	Pt(3) - P(1) -C(111)	118.0(3)
B(5) - B(4) - B(9)	58.6(7)	Pt(3) - P(1) -C(121)	112.3(4)

B(8)	- B(4) - B(9)	58.2(7)	Pt(3)	- P(1) -C(131)	115.8(4)
C(1)	- B(5) - B(4)	58.5(6)	C(111)	- P(1) -C(121)	102.6(5)
C(1)	- B(5) - B(6)	58.5(7)	C(111)	- P(1) -C(131)	105.2(5)
B(4)	- B(5) - B(9)	59.9(7)	C(121)	- P(1) -C(131)	100.8(5)
B(6)	- B(5) -B(10)	59.2(7)	P(1)	-C(111)-C(112)	117.6(8)
B(9)	- B(5) -B(10)	61.9(7)	P(1)	-C(111)-C(116)	123.9(8)
C(1)	- B(6) - C(2)	54.7(6)	C(112)	-C(111)-C(116)	118.4(10)
C(1)	- B(6) - B(5)	58.8(7)	C(111)	-C(112)-C(113)	121.1(10)
C(2)	- B(6) -B(11)	56.7(7)	C(112)	-C(113)-C(114)	119.1(11)
B(5)	- B(6) -B(10)	60.8(7)	C(113)	-C(114)-C(115)	120.4(12)
B(10)	- B(6) -B(11)	61.2(7)	C(114)	-C(115)-C(116)	120.4(11)
Pt(3)	- B(7) - C(2)	69.6(5)	C(111)	-C(116)-C(115)	120.6(10)
Pt(3)	- B(7) - B(8)	66.0(5)	Pt(3)	- P(2) -C(211)	119.7(3)
C(2)	- B(7) -B(11)	57.8(7)	Pt(3)	- P(2) -C(221)	112.3(4)
B(8)	- B(7) -B(12)	59.5(7)	Pt(3)	- P(2) -C(231)	115.2(4)
B(11)	- B(7) -B(12)	60.4(7)	C(211)	- P(2) -C(221)	105.5(5)
Pt(3)	- B(8) - B(4)	68.4(5)	C(211)	- P(2) -C(231)	101.9(5)
Pt(3)	- B(8) - B(7)	67.0(5)	C(221)	- P(2) -C(231)	99.8(5)
B(4)	- B(8) - B(9)	59.4(7)	P(2)	-C(211)-C(216)	116.7(8)
B(7)	- B(8) -B(12)	59.0(7)	P(2)	-C(211)-C(212)	123.2(8)
B(9)	- B(8) -B(12)	60.7(7)	C(216)	-C(211)-C(212)	120.1(10)
B(4)	- B(9) - B(5)	61.6(7)	C(211)	-C(216)-C(215)	119.0(12)
B(4)	- B(9) - B(8)	62.4(7)	C(216)	-C(215)-C(214)	119.1(13)
B(5)	- B(9) -B(10)	59.2(7)	C(215)	-C(214)-C(213)	120.4(14)
B(8)	- B(9) -B(12)	59.7(7)	C(214)	-C(213)-C(212)	120.0(13)
B(10)	- B(9) -B(12)	59.8(7)	C(211)	-C(212)-C(213)	121.3(11)

The platinum atom and the carbaborane cage define a highly distorted icosahedron. The nature of the distortions are: 1) a lateral slippage of the Pt fragment with respect to the centroid of the B_5 belt; 2) a folding of the C_2B_3 face; and 3) a small slippage of the C_2B_3 face over the B_5 belt. These are discussed below (see also section 1.4).

1) Pt fragment slippage.

This is denoted by Δ and was described in section 1.4. For **1**, Δ= +0.39Å. This is of similar magnitude to the reported values of Δ for 3,3-$(PEt_3)_2$-3,1,2-$PtC_2B_9H_{11}$[27] and for the two crystallographically independent molecules of 3,3-$(PMe_2Ph)_2$-3,1,2-$PtC(CH_2OCH_3)C(H)B_9H_9$ in the asymmetric fraction of the unit cell[69] (see table 2.4). The direction of this slippage (σ) is at an angle to the vector joining B(8) and the mid-point of the C(1)-C(2) bond, of 35.7°. Two other examples

of slip angles are included in table 2.4.

2) Folding of the C_2B_3 face.

A folding of the C(1),C(2),B(4),B(7),B(8) face, about an axis approximately through C(2) and B(4) is observed. This results in folding angles of 7.25° and 2.76° and a relative movement of C(1),B(7) and B(8) towards the B_5 belt. Usually this type of folding occurs about an axis through B(4) and B(7) and θ and ϕ are defined for this instance (see section 1.4). However, in this case θ is defined as the angle between the plane passing through C(2), B(4), B(7) and B(8) and that through the B_5 belt (*i.e.* 2.76°). ϕ is defined as the angle between the plane through C(1), C(2) and B(4) and that through the B_5 belt (*i.e.* 7.25°). Some other examples of θ and ϕ are shown in table 2.4.

3) Slippage of the C_2B_3 face.

A small slippage (denoted by Q) of the C(1), C(2), B(4), B(7), B(8) face, with respect to the lower (B_5) belt was observed. Its magnitude (0.09Å) is comparable to that observed in some other complexes (see table 2.4). The slippage is in the same direction as the Pt slippage and leads to a slight over-estimate of Δ.

Table 2.4. Distortion Parameters.

Complex	Δ/Å	σ/°	Q/Å	θ/°	ϕ/°	Av.χ/°
(P)	0.42	-	0.1	4.7	4.4	21
(A)	0.414	52.1	0.12	2.29	8.34	25.1
(B)	0.441	61.6	0.11	2.96	8.32	22.6
1	0.388	35.7	0.09	2.76	7.25	21.1

(P) is 3,3-$(PEt_3)_2$-3,1,2-$PtC_2B_9H_{11}$.
(A) and (B) represent the two crystallographically independent molecules in the asymmetric portion of the unit cell of 1-(CH_2OCH_3)-3,3-$(PMe_2Ph)_2$-3,1,2-$PtC_2B_9H_{10}$.
Q= Lateral slippage of C_2B_3 belt w.r.t. centroid of B_5 face.

χ is the substituent elevation angle which, for a normal icosahedron, is found to be approximately 26°[27]. The elevation angles for the substituents bound to the C_2B_3 face of **1** have been calculated relative to the least squares plane through this belt. The individual angles are shown in table 2.5.

Table 2.5 Individual Substituent Elevation Angles for the C_2B_3 Face of 1.

Substituent	χ/°
Ph	27.3
H(2)	20.7
H(4)	20.9
H(7)	14.8
H(8)	21.9

The distorted nature of **1** is further reflected in the variation of the length of metal connectivities to the C_2B_3 face. The three Pt-B bond lengths are all fairly similar (Pt-B(4) = 2.313(12)Å, Pt-B(7) = 2.257(12)Å, Pt-B(8) = 2.239(12)Å). However, the Pt-C distances are longer, but with the Pt-C(2) distance of 2.326(10)Å considerably shorter than the Pt-C(1) distance of 2.596(10)Å. This last interaction, involving the phenyl- substituted carbon atom, is virtually non-bonding.

The C(1)-C(2) bond length in **1** of 1.594(14)Å is significantly longer than that found in the unsubstituted $(PEt_3)_2PtC_2B_9H_{11}$ (1.529(10)Å)[27]. It is well documented that going from a *closo*- to a *nido*- structure causes a reduction in the C-C bond length. For example[70], in 1-(CH_2OCH_3)-*closo*-1,2-$C_2B_{10}H_{11}$ the C-C bond lengths are found to be 1.636(9)Å and 1.649(8)Å for the two crystallographically independent molecules in the asymmetric fraction of the unit cell. These are significantly longer than that observed in the mono-anionic [7-(CH_2OCH_3)-*nido*-7,8-$C_2B_9H_{11}$]$^-$, which is found to be 1.544(6)Å. Hence, it can be suggested that in P_2Pt-carbaborane complexes, the greater the slippage of the metal fragment over the C_2B_3 face the more the structure will resemble a *nido*- rather than a *closo*- one and the shorter the C-C bond length will be. Thus the smaller slippage in **1** compared to that observed in

the unsubstituted analogue can help to rationalise the longer C-C bond length observed in the former case. This principle is further demonstrated in the mono-ether substituted complex $(PMe_2Ph)_2PtC_2B_9H_{10}(CH_2OCH_3)$[69]. The C-C bond lengths in the 2 forms are 1.550(12)Å and 1.527(12)Å, the longer of the two being that in the less slipped structure, molecule A (Δ= 0.414Å compared to 0.441Å).

Another point to note about **1** is that the phenyl ring attached to C(1) is twisted, with the side of the ring adjacent to C(2) below C(1) and the other side (adjacent to B(4)) above C(1). The twist angle has been calculated to be 38.9° (away from parallel to the cage C-C bond), giving rise to a θ_{phenyl} value of 51.1°. This latter figure can be compared with the predicted value of 90° (see section 1.4). There appears to be an interaction between this phenyl group and a hydrogen atom on one of the phosphino-phenyl rings. This proton (H(112)) points towards the centre of the cage-phenyl ring 2.72Å away. This is less than the sum of the van der Waals radius of a hydrogen atom plus the half thickness of a phenyl ring (= 1.2Å + 1.85Å[64]). The twist described above may be such as to maximise this favourable interaction (see figure 2.2). In the observed conformation, the two phenyl rings are almost orthogonal to each other, the calculated angle between the two being 88.4°. A similar type of interaction has been observed[71] in the complex $C_2H_2B_{10}Cl_{10}$....PPh_3O, in which the acidic cage C-H proton points towards the centre of one of the phosphine-oxide phenyl groups.

The two phosphino-phenyl rings in **1** are aligned almost graphitically but twisted 10.52°, relative to each other. The two centres of gravity are 3.66Å apart, which can be compared to twice the half thickness of a phenyl ring which is estimated to be (2 x 1.85Å = 3.70Å[64]).

Figure 2.2 **Alternative View of 1.**

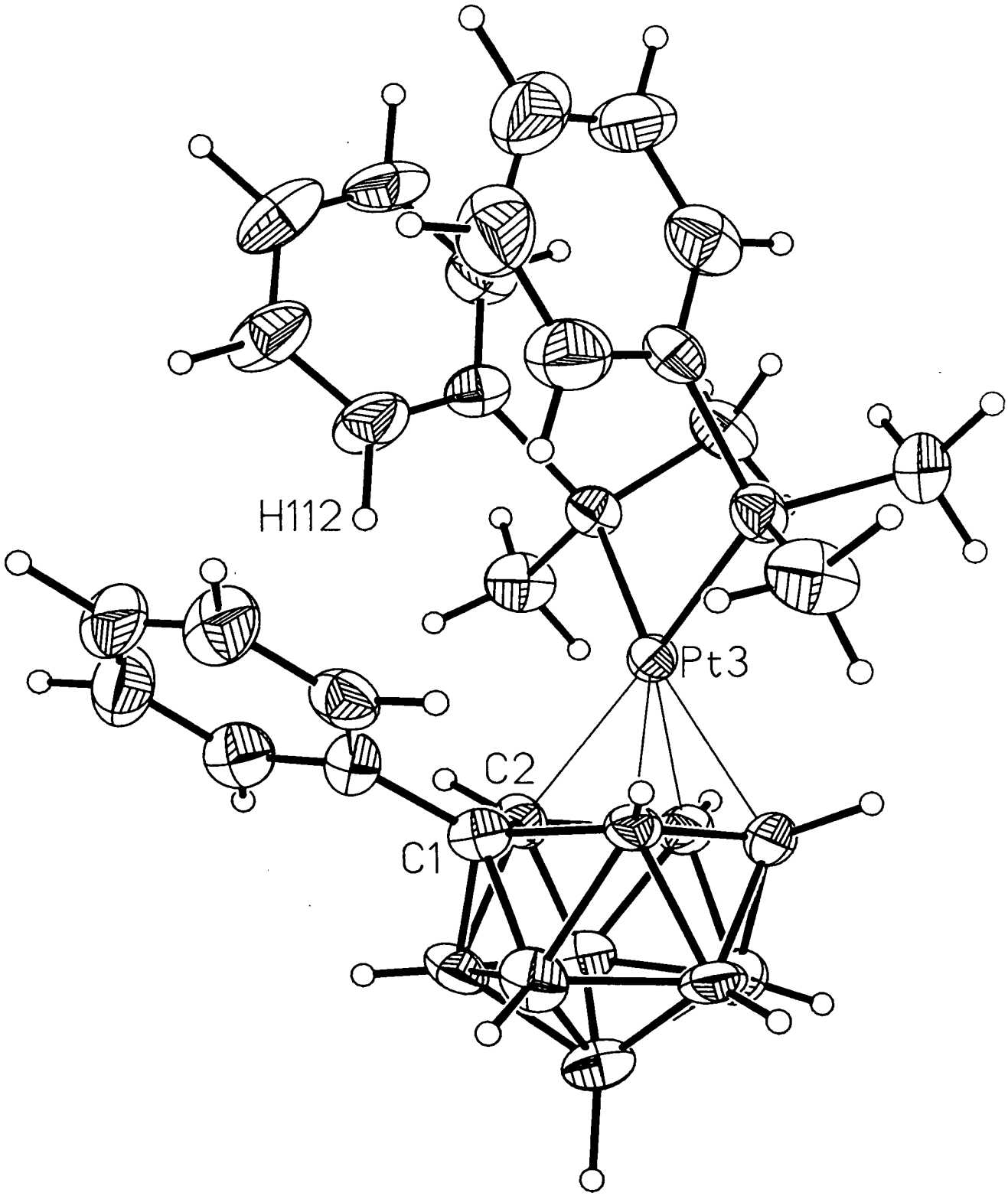

The packing of **1** in the unit cell is shown in figure 2.3. It can be noted that the phosphino-phenyl groups in distinct molecules appear to be aligned in a channel although they are not close enough to be considered graphitically packed.

Figure 2.3

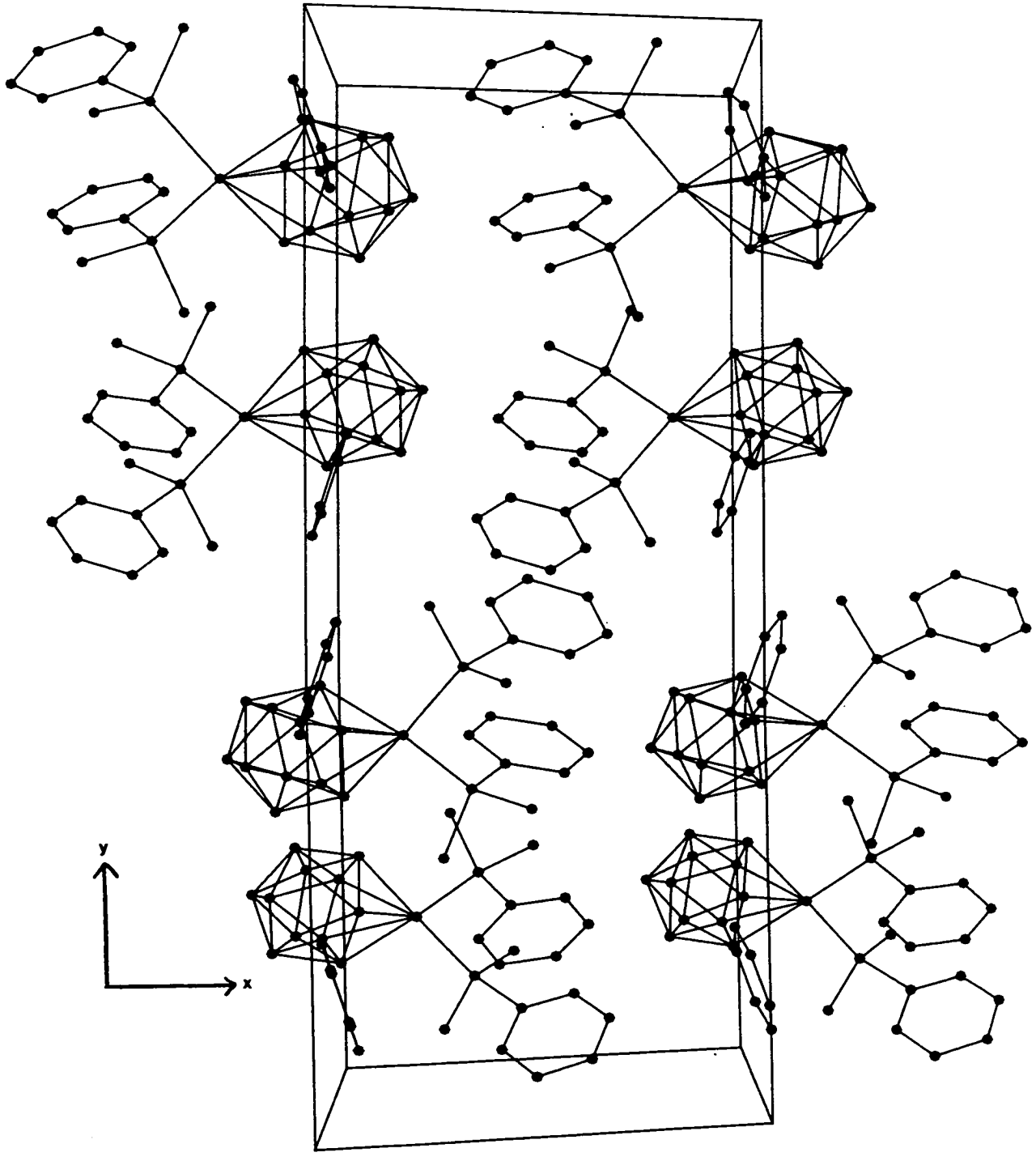

The geometry at the platinum centre can be considered to be *pseudo-* square planar, with a P-Pt-P angle of 95.05(9)°, similar to that observed in other platinum bis-phosphine carbaborane complexes [27,69].

The predicted conformation of ML_2 fragments with respect to (carba)borane *nido-* faces was discussed previously (section 1.4). To recap, when the carbaborane has two carbon atoms adjacent on the *nido*-face, the plane through the metal fragment is expected to lie perpendicular to the idealised cage mirror plane. In **1**, this angle is found to be 52.8°(*i.e.* the plane through the metal fragment is rotated 37.2° away from its predicted position).

A small rotation of the P_2Pt plane (of 13.9°) was observed in $(PEt_3)_2PtC_2B_9H_{11}$[27]. Similarly, for 1,1-$(PMe_2Ph)_2$-2,4-Me_2-1,2,4-$PtC_2B_9H_9$[72], where the carbons are non-adjacent on the metal-bonded face, the PtP_2 fragment is rotated by 10.1° from its predicted conformation, in which the PtP_2 plane would be parallel to the cage mirror plane. In both these examples, this rotation was believed to result from alleviation of unfavourable intra-molecular contacts involving the alkyl-phosphine hydrogen atoms and the hydrogen atoms on the C_2B_3 face. However, in the case of **1**, the observed rotation is clearly more significant. Whereas a rotation of approximately 10° would cost little energetically, a rotation of 37° would require much more than 4 times this energy.

The preferred orientations of ML_2 fragments described were calculated for unsubstituted carbaboranes (see section 1.4). It would be expected that in symmetrically di-substituted carbaboranes, the same conformation of the ML_2 fragment would be preferred. However, there is some evidence to suggest that asymmetric (or mono) substitution alters the preferred orientation. In the case of the mono-ether substituted complex 1-(CH_2OCH_3)-3,3-$(PMe_2Ph)_2$-3,1,2-$PtC_2B_9H_{10}$[69], E.H.M.O. calculations indicated that the lowest energy conformation has the ML_2

fragment aligned along an axis through B(4) and between B(7) and C(2). This conformation was observed in the crystal structure (see figure 2.4).

Figure 2.4

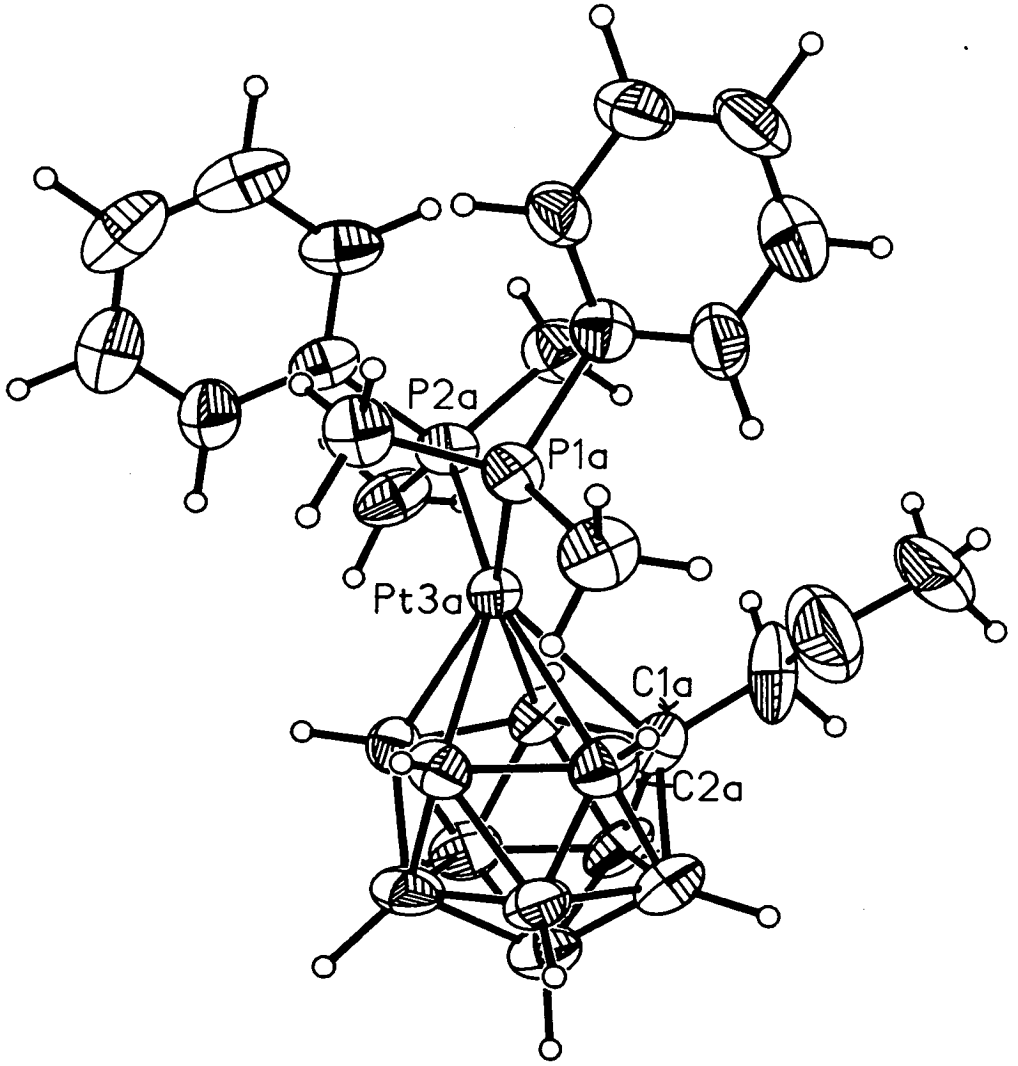

To investigate if a similar change in preferred ML_2 conformation could be predicted for **1**, an E.H.M.O. calculation was performed, considering the di-anionic carbaborane moiety $[C_2B_9H_{10}Ph]^{2-}$ (See Chapter 5). The homo, which is concentrated on the C_2B_3 face, is depicted in figure 2.5. The homo in the dianion is equivalent to the lumo in the neutral species.

In the ligand h.o.m.o. the nodal plane passes through B(8) and the mid-point of the C(1) - C(2) bond. This is identical to that previously reported for the unsubstituted carbaborane and was confirmed by a similar E.H.M.O. calculation for the unsubstituted $[C_2B_9H_{11}]^{2-}$ dianion, using the same model (see figure 2.5). It can be concluded, then, that phenyl substitution does not alter the characteristics of the frontier molecular orbitals of a *nido*-C_2B_9 ligand. On this basis, a perpendicular orientation of the $\{P_2Pt\}$ fragment with respect to the nodal plane is predicted. In **1** the observed rotation of the metal fragment will result in less efficient overlap of metal-fragment h.o.m.o.-ligand l.u.m.o. Hence, **1** can be considered ground-state destabilised, relative to its unsubstituted carbaborane analogue. This rotation of the plane of the metal fragment results from the steric influence of the cage-phenyl substituent.

Figure 2.5 **HOMOs of $C_2B_9H_{10}Ph^{2-}$ and $C_2B_9H_{11}^{2-}$.**

(HOMO of dianion equivalent to LUMO on neutral species)

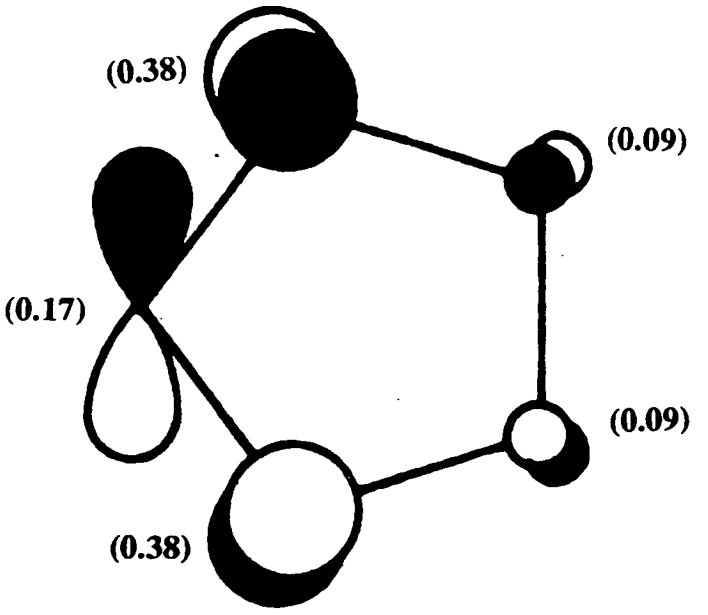

$(C_2B_9H_{11})^{2-}$

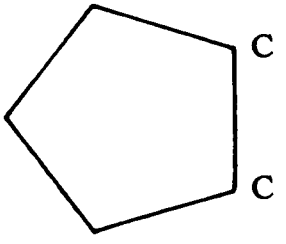

(Reduced Charge Matrix)

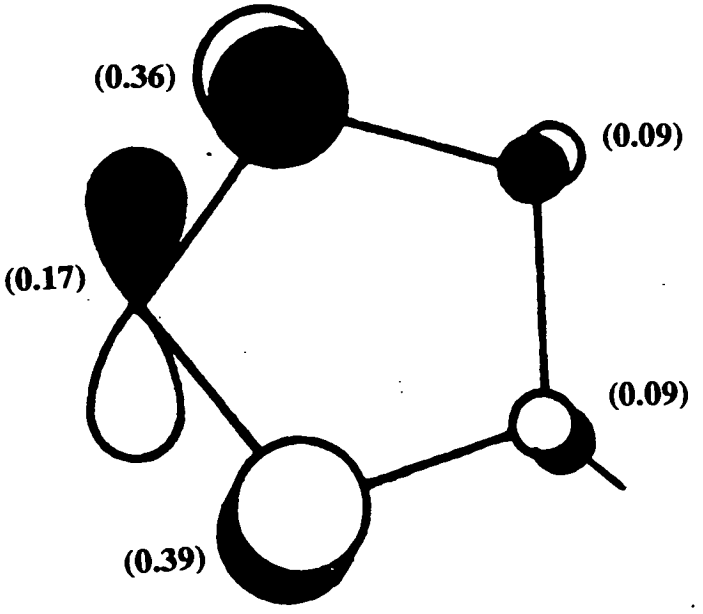

$(C_2B_9H_{10}Ph)^{2-}$

2.4 An N.M.R. Study of 1.

The room temperature $^{11}B\{^1H\}$ n.m.r. spectrum of **1** was recorded in $CDCl_3$ and is shown in figure 2.6. The high frequency signal (at δ= +11.01p.p.m.), corresponding to one boron atom, shows platinum-boron coupling ($^1J^{195}Pt$-B = 225Hz.) and can tentatively be assigned as being due to B(8), which has been noted to give rise to a relatively high frequency shift in a range of slipped carbametallaboranes[60]. The extent of shift of this signal has been related to the magnitude of the slippage of the metal atom over the carbaborane face, and is considered in Chapter 3.

There are a further 6 boron resonances observed in the spectrum, at δ(p.p.m.)= -2.46, -4.36, -7.01, -14.82, -18.51 and -20.35, in the ratio 1:1:1:3:1:1. However, low solubility in the solvent and poor resolution of the spectrum prevent any further assignments being made. In the proton coupled spectrum, all the signals are doublets (with ^{1}JB-H = 120-170Hz.), indicating that all boron atoms are bound to a terminal hydrogen atom.

The ^{1}H n.m.r. spectrum of **1** is complex. The main features are a signal denoting the cage C-H at 3.60p.p.m., methyl protons at *circa* 1.71 p.p.m and phenyl protons at 7.20 and 7.50p.p.m. The last 3 of these resonances are broad, complex multiplets. The methyl protons on one phosphine moiety are magnetically inequivalent to those in the other phosphine group, irrespective of the rate of rotation of the metal-fragment, due to a given proton coupling to one phosphorus atom by a different magnitude than it couples to the second. In this case, the long range (^{4}JPH) coupling is believed to be zero (as the proton spectrum of the *cis*-$PtCl_2(PMe_2Ph)_2$ [73] only exhibits a ^{2}JPH coupling and hence the methyl protons are all equivalent, on the n.m.r. timescale). In **1**, however, the $\{Pt(PMe_2Ph)_2\}$ moiety lies above an asymmetric carbaborane face and hence the two methyl groups are inequivalent,

Figure 2.6

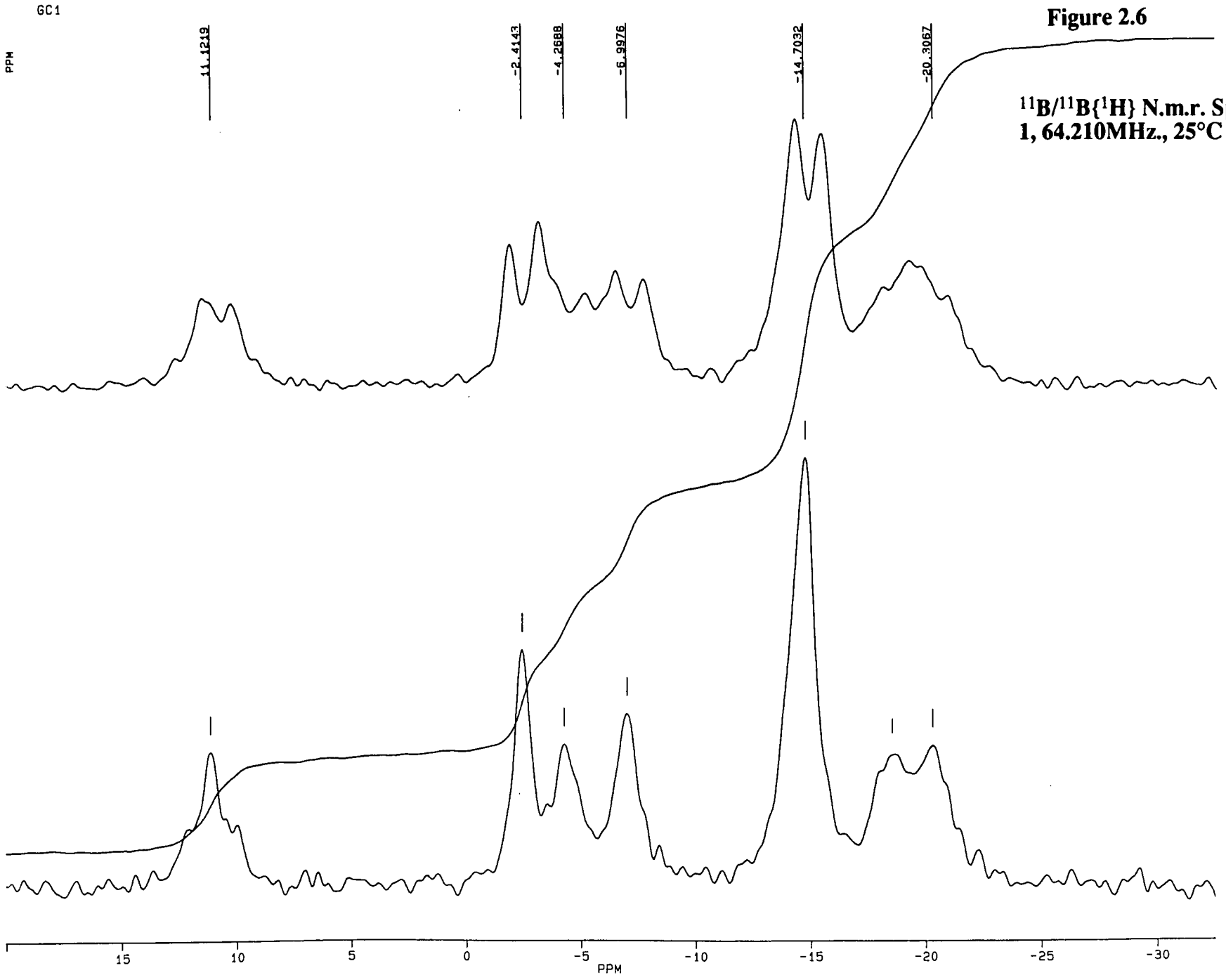

$^{11}B/^{11}B\{^{1}H\}$ N.m.r. Spectra of 1, 64.210MHz., 25°C (298K).

unless there is rapid rotation about the Pt-cage bonding, on the n.m.r. timescale. This inequivalence is the origin of the observed second order pattern.

The $^{31}P\{^{1}H\}$ spectrum consists of a singlet (δ= -12.08p.p.m.), with doublet satellites ($^{1}J^{195}Pt\text{-}P$ = 3227Hz) (see figure 2.7). However, the satellite peaks are considerably broader than the central resonance. This broadening cannot be explained by exchange processes (either inter- or intra- molecular), as such processes would render all three signals equally broad.

Although the central resonance appears as a singlet, it could actually consist of two different phosphorus signals if the chemical shifts of the two nuclei were co-incident, or were similar enough to become averaged. The presence of two different phosphorus environments would be expected if there was hindered rotation about the platinum- cage bonding within a single compound, due to the asymmetric nature of the C_2B_3 face, or if there were two distinct carba-platinaborane complexes present. To clarify this, a variable temperature $^{31}P\{^{1}H\}$ n.m.r. study was undertaken.

At -60°C (213K) in $CDCl_3$, the broad satellites split into two sets and are slightly sharper (see figure 2.8). The major peak tends towards an AB signal, although this is not fully resolved. This implies that there are two phosphorus environments within a single molecule, at this temperature. In the related complex, $1\text{-}(CH_2OCH_3)\text{-}3,3\text{-}(PMe_2Ph)_2\text{-}3,1,2\text{-}PtC_2B_9H_{10}$[69], at room temperature, one phosphorus resonance, with two sets of ^{195}Pt satellites, is observed, in CD_2Cl_2. At -66°C (207K), a fully resolved AB pattern is seen.

Cooling a sample of **1** led to an arrestment of rotation about the Pt- cage bonding, so it would be predicted that warming the sample would facilitate this rotation. The $^{31}P\{^{1}H\}$ n.m.r. spectrum of **1**, at +55°C (328K) shows the expected sharpening of the three signals (see figure 2.9). The singlet occurs at δ = -11.98 p.p.m. with $^{1}J^{195}Pt\text{-}P$ = 3316Hz.

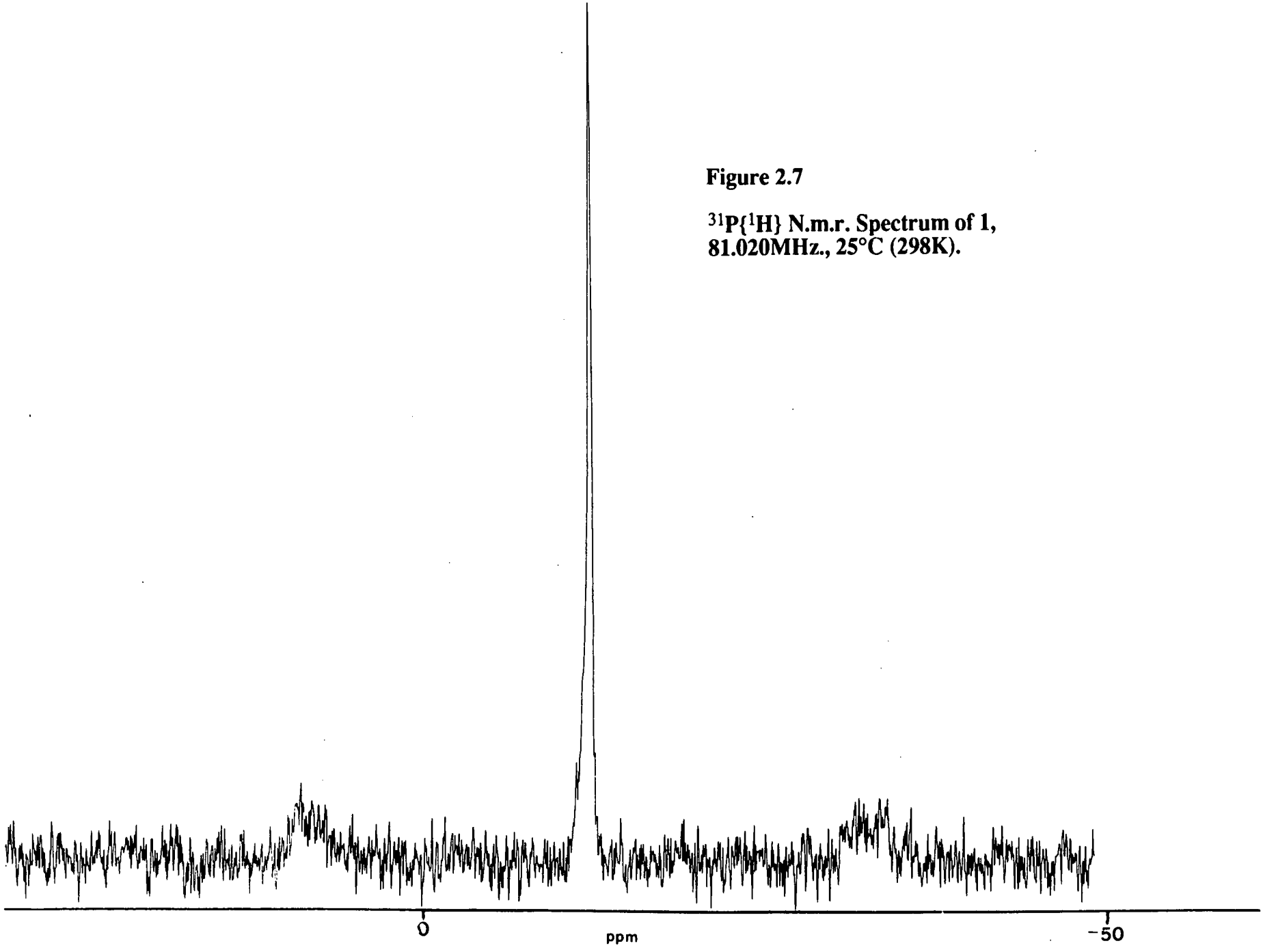

Figure 2.7

$^{31}P\{^{1}H\}$ N.m.r. Spectrum of 1, 81.020MHz., 25°C (298K).

Figure 2.8

$^{31}P\{^{1}H\}$ N.m.r. Spectrum of 1, 81.020MHz., -60°C (213K).

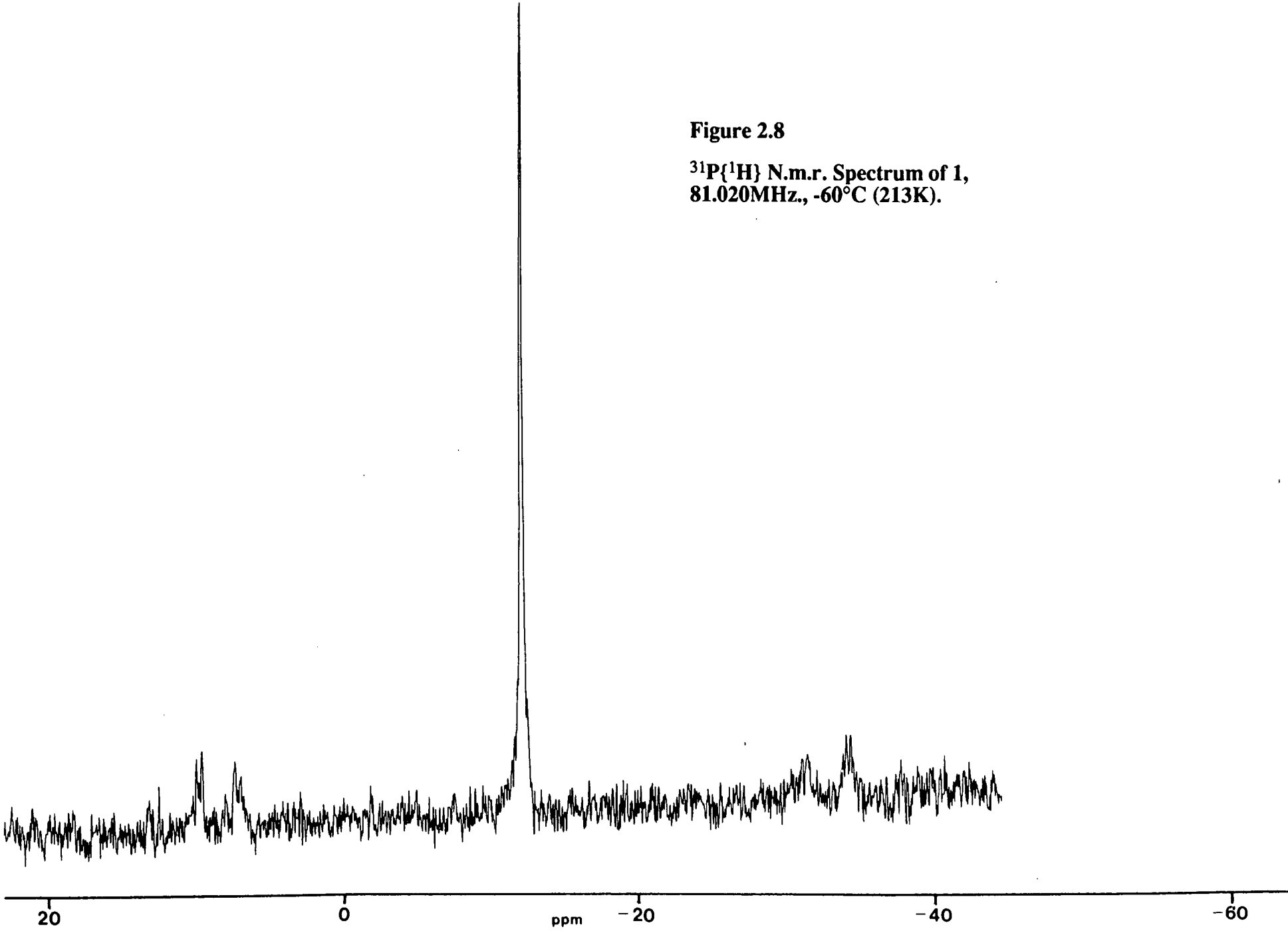

Figure 2.9

$^{31}P\{^{1}H\}$ N.m.r. Spectrum of 1, 81.020MHz.,+55°C (328K).

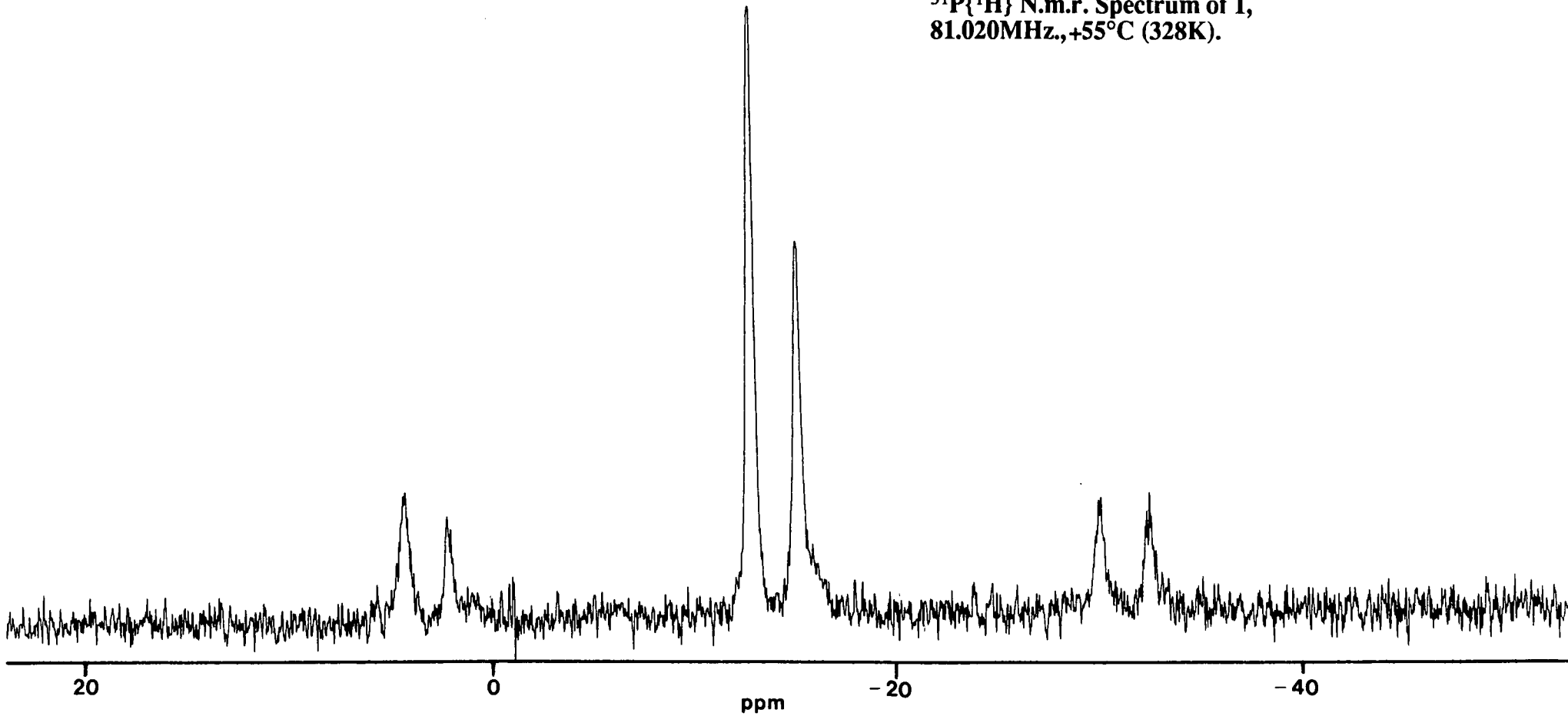

However, another set of peaks is also present (singlet at δ= -14.69 p.p.m. with doublet satellites $^{1}J^{195}Pt\text{-}P$= 3350Hz.). After prolonged warming at this temperature, the signal due to **1** has disappeared while that corresponding to the new species has intensified (see figure 2.10). In fact, there are two new species present, in the approximate ratio 4:1. The major thermolysis product, **2**, resonates at -14.47 p.p.m. with doublet satellites ($^{1}J^{195}Pt\text{-}P$= 3327Hz.), and a similar pattern is observed for the minor product, **3** (singlet -15.30p.p.m., $^{1}J^{195}Pt\text{-}P$= 3228Hz.). Moreover, during warming, the solution changed colour from deep to pale yellow.

A variable temperature $^{31}P\{^{1}H\}$ n.m.r. study of a mixture of **2** and **3** was carried out. At -60°C (213K), the spectrum consists of a singlet, denoting **3** (at δ= -14.83 p.p.m.) with doublet satellites ($^{1}J^{195}Pt\text{-}P$= 3220Hz.), and a fully resolved AB pattern due to **2**, and its doublet satellites (see figure 2.11). The calculated parameters[74] for this system are δP_1= -13.76 p.p.m., δP_2= -14.14 p.p.m., $^{1}J^{195}Pt\text{-}P_1$= 3313.8Hz, $^{1}J^{195}Pt\text{-}P_2$= 3309.2Hz. and $^{2}JP_1\text{-}P_2$ =27.9 Hz. The appearance of this pattern indicates that at low temperature, there is hindered rotation about the platinum- cage bonding, in **2**.

Figure 2.10

$^{31}P\{^{1}H\}$ N.m.r. Spectrum of 2 and 3, 81.020MHz., 25° (298K).

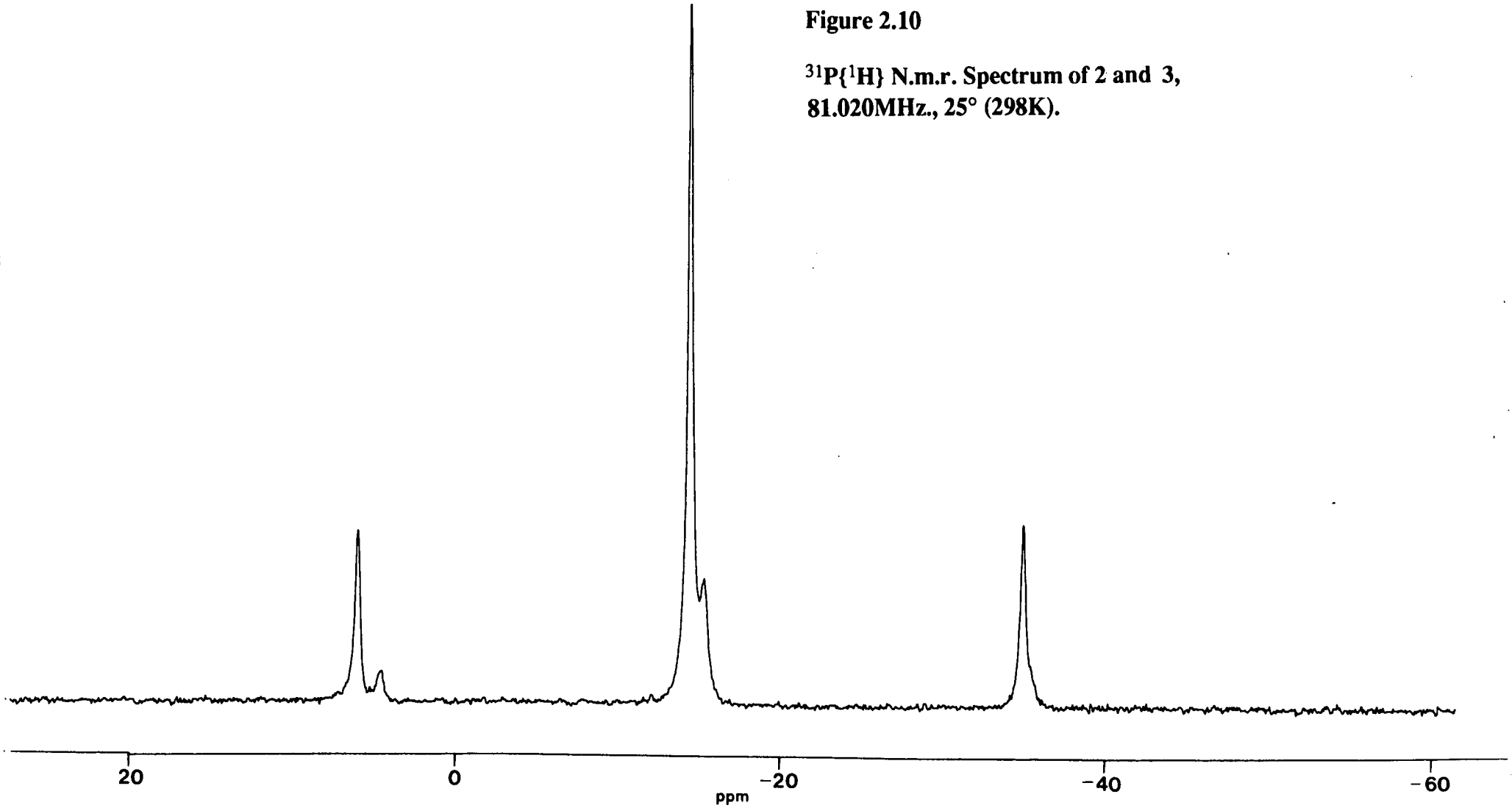

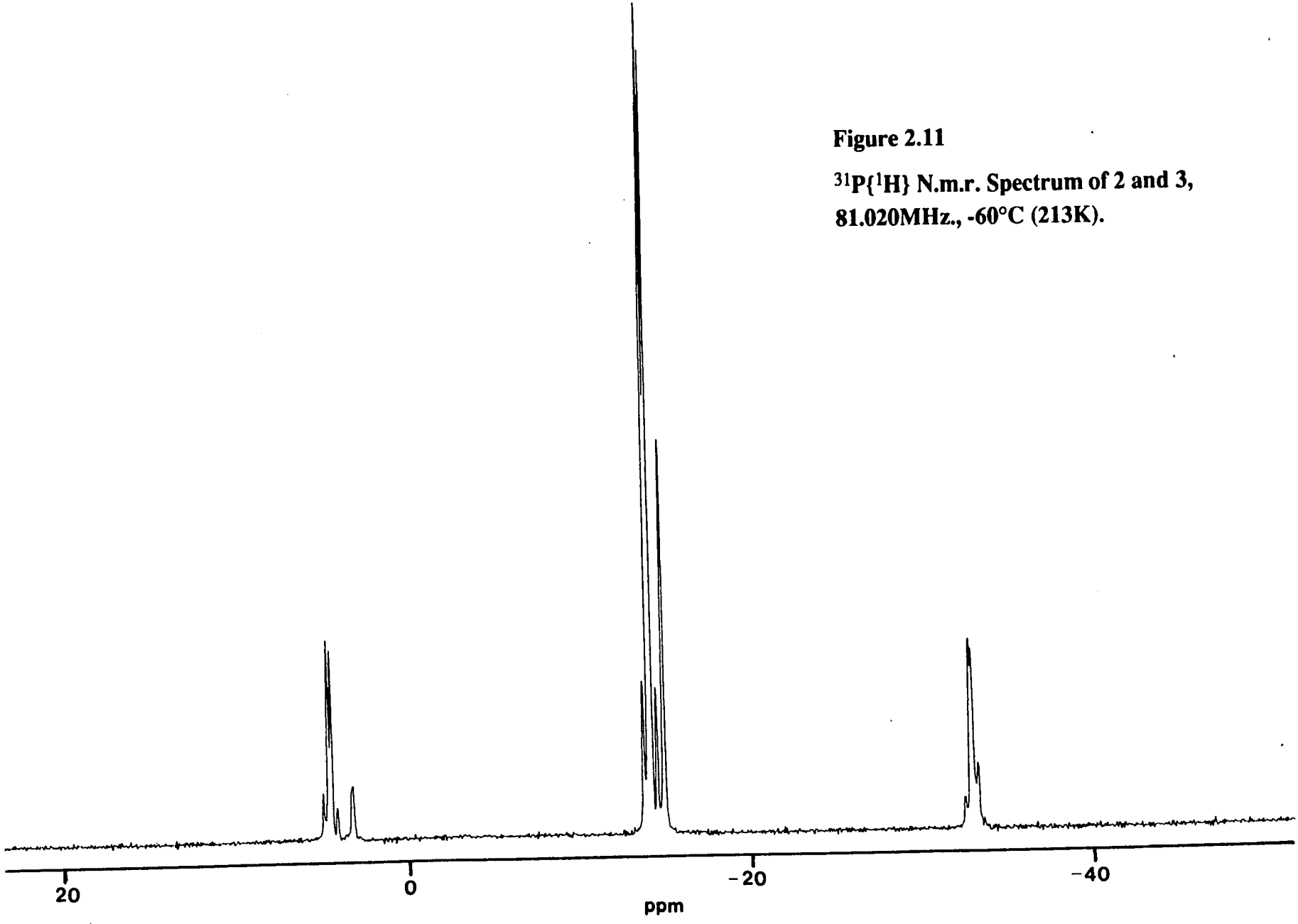

Figure 2.11

$^{31}P\{^{1}H\}$ N.m.r. Spectrum of 2 and 3, 81.020MHz., -60°C (213K).

2.5 Identification of the Thermolysis Products of 1.

The identities of 2 and 3 were established by comparing their spectroscopic data with those obtained by Mingos *et al*[66], for the products of an analogous reaction. Using a microwave technique which was developed by this group, the reaction between cis-$PtCl_2(PMe_2Ph)_2$ and the mono-anionic carbaborane $[C_2B_9H_{11}Ph][NHMe_3]$ had been studied. These reagents were placed in a sealed vessel, in the presence of $NHMe_2$, and exposed to micro-wave radiation (2540MHz., 500W) for 30 minutes, in 10 atmospheres of ethanol. During the reaction, the temperature was believed not to have exceeded 200°C. Two yellow, isomeric carba-platinaboranes were produced, which were separated by two stage preparative t.l.c. They were characterised by n.m.r. spectroscopy and FAB mass spectrometry and a single crystal X-ray diffraction study of each was also carried out. It is interesting to note that when the same reagents were heated in ethanol, in a sealed Teflon vessel, but in the absence of microwave radiation, no reaction was observed[75], even after several days at reflux temperature.

The $^{31}P\{^1H\}$ n.m.r. spectrum of the first microwave-generated isomer consists of a singlet (δ= -15.43p.p.m.) with doublet satellites($^1J^{195}Pt$-P= 3327Hz.) and corresponds to 2. The $^{11}B\{^1H\}$ spectrum, in CD_2Cl_2, is a broad band within which 8 boron environments can be detected (in the ratio 1:2:1:1:1:1:1, δ(p.p.m.)= -8.9, -10.5, -12.4, -15.3, -16.8, -19.9 and -26.0. However, the high frequency boron resonance, observed in the spectrum of 1, is absent suggesting that 2 does not contain a C_2B_3 face. The crystal structure conclusively shows that the two cage carbons have moved apart, with the carbon bearing the phenyl substituent now occupying position 11 in the lower belt. Selected bond lengths are given in table 2.6. A perspective view of a single molecule is shown in figure 2.12.

Figure 2.12

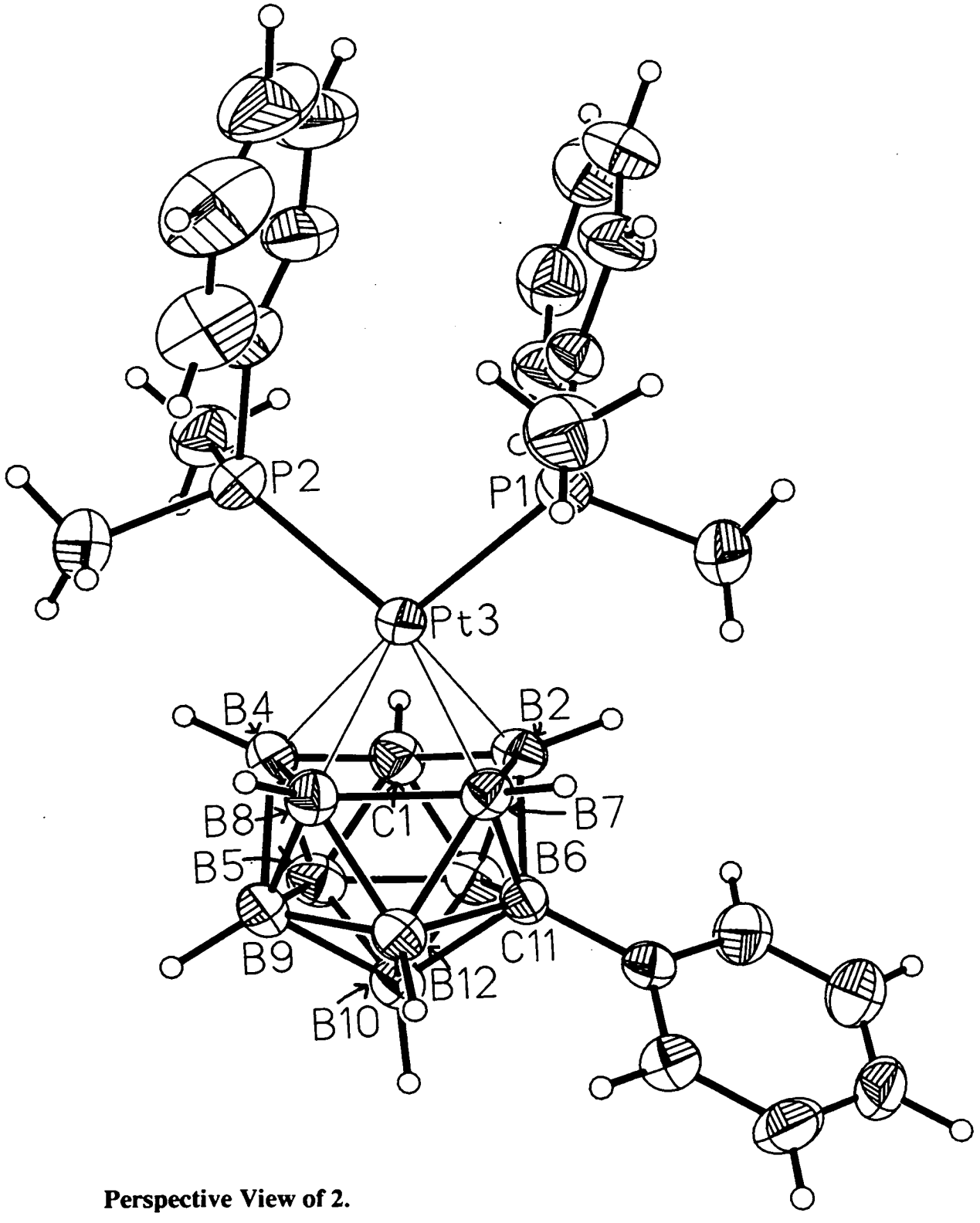

Perspective View of 2.

Table 2.6 Selected Bond Lengths, in 2, Å, with Standard Deviations.

Pt(3)	- P(2)	2.2864(14)	B(2)	-C(11)	1.756(8)
Pt(3)	- P(1)	2.2909(14)	B(4)	- B(5)	1.815(8)
Pt(3)	- C(1)	2.610(5)	B(4)	- B(8)	1.872(8)
Pt(3)	- B(2)	2.222(6)	B(4)	- B(9)	1.800(8)
Pt(3)	- B(4)	2.293(6)	B(5)	- B(6)	1.746(8)
Pt(3)	- B(7)	2.199(6)	B(5)	- B(9)	1.781(9)
Pt(3)	- B(8)	2.231(6)	B(5)	-B(10)	1.745(9)
P(2)	-C(211)	1.811(4)	B(6)	-B(10)	1.754(8)
P(2)	-C(221)	1.822(7)	B(6)	-C(11)	1.712(7)
P(2)	-C(231)	1.826(7)	B(7)	- B(8)	1.797(8)
P(1)	-C(111)	1.821(4)	B(7)	-C(11)	1.735(7)
P(1)	-C(121)	1.822(7)	B(7)	-B(12)	1.783(8)
P(1)	-C(131)	1.826(8)	B(8)	- B(9)	1.768(9)
C(1)	- B(2)	1.700(8)	B(8)	-B(12)	1.772(8)
C(1)	- B(4)	1.700(7)	B(9)	-B(10)	1.778(9)
C(1)	- B(5)	1.677(8)	B(9)	-B(12)	1.769(9)
C(1)	- B(6)	1.647(7)	B(10)	-C(11)	1.738(8)
C(1)	-C(101)	1.515(6)	B(10)	-B(12)	1.752(8)
B(2)	- B(6)	1.834(8)	C(11)	-B(12)	1.736(8)
B(2)	- B(7)	1.871(8)	C(11)	-C(201)	1.526(6)

The plane through the $\{PtP_2\}$ fragment lies at an angle of 80.8° to the idealised cage mirror plane (which passes through C(1), B(10) and B(12)). This is close to the predicted perpendicular alignment for an ML_2 fragment associated with a CB_4 *nido*-face.

The structure of **2** exhibits similar distortions to those observed in **1**. If the metal-cage bonding is considered, the four Pt-B distances are similar (Pt-B(2)= 2.233(5)Å, Pt-B(4)= 2.281(5)Å, Pt-B(7)= 2.211(4)Å and Pt-B(8)= 2.246(5)Å). However, the Pt-C interaction is virtually non-bonding (Pt-C(1)= 2.581(4)Å). The Pt atom is slipped away from the centre of the CB_4 face (Δ= 0.36Å). In this case the slippage is defined as being negative (*i.e.* away from the unique atom in the *nido*-face

[C(1)]). The direction of this slippage with respect to the vector linking the mid-point of the B(7)-B(8) bond with C(1) is 17.0°(= σ).

There is a small lateral slippage of the upper CB_4 face, of 0.08Å, over the lower belt.The metal-bonded face is folded about an axis through B(2) and B(4), giving rise to folding parameters of θ= 4.17° and ϕ= 11.88°. The average elevation angle for the substituents on the upper belt (χ) is 18.2°, indicating that the substituents are bent away from the metal. The geometry at the metal centre can be considered to be *pseudo*-square planar with a P-Pt-P angle of 97.70(4)°.

The $^{31}P\{^1H\}$ n.m.r. spectrum of the second microwave-generated isomer (CD_2Cl_2) consists of a singlet (δ = -15.37 p.p.m.) with doublet satellites ($^1J^{195}Pt\text{-}P$ = 3258Hz.). This corresponds to the observed spectrum of **3**. The $^{11}B\{^1H\}$ n.m.r. spectrum, in CD_2Cl_2, consists of a broad band within which 5 boron signals can be detected. These occur in the ratio 2:2:1:3:1 (δ(p.p.m.)= -7.7, -12.6, -16.5, -22.2 and -26.1). There is no high frequency boron resonance, indicating the absence of a C_2B_3 face.

This is confirmed by the crystal structure which shows that in this case the carbon atom bearing the hydrogen substituent has migrated to position 11 in the lower belt. A perspective view of a single molecule of **3** is shown in figure 2.13. Selected bond lengths are given in table 2.7.

The four platinum-boron connectivities are of similar lengths (Pt-B(2)= 2.237(8)Å, Pt-B(4)= 2.275(8)Å, Pt-B(7)= 2.211(9)Å and Pt-B(8)= 2.212(9)Å), while the platinum-C(1) interaction is virtually non-bonding (Pt-C(1)= 2.622(8)Å). The plane through the ML_2 fragment is almost orthogonal to the idealised cage mirror plane (PtP_2-{C(1)B(10)B(12)}= 87.1°).

Figure 2.13

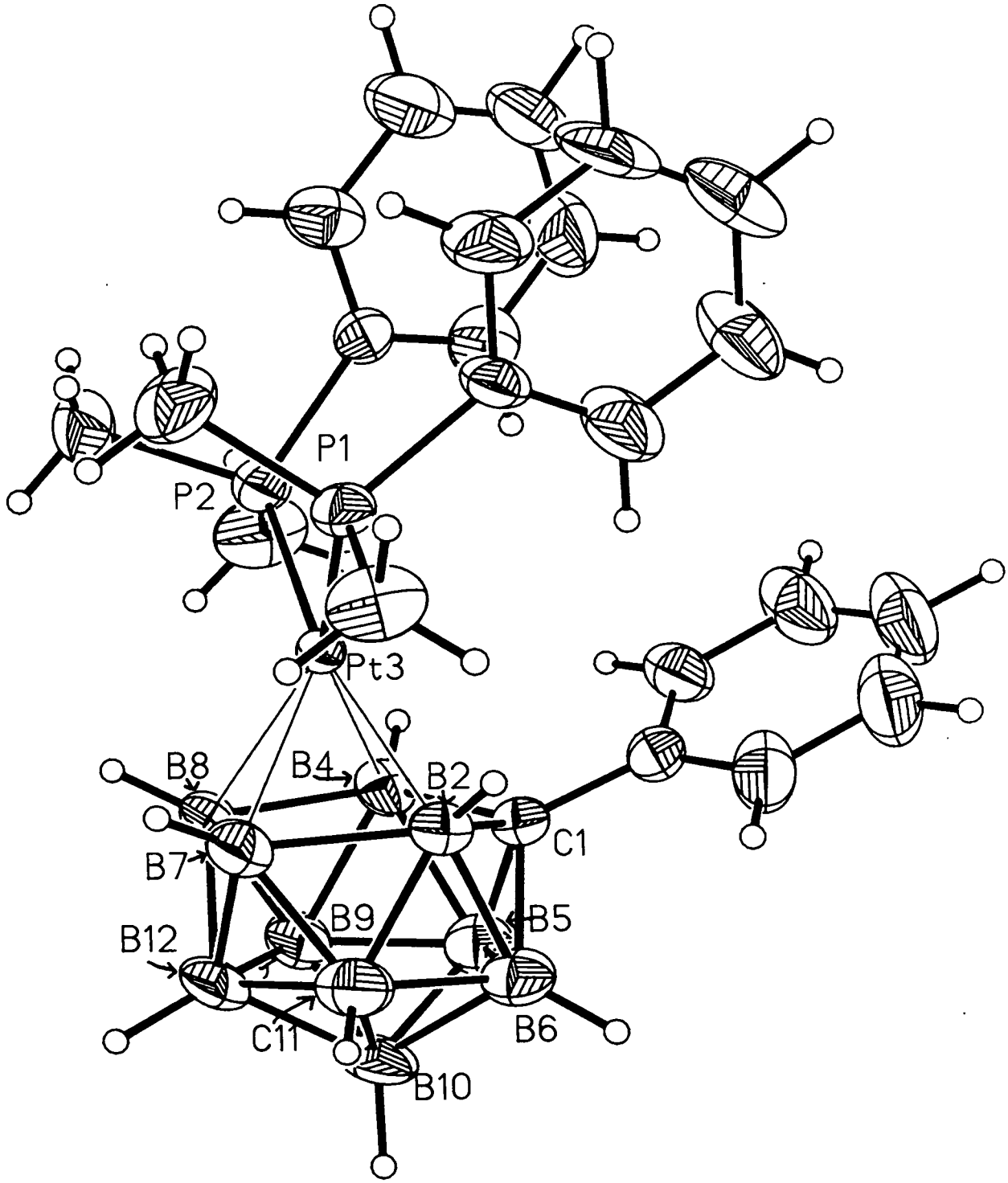

Perspective View of 3.

Table 2.7 Selected Bond Lengths in 3, Å, with Standard Deviations.

Pt(3)	- C(1)	2.622(8)	B(9)	-B(12)	1.766(14)
Pt(3)	- B(2)	2.237(8)	B(10)	-C(11)	1.742(14)
Pt(3)	- B(4)	2.275(8)	B(10)	-B(12)	1.764(14)
Pt(3)	- B(7)	2.211(9)	C(11)	-B(12)	1.727(14)
Pt(3)	- B(8)	2.212(9)	C(101)	-C(102)	1.405(13)
Pt(3)	- P(1)	2.2988(21)	C(101)	-C(106)	1.380(13)
Pt(3)	- P(2)	2.2963(22)	C(102)	-C(103)	1.408(16)
C(1)	- B(2)	1.700(11)	C(103)	-C(104)	1.377(18)
C(1)	- B(4)	1.704(11)	C(104)	-C(105)	1.400(17)
C(1)	- B(5)	1.684(12)	C(105)	-C(106)	1.396(15)
C(1)	- B(6)	1.665(12)	P(1)	-C(111)	1.821(8)
C(1)	-C(101)	1.494(11)	P(1)	-C(121)	1.827(9)
B(2)	- B(6)	1.836(13)	P(1)	-C(131)	1.816(10)
B(2)	- B(7)	1.866(13)	C(111)	-C(112)	1.374(13)
B(2)	-C(11)	1.730(12)	C(111)	-C(116)	1.389(12)
B(4)	- B(5)	1.838(12)	C(112)	-C(113)	1.388(15)
B(4)	- B(8)	1.882(12)	C(113)	-C(114)	1.382(16)
B(4)	- B(9)	1.798(12)	C(114)	-C(115)	1.372(16)
B(5)	- B(6)	1.767(13)	C(115)	-C(116)	1.377(15)
B(5)	- B(9)	1.770(13)	P(2)	-C(211)	1.825(9)
B(5)	-B(10)	1.760(14)	P(2)	-C(221)	1.820(11)
B(6)	-B(10)	1.763(14)	P(2)	-C(231)	1.816(11)
B(6)	-C(11)	1.705(13)	C(211)	-C(216)	1.378(15)
B(7)	- B(8)	1.821(13)	C(211)	-C(212)	1.376(13)
B(7)	-C(11)	1.700(13)	C(216)	-C(215)	1.383(17)
B(7)	-B(12)	1.770(14)	C(215)	-C(214)	1.358(17)
B(8)	- B(9)	1.767(13)	C(214)	-C(213)	1.375(16)
B(8)	-B(12)	1.762(13)	C(213)	-C(212)	1.396(15)
B(9)	-B(10)	1.770(14)			

The distortions exhibited in **3** are similar to those described for **1** and **2**. The Pt atom is slipped by 0.42Å away from the centroid of the CB_4 plane, towards the four boron atoms (negative Δ). The slip angle (σ) is 11.1°, while the upper belt is slipped by 0.09Å, from the centroid of the lower CB_4 belt. The metal-bonded face is folded about an axis through B(2) and B(4), giving rise to folding angles of 4.52° and 11.08°, for θ and ϕ, respectively. Unusually, the substituents on this face are not bent

away from the metal (average χ= 26.5°). The geometry at the metal centre is *pseudo*-square planar with a P-Pt-P angle of 95.82(8)°.

The cage phenyl ring shows a slight (37.9°) twist, similar to that observed in **1**, away from B(2). There appears to be an interaction between this ring and a proton on one of the phosphino-phenyl rings (H(112)), which is 2.80Å away from the centroid of the cage-phenyl ring. The least-squares planes through these phenyl rings are virtually orthogonal to each other (the calculated angle is 89.3°). The two phosphino-phenyl rings are aligned almost graphitically, with the centres of gravity of the two 3.71Å apart, but twisted slightly relative to each other (by 10.9°).

The molecular geometries of **1** and **3** are practically superimposable, even down to small details such as the orientations and interactions of the three phenyl groups and the phosphorus atom positions. In fact, they are crystallographically isomorphous, and differ only in the nature of the atom at position 2 in the cage (carbon in **1** and boron in **3**).

The r.m.s. misfit method[76] provides an empirical measure of the overall geometrical similarity between structurally similar groups. The best fit is found between the two sets of atomic co-ordinates so as to minimise $\Sigma\delta_i$, where δ_i is the distance between the corresponding members of an atom pair. The r.m.s. misfit between two sets of n atoms is then defined as the square root of $\Sigma(\delta_i)/n$. This typically gives a value of less than 1Å, for structurally similar groups. An r.m.s. misfit calculation was performed in which the whole molecules (less H atoms) **1** and **3** were compared and yielded a value of 0.09Å. **1** and **3** represent unusual examples of geometric isomers which are isomorphous. This suggests that the crystal packing is determined by hydrocarbon contacts, rather than by the alignment of molecular dipoles.

2.6 Alternative Methods of Thermolysis of 1

The isomerisation of **1** could also be effected by heating in toluene, at reflux temperature, for 30 minutes. **2** and **3** were again formed in the approximate ratio 4:1. However, when **1** is heated in decalin (decahydronaphthalene) at reflux temperature (circa. 200°C) **2** and **3** are produced in the approximate ratio 3:4. The $^{31}P\{^{1}H\}$n.m.r.spectrum of the products of decalin reflux of **1** are shown in figure 2.14 while the $^{11}B\{^{1}H\}$ n.m.r. spectrum is shown in figure 2.15 Hence, it appears that higher temperatures favour the formation of (3). This isomer may lie at the global energy minimum by virtue of having the cage carbons separated while also retaining the favourable interaction between a hydrogen atom bound to a phosphino-phenyl group and the cage-phenyl ring. A summary of the isomerisation of **1** is shown in figure 2.16.

Figure 2.16 Thermally Induced Isomerisation of 1.

$[1\text{-}Ph\text{-}3,3\text{-}(PMe_2Ph)_2\text{-}3,1,2\text{-}PtC_2B_9H_{10}]$

1

$\downarrow$ (Δ)

$[11\text{-}Ph\text{-}3,3\text{-}(PMe_2Ph)_2\text{-}3,1,11\text{-}PtC_2B_9H_{10}]$

2

+

$[1\text{-}Ph\text{-}3,3\text{-}(PMe_2Ph)_2\text{-}3,1,11\text{-}PtC_2B_9H_{10}]$

3

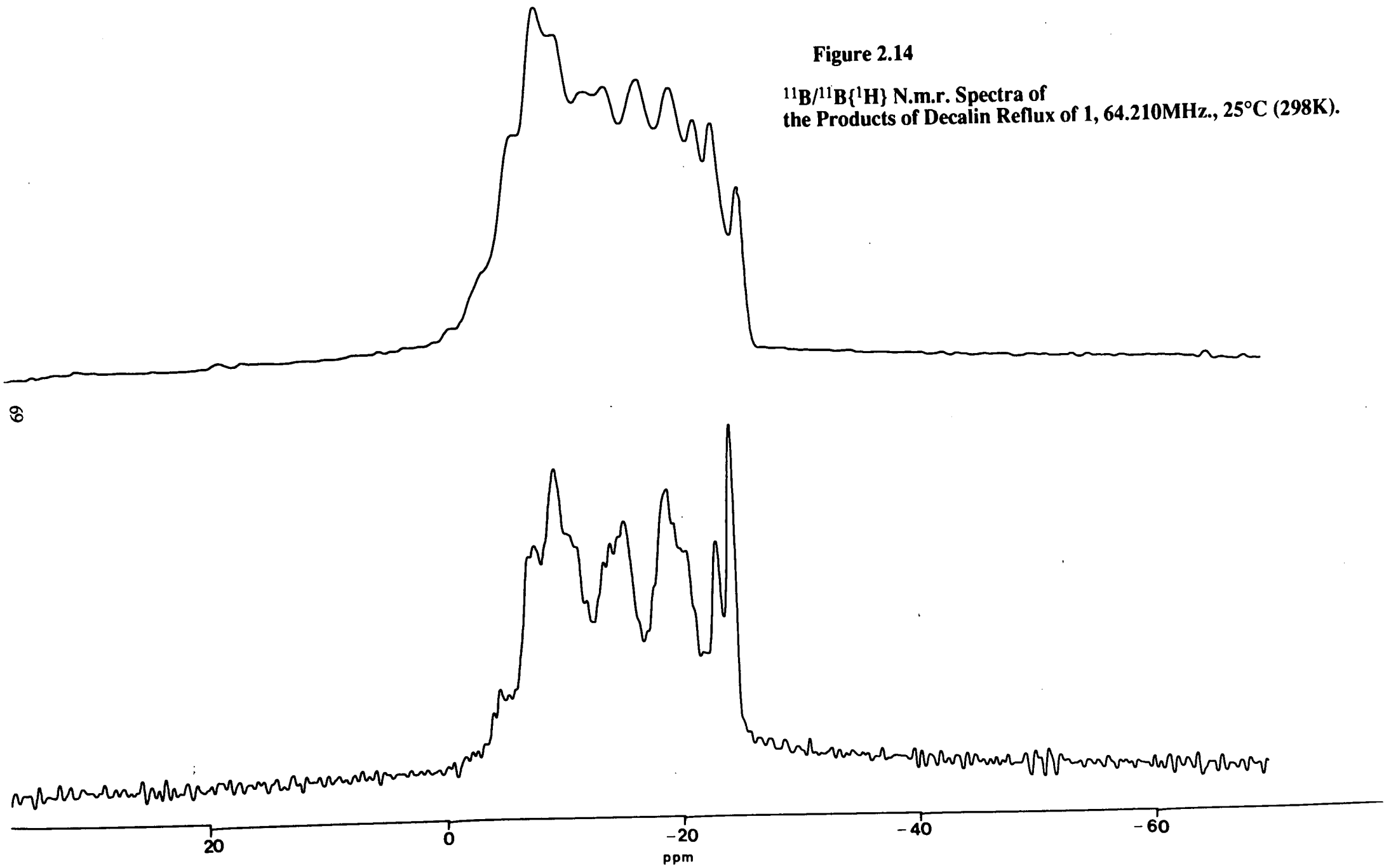

Figure 2.14

$^{11}B/^{11}B\{^1H\}$ N.m.r. Spectra of the Products of Decalin Reflux of 1, 64.210MHz., 25°C (298K).

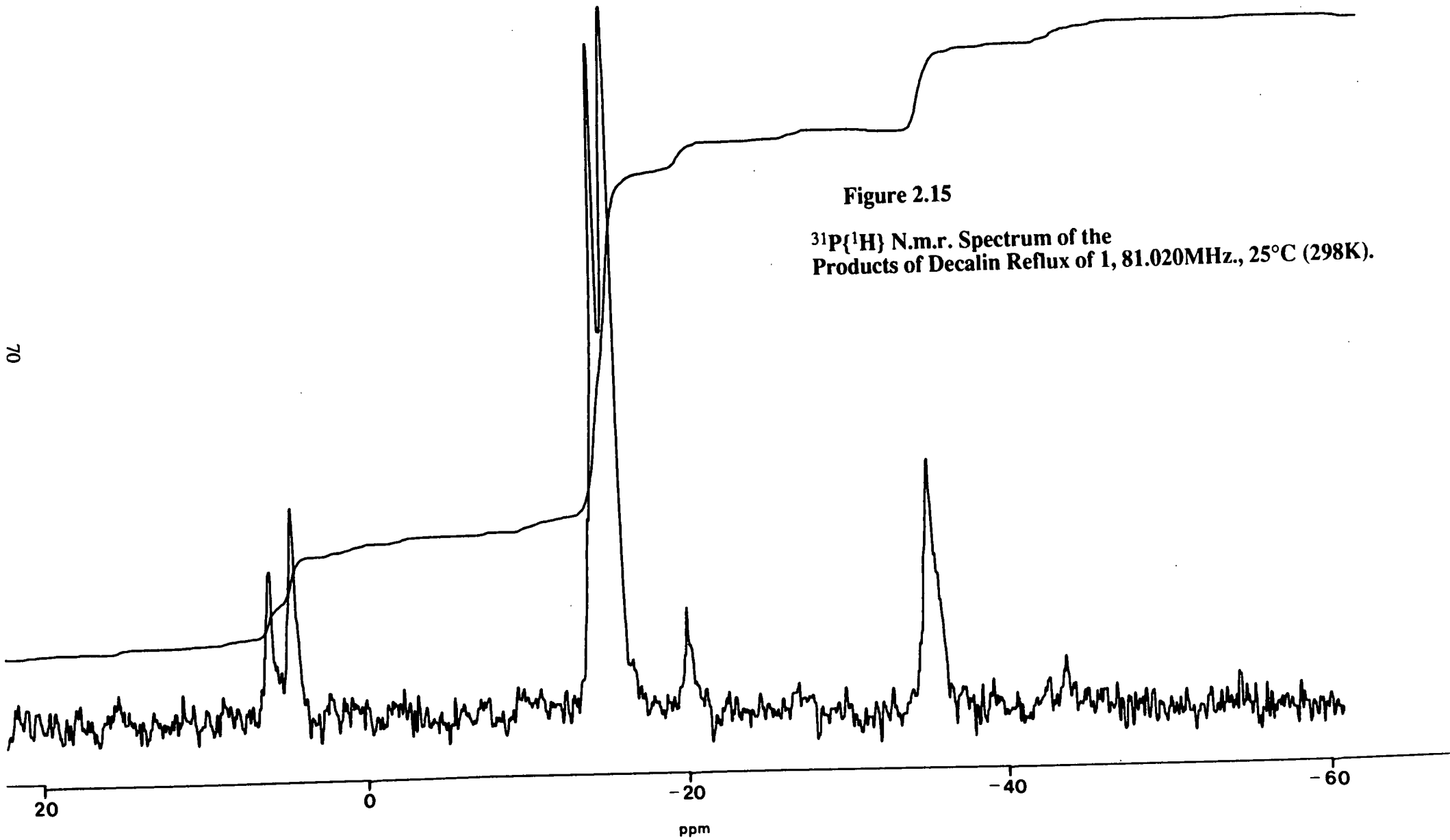

Figure 2.15

$^{31}P\{^{1}H\}$ N.m.r. Spectrum of the Products of Decalin Reflux of 1, 81.020MHz., 25°C (298K).

2.7 Other Examples of Polytopal Rearrangements.

Skeletal rearrangements, involving migration of atoms on the polyhedral surface of carbaboranes, are well known and give rise to a range of positional isomers. The driving force of such processes is usually considered to be the mutual coulombic repulsion experienced by the two adjacent carbon atoms, which are relatively positively charged. Separation of these atoms is commonly the outcome of rearrangement.

The earliest reported[77] example of such a polytopal isomerisation was that of 1,2-$C_2B_{10}H_{12}$ (ortho-carborane). At 450° this is found to rearrange to the 1,7-isomer (meta-carborane), in which the carbons are non-adjacent. This, in turn, undergoes a further rearrangement, at 600°, to form the 1,12-isomer (para-carborane)[78], which is the most thermodynamically stable of the three forms [79]. This process is shown in figure 2.17.

Figure 2.17

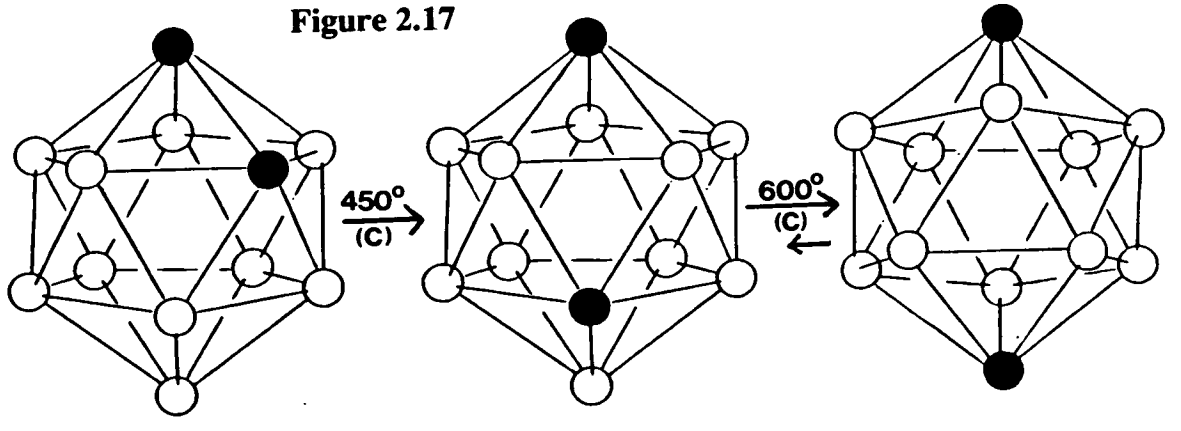

ortho-carborane **meta-carborane** **para-carborane**

The temperature at which this type of isomerisation occurs can be significantly reduced by introduction of bulky substituents on the cage carbon atoms. Hence, the isomerisation of 1,2 bis-dimethylsilyl-carbaborane occurs at 280°C[80].

The relative stabilities of the three positional isomers of the 12-vertex carbaborane are altered by the introduction of a double negative charge, whence all three are of

similar energy. In fact, the reverse isomerisation of 1,7- to 1,2-carbaborane can be observed, by first generating the 1,7-dianion in Na/liquid ammonia and then re-oxidising with $KMnO_4$ to form the neutral 1,2-carbaborane[81].

Carbametallaboranes can also undergo polytopal rearrangements. One of the first reported[82] examples of such a process involved the vapour-phase isomerisation of (η^5-Cp)-3,1,2-$CoC_2B_9H_{11}$ and its C,C-dimethyl-substituted analogue. This required temperatures of 400-700°C and yielded a variety of rearranged products. The presence of a metal atom as well as two carbon atoms in the polyhedral skeleton dramatically increases the number of possible isomers. Several of these were observed, including one in which the the carbon atoms remained adjacent, but with one shifted away from the metal. The separation of the positively charged metal fragment and a $\delta+$ carbon atom has been cited as a possible explanation for the formation of this isomer.

In the analogous complex where the carbon atoms are linked by a trimethylene bridge, which renders carbon atom separation impossible, heating to 500-650°C yields three isomers in which one or both of the carbon atoms have migrated away from the metal[82].

In complexes with no repulsive C-C interaction to facilitate rearrangement, this may nevertheless occur[83]. At 450°, (η^5Cp)-$NiCB_{10}H_{11}$ isomerises to give two products. In the first of these, the carbon atom which was vicinal to the metal now occupies a site on the lower belt. The second positional isomer has the carbon atom antipodal to the metal.

Another example where rearrangement occurs without resulting in carbon separation is provided by Ni and Pd bis-dicarbollyl complexes[84]. Three classes of these compounds have been observed (see figure 2.18).

Figure 2.18

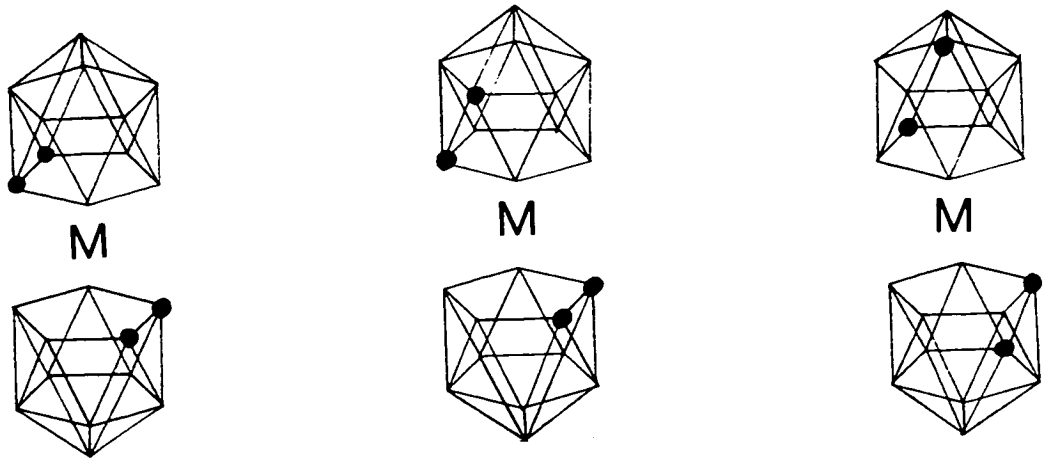

Class A, Class B and Class C Complexes.

In the first (A), the two carbons in each cage are adjacent on the metal-bonded face, and are *cis*- to the carbon atoms in the other cage. At higher temperatures, a carbon atom in one cage shifts to the lower belt, while still staying adjacent to the other carbon in that cage (to form type B). Raising the temperature further causes a carbon on the other cage to undergo a similar movement (to form type C). Electrostatic repulsion between the carbon atoms of different cages and between the carbon and metal atoms provide rationales for these reorganisations.

A steric effect is also apparent- whereas the C,C-dimethyl substituted species rearrange at 0-100°C, the unsubstituted Ni complex requires temperatures of 360-400°(at reduced pressure). In the related complexes in which the cage carbons are linked via a trimethylene group[85], carbon migration away from the metal atom occurs although the carbons must remain adjacent.

The first examples of fully characterised 3,1,11-carbametallaboranes were reported by Hawthorne *et al*, in 1984[48]. The complex $[(PEt_3)_4Rh][(nido\text{-}7\text{-}Me\text{-}8\text{-}Ph\text{-}7,8\text{-}C_2B_9H_{10}]$, was found to undergo a thermally

induced reorganisation, at 60°C (333K), in thf, to yield 1-Me-11-Ph-3,3-$(PEt_3)_2$-3-H-3,1,11-$RhC_2B_9H_9$, which has been identified by a crystallographic determination. The isomerisation was thought to proceed via formation and subsequent rearrangement of the 3,1,2-rhodacarbaborane. Similar species were produced bearing different phosphine ligands, when rhodium was replaced by iridium and also when the C,C-dimethyl-substituted carbaborane was studied. In addition, a similar iridium-monophenylcarbaborane complex was synthesised from 1-Ph-3,3-$(PPh_3)_2$-3-H-3,1,2-$IrC_2B_9H_{10}$ by heating to reflux temperature in toluene for *circa* 30 hours, to yield 2,2-$(PPh_3)_2$-2-H-8-Ph-2,1,8-$IrC_2B_9H_{10}$. This product has been characterised by an X-ray diffraction study [47] (the 2,1,8-isomer is equivalent to a 3,1,11-isomer using an older numbering convention).

The rearrangement of these asymmetrically substituted carbametallaboranes gives rise to the possibility of two 3,1,11-isomers- one with the (CPh) group occupying position 11 and the other with the second cage carbon atom at this position. However, in each case, only the former of these is observed. This is in contrast to the rearrangement of **1** which generates both the possible 3,1,11-isomers.

Even lower temperatures were required to facilitate the polytopal rearrangement of complexes of the type $[NEt_4][1,2\text{-}Me_2\text{-}3,3\text{-}(CO)_2\text{-}3(\equiv R)\text{-}3,1,2\text{-}WC_2B_9H_9]$, R=alkyl or aryl[86]. For example, when $R=CC_6H_4Me$, at room temperature, in aqueous HCl, with CO saturation, the 2,1,8-carbametallaborane $[NEt_4][1,8\text{-}Me_2\text{-}11\text{-}(CH_2C_6H_4Me)\text{-}2,2,2\text{-}(CO)_3\text{-}2\text{-}Cl\text{-}2,1,8\text{-}WC_2B_9H_9]$ is produced (similarly with aqueous HI). In this case, as well as C-migration, the alkyl group formerly bound to the metal centre inserts into the B-H bond at B(11). Subsequent experiments on these complexes indicated that the insertion of the alkyl group into the B-H bond is independent of the isomerisation process. Remarkably the isomerisation proved to be reversible. Reacting a CO saturated solution of the

2,1,8-isomer with excess $AgBF_4$ at room temperature, yielded a mixture of two products (see figure 2.19).

Figure 2.19

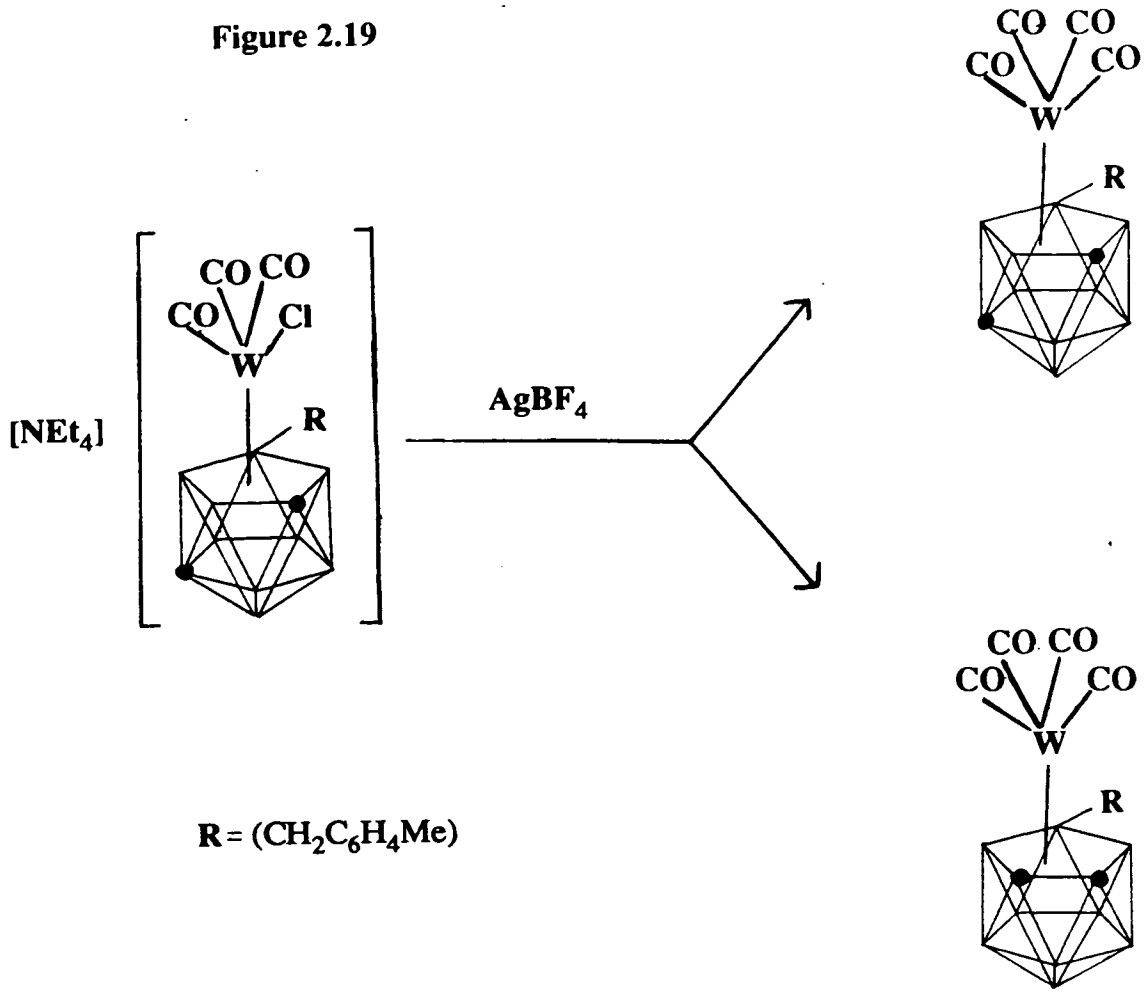

R = $(CH_2C_6H_4Me)$

One of these was 1,2-Me_2-8-$(CH_2C_6H_4Me)$-3,3,3,3-$(CO)_4$-3,1,2-$WC_2B_9H_9$, in which the carbon atoms are once again adjacent. The other product is 1,8-Me_2-11-$(CH_2C_6H_4)$-2,2,2,2-$(CO)_4$-2,1,8-$WC_2B_9H_9$. This unexpected reverse isomerisation has yet to be rationalised. In addition, the question arose[87] as to whether the formation of the 2,1,8-isomer proceeded with B-H insertion or isomerisation occurring first. When the Mo-analogue was treated with aqueous HI, as above, 2 species were observed. The first was the 2,1,8-isomer: $[NEt_4]$[1,8-Me_2-2,2,2-$(CO)_3$-2-I-11-$(CH_2C_6H_4Me$-4)-2,1,8-$MoC_2B_9H_9$]. The other product was a 3,1,2-isomer in which insertion into the B-H bond had occurred,

i.e. $[NEt_4][1,2\text{-}Me_2\text{-}2,2,2\text{-}(CO)_3\text{-}2\text{-}I\text{-}8\text{-}(CH_2C_6H_4Me\text{-}4)\text{-}3,1,2\text{-}MoC_2B_9H_9]$. This was converted to the 2,1,8-isomer within 10 hours at ambient temperature. Hence, it appears that alkyl insertion into a B-H bond occurs prior to skeletal isomerisation. Further, rearrangement of the Mo-species is less facile than that of the W-analogues.

This was also apparent when the isomerisation of the species $[N(PPh_3][1,2\text{-}Me_2\text{-}3\text{-}(\eta^3C_3H_5)\text{-}3,3\text{-}(CO)_2\text{-}3,1,2\text{-}MC_2B_9H_9]$, M= Mo, W, by stirring with aqueous HI, in a CO saturated CH_2Cl_2 solution[87], were studied. Whereas the W species isomerises virtually quantitatively to the 2,1,8-isomer the Mo-analogue gives rise to the complex $[NEt_4][1,2\text{-}Me_2\text{-}3\text{-}I\text{-}3,3,3\text{-}(CO)_3\text{-}3,1,2\text{-}MoC_2B_9H_9]$. In order to form the 2,1,8-Mo-carbaborane, heating to reflux temperature was required, or alternatively *circa* 10% conversion was observed after 10 days at ambient temperature. The relative ease of isomerisation of third row carbametallaboranes with respect to their second row metal analogues is discussed in chapter 4.

2.8 Postulated Mechanisms of Polytopal Rearrangements.

There has been much speculation as to the mechanism of skeletal rearrangements, however no definitive mechanism has yet been established. The principal mechanistic suggestions are described below. The earliest proposal was Lipscomb's[88] diamond-square-diamond (d.s.d.) mechanism, which successfully explained the isomerisation of ortho- to meta-carborane. This involves breaking of the common linkage between two adjacent triangular faces of polyhedral atoms to form a square face. This face can then revert to the original triangle pair or alternatively, a bond may be formed orthogonal to the original one. In an icosahedron, six such steps are required to yield a 1,2- to 1,7-isomerisation. If these d.s.d. cycles occur simultaneously then it was suggested a cuboctahedral intermediate could be produced. A single d.s.d. process is shown in figure 2.20, and a full 1,2 - 1,7

isomerisation via this mechanism is depicted in figure 2.21.

Figure 2.20

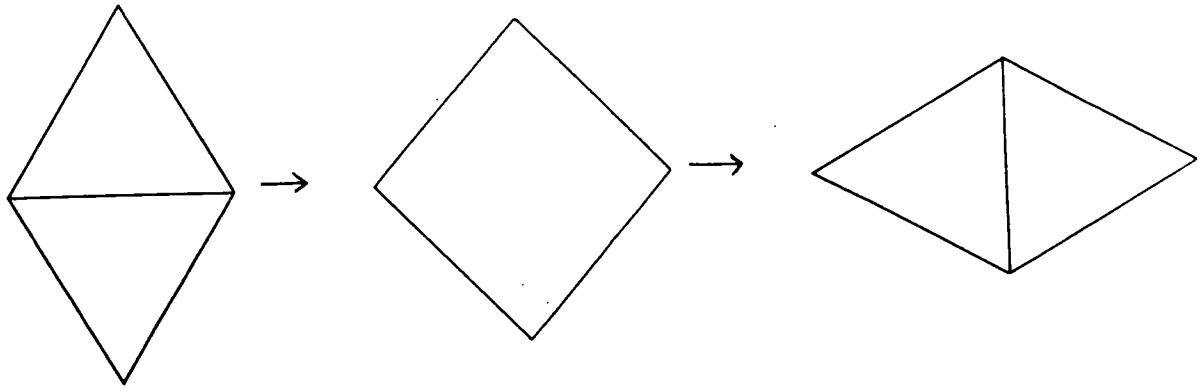

A Single Diamond-Square-Diamond Process.

This simple mechanism cannot account for the further isomerisation of the 1,7-carbaborane to the 1,12-isomer. The observation of this isomer led Lipscomb to suggest a more complex variation - the modified d.s.d. mechanism[89]. In this case, rotations of trigonal faces in the cuboctahedral intermediate were permitted. When the preferential rotation of certain faces was taken into account, the product distribution for the isomerisation of 1,2-Me_2-9,12-Cl_2-1,2-$C_2B_{10}H_8$ could be modelled[148]. A related mechanism "the d.s.d. twist" involves only rotation of square faces[90].

Rather than introduce variations in the behaviour of the cuboctahedral intermediate, the formation of a complementary anticuboctahedral intermediate has been suggested[91]. This can be formed by breaking a different set of bonds in the icosahedron, but crucially, the antipodal relationship of vertices need not be maintained. The 1,7 - 1,12 carbaborane isomerisation (as well as the other documented rearrangements) can be rationalised by this mechanism which requires only simple diamond-square-diamond steps as illustrated in figure 2.22.

Figure 2.21

1,2- to 1,7- Isomerisation via a Cubeoctahedral Intermediate.

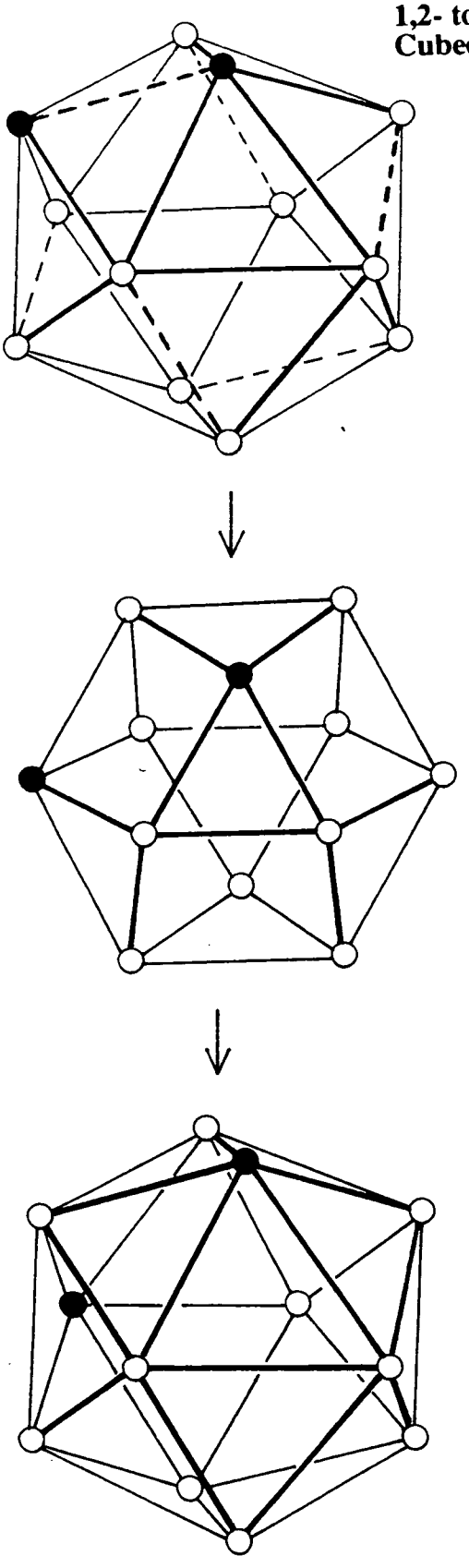

Figure 2.22

1,2- to 1,7- to 1,12- Isomerisation via an Anti-cubeoctahedral Intermediate.

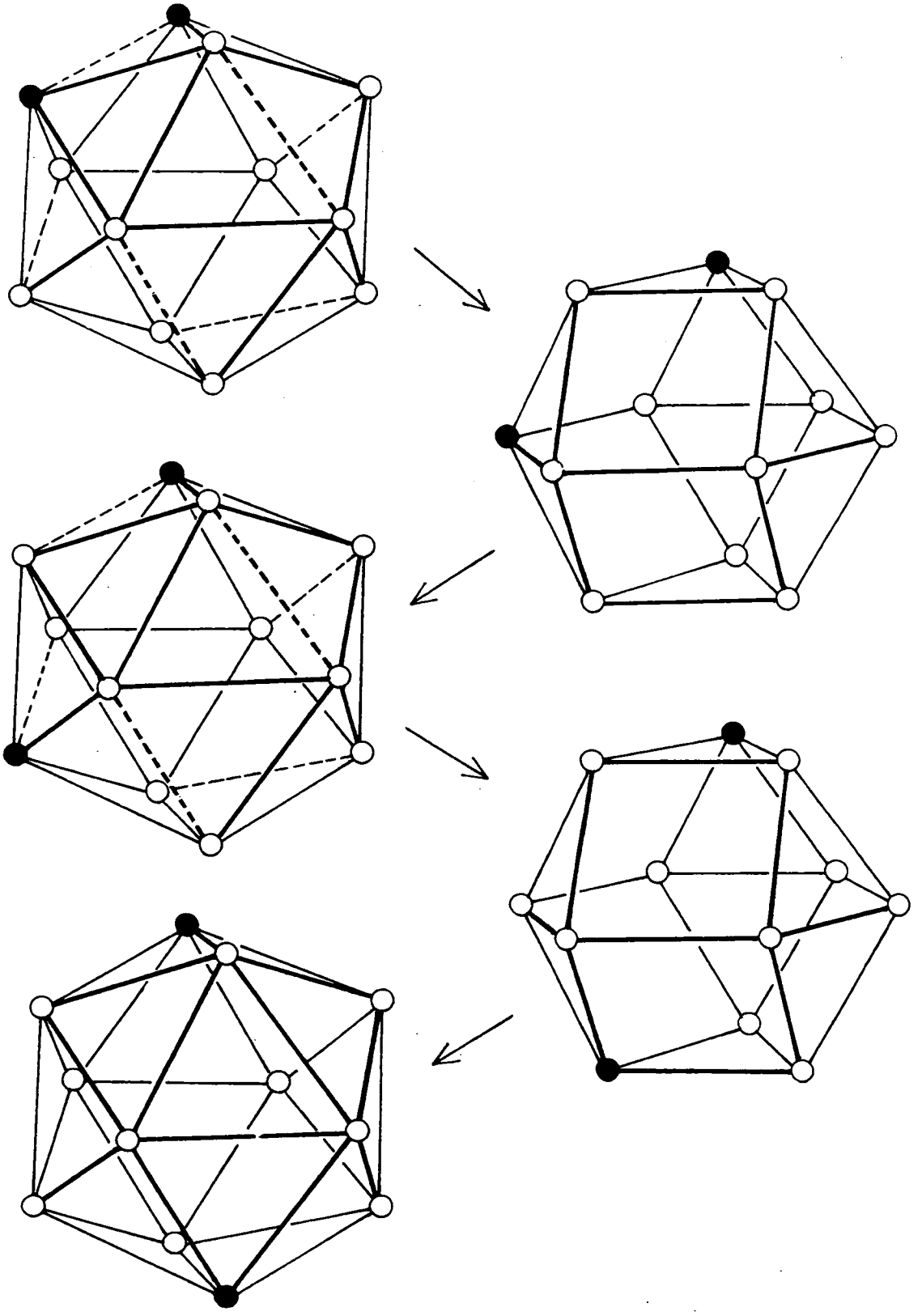

Mechanisms involving neither of these polyhedral intermediates have also been invoked. Grafstein and Dvorak[92] devised a mechanism involving the mutual rotation of pentagonal pyramids, within the icosahedron. This was used to successfully account for the product distribution in the rearrangements of chloro-phosphacarbaboranes (*e.g.*12-Cl-1,2-$CPB_{10}H_{10}$)[90].

The simple proposal involving the rotation of triangular faces in the icosahedral ground state (of Muetterties and Knoth[93]) gave rise to the unifying "extended-triangle-rotation" mechanism. This was suggested by Wu and Jones[94], as being applicable to all previously reported rearrangements. Polyhedral atoms were defined as being of two classes - framework atoms or middle triangle atoms (see figure 2.23).

Figure 2.23

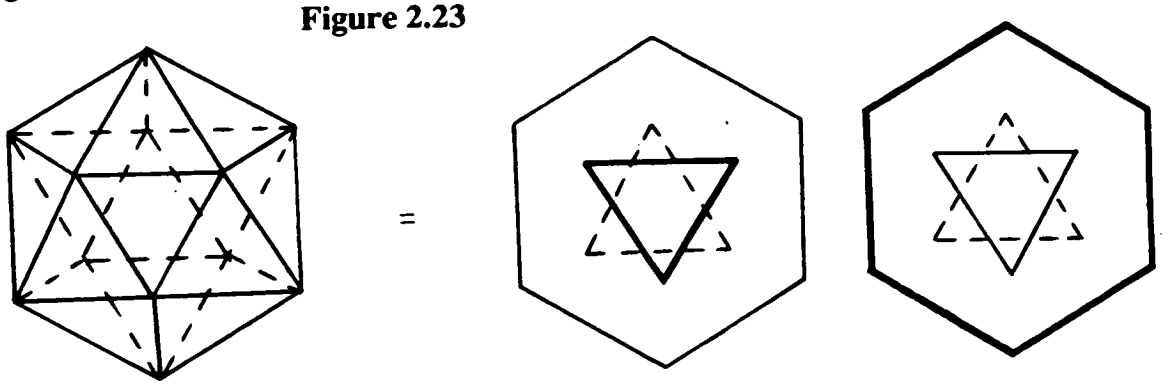

(Only one of the pairs is emphasized in the diagram.)

Rearrangement could be effected by various combinations of rotations of the middle triangles. Preferential rotation of certain triangles (depending on *e.g.* the nature of substituents or of polyhedral atoms) and hence product distributions could be explained. However, at this time there exists too small a body of knowledge to allow the prediction of the lowest energy triangular rotations, which limits the application of this mechanism.

A final proposed mechanism[90] differs considerably from the rest, in that it

involves opening of the *closo*-icosahedron to give a 12-vertex *nido*-species. This is formally a *nido*-fragment of a 13-vertex docosahedron. Various d.s.d.-type processes are permitted to occur at the *nido*-face to produce new configurations which can then re-close to form new icosahedra. By varying the pattern of reorganisation within this intermediate, formation of all the observed isomers can be explained. Edvenson and Gaines[95] have demonstrated that variation of the nature of the processes occurring within the intermediate can render this mechanism equivalent to all the other proposed rearrangement pathways. Therefore, this provides a potential widely-applicable mechanism. It is particularly convincing when applied to the case of the rearrangement of carbametallaboranes in which the metal is often found to be loosely bonded to one or more atom(s) in the ligated face. By the breaking of three of these metal-B (or C) bonds and the formation of one, the metal vertex could become part of a six-membered *nido*-face. This would be unlikely to require a large expenditure of energy.

This mechanism has been suggested[87] as being involved in the formation of the 2,1,8-M-species (M= W, Mo) discussed in the previous section, by reaction of CO and aqueous HI with the 3,1,2-M-complexes. Attack of the metal centre by I^- could lead to the formation of a 12-vertex *nido*-carbametallaborane. A diamond-square-diamond cycle with rotation of a CBB triangular face, followed by closure of the *nido*-intermediate, would give the observed products.

There are numerous examples of the theoretical consideration of these mechanisms[96], but these are beyond the scope of this discussion. It should be noted, however, that in the case of an asymmetrically substituted carbametallaborane the symmetry of the molecule is dramatically reduced from that of the molecules usually discussed and this will significantly alter the symmetry-allowed processes.

2.9 Consideration of the Isomerisation of 1.

At this time, little can be concluded about the mechanism of rearrangement of **1**. However, the crystal structure shows significant distortions from an idealised icosahedral structure, which may contribute to lowering the activation energy to the rearrangement process. The formation of 2 isomeric carbaplatinaboranes, one of which (**3**) is as sterically crowded as **1**, indicates steric considerations are not predominant. However, it was noted earlier that an unfavourable steric interaction between the (CPh) unit and the metal fragment leads to a ground state destabilisation of **1**, with respect to its unsubstituted analogue. This destabilisation may lower the activation energy to rearrangement sufficiently to permit a facile isomerisation to occur. A schematic representation of this is shown in figure 2.24.

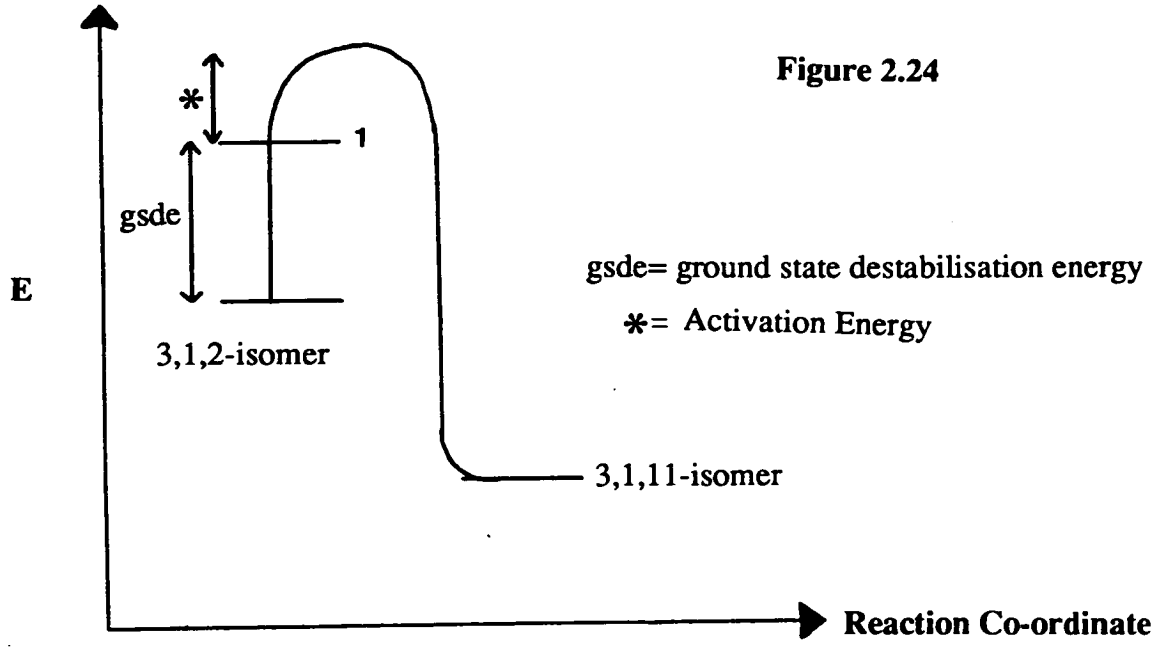

Figure 2.24

It can also be noted that the magnitude of the rotation of the plane through the $\{P_2Pt\}$ fragment is such that in the ground state of **1** it is aligned in the same conformation as it would be predicted to occupy if the carbaborane face was of the CB_4 type, with C(1) being the sole carbon atom and C(2) being replaced by a boron atom *i.e.* with the $\{P_2Pt\}$ fragment lying parallel to the B(7)-B(8) bond.

2.10 Formation and Characterisation of the $\{(PMe_2Ph)_2Pt\}$ Complex of (C-Ph) Disubstituted Carbaborane.

When cis-$PtCl_2(PMe_2Ph)_2$ was stirred with $Tl_2C_2B_9H_9Ph_2$, in CH_2Cl_2, at room temperature, a soluble yellow product was formed (along with TlCl) and was purified by column chromatography (alumina/CH_2Cl_2). Subsequent preparative t.l.c. was required on some occasions to yield the pure product, **4**.

Microanalysis is consistent with the formulation $B_9C_{30}H_{41}P_2Pt$, molecular weight 756. The solution i.r. spectrum (CH_2Cl_2) indicates the presence of borane (B-H stretch at 2545cm^{-1}) as well as the PMe_2Ph ligand.

The $^{11}B\{^1H\}$ n.m.r. spectrum in $CDCl_3$ is poorly resolved, under standard conditions (at 64.210MHz.). However, the spectrum at higher field (192.630MHz.) is more informative and indicates the presence of 8 boron environments in the ratio 2:1:1:1:1:1:1:1. These resonances occur at δ(p.p.m.)= -3.81, -6.52, -8.41, -12.43, -13.16, -14.69, -17.55, -22.48, none of which exhibit discernible coupling to the platinum nucleus. The proton coupled spectrum shows 8 doublets indicating that each boron atom is bound to a terminal hydrogen atom (^{1}JB-H= 95-165Hz.) (see figure 2.25).

The $^{31}P\{^1H\}$ n.m.r. spectrum consists of a singlet (δ = -14.94 p.p.m.) with doublet satellites ($^1J^{195}$Pt-P=3257Hz.). The spectrum at -50°C (223K) is a fully resolved AB pattern, mirrored in the doublet satellites (see figure 2.26). This indicates that, at low temperature, there is restricted rotation about the Pt-cage bonding, on the n.m.r. timescale, which renders the two phosphorus nuclei inequivalent. Calculation of the parameters[75] from this spectrum yields δP_1= -14.25p.p.m., δP_2= -14.80p.p.m., $^2JP_1$-P_2= 26.70Hz., $^1J^{195}$Pt-P_1= 3228.7Hz. and $^1J^{195}$Pt-P_2= 3261.2Hz.

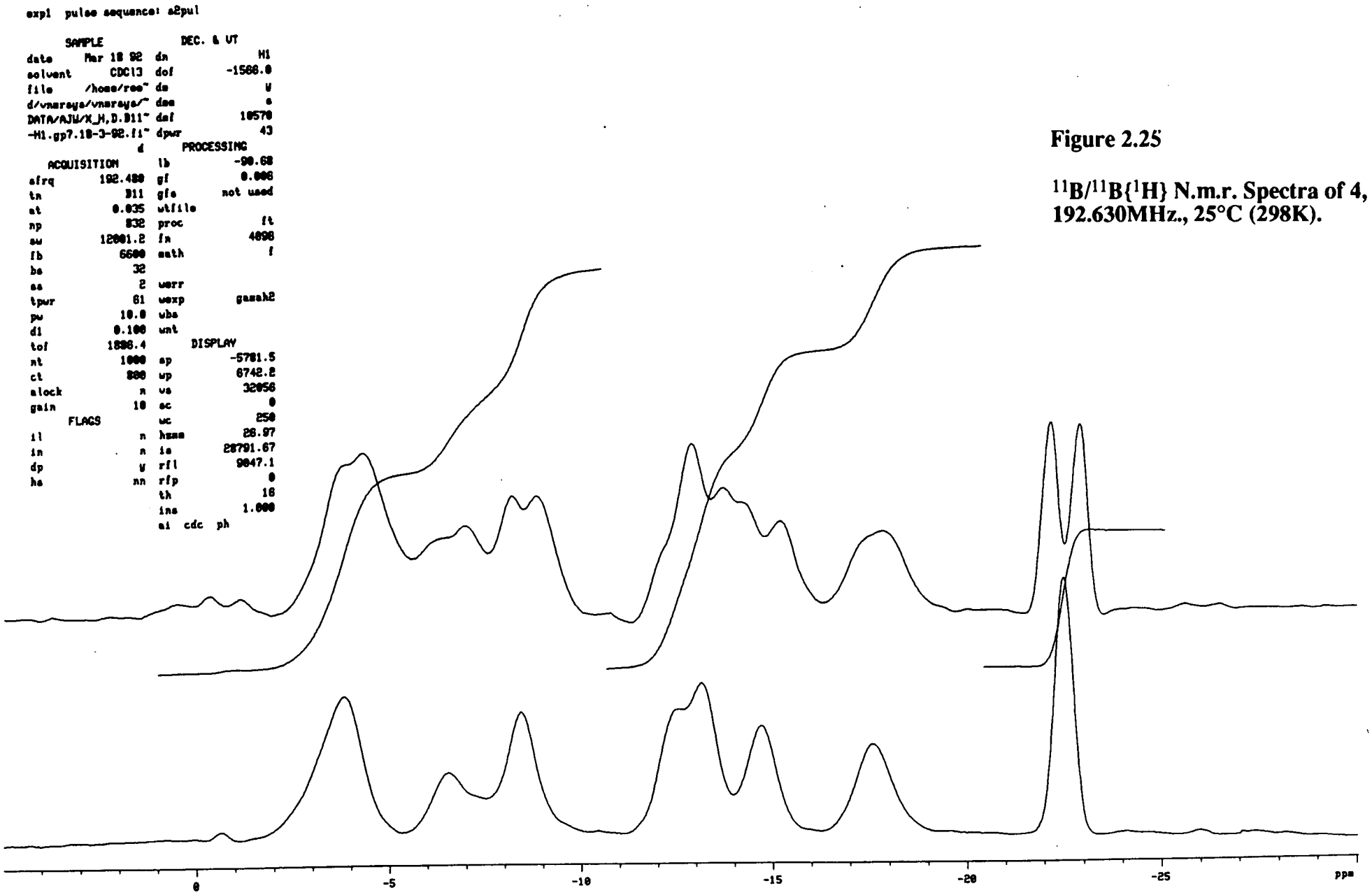

Figure 2.25

$^{11}B/^{11}B\{^{1}H\}$ N.m.r. Spectra of 4, 192.630MHz., 25°C (298K).

Figure 2.26

$^{31}P\{^{1}H\}$ N.m.r. Spectrum of 4, 81.020MHz., -50° (223K).

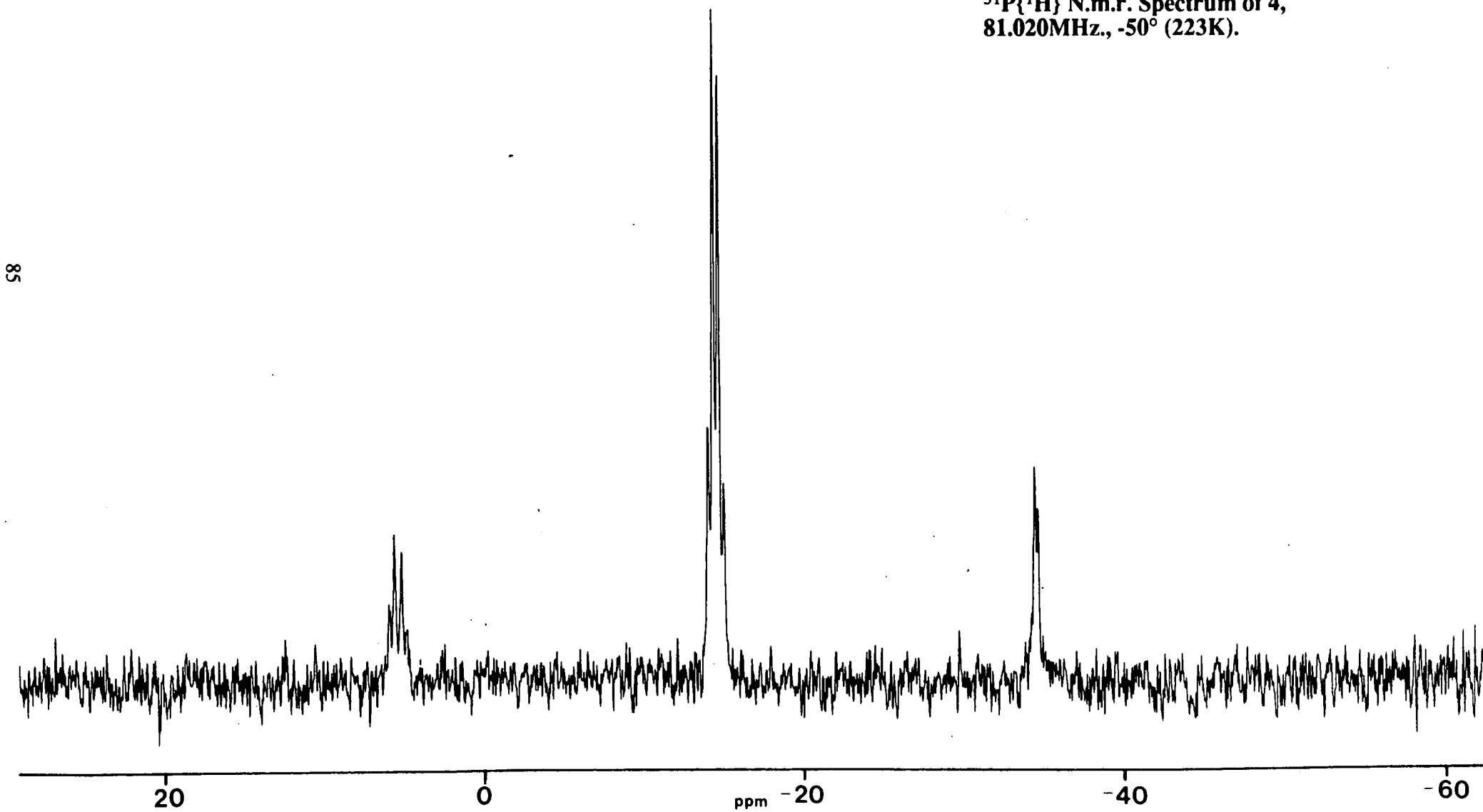

The room temperature ^1H n.m.r. spectrum is complex. The signal denoting the methyl protons is a broad second-order resonance centred on 1.50p.p.m., while there are two complex signals arising from the phenyl-protons at 7.17 and 7.50 p.p.m. (one corresponding to the cage-phenyl protons and the other to the phosphino-phenyl protons).

2.11 Crystal Structure of 4.

Yellow, single crystals suitable for X-ray diffraction study were obtained by slow diffusion of n-hexane into a solution of **4** in CH_2Cl_2, at -30°C (243K). Data collection and structure refinement were carried out in a similar manner to that for **1** and full details appear in chapter 5. **4** forms discrete, neutral, monomeric molecules, with no imposed symmetry.

Selected bond lengths and angles are given in tables 2.8 and 2.9 respectively. A perspective view of a single molecule is depicted in figure 2.27. The striking feature relating to this structure is that the two cage carbons have separated, even under the mild conditions employed for the reaction. These atoms are separated in a similar fashion to those in **2** and **3** to yield the compound 1,11-Ph_2-3,3-$(PMe_2Ph)_2$-3,1,11-$PtC_2B_9H_9$, **4**.

Figure 2.27

Perspective View of 4.

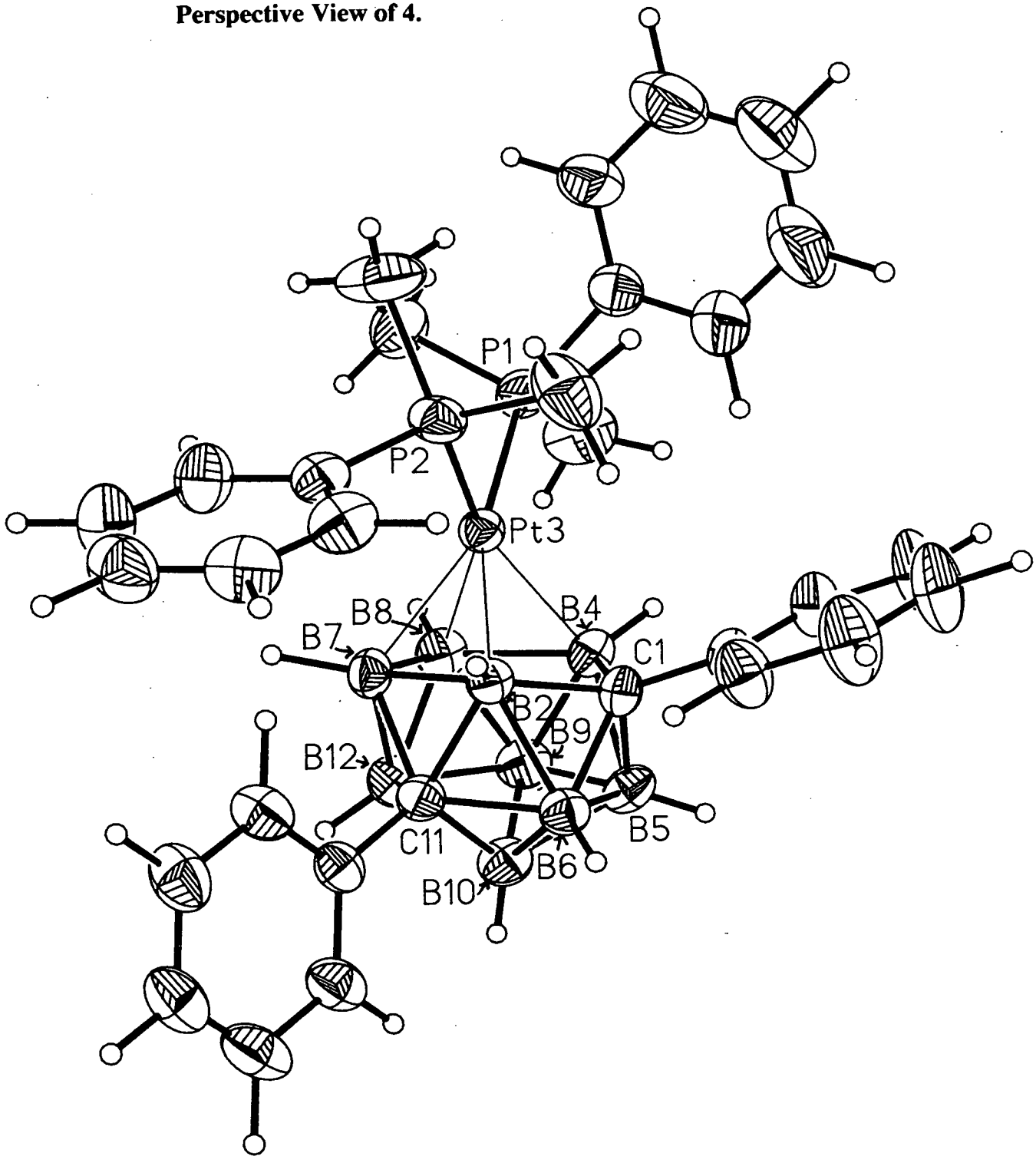

Table 2.8 Selected Bond Lengths in 4, Å, with Standard Deviations.

Pt(3) - P(2)	2.2864(14)	B(2) - C(11)	1.756(8)
Pt(3) - P(1)	2.2909(14)	B(4) - B(5)	1.815(8)
Pt(3) - C(1)	2.610(5)	B(4) - B(8)	1.872(8)
Pt(3) - B(2)	2.222(6)	B(4) - B(9)	1.800(8)
Pt(3) - B(4)	2.293(6)	B(5) - B(6)	1.746(8)
Pt(3) - B(7)	2.199(6)	B(5) - B(9)	1.781(9)
Pt(3) - B(8)	2.231(6)	B(5) -B(10)	1.745(9)
P(2) -C(211)	1.811(4)	B(6) -B(10)	1.754(8)
P(2) -C(221)	1.822(7)	B(6) -C(11)	1.712(7)
P(2) -C(231)	1.826(7)	B(7) - B(8)	1.797(8)
P(1) -C(111)	1.821(4)	B(7) -C(11)	1.735(7)
P(1) -C(121)	1.822(7)	B(7) -B(12)	1.783(8)
P(1) -C(131)	1.826(8)	B(8) - B(9)	1.768(9)
C(1) - B(2)	1.700(8)	B(8) -B(12)	1.772(8)
C(1) - B(4)	1.700(7)	B(9) -B(10)	1.778(9)
C(1) - B(5)	1.677(8)	B(9) -B(12)	1.769(9)
C(1) - B(6)	1.647(7)	B(10) -C(11)	1.738(8)
C(1) -C(101)	1.515(6)	B(10) -B(12)	1.752(8)
B(2) - B(6)	1.834(8)	C(11) -B(12)	1.736(8)
B(2) - B(7)	1.871(8)	C(11) -C(201)	1.526(6)

Table 2.9 Selected Bond Angles in 4, °, with Standard Deviations.

P(2) -Pt(3) - P(1)	96.23(5)	B(5) - B(6) -B(10)	59.8(3)
C(1) -Pt(3) - B(2)	40.21(19)	B(10) - B(6) -C(11)	60.2(3)
C(1) -Pt(3) - B(4)	39.91(17)	Pt(3) - B(7) - B(2)	65.6(3)
B(2) -Pt(3) - B(7)	50.08(22)	Pt(3) - B(7) - B(8)	67.0(3)
B(4) -Pt(3) - B(8)	48.86(21)	B(2) - B(7) -C(11)	58.1(3)
B(7) -Pt(3) - B(8)	47.87(21)	B(8) - B(7) -B(12)	59.3(3)
Pt(3) - P(2) -C(211)	117.00(15)	C(11) - B(7) -B(12)	59.1(3)
Pt(3) - P(2) -C(221)	112.34(23)	Pt(3) - B(8) - B(4)	67.3(3)
Pt(3) - P(2) -C(231)	116.43(24)	Pt(3) - B(8) - B(7)	65.1(3)
C(211)- P(2) -C(221)	106.4(3)	B(4) - B(8) - B(9)	59.2(3)
C(211)- P(2) -C(231)	102.0(3)	B(7) - B(8) -B(12)	59.9(3)
C(221)- P(2) -C(231)	100.8(3)	B(9) - B(8) -B(12)	60.0(3)
Pt(3) - P(1) -C(111)	113.86(13)	B(4) - B(9) - B(5)	60.9(3)
Pt(3) - P(1) -C(121)	112.61(23)	B(4) - B(9) - B(8)	63.3(3)
Pt(3) - P(1) -C(131)	120.38(24)	B(5) - B(9) -B(10)	58.7(3)
C(111)- P(1) -C(121)	105.4(3)	B(8) - B(9) -B(12)	60.1(3)
C(111)- P(1) -C(131)	100.5(3)	B(10) - B(9) -B(12)	59.2(3)
C(121)- P(1) -C(131)	102.2(3)	B(5) -B(10) - B(6)	59.9(3)
Pt(3) - C(1) - B(2)	57.53(25)	B(5) -B(10) - B(9)	60.7(3)
Pt(3) - C(1) - B(4)	59.97(23)	B(6) -B(10) -C(11)	58.7(3)
Pt(3) - C(1) -C(101)	112.6(3)	B(9) -B(10) -B(12)	60.1(3)
B(2) - C(1) - B(6)	66.4(3)	C(11) -B(10) -B(12)	59.7(3)
B(2) - C(1) -C(101)	119.6(4)	B(2) -C(11) - B(6)	63.8(3)
B(4) - C(1) - B(5)	65.0(3)	B(2) -C(11) - B(7)	64.8(3)
B(4) - C(1) -C(101)	122.9(4)	B(2) -C(11) -C(201)	118.3(4)
B(5) - C(1) - B(6)	63.4(3)	B(6) -C(11) -B(10)	61.1(3)
B(5) - C(1) -C(101)	119.0(4)	B(6) -C(11) -C(201)	115.6(4)
B(6) - C(1) -C(101)	117.4(4)	B(7) -C(11) -B(12)	61.8(3)
Pt(3) - B(2) - C(1)	82.3(3)	B(7) -C(11) -C(201)	116.3(4)
Pt(3) - B(2) - B(7)	64.3(3)	B(10) -C(11) -B(12)	60.6(3)
C(1) - B(2) - B(6)	55.4(3)	B(10) -C(11) -C(201)	120.0(4)

B(6) - B(2) -C(11)	56.9(3)	B(12) -C(11) -C(201)	121.1(4)
B(7) - B(2) -C(11)	57.0(3)	B(7) -B(12) - B(8)	60.7(3)
Pt(3) - B(4) - C(1)	80.1(3)	B(7) -B(12) -C(11)	59.1(3)
Pt(3) - B(4) - B(8)	63.83(25)	B(8) -B(12) - B(9)	59.9(3)
C(1) - B(4) - B(5)	56.9(3)	B(9) -B(12) -B(10)	60.7(3)
B(5) - B(4) - B(9)	59.0(3)	B(10) -B(12) -C(11)	59.8(3)
B(8) - B(4) - B(9)	57.5(3)	C(1) -C(101)-C(106)	120.0(3)
C(1) - B(5) - B(4)	58.1(3)	C(1) -C(101)-C(102)	120.0(3)
C(1) - B(5) - B(6)	57.5(3)	C(11) -C(201)-C(202)	119.3(3)
B(4) - B(5) - B(9)	60.1(3)	C(11) -C(201)-C(206)	120.7(3)
B(4) - B(5) -B(10)	106.6(4)	P(2) -C(211)-C(212)	123.4(3)
B(9) - B(5) -B(10)	60.6(3)	P(2) -C(211)-C(216)	116.6(3)
C(1) - B(6) - B(2)	58.2(3)	P(1) -C(111)-C(112)	118.0(3)
C(1) - B(6) - B(5)	59.2(3)	P(1) -C(111)-C(116)	122.0(3)
C(1) - B(6) -B(10)	107.3(4)		

The platinum atom and the carbaborane cage define a distorted icosahedron, the nature of the distortions being similar to those described earlier. The four metal-boron bonds to the CB_4 face are of similar lengths (Pt-B(2)= 2.222(6)Å, Pt-B(4)= 2.293(6)Å, Pt-B(7)= 2.199(6)Å and Pt-B(8)= 2.231(6)Å). However, the platinum- facial-carbon interaction is virtually non-bonding (Pt-C(1)= 2.610(5)Å).

The platinum atom is slipped over the CB_4 face, away from the carbon atom (Δ= -0.36Å), at an angle of 17.2° from the vector linking C(1)and the mid-point of the B(7)-B(8) bond (= σ). The upper CB_4 belt is slipped 0.08Å, with respect to the centroid of the lower belt, in the same sense as Δ, leading to a slight over-estimate of this value. The metal-bonded face is folded with respect to the lower belt, about an axis through B(2) and B(4) making folding angles of 3.52° and 11.38° for θ and ϕ, respectively. The average elevation angle of the substituents on the metal-bonded face is 20.6°(= χ), indicating that these are bent slightly away from the metal. The cage-phenyl ring is twisted slightly (by 19.4°) with respect to the lower CB_4 girdle.

The geometry at the platinum centre can be considered to be *pseudo*-square planar with the P-Pt-P angle of 96.23(5)°. The plane through the PtP_2 fragment is predicted to lie perpendicular to the idealised cage mirror plane in a carbaborane containing a CB_4 metal-bonded face (see section 1.4). The calculated angle between the PtP_2

plane and the plane through C(1), B(10) and B(12), in **4**, is 79.1° (*i.e.* a rotation of 10.9° away from the expected orientation is observed).

This magnitude of rotation has been observed in other carbaplatinaborane complexes[27] and was explained as being due to intra-molecular contacts involving alkyl-phosphino hydrogen atoms and cage hydrogen atoms. In this case, another possible explanation can be envisaged. Within a single molecule there are interactions involving phenyl hydrogen atoms and nearby phenyl rings, similar to those observed in **1** and **3**. These protons point towards the centre of the ring and are at a distance less than the sum of the van der Waals radii of a hydrogen atom and the half thickness of a phenyl ring (= 1.2Å + 1.85Å[64]). The interactions between H(202) and the almost orthogonal (calculated angle= 80.8°) phosphino-phenyl ring (2.85Å away) and between H(216) and the almost orthogonal (calculated angle= 77.4°) cage phenyl ring (3.01Å away) are indicated in figure 2.28. It is plausible that the $\{P_2Pt\}$ fragment is rotated slightly such as to maximise these interactions.

A diagram of the packing of **4** in the unit cell (figure 2.29)shows no significant inter-molecular interactions.

Figure 2.28

Alternative View of 4.

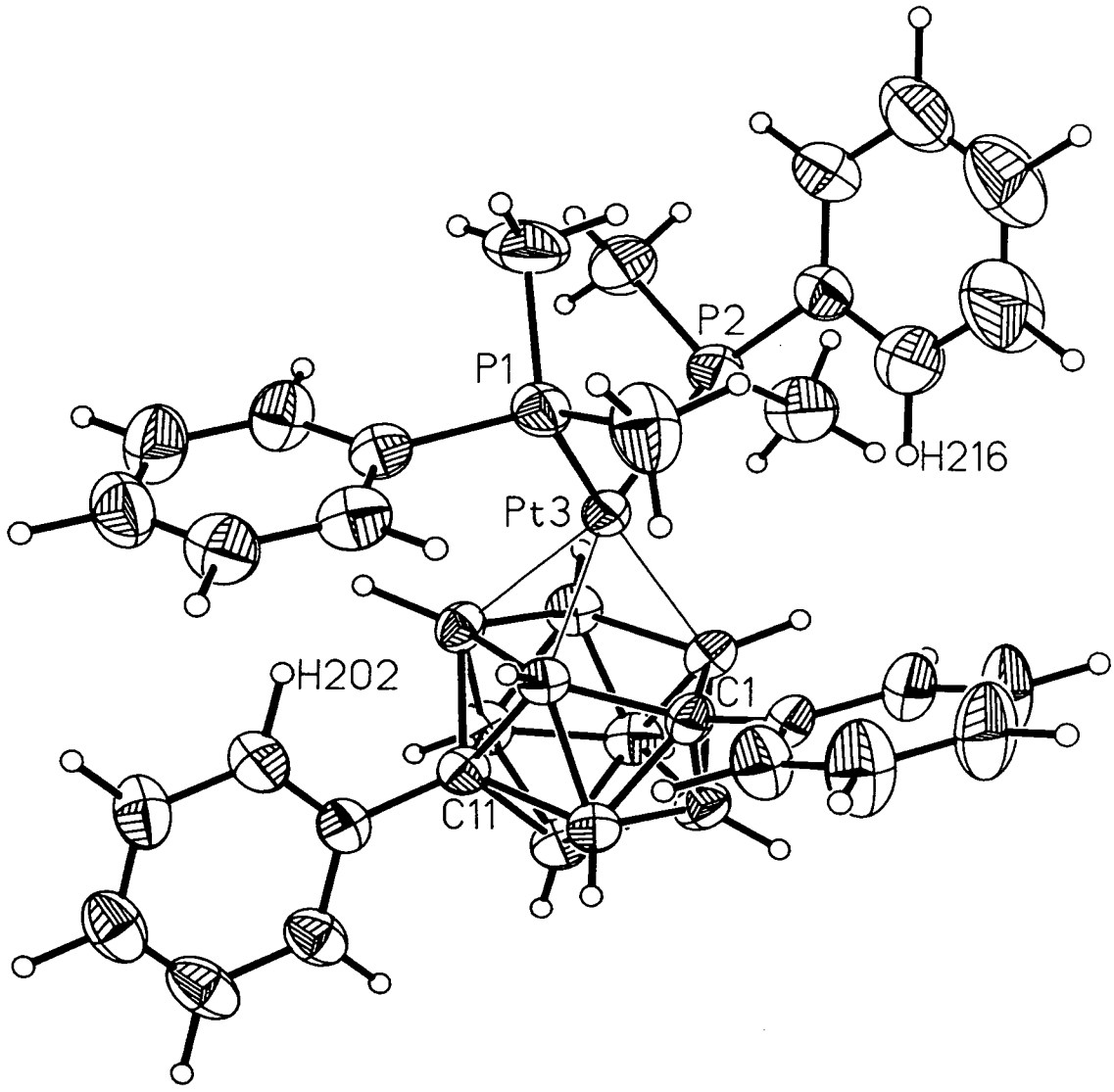

Figure 2.29

Packing Diagram of 4.

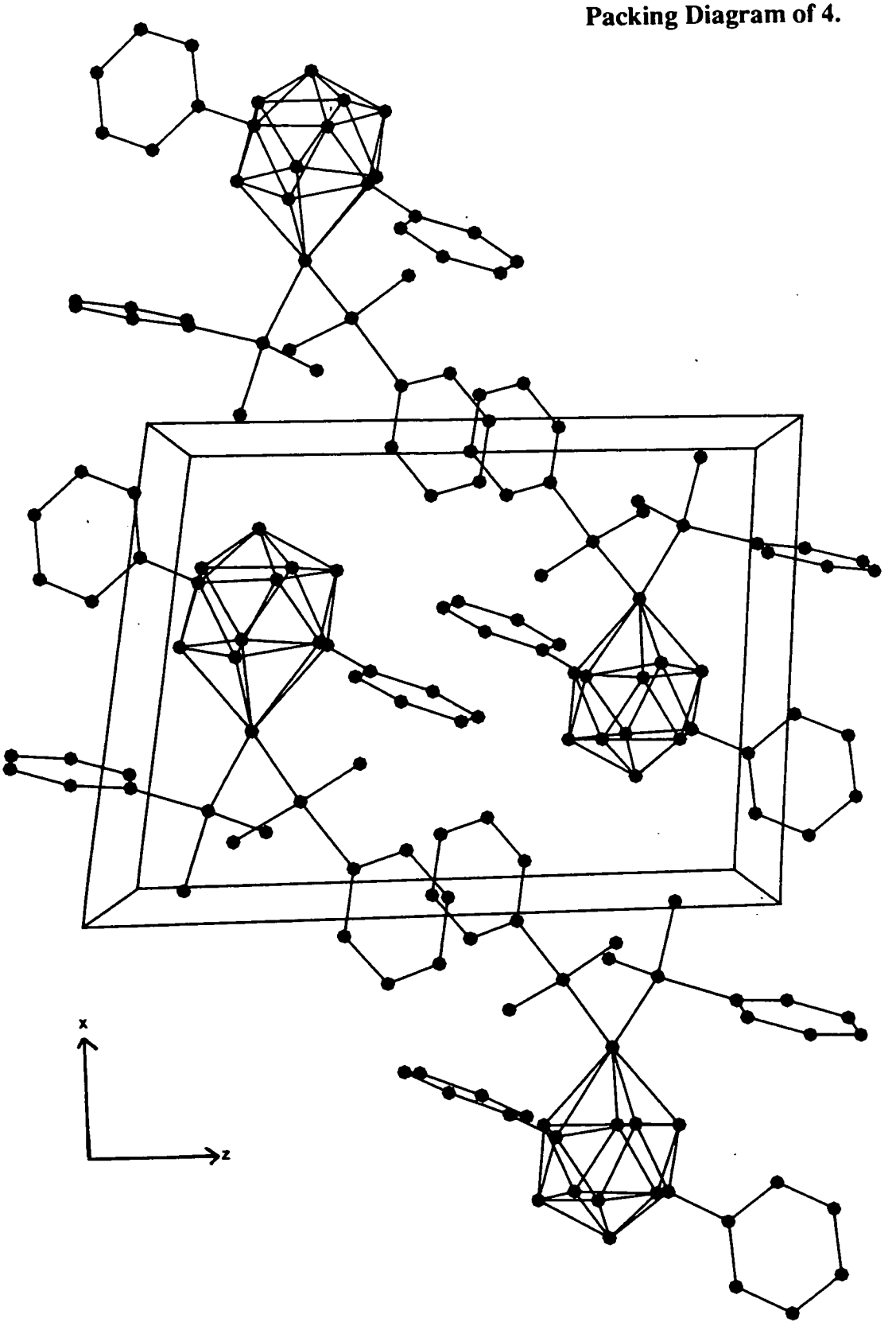

2.12 Consideration of the Factors Leading to the Formation of 4.

In order to examine the factors which lead to the exclusive formation of the rearranged 1,11-Ph_2-3,3-$(PMe_2Ph)_2$-3,1,11-$PtC_2B_9H_9$ isomer, the expected structure of the target compound 1,2-Ph_2-3,3-$(PMe_2Ph)_2$-3,1,2-$PtC_2B_9H_9$ must be considered. A symmetrically di-substituted carbaborane would be expected to give rise to frontier molecular orbitals with similar characteristics to those of the unsubstituted carbaborane. Hence, the $\{PtP_2\}$ fragment is predicted to lie perpendicular to the idealised cage mirror plane. However, in this conformation there would be a severe unfavourable steric interaction between the cage-phenyl groups and the metal fragment, which could not be alleviated by a simple rotation of this fragment. This steric crowding at the metal-bonded face is thought to lower the barrier to rearrangement sufficiently to allow isomerisation to occur at room temperature.

It is believed that the 3,1,2-isomer must initially be formed and that this then spontaneously isomerises to the 3,1,11-form. The basis for this is that a range of metalla-complexes have previously been prepared from the same carbaborane ligand source, $[Tl_2C_2B_9H_9Ph_2]$. Some of these have been structurally characterised[43,49,63], and all have the two cage carbons adjacent on the metal-bonded face. From this it can be concluded that the cage carbons are adjacent in the starting material and that they remain adjacent under the conditions employed for the reaction.

An analogous formation and spontaneous isomerisation of a 3,1,2-rhoda-methylphenyl-carbaborane was mentioned earlier[48]. This involves the formation of 1-Me-11-Ph-3,3-$(PEt_3)_2$-3-H-3,1,11-$RhC_2B_9H_9$ from $[(PEt_3)_4Rh][nido$-7-Me-8-Ph-7,8-$C_2B_9H_{10}]$.

Some of the highly distorted metalla-complexes of diphenylcarbaborane were discussed in section 1.8. It may appear surprising that we see a sterically driven

rearrangement when the metal fragment is $\{P_2Pt\}$ yet not in any of these other cases. Even when the fragment is the sterically bulky $\{Cp^*Rh\}$, the cage carbon atoms remain adjacent (although they are not formally bonded to each other)[43]. This suggests that in the case of the $\{P_2Pt\}$ complex a low energy pathway for rearrangement exists, whereas for the $\{Cp^*Rh\}$ complex it does not. However, the spontaneous isomerisation of the 3,1,2-rhoda-methylphenyl-carbaborane species described above, suggests that it is not the difference in the nature of the metal atom which is important but the ligands it bears. A comparison of space-filling diagrams of the {RhCp*} fragment and the $\{Pt(PMe_2Ph)_2\}$ fragment (see figure 2.30) shows that although the Cp* ligand is bulky, the fragment is virtually planar. In contrast, the two phosphine ligands in the $\{PtP_2\}$ fragment appear to be more angularly demanding and hence are likely to interfere with any substituents on the metal-bonded face.

It is not clear what the actual pathway for this rearrangement is. Some suggested mechanisms have been described in section 2.7. If Lipscomb's diamond-square-diamond mechanism[88] is considered, then it can be noted that to go from a 3,1,2-species to a 3,1,11-isomer would require two sets of 6 concerted d.s.d. processes. If the formation of the first cuboctahedral intermediate (or anti-cuboctahedral intermediate) involves cleavage of the C-C bond then this mechanism will lead to the formation of a 3,1,7-species, in which the two carbon atoms are non-adjacent on the metal-bonded face. To form the 3,1,11-isomer another set of 6 d.s.d. processes would have to occur.

If this mechanism was indeed occurring during the formation of **4**, then a complex incorporating the $\{(PMe_2Ph)_2Pt\}$ fragment, of the type $1,7\text{-}Ph_2\text{-}3,1,7\text{-}PtC_2B_9H_9$, would be expected to spontaneously isomerise. Conversely, if a stable complex of this type could be formed, then this would suggest that a d.s.d. mechanism was not important, in this case.

Figure 2.30

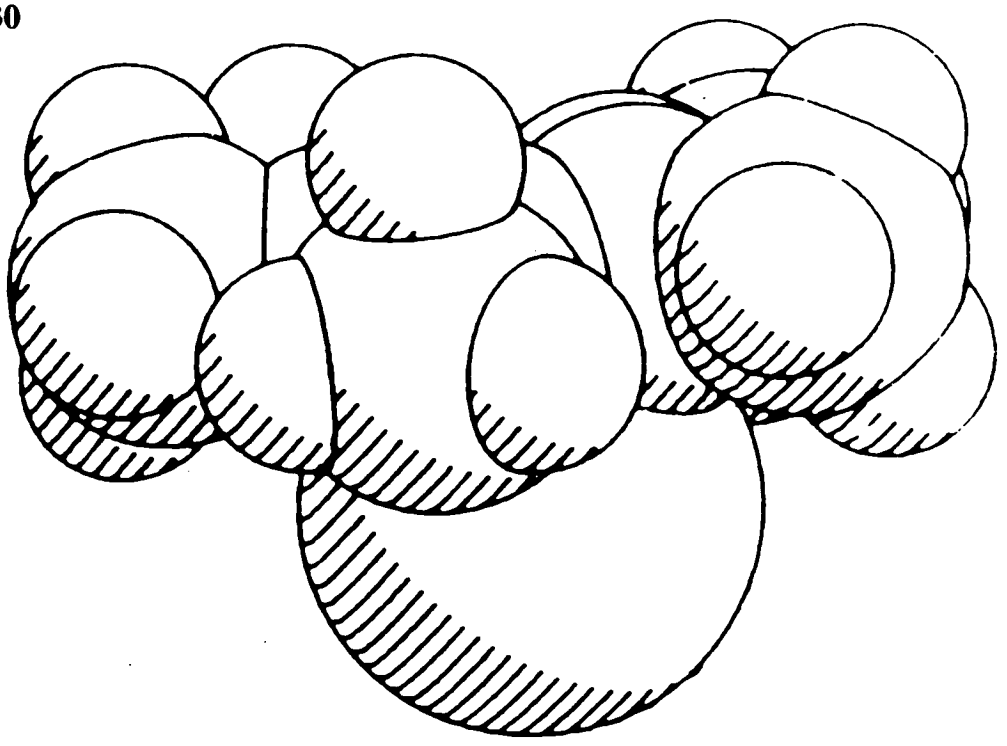

Space-filling Diagrams of the {RhCp*} and {Pt(PMe_2Ph)$_2$} Fragments.

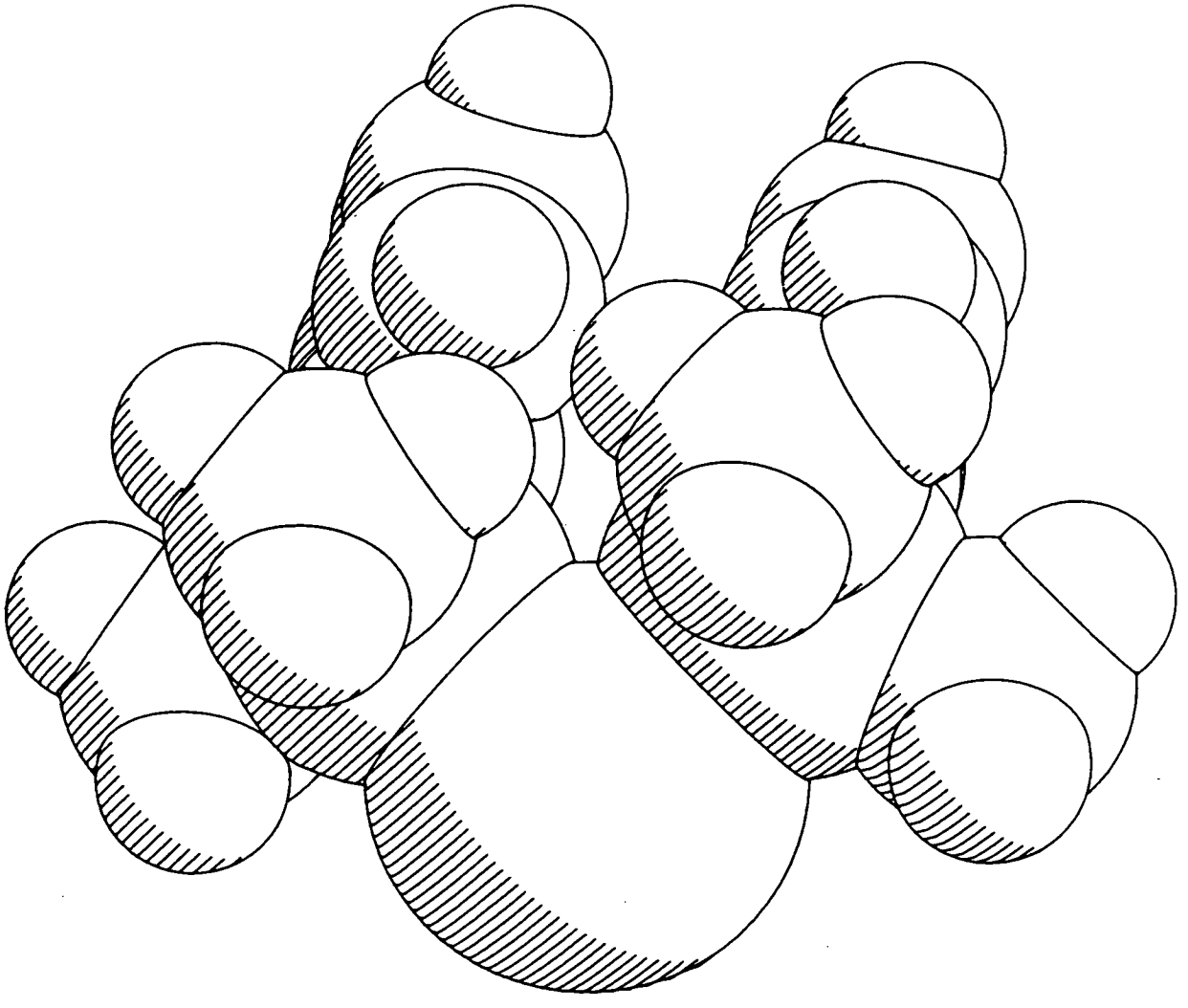

Complexes of this type are known for C,C-dimethyl carbaborane e.g.1,1-$(PMe_2Ph)_2$-2,4-Me_2-1,2,4-$PtC_2B_9H_9$[72] (this is equivalent to the 3,1,7-species). However, the analogous complexes of diphenylcarbaborane have not been reported. Attempted synthesis of such a species would provide worthwhile information as to the rearrangement pathway.

2.13 Conclusions.

Reaction of carbaborane dianions with platinum-bisdimethylphenylphoshine salts readily yield carbaplatinaborane complexes. In the case of the mono-phenyl substituted carbaborane, the 3,1,2-platina-species is formed. This shows a highly distorted icosahedral structure, and has been shown to be ground state destabilised. The destabilisation facilitates a low temperature polytopal rearrangement, to form two isomeric carbaplatinaboranes. However, when the carbaborane is di-phenyl substituted, steric crowding at the metal-bonded face leads to the formation of the 3,1,11-isomer and the 3,1,2-isomer is not isolated.

Chapter 3.

Other Platinum Bis-(Phosphine)-Carbaborane Complexes.

3.1 Introduction.

This chapter describes the effects of varying the phosphorus ligand (P) on complexes of the type $[(P_2Pt)C_2B_9H_{10}Ph]$ and $[(P_2Pt)C_2B_9H_9Ph_2]$. These ligands are classified in terms of their cone angle[97], which gives a measure of their steric influence, and an electronic factor, indicating their ability to act as an electron donor ligand[98]. The effect of varying P on the n.m.r. spectra of the carbaborane complexes is considered. A preliminary investigation into the electrochemistry of these species is also discussed. The phosphorus ligands employed were as follows: PCy_3; $P(p\text{-tolyl})_3$; PPh_3; PEt_3; dppe; PMe_3 and $P(OMe)_3$.

In light of the results described in the previous chapter, where P= PMe_2Ph, the following questions arose: In the case of the $[(P_2Pt)C_2B_9H_{10}Ph]$ complexes- could decreasing the size of P prevent the occurrence of a facile isomerisation? Conversely, could increasing the size of P force this isomerisation to occur spontaneously, at room temperature? For the $[(P_2Pt)C_2B_9H_9Ph_2]$ complexes- could reducing the size of P permit the formation of the unrearranged 3,1,2-platinacarbaborane as an isolatable product?

3.2 The Cone Angle of Phosphorus Ligands.

Changing the substituents on phosphorus ligands can cause marked changes in their metal complexes. Although such variations were often described in terms of the electronic effect of the substituent groups, Tolman[97] recognised that it is often the steric effect of these groups which is dominant. In 1970, he developed an empirical measure of this steric influence- the cone angle. He used this to account for the observed stabilities of complexes of the type NiP_4, to ligand substitution. The cone angles were measured using CPK molecular models.

The cone angle (Θ), for a symmetric ligand (*i.e.* one in which the three substituents are the same) is defined as the apex angle of a cylindrical cone, centred 2.28Å from the middle of the phosphorus atom, which just touches the van der Waals radii of the outermost atoms (see figure 3.1). The substituents are oriented such as to give the smallest possible cone angle. In the case of an asymmetrically substituted phosphorus ligand ($PX_1X_2X_3$) an approximate group addivity is employed[99]. This assumes that the orientation of a substituent in $P(X_1)_3$, which minimises the cone angle, is the same as that which minimises Θ in $PX_1X_2X_3$. Hence, Θ can be defined as $2/3\Sigma_{i=1}^{3}\ \Theta_i/2$.

Figure 3.1

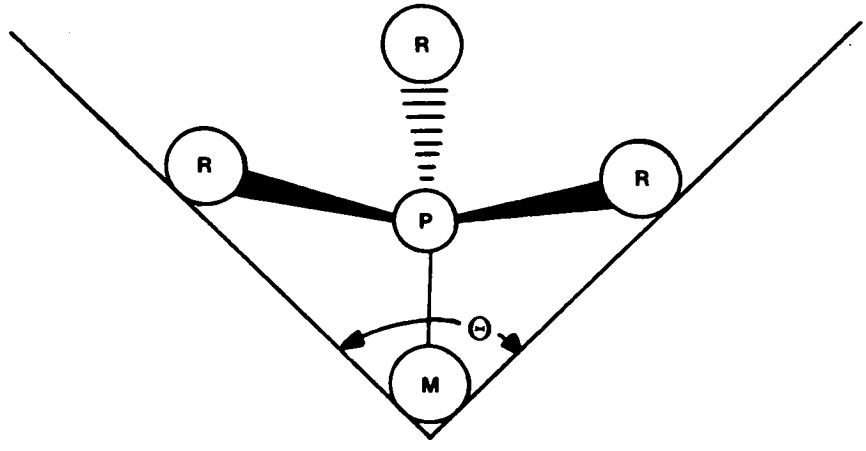

The simple model-based method of determination of Θ has a number of limitations. While for ligands with fixed geometries or few internal degrees of freedom (*e.g.* PMe_3), the cone angle can be measured to within ±2°, for ligands with more degrees of freedom (*e.g.* PCy_3), Θ can only be estimated within ±10°. The possibility also arises, for more complex ligands, that the minimum cone angle may introduce strain, and may not, realistically, be attained. Even symmetric ligands may not exhibit cylindrical symmetry in real complexes. For example, in the species $[Au(PPh_3)_3]^+$[100], the ligands are meshed together allowing a graphitic interaction between certain phenyl rings.

The P-M bond length was assumed to be 2.28Å, but in real complexes substantial variation from this may occur. However, Tolman[99] calculated that even a relatively large deviation from this value would not alter the cone angle by more than 3 or 4°. In any case, when complexes of the same metal are being compared, the M-P distance will be virtually constant. Finally, the geometry at the phosphorus centre was taken to be tetrahedral. However, for ligands with small cone angles, the observed angles at the phosphorus centre are considerably less than 109.5°. With increasing cone angle these angles tend towards the tetrahedral value. When angles at the phosphorus atom are below 109.5° this leads to an over-estimation of Θ.

In an attempt to overcome these difficulties, a number of alternative methods of measuring Θ have been developed[101] which are based on computer modelling or mathematical techniques. However, for the purposes of the current work, Tolman's cone angles were considered to provide an adequate measure of the steric influence of phosphorus ligands. Indeed, Tolman has provided a convincing description of the variation of a number of physical properties with these simply determined values of Θ[99]. The cone angles for the phosphorus ligands employed in this, and the previous chapters, are given in table 3.1[99].

Table 3.1 The Cone Angles of Selected Phosphorus Ligands.

Ligand	Cone Angle(Θ)/°
$P(OMe)_3$	107
PMe_3	118
PMe_2Ph	122
dppe	125
PEt_3	132
PPh_3	145
$P(p\text{-}tol)_3$	145
PCy_3	170

3.3 The Electronic Influence of Phosphorus Ligands.

An electronic factor for phosphorus ligands was defined in terms of the A_1 stretching frequency of the (CO) groups in complexes of the type $Ni(CO)_3P$. The position of this band can be measured with an accuracy of $\pm 0.3 cm^{-1}$. The smaller the value of ν_{CO} the more basic the ligand. A similar method of ranking phosphorus ligands was suggested by Strohmeier[102], but that utilised here was reported by Tolman, in 1970[98]. The value of ν for $P(o\text{-}tol)_3$ and $P(p\text{-}tol)_3$ (which posess cone angles which differ considerably) are virtually identical (2066.6 and $2066.7 cm^{-1}$, respectively). This indicates that ν is truly a measure of electronic effects and is not related to a steric factor. The values of ν for the ligands employed in this and the previous chapters are given in table 3.2[99].

Table 3.2 The Electronic Factor of Selected Phosphorus Ligands.

Ligand	ν_{CO} (cm^{-1})
PCy_3	2056.1
PEt_3	2061.7
PMe_3	2064.1
PMe_2Ph	2065.3
$P(p\text{-}tol)_3$	2066.7
dppe	(2067.3)
PPh_3	2068.9
$P(OMe)_3$	2079.5

The value for dppe was estimated using the substituent additivity relationship: $\nu = (2056.1 + a_1 + a_2 + a_3)cm^{-1}$, for P123 [99] and taking 1 and 2 to be Ph and 3 to be Me (a_i is the additivity constant for substituent i).

In the following sections a series of (P_2Pt)-carbaborane complexes are described in order of increasing cone angle of the phosphorus ligand (P).

3.4 Platinum Bis-(trimethylphoshite)-Carbaborane Complexes.

The reaction between $Tl_2C_2B_9H_{10}Ph$ and *cis*-$PtCl_2(P(OMe)_3)_2$ was carried out in CH_2Cl_2, yielding a soluble product. This was separated and purified by column chromatography (alumina/CH_2Cl_2). A mobile yellow band was collected and yielded a crystalline solid, **5**, in moderate yield, on removal on solvent *in vacuo*. The i.r. spectrum of this species (CH_2Cl_2) indicates the presence of borane (νB-H= 2540cm^{-1}) and the $P(OMe)_3$ ligand (ν= 1175 and 1040cm^{-1}). The $^{31}P\{^1H\}$ n.m.r. spectrum of **5** consists of a singlet (at δ= 104.95p.p.m.), with doublet satellites ($^1J^{195}$Pt-P= 5478.0Hz.) (see figure 3.2). These resonances show some structure, although an AB pattern is not fully resolved. This indicates that there is some restriction to rotation of the $\{PtP_2\}$ fragment, at room temperature, on the n.m.r. timescale.

The large Pt-P coupling constant observed is typical of platinum bis-phosphite complexes[103] and arises as follows. The major factor influencing the coupling is believed to be the degree of s-character in the σM-P bond[40]. This is increased by the presence of π-acceptor substituents on the phosphorus atom which increase the p-character of the phosphorus-substituent bonds and, hence, increase the s-character of the phosphorus-metal bond. Similarly, in ligands with small cone-angles, the SPS (substituent-phosphorus-substituent) angle is less than the tetrahedral angle implying increased p-character in the substituent-phosphorus bond, thereby increasing the s-character of the phosphorus-metal bond. Both these effects may be important here, the phosphite ligand being more electronegative than a phosphine ligand, while possessing a smaller cone angle. Hence, the observed increase in platinum-phosphorus coupling constant may be understood.

The $^{11}B\{^1H\}$ spectrum of **5** consists of 7 resonances, in the ratio 1:1:2:2:1:1:1 (see figure 3.3).

Figure 3.2

$^{31}P\{^{1}H\}$ n.m.r. spectrum of 5, 81.020MHz., 25°C (298K).

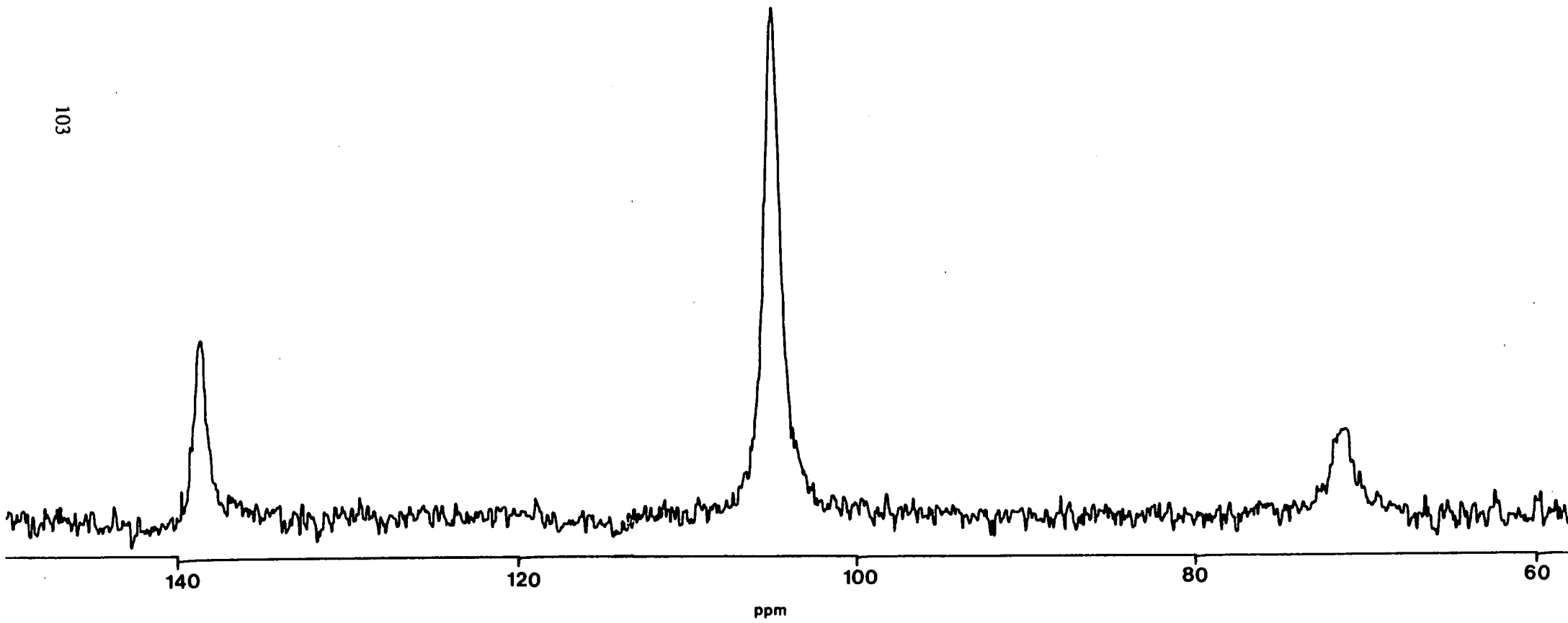

Figure 3.3

$^{11}B/^{11}B\{^1H\}$ n.m.r. spectra of 5, 64.210MHz., 25°C (298K).

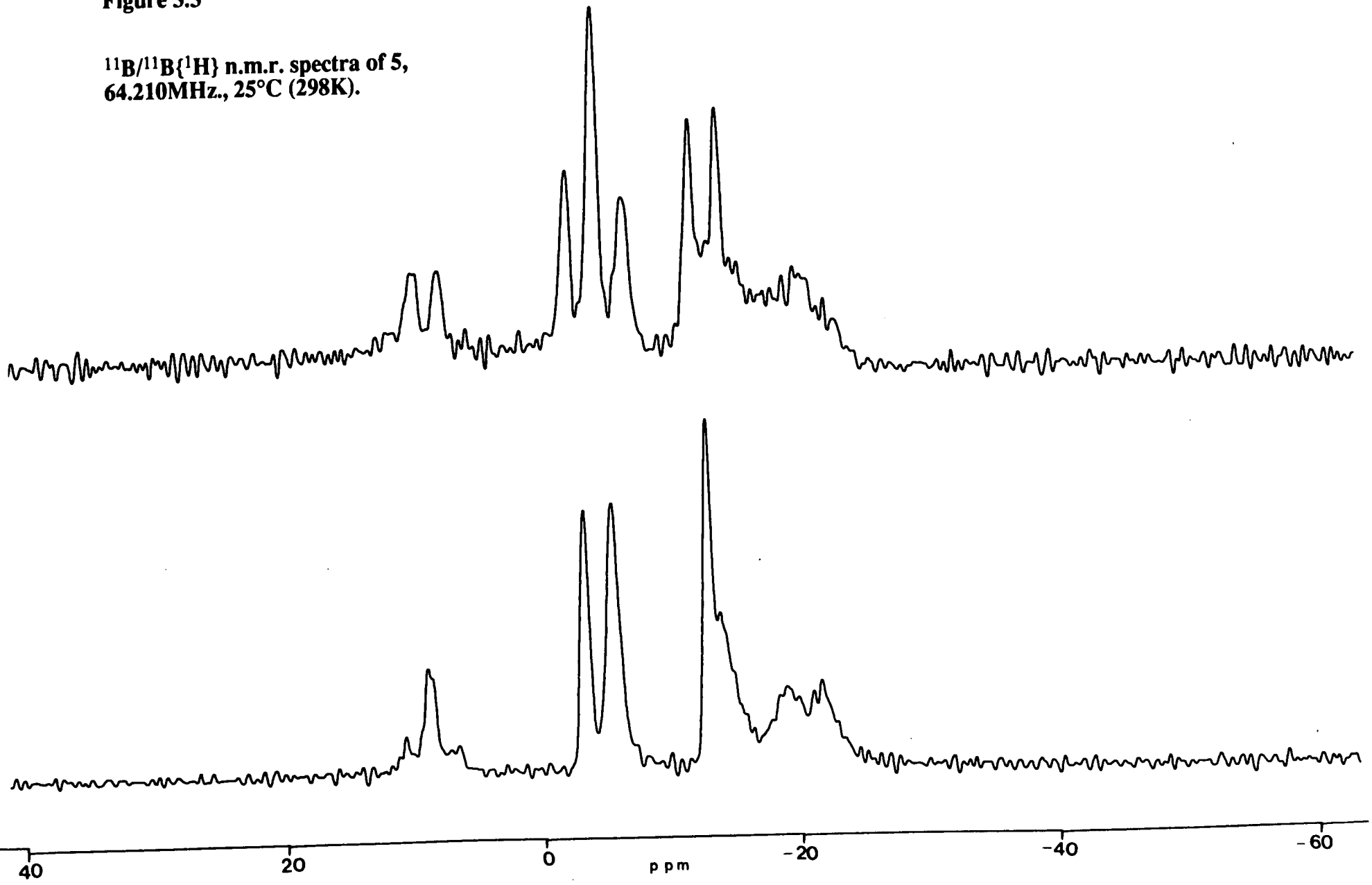

There is a high frequency signal (at δ = +8.97p.p.m.) suggesting the presence of a C_2B_3 metal-bonded face. This boron nucleus shows coupling to the Pt nucleus ($^1J^{195}$Pt-P= 260Hz.). Additionally, in the H-coupled ^{11}B spectrum, each resonance exhibits coupling to a proton, in the range ^{1}JB-H= 110-150Hz. The ^{1}H n.m.r. spectrum of **5** shows 4 signals (see figure 3.4). There are two resonances due to the cage phenyl protons; a doublet (δ= 7.48p.p.m.,^{3}JH-H = 6.6Hz.) integrating for two protons and a multiplet (centred on 7.15p.p.m.) integrating for 3 protons. The signal corresponding to the cage C-H appears at 4.21p.p.m., while that due to the phosphito-protons is an apparent triplet centred on 3.53p.p.m. and integrating for 18 protons. The second-order nature of this signal is typical of phosphito-metal complexes[104] and arises as follows[105]. There is a 3 bond coupling between a proton and the phosphorus nucleus in the same phosphite group. This can be estimated from the two outer lines of the signal, and is typically *circa.* 10Hz. (in **5** ^{3}JH-P = 12.6Hz.). Additionally, there is a 4 bond ^{195}Pt-H coupling of about 2.5Hz. The two phosphorus nuclei in a given platinum bis-phosphite moiety are chemically equivalent but magnetically inequivalent. Thus, there will also be a weak coupling between a given proton and the phosphorus of the other phosphite moiety, 5 bonds away. This coupling increases the separation of the two outer lines of the signal and leads to a slight over-estimation of ^{3}JH-P. These small couplings give rise to the complex signal observed. From the evidence presented above, it was concluded that **5** was an analogous species to **1**, with the $\{Pt(P(OMe)_3)_2\}$ fragment bound to the C_2B_3 carbaborane face, *i.e.* 1-Ph-3,3-$(P(OMe)_3)_2$-3,1,2-$PtC_2B_9H_{10}$.

Figure 3.4

^{1}H n.m.r. spectrum of 5, 200.130MHz., 25°C (298K).

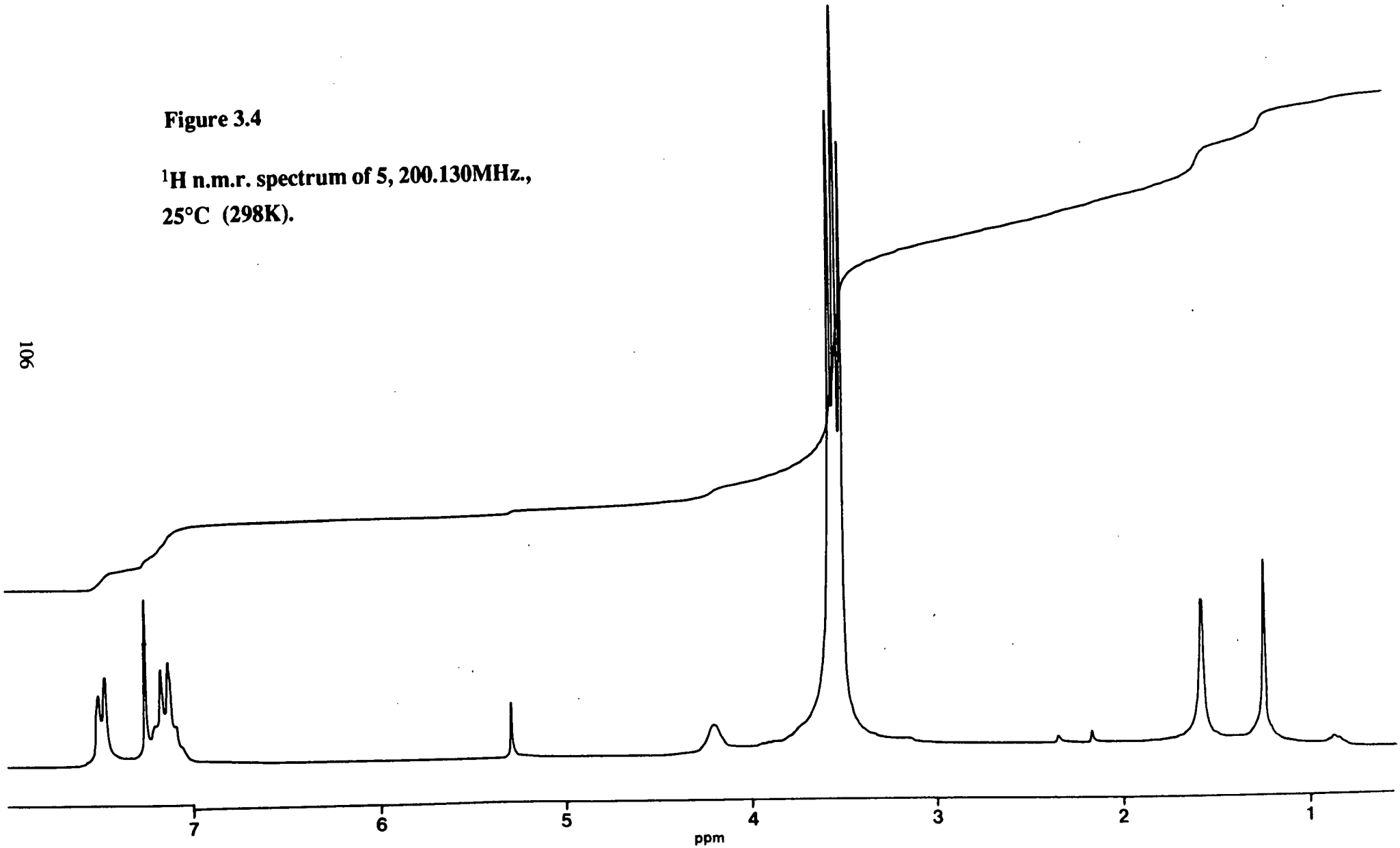

A sample of **5** was heated in toluene, at reflux temperature, for 30 minutes. On removal of solvent *in vacuo* a pale yellow solid was afforded, and the n.m.r. spectra of this residue were recorded. The $^{11}B\{^1H\}$ spectrum ($CDCl_3$) consists of 5 resonances, in the range δ= -5.65p.p.m. to -20.53p.p.m., in the ratio 3:1:1:2:2. Crucially, there is no longer a high frequency boron resonance. The proton coupled spectrum contains 5 doublets with ^{1}JB-H in the range 130Hz. to 160Hz., indicating that each boron atom is bound to a terminal hydrogen atom.

The $^{31}P\{^1H\}$ spectrum of the thermolysis product is a singlet at δ= 114.99p.p.m. with doublet satellites ($^1J^{195}$Pt-P= 5388.6Hz.) (see figure 3.5). This suggests that a single product has been formed, in which there is free rotation about the platinum-cage axis. However, the ^{1}H n.m.r. spectrum indicates that there are, in fact, two species present, in the approximate ratio 2:1 (see figure 3.6). Each of these shows an apparent triplet arising from the (OMe) protons (centred on δ= 3.71p.p.m., and with ^{3}JP-H = 12.6Hz., for the major species and at 3.15p.p.m. with ^{3}JP-H = 17.0Hz., for the minor species). There are resonances due to the cage C-H at δ= 2.82p.p.m. and 1.83p.p.m. for the major and minor products, respectively. The more abundant product shows two signals in the phenyl region of the spectrum, centred on δ 7.41p.p.m. and 7.13p.p.m., which are both multiplets. Similarly, the other product gives rise to 2 multiplets in the phenyl region, centred on δ 7.44p.p.m. and 7.21p.p.m..

Figure 3.5

$^{31}P\{^{1}H\}$ n.m.r. spectrum of the product(s) of thermolysis of 5, 81.020MHz., 25°C (298K).

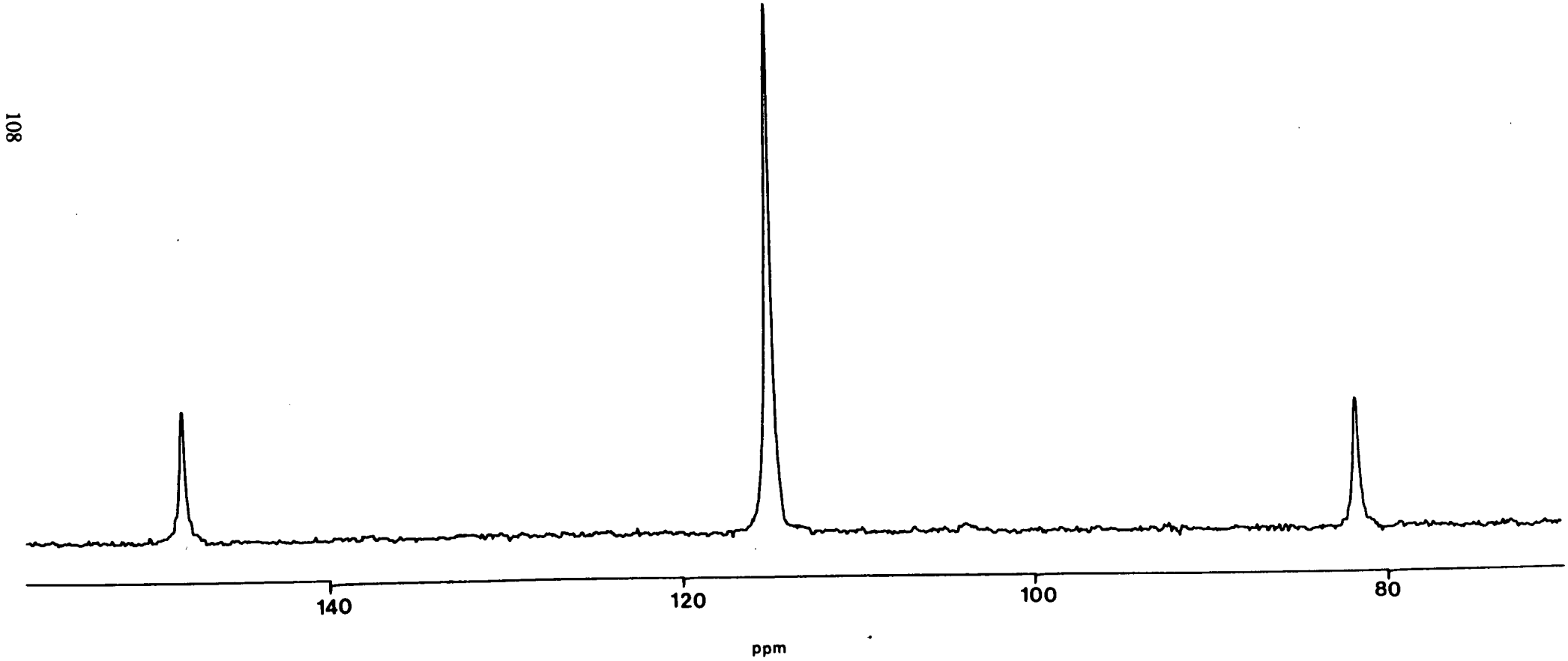

Figure 3.6

^{1}H n.m.r spectrum of the product(s) of thermolysis of 5, 200.130MHz., 25°C (298K).

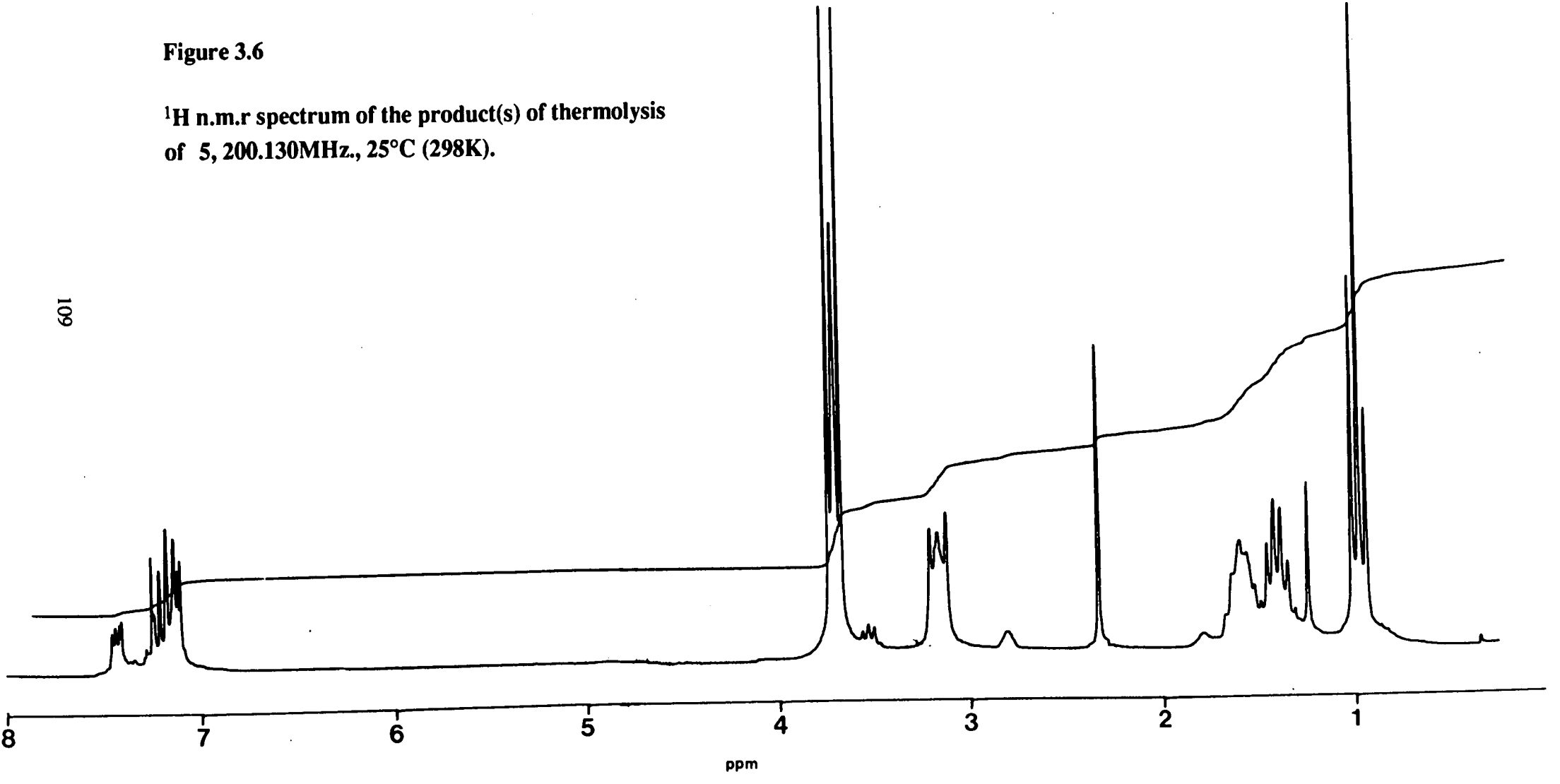

The similarity between the spectra of these 2 products suggests that they are isomeric and may be analogues of **2** and **3** with the formulae 1-Ph-3,3-$(P(OMe)_3)_2$-3,1,11-$PtC_2B_9H_{10}$ and 11-Ph-3,3-$(P(OMe)_3)_2$-3,1,11-$PtC_2B_9H_{10}$. However, it is not clear which of these isomers corresponds to the major observed product and which to the minor. With the relatively sterically undemanding $P(OMe)_3$ ligand on the metal fragment, the thermodynamically-favoured product would be expected. For the isomerisation of **1** this appeared to be **3**, with the Ph substituent remaining on the metal bonded face. However, this was believed to be favoured due to a stabilising intramolecular interaction involving a phosphino-phenyl group which would not be possible in the alkyl-phosphito complex. In addition, the relatively strong π-acceptor phosphite ligands may give rise to a less slipped structure for the carbaborane complex than would be predicted for the analogous phosphine complex, in which case the steric interaction between the metal-fragment and the cage-carbon substituent would be greater. This may favour the formation of the 3,1,11-isomer in which the metal-bonded face is less sterically crowded.

There are further anomalies resulting from this thermolysis reaction. The proton spectrum of the products contains 3 extraneous peaks. Two of these appear to be 6-line patterns centred on δ= 1.40p.p.m. and 1.59p.p.m., in the ratio 1:1, both with coupling constants of about 7Hz., while the other signal is a triplet at 0.98p.p.m. exhibiting similar coupling. This could suggest that some decomposition has occurred. However, this would be expected to result in the appearance of some extra signals in the ^{31}P n.m.r. spectrum. This consists only of one sharp singlet with 2 sharp satellites and indeed the existence of 2 isomerisation products can only be rationalised by assuming these have identical chemical shifts and coupling constants.

Given these problems of identifying the products little can be concluded about this reaction. An attempt was made to overcome them by recording the n.m.r. spectra in a

different solvent. If there were indeed 2 phosphito-complexes present the chemical shifts may become sufficiently different from each other for two signals to be observable. However, in d_6-acetone there was extensive decomposition to yield a white, insoluble material and this reaction was not pursued further.

When $Tl_2C_2B_9H_9Ph_2$ was reacted with *cis*-$PtCl_2(P(OMe)_3)_2$ in CH_2Cl_2, a soluble orange product was obtained. This was separated from the reaction mixture and purified by column chromatography. An orange mobile band was collected and this yielded an orange solid on removal of solvent *in vacuo*. Subsequent attempts at further chromatographic purification indicated that there may be more than one compound present (or the product may undergo decomposition in solution) but a suitable set of conditions to allow adequate separation of these constituents could not be found. The spectra of the crude product, **6**, were therefore recorded.

The solution i.r. spectrum of **6** (CH_2Cl_2) shows the presence of borane (ν= 2535cm^{-1} (B-H)) and the $P(OMe)_3$ moiety (ν= 1170cm^{-1}, 1110cm^{-1} and 1010cm^{-1}). In the $^{11}B\{^1H\}$ spectrum ($CDCl_3$) there are 9 resonances, in the range δ= -5.70p.p.m. to -35.05p.p.m., each due to one boron atom. The proton coupled spectrum indicates that all of these are bonded to terminal hydrogen atoms, with ^1JB-H in the range 110 to 170Hz. The $^{31}P\{^1H\}$ spectrum of **6** consists of a poorly resolved AB signal at δ= 114.4p.p.m. which appears as a broad singlet with a little structure, from which a mutual P-P coupling of 26Hz. can be estimated. Similarly the doublet satellites are ill-resolved and only an average platinum-phosphorus coupling constant can be measured ($^1J^{195}$Pt-P= 5325.5Hz.). This is indicative of there being restricted rotation about the Pt-cage bonding, resulting in the observation of two different phosphorus environments within the same molecule.

The ^1H n.m.r. spectrum of **6** is complex, confirming the impurity of the sample. There are two signals in the (OMe) region of the spectrum, a second order pattern

centred on δ 3.75p.p.m. and a doublet of doublets centred on δ 3.54p.p.m., with coupling constants of 18.3Hz. and 6.1Hz., respectively. In the phenyl region there are 5 signals, 3 of which are complex multiplets (centred on δ 6.91p.p.m., 7.04p.p.m. and 7.20p.p.m.). In addition, there is a doublet of doublets at δ 7.46p.p.m. showing couplings of 8.2Hz. and 1.7Hz. and a second order resonance centred on δ 7.55p.p.m.

From these spectra it was concluded that the major constituent of the crude product mixture was the analogous species to **4**, namely 1,11-Ph_2-3,3-$(P(OMe)_3)_2$-3,1,11-$PtC_2B_9H_9$. Hence, even with the the relatively small phosphorus ligands on the metal fragment, the 3,1,2-isomer is not isolatable and is, presumably, spontaneously isomerised to the 3,1,11-isomer. As described before, however, the π-acceptor phosphite ligands may induce a less slipped structure in the carbametallaborane, in which there is a greater steric interaction between the metal fragment and the cage substituents than would be predicted purely from consideration of the ligand cone angle. This steric interaction may lead to the observed facile isomerisation.

3.5 Platinum Bis-(trimethylphosphine)-Carbaborane Complexes.

The reaction between $Tl_2C_2B_9H_{10}Ph$ and *cis*-$PtCl_2(PMe_3)_2$, in CH_2Cl_2, yields several products. The major product was separated from the others by two-stage column chromatography (alumina/CH_2Cl_2 followed by alumina/3:1 CH_2Cl_2). This yielded a yellow crystalline solid on recrystallisation from CH_2Cl_2/Et_2O.

This product, **7**, was characterised by i.r. and n.m.r. spectroscopies. The solution i.r. spectrum (CH_2Cl_2) confirms the presence of borane (ν= 2510cm^{-1}). The $^{11}B\{^1H\}$ n.m.r. spectrum consists of 7 signals in the ratio 1:1:1:1:1:3:1, including a high frequency resonance at δ +11.51p.p.m. which shows coupling to the metal nucleus of 270Hz. The proton coupled spectrum contains 7 doublets with ^{1}JB-H in the range 120 to 170Hz. (see figure 3.7). The $^{31}P\{^1H\}$ spectrum of **7** consists of one singlet (at δ = -42.79p.p.m.) with doublet satellites ($^1J^{195}$Pt-P= 3240.3Hz.). This suggests there is rapid rotation about the platinum-cage axis at room temperature, on the n.m.r. timescale, which renders the phosphorus nuclei equivalent. The ^{1}H n.m.r. spectrum contains a broad signal at δ 2.16p.p.m. which integrates for 18 protons and can be assigned to the methyl protons. There is a resonance at δ 3.77p.p.m. due to the single cage C-H and two multiplets denoting the phenyl protons centred on δ 7.16 and 7.54p.p.m. integrating for 3 and 2 protons, respectively. From this data it was concluded that **7** was analogous to **1**, with the formula 1-Ph-3,3-$(PMe_3)_2$-3,1,2-$PtC_2B_9H_{10}$.

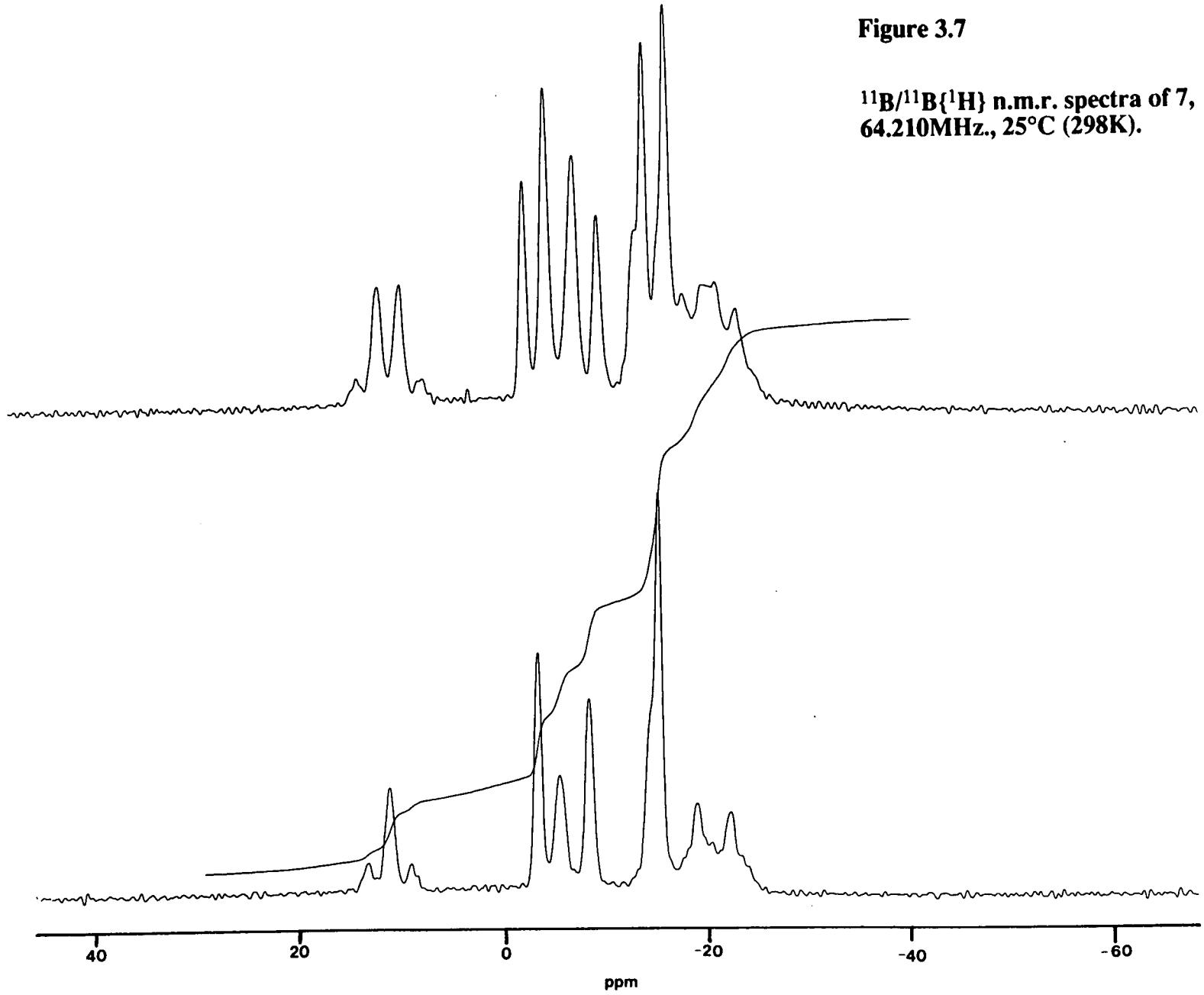

Figure 3.7

$^{11}B/^{11}B\{^{1}H\}$ n.m.r. spectra of 7, 64.210MHz., 25°C (298K).

Heating a sample of **7** in toluene produced a pale yellow product mixture. The $^{11}B\{^1H\}$ n.m.r. spectrum of this consists of 8 signals, in the range δ= -4.99 to -24.34p.p.m., in the ratio 1:1:1:1:1:1:2:1. The proton coupled spectrum comprises 8 doublets with ^{1}JB-H in the range 130-160Hz. The $^{31}P\{^1H\}$ n.m.r. spectrum consists of a singlet at δ= -19.98p.p.m. with doublet satellites ($^1J^{195}$Pt-P= 3278.7 Hz.). The three peaks are all extremely broad but show no fine structure (see figure 3.8), suggesting that there may be two distinct complexes present with similar chemical shifts and coupling constants. Alternatively, there may simply be one complex in which hindered rotation about the Pt-cage bonding renders the phosphorus nuclei inequivalent.

The proton spectrum contains three resonances in the methyl region of the spectrum; a complex multiplet centred on δ 1.58p.p.m., an apparent triplet centred on δ 1.73p.p.m. and with $|^2$JP-H + ^{4}JP-H$|$ = 9.6Hz (estimated from the separation of the 2 outer lines[105]) and a small apparent triplet at δ = 3.15 with $|^2$JP-H + ^{4}JP-H$|$ ≈15Hz. A resonance denoting a cage C-H proton appears at δ 2.53p.p.m. and there are 3 multiplets in the phenyl region of the spectrum (centred on 7.04, 7.10 and 7.42p.p.m.). The complexity of this spectrum suggests there may be more than one species present. It can be tentatively suggested that there are two complexes present, of a similar nature to the 3,1,11-isomers discussed elsewhere.

Figure 3.8

$^{31}P\{^{1}H\}$ n.m.r. spectrum of the products of thermolysis of 7, 81.020MHz., 25°C (298K).

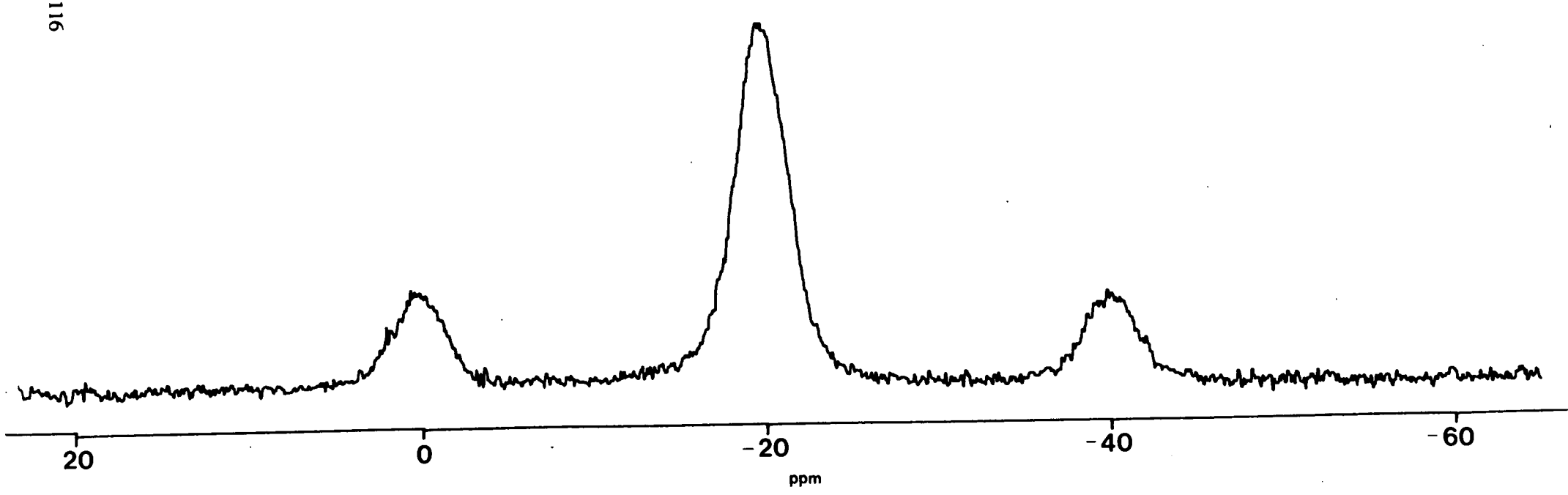

When $Tl_2C_2B_9H_9Ph_2$ and *cis*-$PtCl_2(PMe_3)_2$ were stirred in CH_2Cl_2, an orange/brown soluble product was formed, along with TlCl. Separation was effected by column chromatography, whence the brown mobile band yielded a brown solid, **8**, on removal of solvent *in vacuo*. The $^{11}B\{^1H\}$ n.m.r. spectrum of **8** consists of a broad envelope (from δ= -5.30p.p.m. to -23.67p.p.m.) within which 5 resonances can be distinguished. The proton coupled spectrum indicates that each boron atom is attached to a terminal hydrogen atom (^{1}JB-H= 140-160Hz.). The $^{31}P\{^1H\}$ spectrum consists of two signals (at δ= -26.22p.p.m. and -27.12p.p.m.) each with doublet satellites ($^1J^{195}$Pt-P= 3225.0Hz. and 3210.9Hz., respectively). These inequivalent phosphorus nuclei show a small mutual coupling of less than 10Hz., indicating that they occur within a single molecule, in which there is hindrance to rotation about the metal-cage axis. The ^1H n.m.r. spectrum of **8** consists of a multiplet centred on δ 1.59p.p.m. denoting the methyl protons and two multiplets centred on δ 7.30 and 7.51p.p.m. due to the phenyl protons.

The absence of a high frequency boron resonance in the ^{11}B n.m.r. spectrum, together with the observation of 2 signals in the ^{31}P n.m.r. spectrum, suggest that a polytopal rearrangement has occurred. If this is assumed to be of a similar nature to that giving rise to **4**, then **8** can be concluded to be 1,11-Ph_2-3,3-$(PMe_3)_2$-3,1,11-$PtC_2B_9H_9$.

3.6 Platinum (Dppe)-Carbaborane Complexes.

Dppe (diphenylphosphinoethane, $Ph_2PCH_2CH_2PPh_2$) is markedly different from the other phosphorus ligands utilised in this work, in that it acts as a bidentate ligand. Co-ordination of this ligand to the metal atom was assumed to preclude any processes involving subsequent cleavage of one of the Pt-P bonds, due to the chelate effect.

When $Tl_2C_2B_9H_{10}Ph$ and $PtCl_2$(dppe) were reacted, in CH_2Cl_2, a yellow soluble product was formed along with TlCl. Chromatographic purification readily afforded a lemon yellow solid, **9**, in moderate yield. The solution i.r. spectrum of **9** indicates the presence of borane (νB-H = 2510cm^{-1}). The $^{11}B\{^1H\}$ n.m.r. spectrum ($CDCl_3$) consists of 6 resonances in the ratio 1:2:1:3:1:1. The highest frequency of these (at δ= 14.18p.p.m.) shows coupling to the platinum nucleus of 300Hz. and can be tentatively assigned to B(8). The proton- coupled spectrum is 6 doublets (with ^1JB-H= 130-160Hz.) confirming that each boron atom is bound to a terminal hydrogen atom.

The $^{31}P\{^1H\}$ n.m.r. spectrum of **9** is a singlet (at δ = 48.21p.p.m.) with doublet satellites ($^1J^{195}$Pt-P = 3286.8Hz.). This is consistent with there being rapid rotation about the Pt-cage axis, on the n.m.r. timescale, which renders the two phosphorus atoms equivalent. The ^1H n.m.r. spectrum is complex. There is a second order signal centred on δ 2.20p.p.m. arising from the $C\underline{H}_2$ protons in the dppe ligand. The cage C-$\underline{H}$ resonates at δ 3.20p.p.m. and there are 4 multiplets in the phenyl region of the spectrum (centred on δ 6.61p.p.m., 7.26p.p.m., 7.51p.p.m. and 7.72p.p.m.) From this spectroscopic evidence it was concluded that **9** has the formula 1-Ph-3-dppe-3,1,2-$PtC_2B_9H_{10}$.

A sample of **9** was dissolved in toluene and heated at reflux temperature for 30 minutes, during which time the solution became lighter in colour. Removal of the

solvent *in vacuo* yielded a pale yellow residue. The $^{11}B\{^1H\}$ n.m.r. spectrum of this residue consists of 5 resonances in the range δ = -7.26p.p.m. to -21.25p.p.m. The high frequency resonance observed in the spectrum of **9** is no longer present, indicating that the thermolysis product does not contain a C_2B_3 face. The $^{31}P\{^1H\}$ n.m.r. spectrum of this product is a singlet at δ= 46.52p.p.m. with doublet satellites, ^1JPt-P= 3377.6Hz. (see figure 3.9), suggesting that a single isomerisation product had been formed, in which there is facile rotation about the metal-cage axis. The ^1H n.m.r. spectrum contains a broad signal centred on δ 2.63p.p.m. corresponding to the $C\underline{H}_2$-protons. The cage C-$\underline{H}$ resonates at δ 3.27p.p.m. and there are three signals in the phenyl region. Two of these are multiplets, centred on δ 7.25p.p.m. and 7.75p.p.m., while the third is a 12.3Hz. doublet (at δ 7.53p.p.m.). Assignment of the last three of these resonances was not possible.

Thus, thermolysis of **9** gives rise to one product, believed to be one of the two possible 3,1,11-isomers. Identification of which of the two had been formed was not possible. The fact that only one was produced can be explained using a number of different approaches. Although the dppe ligand has a relatively small cone angle it is fairly rigid, hence the metal fragment is less flexible than one bearing two mono-dentate phosphorus ligands and, consequently, there is less scope for avoidance of steric interaction between the metal fragment and the cage carbon substituents. This potential steric crowding at the metal-bonded face may favour the sole formation of the less crowded 3,1,11-isomer *i.e.* 11-Ph-3-(dppe)-3,1,11-$PtC_2B_9H_{10}$.

Alternatively, **9** may isomerise via a different pathway to the other carbaplatinaborane complexes, due to rupture of a Pt-P bond being relatively disfavoured in this case. The alternative mechanism may favour rearrangement to one or other of the two 3,1,11-isomers.

Figure 3.9

$^{31}P\{^{1}H\}$ n.m.r. spectrum of the thermolysis product of 9, 81.020MHz., 25°C (298K).

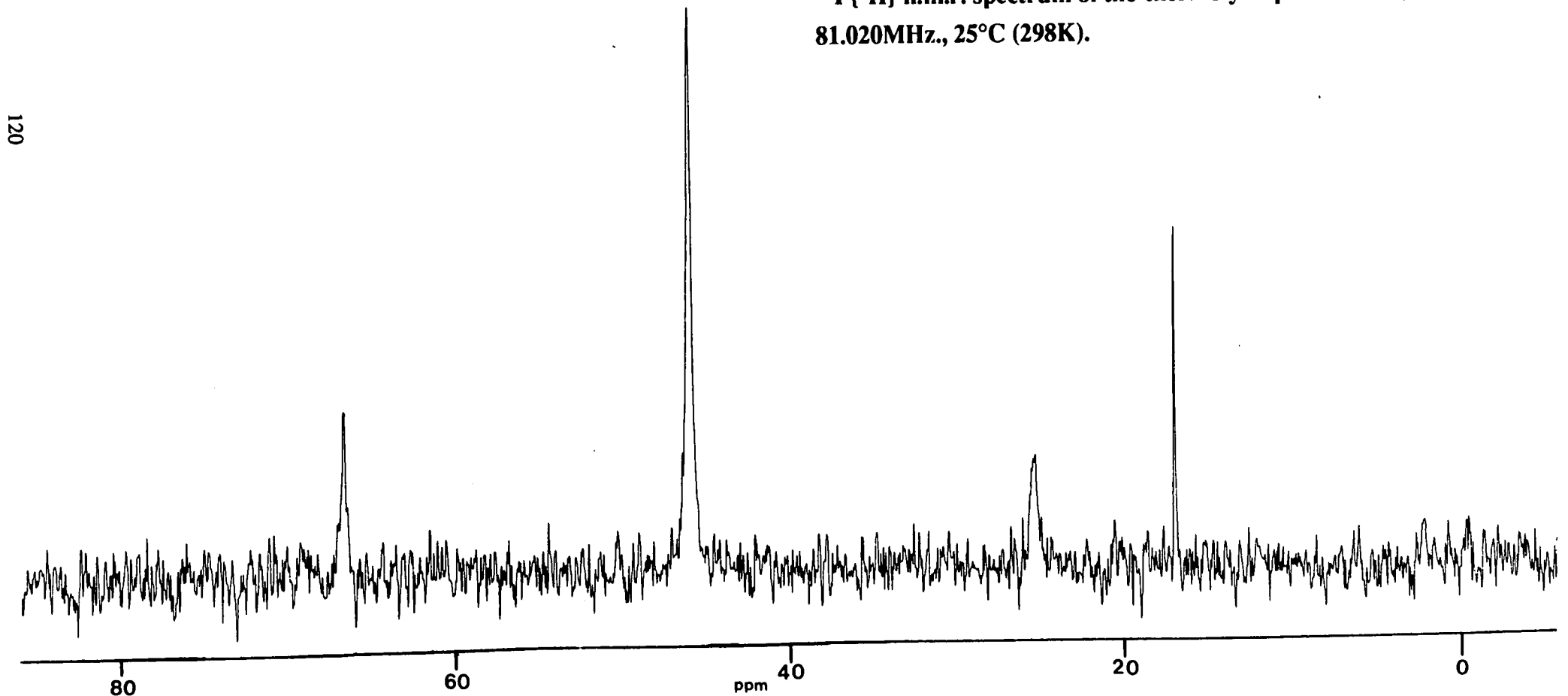

Even if the rearrangement pathway of **9** is similar to that of the other complexes described, the co-ordination of a bidentate ligand may sufficiently alter the geometry and nature of bonding at the metal centre to favour rearrangement to only one of the isomers. The fact that a 3,1,11-isomer is formed, at all, indicates that, for this specific complex, the pathway must not involve a phosphine dissociation step.

The reaction between $Tl_2C_2B_9H_9Ph_2$ and $PtCl_2$(dppe) was attempted by a similar method to that employed previously to yield a deep yellow product, **22**. The i.r. spectrum (CH_2Cl_2) confirms the presence of borane (νB-H= 2540cm^{-1}) and of dppe (ν= 1410cm^{-1}, broad). The $^{11}B\{^1H\}$ n.m.r. spectrum of this species shows 8 resonances in the ratiol:1:1:1:2:1:1:1in the range δ = -1.78p.p.m. to -34.98p.p.m. Each of these signals becomes a doublet in the proton coupled spectrum, with ^{1}JB-H in the range 120 to 170Hz. The complex is prone to decomposition and during spectral accumulation a white precipitate is slowly deposited. From the $^{31}P\{^1H\}$ n.m.r. spectrum there is evidence that this is the salt $[PtCl_4]^{2-}[Pt(dppe)_2]^{2+}$. There is also a less intense signal denoting a second non-carbaborane containing platinum-phosphine complex. The complex **22** exhibits two phosphorus environments which give rise to singlets at δ= 44.55p.p.m. with $^1J^{195}$Pt-P= 3268.8Hz. and δ= 46.17p.p.m. with $^1J^{195}$Pt-P= 3296.6Hz. The peaks show evidence for a small (<5Hz.) PP coupling (see figure 3.10). The inequivalence of the two nuclei suggests there is restricted rotation about the metal-fragment to cage bonding. The ^{1}H n.m.r. spectrum is complex in the phenyl region of the spectrum, showing 6 broad multiplets. The signal denoting the dppe-C$\underline{H}_2$ protons is broad, centred on δ= 2.3p.p.m. From the above evidence it was concluded that **22** was the 3,1,11-isomer, 1,11-Ph_2-3-dppe-3,1,11-$PtC_2B_9H_9$.

The isolation of this skeletal isomer suggests that rearrangement occurs via a route which does not involve cleavage of the metal-phosphorus bond.

Figure 3.10

$^{31}P\{^{1}H\}$ n.m.r. spectrum of 22, 81.020MHz., 25°C (298)K.

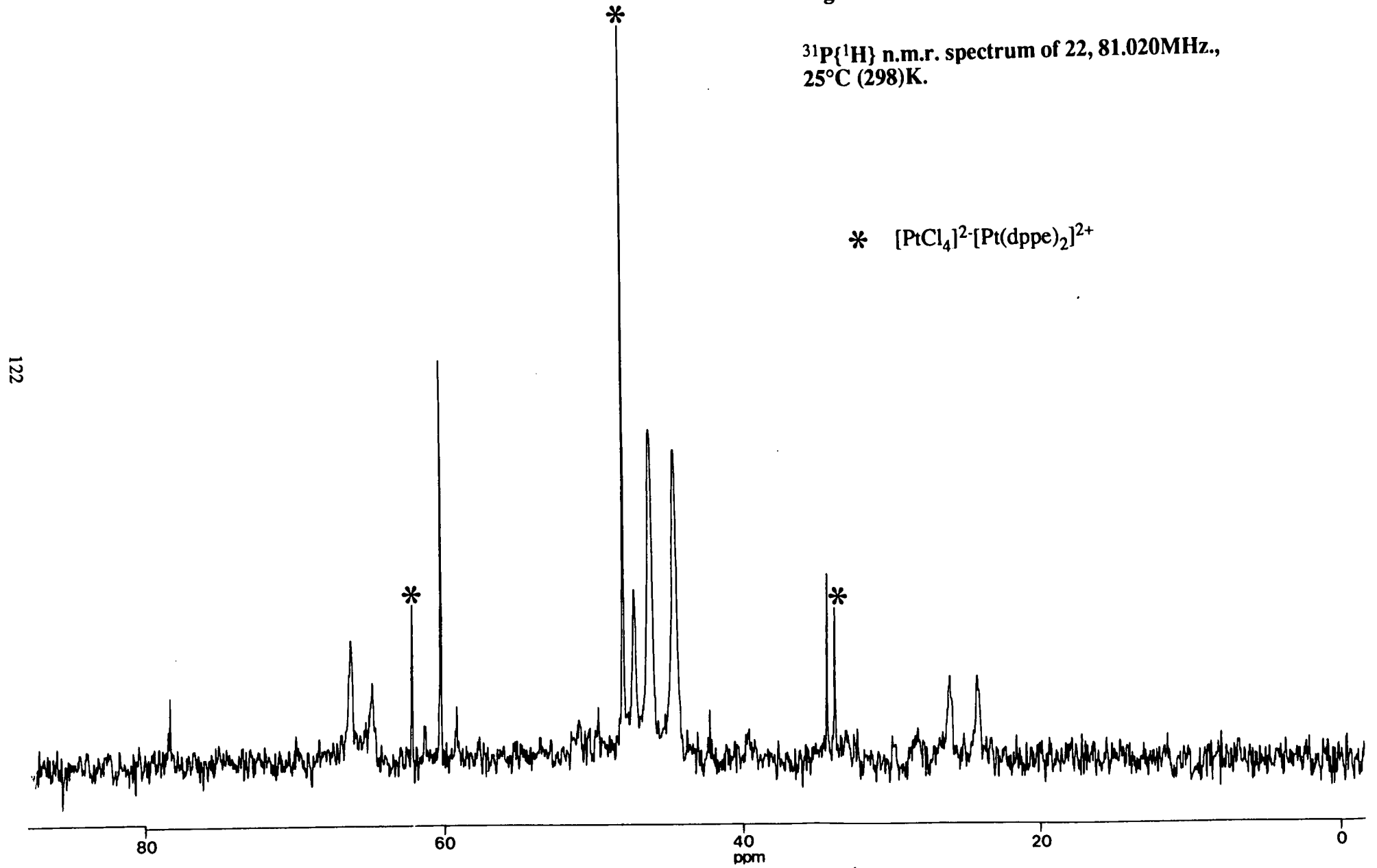

3.7 Platinum Bis-(triethylphosphine)-Carbaborane Complexes.

The reaction of $Tl_2C_2B_9H_{10}Ph$ with *cis*-$PtCl_2(PEt_3)_2$ was carried out to yield an orange-red soluble product. Recrystallisation from CH_2Cl_2/Et_2O afforded orange-red crystals, **10**. Microanalysis was consistent with the formulation $B_9C_{20}H_{45}P_2Pt$, molecular weight 639.6. A solution i.r. spectrum of **10** confirms the presence of borane (νB-H = 2530cm^{-1}). The $^{11}B\{^1H\}$ n.m.r. spectrum of **10** consists of 8 resonances, in the ratio 1:1:1:1:2:1:1:1 (see figure 3.11). The signal at highest frequency (δ = +13.87p.p.m.) shows coupling to the platinum nucleus ($^1J^{195}Pt$-B= 254Hz.) and can tentatively be assigned to B(8). The proton coupled spectrum comprises 8 doublets with ^1JB-H in the range 120-160Hz.

The $^{31}P\{^1H\}$ n.m.r. spectrum of **10** consists of two singlets (at δ= +13.68p.p.m. and +8.59 p.p.m.) each with doublet satellites ($^1J^{195}Pt$-P= 3038.5Hz. and 3388.0Hz., respectively) (see figure 3.12). There is a mutual coupling between the two phosphorus nuclei of approximately 10Hz. indicating that the two phosphorus environments exist within the one molecule, probably as a result of there being restricted rotation of the $\{Pt(PEt_3)_2\}$ fragment over the asymmetrically substituted C_2B_3 face, on the n.m.r. timescale.

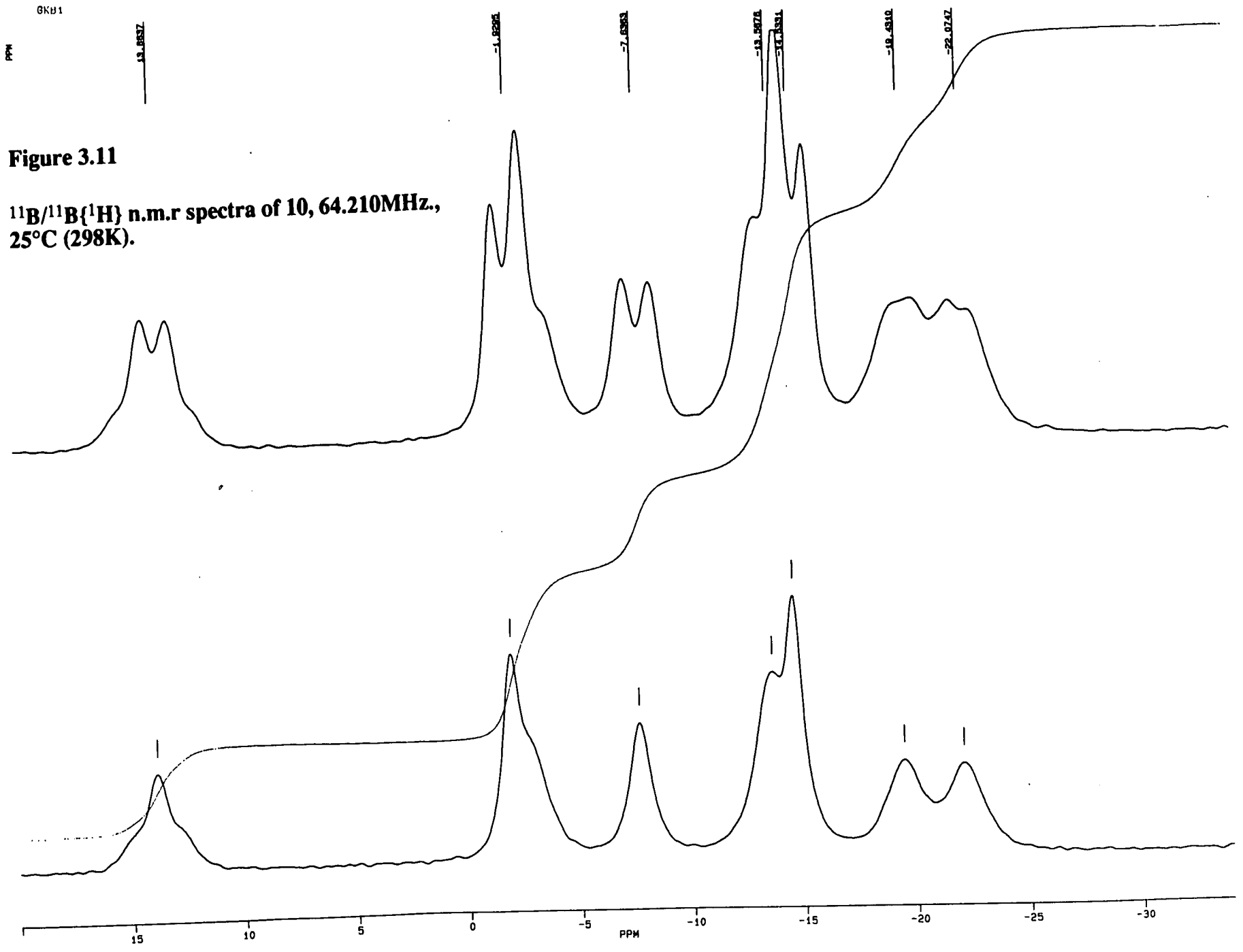

Figure 3.11

$^{11}B/^{11}B\{^{1}H\}$ n.m.r spectra of 10, 64.210MHz., 25°C (298K).

Figure 3.12

$^{31}P\{^{1}H\}$ n.m.r spectrum of 10, 81.020MHz., 25°C (298K).

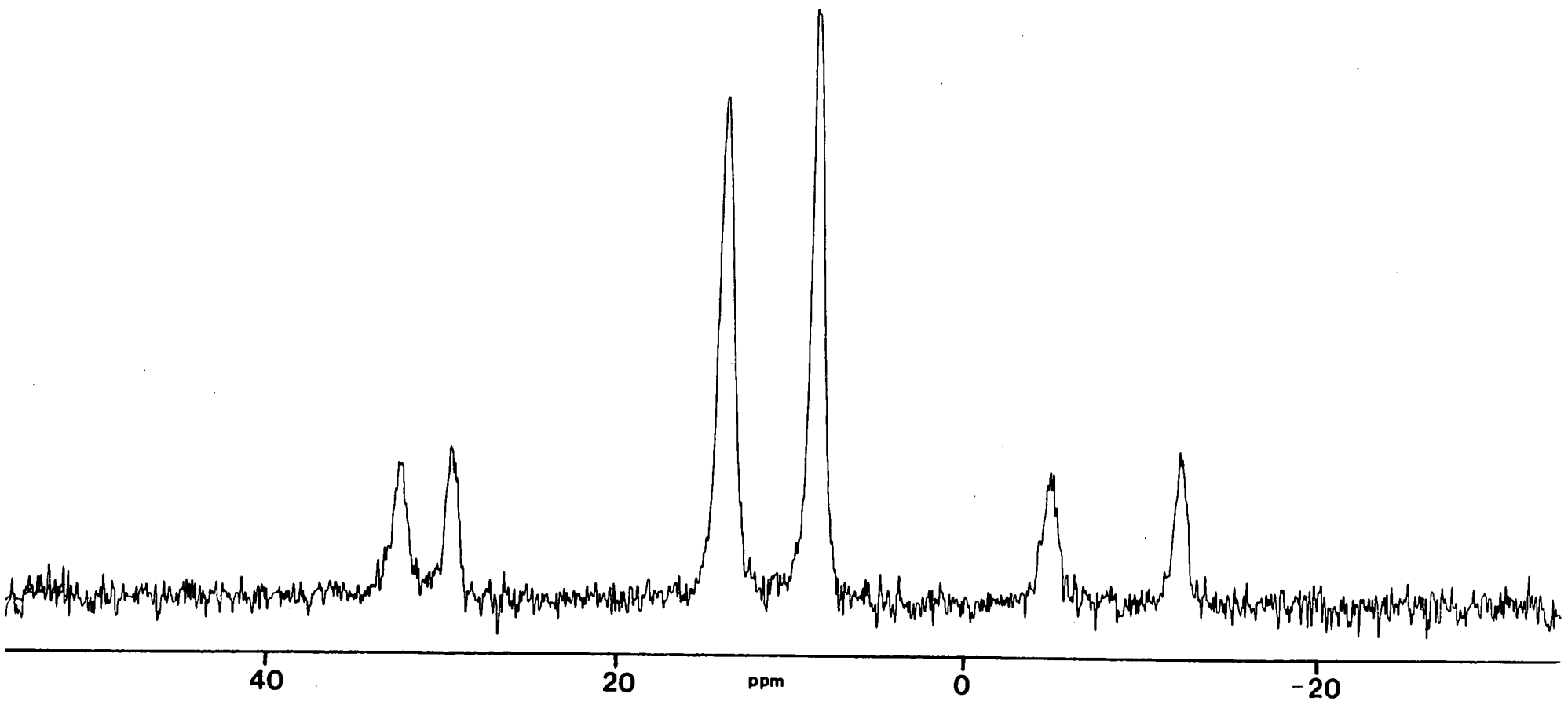

Figure 3.13

^{1}H n.m.r. spectrum of 10, 200.130MHz., 25°C (298)K.

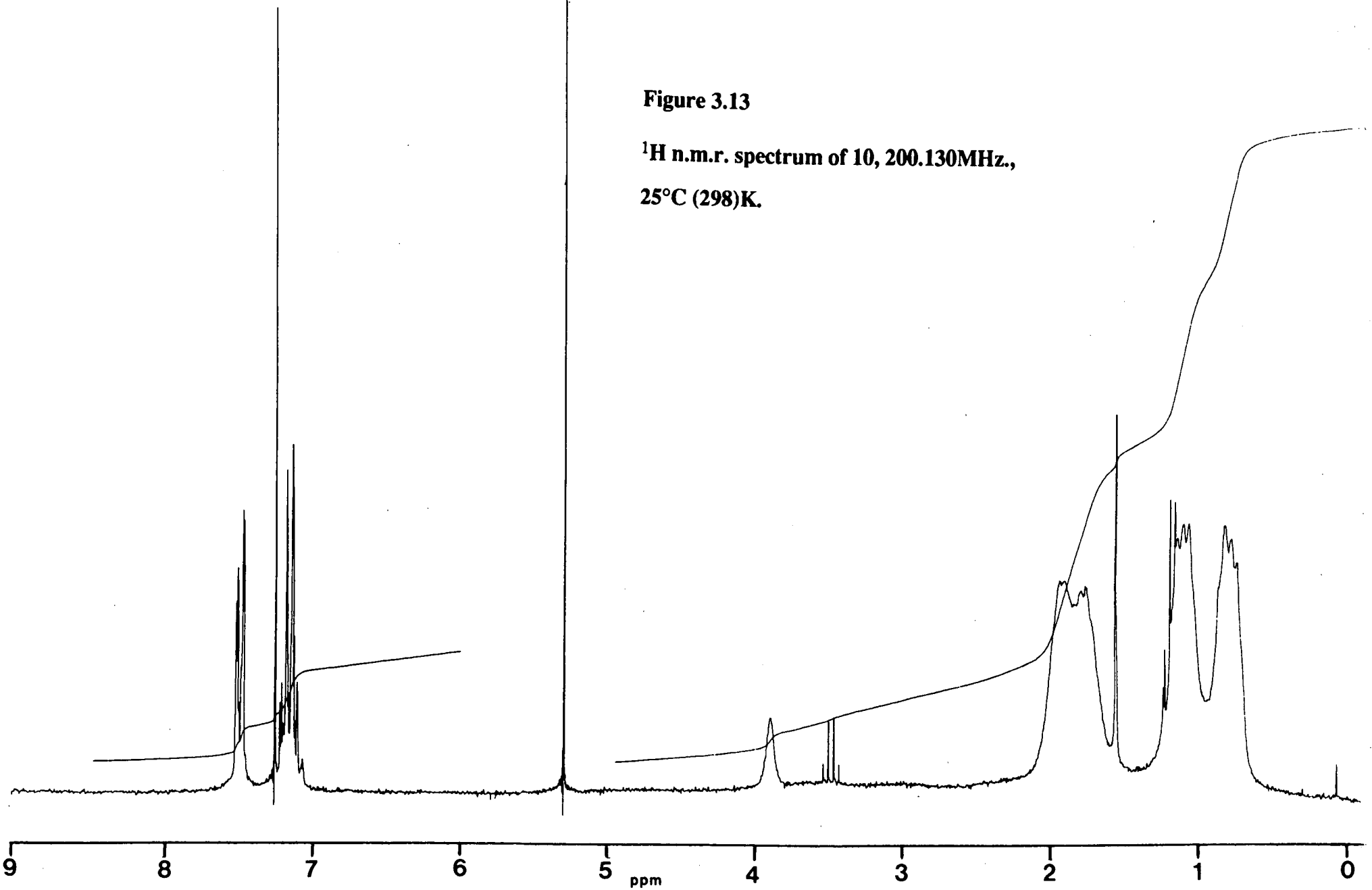

The ^{1}H n.m.r. spectrum of **10** is second order in the ethyl region (see figure 3.13).

There are 2 broad signals centred on δ= 1.80 and 1.93p.p.m., corresponding to the 2 inequivalent sets of $C\underline{H}_2$ protons, and 2 broad resonances centred on δ= 0.83 and 1.12p.p.m. due to the $C\underline{H}_3$ groups. The cage C-H resonates at δ 3.89p.p.m. while there are two signals corresponding to the phenyl protons. The first of these is a doublet of doublets centred on δ 7.49p.p.m. with coupling constants of 9Hz. and 1.5Hz. and integrating for 2 protons. The other signal is a complex multiplet, centred on δ 7.13p.p.m, which integrates for 3 protons. From the available data it was concluded that **10** was analogous to **1** with the formula 1-Ph-3,3-$(PEt_3)_2$-3,1,2-$PtC_2B_9H_{10}$.

When a sample of **10** was dissolved in toluene and heated at reflux temperature for 30 minutes a pale yellow product mixture was produced. The $^{11}B\{^{1}H\}$ n.m.r. spectrum consists of six signals in the range δ= -4.73p.p.m. to -23.63p.p.m. The high frequency boron resonance, indicative of the presence of a C_2B_3 metal-bonded face, is no longer present. The $^{31}P\{^{1}H\}$ n.m.r. spectrum indicates that are were two products in the mixture, in the ratio of greater than ten to one (see figure 3.14). The major product contains two different phosphorus environments which give rise to signals at δ +7.82p.p.m. and 6.56p.p.m. each of which shows coupling to the platinum nucleus ($^{1}J^{195}Pt$-P= 3257.0Hz. and 3288.3Hz., respectively). There is a small coupling, of less than 10Hz., between these two nuclei. In contrast, the minor product exhibits only one signal, at δ 4.51p.p.m., with coupling of 3200.2Hz., to the platinum nucleus.

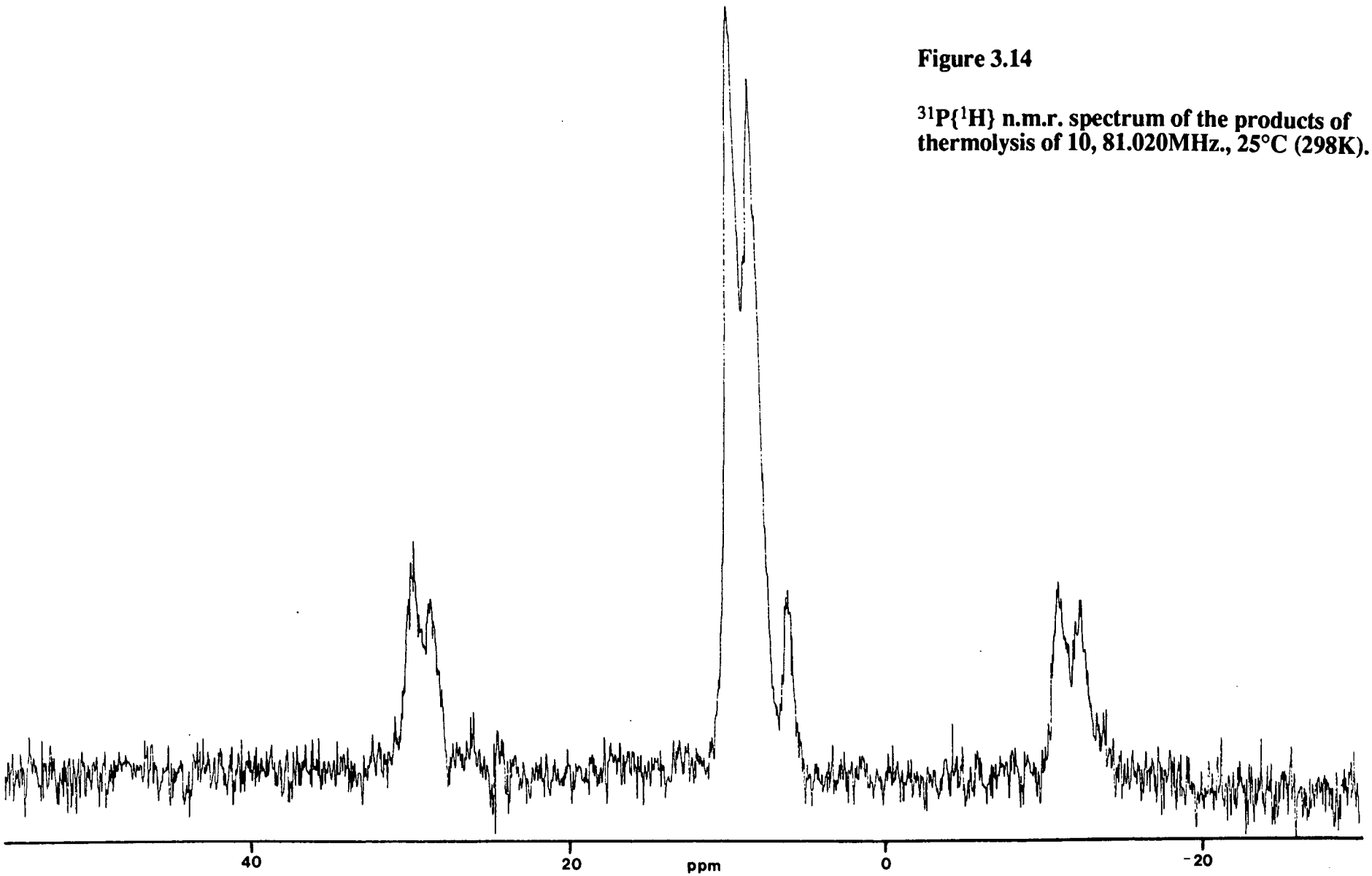

Figure 3.14

$^{31}P\{^{1}H\}$ n.m.r. spectrum of the products of thermolysis of 10, 81.020MHz., 25°C (298K).

Figure 3.15

^{1}H n.m.r. spectrum of the products of thermolysis of 10., 200.130MHz., 25°C (298K).

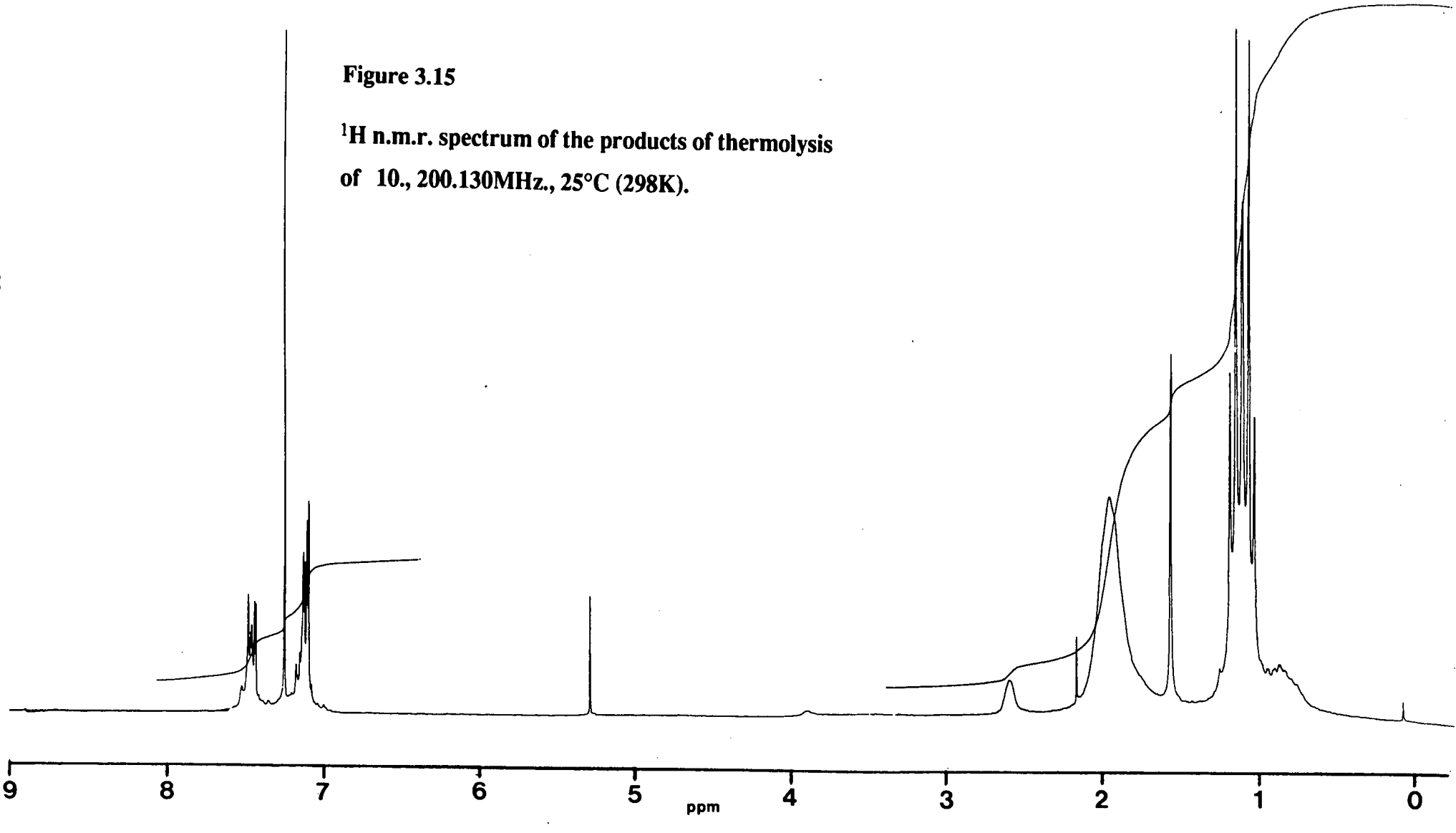

The ^1H n.m.r. spectrum (see figure 3.15) shows a doublet of triplets centred on δ= 1.11p.p.m. (with $^3JP\text{-}H$ = 16.3Hz. and $^3JCH_2\text{-}H$= 7.5Hz.) which integrates for the 18 $C\underline{H}_3$ protons. The signal corresponding to the $C\underline{H}_2$ protons is a broad multiplet, centred on δ 1.94p.p.m. which integrates for 12 protons. The cage C-$\underline{H}$ resonates at δ 2.60p.p.m. and there are two multiplets in the phenyl region at δ 7.13p.p.m. and 7.54p.p.m., representing 3 and 2 protons respectively.

With no further data on these products it is impossible to identify them with any certainty. However, if it is assumed that they are analogous to the rearranged isomers **2** and **3**, then their formation can readily be explained. In **10** the metal fragment is more sterically demanding than it is in **1**, where the phosphine is the smaller PMe_2Ph. Thus, there would be expected to be a greater incentive for rearrangement to the less crowded isomer, analogous to **2**, with the (CPh) unit in position 11. Further, the stabilising intramolecular interaction between the cage-phenyl and the phosphino-phenyl groups, which was noted in **3**, is not possible when the phosphine is tri-alkyl substituted. Therefore, it was concluded that the major thermolysis product is likely to be 11-Ph-3,3-$(PEt_3)_2$-3,1,11-$PtC_2B_9H_{10}$, and the minor one 1-Ph-3,3-$(PEt_3)_2$-3,1,11-$PtC_2B_9H_{10}$.

When $Tl_2C_2B_9H_9Ph_2$ was reacted with *cis*-$PtCl_2(PEt_3)_2$ the major product was a pale orange solid, which was recrystallised to afford yellow crystals of **11**. Microanalysis figures were consistent with the formulation $B_9C_{26}H_{49}P_2Pt$, molecular weight 714.6. The solution i.r. spectrum of **11** indicates the presence of borane (νB-H= 2540cm^{-1}).

The $^{11}B\{^1H\}$ n.m.r. spectrum ($CDCl_3$) consists of 7 resonances in the range δ= -1.74p.p.m. to -24.41p.p.m., in the ratio 1:1:1:1:1:3:1. There is no high frequency boron signal indicating that the product does not contain a C_2B_3 metal-bonded face. The proton coupled spectrum of **11** consists of 7 doublets with $^1JB\text{-}H$ in the range

130Hz.- 150Hz. The $^{31}P\{^{1}H\}$ n.m.r. spectrum shows two signals at δ = +5.76p.p.m. and +4.58p.p.m., which each exhibit coupling to the platinum nucleus ($^{1}J^{195}Pt\text{-}P$= 3206.2Hz. and 3173.1Hz., respectively). There is also a mutual coupling between the two phosphorus nuclei, of 10Hz., indicating that there are two distinct phosphorus environments within a single molecule. While the upper belt is believed to be of the CB_4 type, and therefore has a mirror plane through the carbon atom, the (CPh) on the lower CB_4 belt does not lie in this plane and hence the carbaborane is asymmetric. Therefore, in a static structure, or if there is restricted rotation of the metal-fragment, there will be two different phosphorus environments (see section 3.14).

There are 4 resonances in the phenyl region of the ^{1}H n.m.r. spectrum of **11**. Two are doublets of doublets, each corresponding to 2H, one arising from two protons in each of two inequivalent cage phenyl groups. These occur at δ 7.56p.p.m. with $^{3}JH\text{-}H$ = 10.3Hz. and $^{4}JH\text{-}H$= 1.7Hz. and at δ 7.44p.p.m. with $^{3}JH\text{-}H$= 7.8Hz. and $^{4}JH\text{-}H$ = 1.2Hz. In addition, there are two multiplets at δ 7.16p.p.m. and 7.04p.p.m. each integrating for 3H and corresponding to the other 3 protons in each cage-phenyl moiety. The inequivalence of the two cage-phenyl groups provides strong evidence that the bound carbon atoms have separated. From this and the other spectroscopic data it was concluded that **11** was analogous to **4** with the formula 1,11-Ph_2-3,3-$(PEt_3)_2$-3,1,2-$PtC_2B_9H_9$.

3.8 Platinum Bis-(triphenylphosphine)-Carbaborane Complexes.

When $Tl_2C_2B_9H_{10}Ph$ was reacted with *cis*-$PtCl_2(PPh_3)_2$ an orange soluble product was formed. This was purified by a bulk recrystallisation (CH_2Cl_2/n-hexane) which afforded a fine orange microcrystalline solid **12**, in reasonable yield. Microanalysis figures were consistently found to be too low for the target compound which has the formula $B_9C_{44}H_{45}P_2Pt$, molecular weight 927.8. To establish whether this had indeed been formed, a FAB mass spectrum of **12** was recorded. The principal peaks in this spectrum and their assignments are given in table 3.3. These assignments are based on a molecular ion of formula $[(PPh_3)_2PtC_2B_9H_{10}Ph]^+$, m/z = 928.

Table 3.3 Principal Peaks in the FAB Mass Spectrum of 12.

m/z	Assignment
928	$[(PPh_3)_2PtC_2B_9H_{10}Ph]^+$
719	$[(PPh_3)_2Pt]^+$
642	$[(PPh_2)(PPh_3)Pt]^+$
565	$[(PPh)(PPh_3)Pt]^+$ or $[(PPh_2)_2Pt]^+$
488	$[(PPh)(PPh_2)Pt]^+$
457	$[(PPh_3)Pt]^+$
411	$[(PPh)_2Pt]^+$
380	$[(PPh_2)Pt]^+$

From these results it was concluded that a complex with the composition of the target compound had indeed been formed. A possible explanation for the poor microanalysis figures obtained was that there was incomplete combustion of the

sample.

The i.r. spectrum of **12** (CH_2Cl_2) confirmed the presence of borane (νB-H= 2540cm^{-1}). The $^{11}B\{^1H\}$ n.m.r. spectrum ($CDCl_3$) consists of 7 boron environments in the ratio 1:1:3:1:1:1:1. There is a high frequency boron signal at δ= +21.11p.p.m., which shows coupling to the platinum nucleus of 270Hz. and is indicative of the presence of a C_2B_3 metal-bonded face. The proton coupled spectrum contains 7 doublets indicating that each boron atom is bound to a terminal hydrogen atom (^{1}JB-H= 100-150Hz.). The $^{31}P\{^1H\}$ n.m.r. spectrum of **12** shows the presence of two phosphorus environments (δ= 26.20p.p.m. and 22.25p.p.m.). Each of these resonances is broad and shows some structure, from which a mutual coupling between the two phosphorus nuclei, of approximately 20Hz. can be estimated. This suggests that these different environments arise within the same molecule, as a result of restricted rotation about the platinum-cage bonding. In addition, both signals possess doublet satellites, with $^1J^{195}$Pt-P= 3032.4Hz. and 3438.8Hz., respectively. The ^{1}H n.m.r. spectrum of **12** contains a resonance denoting the cage C-H proton at δ 2.85p.p.m.. There are also two complex multiplets due to the phenyl protons, at δ 6.95 and 7.20p.p.m. From the above evidence it was concluded that a complex analogous to **1** had been formed, namely 1-Ph-3,3-$(PPh_3)_2$-3,1,2-$PtC_2B_9H_{10}$.

When a sample of **12** was warmed at reflux temperature in toluene, the solution lightened in colour. Removal of solvent *in vacuo* yielded an orange residue. The $^{11}B\{^1H\}$ n.m.r. spectrum of this residue ($CDCl_3$) is poorly resolved. However, the absence of a high frequency resonance suggests a change in the nature of the metal-bonded carbaborane face. The $^{31}P\{^1H\}$ n.m.r. spectrum consists of a poorly resolved AB signal at δ= 21.87p.p.m., with doublet satellites ($^1J^{195}$Pt-P= 3408.9Hz.). The resonance is broad, but a mutual P-P coupling of approximately 22Hz. can be observed. This suggests that there is only one thermolysis product, in which there is restricted rotation about the platinum-cage bonding. The ^{1}H n.m.r. spectrum consists

of a signal denoting the cage C-H proton, at δ= 1.57p.p.m. and two resonances in the phenyl region of the spectrum. One of these (at δ 7.45p.p.m.) is broad and structureless, while the other (at δ 7.22p.p.m.) is a complex multiplet. From this evidence it was concluded that thermolysis of **12** gives rise to a single rearranged isomer. It is not clear which of the two possible isomers this is, although, on steric grounds, the isomer with the (CPh) distant from the metal fragment would be favoured *i.e.* 11-Ph-3,3-$(PPh_3)_2$-3,1,11-$PtC_2B_9H_{10}$.

Reaction of $Tl_2C_2B_9H_9Ph_2$ with *cis*-$PtCl_2(PPh_3)_2$, in CH_2Cl_2, yielded an orange soluble product, and TlCl. The former was purified by column chromatography which afforded a yellow solid, **13**. Microanalysis figures were a little low for the target compound of formula $B_9C_{50}H_{49}P_2Pt$, molecular weight 1003.8. However, incomplete combustion of the sample, as for **12**, could account for this discrepancy. The solution i.r. spectrum (CH_2Cl_2) indicated the presence of borane (νB-H= 2540cm^{-1}).

The $^{11}B\{^1H\}$ n.m.r. spectrum ($CDCl_3$) of **13** shows 9 resonances, each corresponding to one boron atom. The highest frequency resonance occurs at δ = +9.30p.p.m., which is in the range where the high frequency boron resonance, in complexes with a C_2B_3 metal-bonded face, has been found to occur. However, in previous cases, when the presence of a C_2B_3 face is proven, this resonance shows a coupling to the platinum nucleus and the next highest resonance is found at approximately 10p.p.m. lower shift. In the case of **13**, however, this resonance shows no coupling to the metal. In fact, the spectrum (see figure 3.16) resembles those of the other 3,1,11-platinacarbaboranes studied (*i.e.* a broad envelope covering a range of 20-40p.p.m.)except that *all* the resonances are at relatively high frequency. It was concluded that the relatively high frequency of this boron resonance was due to the presence of the bulky $\{PtP_2\}$ fragment, rather than being indicative of a change in the nature of the metal-bonded face. The proton coupled ^{11}B spectrum shows a doublet for each signal ($^1JB\text{-}H$= 120-180Hz.) indicating that each boron atom is bonded to a terminal hydrogen atom.

The $^{31}P\{^1H\}$ n.m.r. spectrum of **13** consists of two signals, at δ 24.32p.p.m. and 22.22p.p.m. Each of these possesses doublet satellites ($^1J^{195}Pt\text{-}P$ = 3209.0Hz. and 3305.6Hz., respectively). In addition, there is mutual coupling between the two phosphorus nuclei, of 18.2Hz., indicating that there are two different phosphorus environments within the same molecule. The ^1H n.m.r. spectrum consists of several complex signals denoting the phenyl protons. From this spectroscopic evidence, it was concluded that a complex of a similar nature to **4** had been formed *i.e.* 1,11-Ph_2-3,3-$(PPh_3)_2$-3,1,2-$PtC_2B_9H_9$.

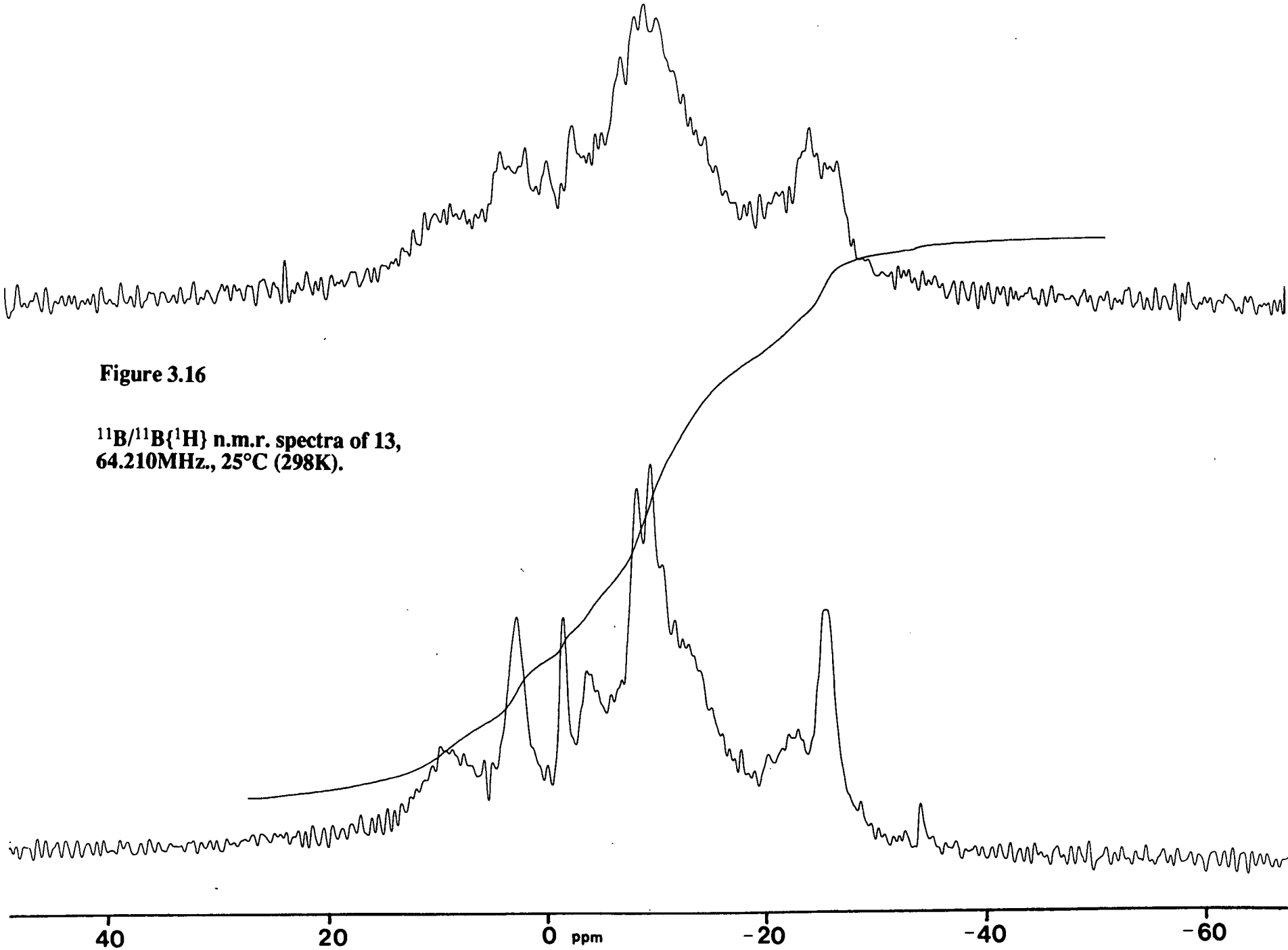

Figure 3.16

$^{11}B/^{11}B\{^{1}H\}$ n.m.r. spectra of 13, 64.210MHz., 25°C (298K).

3.9 Platinum Bis-(tri-p-tolylphosphine)-Carbaborane Complexes.

Tri-p-tolylphosphine has the same cone angle as triphenylphoshine. However, it possesses different electronic properties, being the more basic of the two. Therefore, a comparison of the carbaborane complexes incorporating these fragments may provide information as to the degree, and to which properties, electronic effects are significant.

When $Tl_2C_2B_9H_{10}Ph$ was stirred with *cis*-$PtCl_2(P(p\text{-}tol)_3)_2$, in CH_2Cl_2, an orange soluble product and TlCl were formed. Purification was effected by column chromatography (alumina/CH_2Cl_2) which yielded an orange microcrystalline product, **14**.

The solution i.r. spectrum of **14** (CH_2Cl_2) indicates the presence of borane (νB-H= 2540cm^{-1}) and the $P(p\text{-}tol)_3$ ligand (ν= 1490 and 1440cm^{-1}). The $^{11}B\{^1H\}$ n.m.r. spectrum ($CDCl_3$) is poorly resolved. However, seven resonances can be identified including one at δ= +20.19p.p.m. which shows coupling to the platinum nucleus of approximately 280Hz. In the proton coupled spectrum, there are 7 doublets indicating that each boron atom is bonded to a terminal hydrogen atom (^{1}JB-H= 100-150Hz.). The $^{31}P\{^1H\}$ spectrum shows two phosphorus resonances, at δ= 24.33p.p.m. and 20.33p.p.m. (see figure 3.17). Both of these exhibit coupling to the platinum nucleus (of 3055.6Hz. and 3439.3Hz., respectively) and also a mutual coupling of 27Hz.

Figure 3.17

$^{31}P\{^{1}H\}$ n.m.r. spectrum of 14, 81.020MHz., 25°C (298)K.

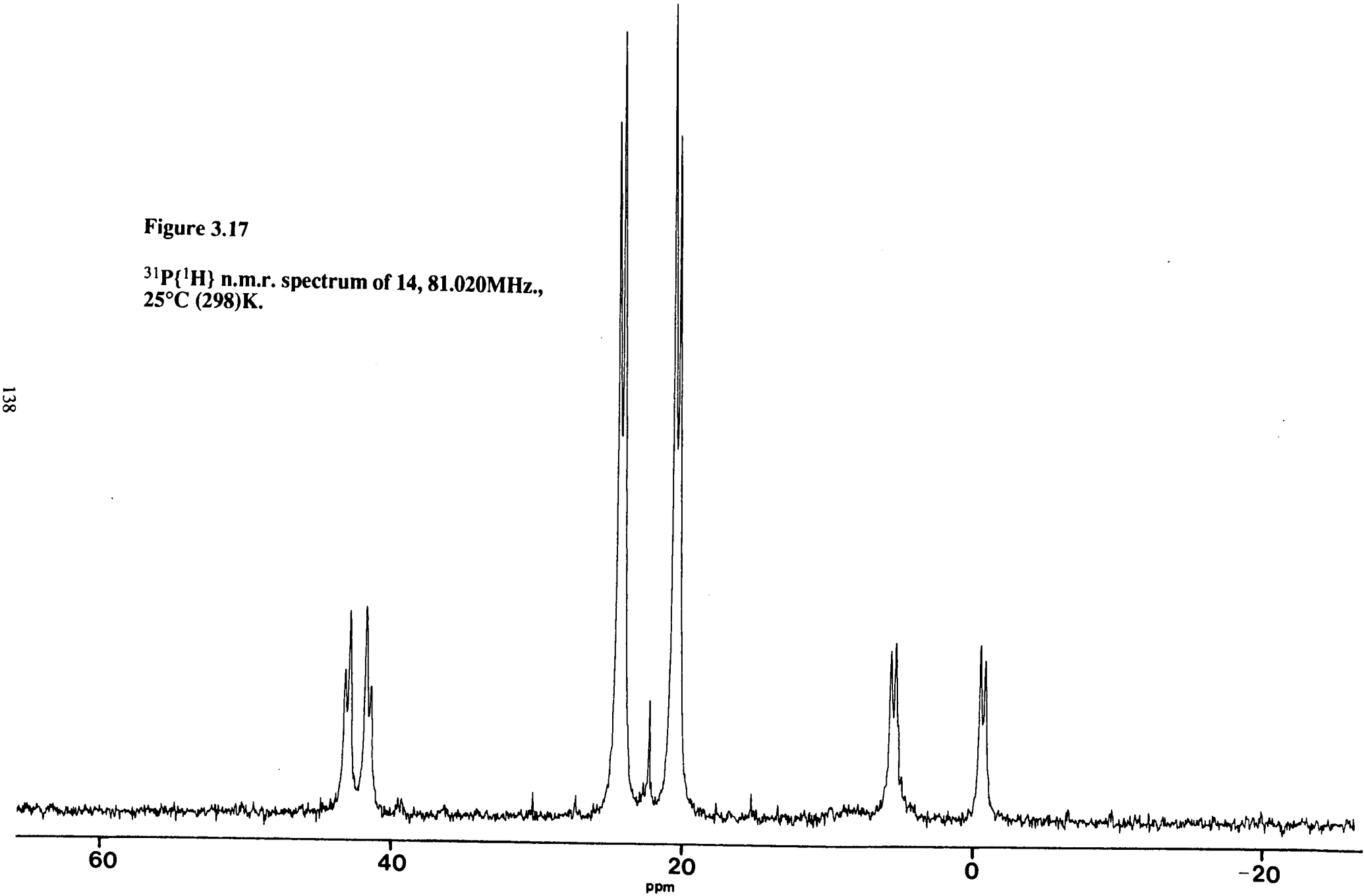

Figure 3.18

^{1}H n.m.r. spectrum of 14, 200.130MHz., 25°C (298)K.

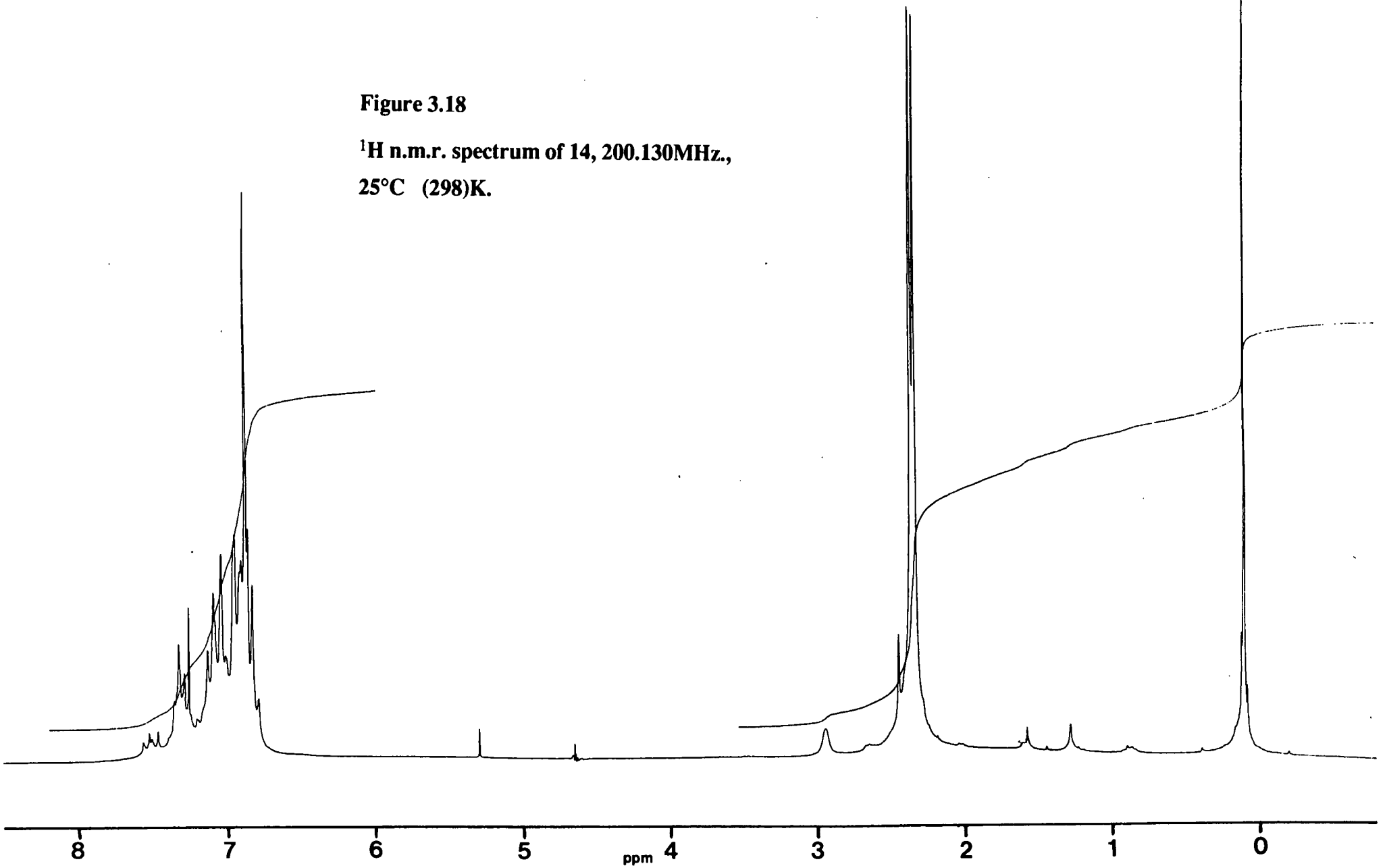

The ^{1}H n.m.r. spectrum of **14** shows a signal due to the cage C-H proton at δ 2.95p.p.m. (see figure 3.18). There are two singlets denoting the protons of the magnetically inequivalent methyl groups in the two p-tolyl ligands (which have a combined integral of 18 protons). The phenyl region of the spectrum is complex, consisting of four multiplets (centred on δ = 7.50p.p.m., 7.32p.p.m., 7.10p.p.m. and 6.90p.p.m.) which integrate for a total of 29 protons. From the above data it was concluded that a complex analogous to **1** had been formed, namely 1-Ph-3,3-$(P(p\text{-}tol)_3)_2$-3,1,2-$PtC_2B_9H_{10}$.

When a sample of **14** was heated in toluene, at reflux temperature, the solution lightened. The n.m.r. spectra of the residue, which remained after removal of solvent *in vacuo*, were recorded. The $^{11}B\{^{1}H\}$ spectrum ($CDCl_3$) is a broad envelope which shows little structure. However, it is apparent that the high frequency boron resonance, indicative of the presence of a C_2B_3, face is now absent. The $^{31}P\{^{1}H\}$ spectrum consists of a poorly resolved AB pattern, centred on δ= 20.02p.p.m., from which a P-P coupling of 26.3Hz. and an average $^{1}J^{195}Pt\text{-}P$ of 3404.9Hz. can be measured (see figure 3.19). This indicates the formation of a single new carbaplatinaborane in which there is hindered rotation about the platinum-cage bonding at room temperature, on the n.m.r. timescale. The ^{1}H n.m.r. spectrum of this product shows a signal due to the cage C-H at δ 3.05p.p.m. There are two singlets corresponding to the magnetically inequivalent sets of p-tolyl methyl protons, at δ 2.32 and 2.37p.p.m. The phenyl region of the spectrum is complicated, containing 3 multiplets centred on δ = 7.34, 7.24 and 6.91p.p.m.

Figure 3.19

$^{31}P\{^{1}H\}$ n.m.r. spectrum of the product of thermolysis of 14, 81.020MHz., 25°C (298K).

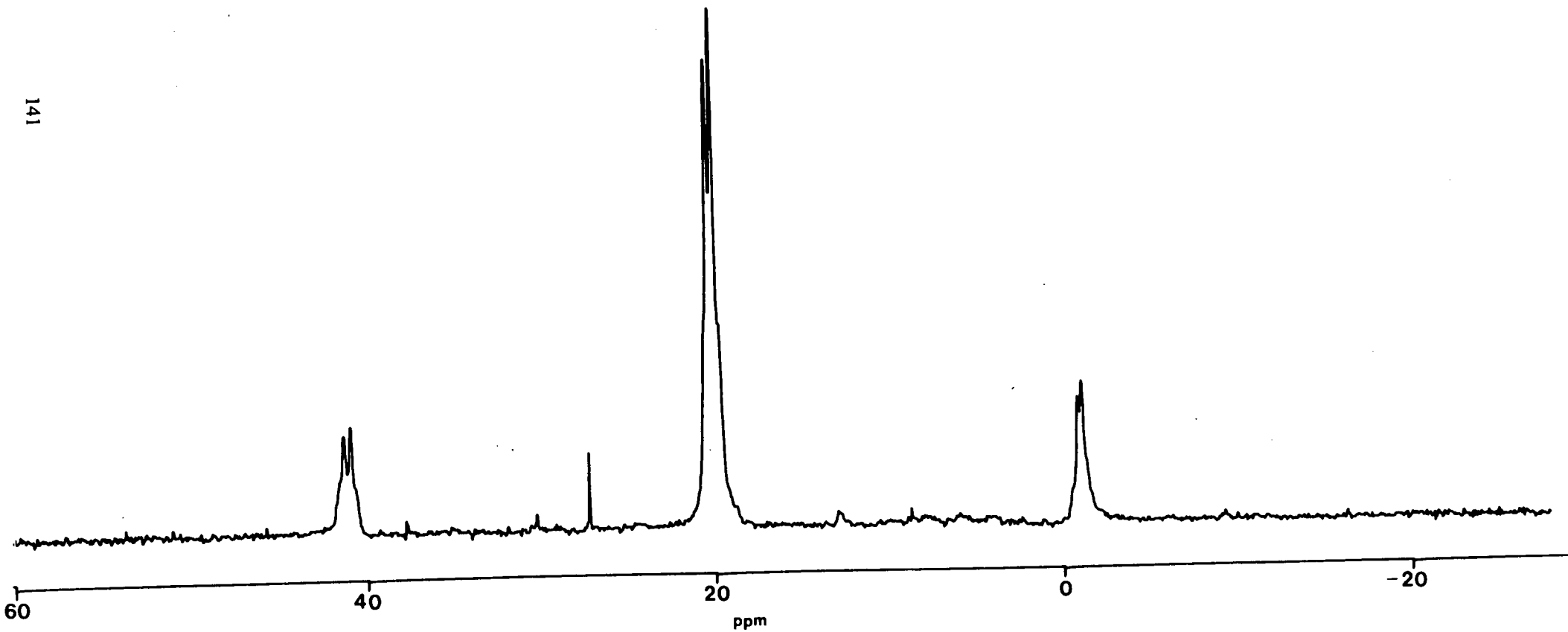

From the above spectral data it was concluded that thermolysis of **14** gives rise to a single rearranged isomer. On steric grounds this would be expected to be the one in which the carbon atom bearing the phenyl group has migrated to the lower belt *i.e.* 11-Ph-3,3-$(P(p\text{-}tol)_3)_2$-3,1,11-$PtC_2B_9H_{10}$.

Reaction of $Tl_2C_2B_9H_9Ph_2$ with *cis*-$PtCl_2(P(p\text{-}tol)_3)_2$, in CH_2Cl_2, yielded an soluble orange product. This was worked up as described previously to afford an orange solid, **15**. A solution i.r. spectrum (CH_2Cl_2) was recorded, indicating the presence of borane (νB-H= 2540cm^{-1} and the $P(p\text{-}tol)_3$) moiety (ν= 1500 and 1450cm^{-1}).

The $^{11}B\{^1H\}$ n.m.r. spectrum of a sample of **15** ($CDCl_3$) consists of 5 resonances in the ratio 1:2:2:3:1. There is no high frequency boron signal, which suggests that the product does not contain a C_2B_3 metal-bonded face. As in the spectrum of **13** all the resonances are at relatively high frequency. In the proton coupled spectrum each signal is split into a doublet (^1JB-H= 100-140Hz.). The $^{31}P\{^1H\}$ n.m.r. spectrum of **15** consists of two singlets at δ= 20.05p.p.m. and 22.65p.p.m. each of which exhibits doublet satellites ($^1J^{195}$Pt-P = 3323.1 and 3228.2Hz., respectively) (see figure 3.20). A mutual coupling is also observed ($^2JP_1$-P_2= 20.4Hz.), indicating that the two environments exist within a single molecule, in which there is restricted rotation about the platinum-cage bonding. The ^1H n.m.r. spectrum contains two singlets due to the inequivalent sets of methyl protons in the two phosphine ligands. There are three multiplets in the phenyl region of the spectrum centred on δ 7.24p.p.m., 6.91p.p.m. and 6.74p.p.m. The combined spectroscopic evidence suggests that a complex analogous to **4** has been formed, namely 1,11-Ph_2-3,3-$(P(p\text{-}tol)_3)_2$-3,1,11-$PtC_2B_9H_9$.

Figure 3.20

$^{31}P\{^{1}H\}$ n.m.r. spectrum of 15, 81.020MHz., 25°C (298)K.

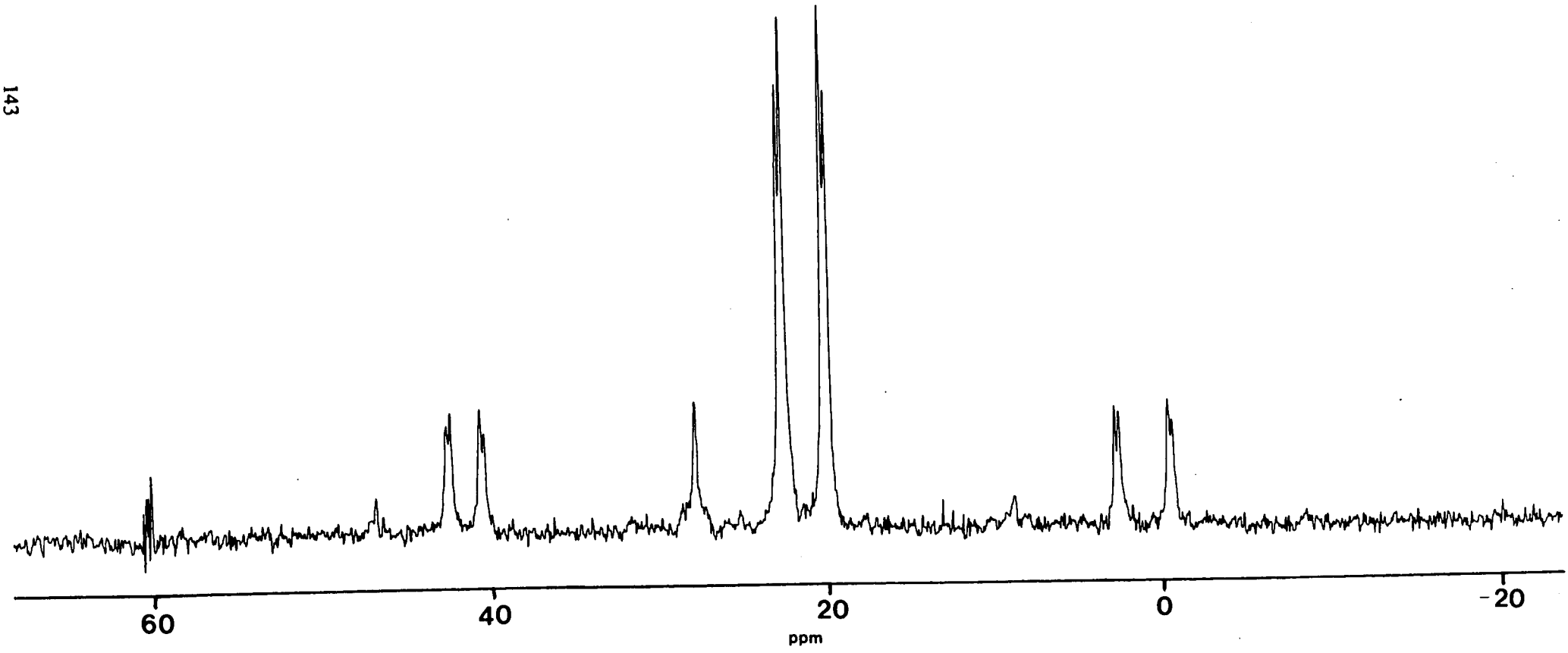

3.10 A Comparison of the Platinum Bis-(triphenylphosphine) Complexes with the Platinum Bis-(tri-p-tolylphosphine) Complexes.

The spectra and observed behaviour of the carbaborane complexes incorporating the $\{Pt(PPh_3)_2\}$ fragment were similar to those of the corresponding carbaborane complexes containing the $\{Pt(P(ptol)_3)_2\}$ fragment.

Considering firstly the complexes of the type $[(P_2Pt)C_2B_9H_{10}Ph]$, it can be noted that the ^{11}B n.m.r. spectra both show a high frequency boron resonance, at similar chemical shift. In fact, the shift in the $\{Pt(PPh_3)_2\}$ complex is at slightly higher frequency, contrary to what would be predicted on the grounds of the e-donating abilities of the ligands. This indicates that, for these two species, the steric bulk of the phosphine ligands may be the dominant factor in determining the magnitude of the slippage in these structures. The correlation of high frequency boron shift with π-acceptor properties of ligands is discussed more fully in section 3.13. Both $^{31}P\{^1H\}$ n.m.r. spectra consist of two phosphorus resonances which exhibit similar coupling to the platinum nucleus and to each other. However, both the signals arising from the $\{Pt(P(p\text{-}tol)_3)_2\}$complex, **14**, occur at slightly lower chemical shift, indicating that the phosphorus nuclei are more shielded, in this case, by the better e-donating substituents.

On heating, **12** and **14** each give rise to one thermolysis product which have similar ^{11}B n.m.r. spectra. Both the $^{31}P\{^1H\}$ spectra consist of poorly resolved AB signals for which the measured couplings are almost identical. Again, the chemical shifts observed in the spectrum of the $\{Pt(P(p\text{-}tol_3)_2\}$ complex, **14**, are to lower frequency. It was concluded that the isomerisations had both given rise to analogous 3,1,11-isomers. The species of the type $[(P_2Pt)C_2B_9H_9Ph_2]$ have ^{11}B and $^{31}P\{^1H\}$ n.m.r. spectra of similar nature with similar chemical shift variations as those

described above.

From these comparisons it was concluded that variation of the electronic properties of ligands of the same steric bulk has no significant effect on the nature or behaviour of their carbaborane derivatives.

3.11 Platinum Bis-(tricyclohexylphosphine)-Carbaborane Complexes.

When $Tl_2C_2B_9H_{10}Ph$ was stirred with *trans*-$PtCl_2(PCy_3)_2$, in CH_2Cl_2, there was no apparent reaction. This was confirmed by a $^{31}P\{^1H\}$ n.m.r. spectrum of the residue which showed only the presence of *trans*-$PtCl_2(PCy_3)_2$. Similarly, there was no reaction when these reagents were stirred in CH_2Cl_2, at reflux temperature, for 3 hours. The residue from this reaction was dissolved in toluene and heated to reflux temperature for 1 hour. There was a slight colouration of the solution, although there was still insoluble yellow $Tl_2C_2B_9H_{10}Ph$ present. A solution i.r. spectrum revealed the presence of borane (νB-H= 2540cm^{-1}). However, the ^{11}B n.m.r. spectrum was extremely complex and suggested that decomposition of the cage may have occurred. The $^{31}P\{^1H\}$ n.m.r. spectrum consists of the signals denoting $PtCl_2(PCy_3)_2$ and also a small singlet at δ +51.15p.p.m., which shows no coupling to the platinum nucleus. This may be a result of some decomposition of the chloro-platinum complex.

It was concluded that the $[Pt(PCy_3)_2]^{2+}$ fragment was sterically too demanding to co-ordinate to [1-Ph-1,2-carbaborane]$^{2-}$. The failure of this reaction was not believed to be a result of the use of the *trans*-chloroplatinum starting material rather than the *cis*-. The basis for this is that the reaction between *trans*-$PtCl_2(PMe_2Ph)_2$ and $Tl_2C_2B_9H_{10}Ph$ has been carried out to yield **1** in similar yield to the analogous reaction using the *cis*-chloroplatinum isomer. The reaction between $Tl_2C_2B_9H_9Ph_2$ and *trans*-$PtCl_2(PCy_3)_2$ was not attempted.

3.12 A Comparison of the ^{11}B N.M.R. Spectra.

Within each of the three classes of complexes studied (*i.e.* [1-Ph-3,3-P_2-3,1,2-$PtC_2B_9H_{10}$], [Ph-3,3-P_2-3,1,11-$PtC_2B_9H_{10}$] and [1,11-Ph_2-3,3-P_2-3,1,11-$PtC_2B_9H_9$]) the ^{11}B n.m.r. spectra are broadly similar. The striking feature of the observed spectra for complexes of the type [1-Ph-3,3-P_2-3,1,2-$PtC_2B_9H_{10}$] is the presence of a relatively high frequency boron resonance which is discussed fully in the next section. Thermolysis of these complexes yields species which no longer possess a resonance of this type. Similarly, the complexes of the type [1,11-Ph_2-3,3-P_2-3,1,11-$PtC_2B_9H_9$] which were synthesised did not exhibit a high frequency signal. There appeared to be no obvious trends in ^{11}B chemical shifts with changing the metal-bound phosphorus ligand.

3.13 The High Frequency Boron Resonance.

It has been recognised[106] that the presence of a high frequency boron resonance in the ^{11}B n.m.r. spectrum is particularly distinctive of a slipped structure (in complexes containing a C_2B_3 metal-bonded face). Further, the magnitude of this shift may reflect the degree of slippage of the metal-fragment[60].

This concept must be used with caution, however, as it has been found[107] that complexes in which the metal atom is either not strongly bonded to the open face (*e.g.* as in $[TlC_2B_9H_{11}]^-$), or is effectively bonded to only one of the boron atoms (*e.g.* as in 3-(PPh_3)-3,1,2-$HgC_2B_9H_{11}$) do not exhibit a high frequency boron resonance.

With this limitation in mind Wallbridge synthesised a range of carbametallaboranes (mainly palladium complexes) with a variety of ligands bound to the metal atom, and studied their ^{11}B n.m.r. spectra. The degree of opening of a carbaborane structure is believed to depend on the occupancy of the e_1^* metal-cage π

antibonding orbital[27] and it has been suggested that the introduction of π- acid ligands onto the metal could produce a more nearly closed polyhedron by delocalising electron density away from the e_1^* orbital onto the ligands[60]. Thus the stronger a π- acceptor ligand bound to the metal centre, the smaller the slippage of the metal fragment over the C_2B_3 face and the lower the expected chemical shift of the high frequency boron resonance.

Broadly speaking, this idea was shown to hold true, with palladium complexes bearing π-neutral N-donor ligands showing a higher shift of the highest frequency resonance than those bearing weak π-acceptor C- donor or alkene complexes, which in turn showed a higher shift than observed for complexes bearing P-donor ligands. The crystal structures of 3-(tmen)-3,1,2-$PdC_2B_9H_{11}$ and 3,3-$(PMe_3)_2$-3,1,2-$PdC_2B_9H_{11}$ (see section 1.9) confirmed that the former exhibited a larger slippage of the metal fragment than the latter and this could be correlated with a higher frequency resonance in the boron n.m.r. spectrum[60].

This correlation was later called into question, however, when the crystal structure of 3-(1,5-COD)-3,1,2-$PdC_2B_9H_{11}$ was determined[65]. This showed a slippage of the metal fragment of similar magnitude to that observed in the analogous {$(PMe_3)_2$Pd} complex. However, the chemical shift of the high frequency boron signal (δ= +17.67p.p.m.) was significantly different from that for the phosphine complex (δ= +6.68p.p.m.) and in fact was more similar to that observed for the {(tmen)Pd} complex. There were also anomalies in the original work which could not readily be explained, e.g. involving the complex 3-(dppe)-3,1,2-$PdC_2B_9H_{11}$ (see later).

While there are clearly problems in comparing specific complexes bearing ligands of a different nature, it was believed that consideration of a series of complexes in which the ligand type is constant and the sole variation is in the electronic properties of the ligands may be more valid. Each of the {Pt(bis-phosphine)} complexes of

$[C_2B_9H_{10}Ph]^{2-}$ described in this and the previous chapters showed a high frequency boron resonance in the ^{11}B n.m.r. spectrum. Table 3.4 shows the value of these shifts, with the phosphorus ligands ordered going from the worst π-acceptor at the top to the best π-acceptor at the bottom.

Table 3.4 Chemical Shifts of the Highest Frequency Boron Resonance in the $^{11}B\{^1H\}$ N.m.r. Spectra of Complexes of the Type 1-Ph-3,3-P_2-3,1,2-$PtC_2B_9H_{10}$.

Phosphorus Ligand (P)	δ(high frequency boron resonance) (p.p.m.)
PEt_3	13.78
PMe_3	11.51
PMe_2Ph	11.00
$P(p\text{-}tol)_3$	20.02
dppe	14.18
PPh_3	21.11
$P(OMe)_3$	8.97

The first three complexes in the table and the last one follow the expected trend, with the shift of the high frequency boron resonance decreasing with increasing π-acceptor ability of the ligands. The other three complexes show higher than predicted shifts, which may be attributed to steric effects. In the cases of the PPh_3 complex, **12**, and the $P(p\text{-tol})_3$ complex, **14**, the large steric bulk of the ligands may cause a larger slippage of the metal fragment than would be predicted on purely electronic grounds (as slippage would decrease the steric interaction between the metal fragment and the cage-phenyl substituent). Although the dppe ligand is smaller, it is more rigid and so cannot adjust in the same way as the bis-monodentate ligands can to reduce interaction with the cage phenyl group. Hence, in the dppe complex this interaction may only be minimised by greater slippage of the metal fragment than would be predicted on purely electronic grounds. Wallbridge also found that the 3-(dppe)-3,1,2-$PdC_2B_9H_{11}$ complex showed an anomalously high shift of the boron resonance compared to the other phosphine complexes which were

studied[60].

When steric constraints are taken into account these complexes show the expected trend in chemical shifts of the high frequency boron resonance. What is not clear, however, is if this provides a justification of the original correlation or if it is merely fortuitous.

3.14 A Comparison of the ^{31}P and ^{1}H N.M.R. Spectra.

The chemical shifts observed in ^{31}P n.m.r. spectra depend on a number of complex factors[108] and a comparison of these would be of little value. However, the structure and number of resonances observed can be of use in assessing the nature of the metal-cage bonding. For complexes of the type [1-Ph-3,3-P_2-3,1,2-$PtC_2B_9H_{10}$], the metal fragment lies over an asymmetrically substituted C_2B_3 face and hence if the structure is static, or if there is restricted rotation of the metal fragment, then the two phosphorus nuclei will be inequivalent. This is observed for complexes incorporating the larger metal fragments *i.e.* {$Pt(P(ptol)_3)_2$} (**14**), {$Pt(PPh_3)_2$} (**12**), {$Pt(PEt_3)_2$} (**10**) and {$Pt(PMe_2Ph)_2$} (**1**) (see chapter 2), in which there is restricted rotation about the metal-cage bonding. For complexes with smaller metal fragments this rotation is more facile and the two phosphorus nuclei can show an average chemical shift value. This is observed for the complex which incorporates the {$Pt(PMe_3)_2$} fragment (**7**). However, in **5** where the metal fragment is the smaller {$Pt(P(OMe)_3)_2$}, some AB structure is observed. The phosphite ligands possess relatively good π-acceptor properties, which may lead to a more closed (less slipped) structure, in **5**. This, in turn may increase the severity of the steric interaction between the metal fragment and the cage-phenyl ligand, thereby restricting rotation of this fragment. Only one phosphorus environment is revealed in the $^{31}P\{^{1}H\}$ n.m.r. spectrum of the {Pt(dppe)} complex. This is perhaps surprising given that **1**, where the phosphine has a smaller

cone angle, exhibits two, and may simply be an effect of the presence of a bidentate ligand. Alternatively, there may conceivably be two phosphorus environments present which have identical chemical shifts and coupling constants.

Although the metal bonded face in the 3,1,11-complexes is symmetric and the lower belt is symmetric these are twisted relative to each other (see figure 3.21) so in a static structure, or where there is hindrance to rotation about the metal-cage bonding, the two phosphorus environments will be inequivalent. All the complexes of the type [1,11-Ph_2-3,3-P_2-3,1,11-$PtC_2B_9H_9Ph_2$], except the one in which the metal fragment is {$Pt(PMe_2Ph)_2$} (see chapter 2), show some degree of inequivalence of the two environments. This can be related to the steric bulk of the metal fragment restricting rotation about the metal-cage connectivities. Even the complex incorporating the small {$Pt(P(OMe)_3)_2$} fragment (**6**) has a $^{31}P\{^1H\}$ n.m.r. spectrum consisting of an AB signal, indicating that there are two distinct phosphorus environments. This may again be attributed to the reduced slippage of the metal fragment increasing the steric interaction with the cage-phenyl group. The $^{31}P\{^1H\}$ n.m.r. spectrum of **4** has only one resonance, suggesting that there is free rotation about the platinum-cage bonding. It is not clear why this is the case given that, the complex **8** (where the metal fragment is the smaller {$Pt(PMe_3)_2$}) exhibits two phosphorus environments. There may, in fact, be two distinct environments in **4** which have the same spectral parameters.

Figure 3.21

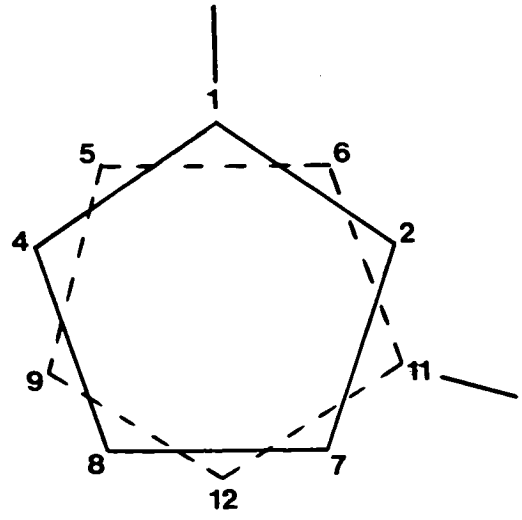

One point of interest which arises from the ^1H spectra concerns the chemical shift of the cage C-H proton. Generally, this proton resonates at higher frequency in the 3,1,2-species than in the analogous 3,1,11-isomers (thermolysis products). A CB_4 face is considered to be more electron rich than a C_2B_3 one[109] and hence a C-H would be relatively shielded when attached to the former and would resonate at lower frequency. Alternatively, this deshielding of the C-H protons in a C_2B_3 face can be thought of as arising from the effect of the carbon atom bearing the proton being adjacent to a relatively δ+ carbon atom.

3.15 Redox Chemistry of Carbaplatinaborane Complexes.

The cyclic voltammetry of the range of carbaplatinaboranes synthesised, in this and the previous chapters, was studied. These studies were confined to one solvent system (CH_2Cl_2) and no attempt was made to quantify the electron transfer steps observed, therefore the conclusions which can be drawn from the results obtained are limited. Full experimental details are described in chapter 5. The redox processes observed for complexes of the type [1-Ph-3,3-P_2-3,1,2-$PtC_2B_9H_{10}$] are presented in table 3.5, in which the phosphorus ligands are ordered in decreasing π-acceptor ability. In the following discussion it is assumed that in the starting species the metal atom is formally in the +2 oxidation state.

The first oxidative process is generally quasi-reversible becoming more reversible with increasing scan rate (v) and decreasing temperature. The oxidation of **1** is the most reversible of those studied, at room temperature, and this is depicted in figure 3.22. In the dppe complex there is no sign of reversibility of the first oxidative process under any set of conditions. The oxidation process became easier as the donor properties of the phosphorus ligand increase. This suggests that the oxidation is metal-based and can tentatively be described as a Pt^{2+} to Pt^{3+} step, with the stronger donor ligands more effectively stabilising the higher oxidation state. The second oxidative process is found to be irreversible under all conditions (see figure

Table 3.5 Redox Processes of 1-Ph-3,3-P_2-3,1,2-$PtC_2B_9H_{10}$ Complexes.

Phosphorus Ligand	$E_{1/2}$/V(Oxid. Range)	$E_{1/2}$/V(Red. Range)
$P(OMe)_3$	+1.30 (qr) +1.42 (i)	-1.54 (i)
PPh_3	+1.25 (qr) +1.81 (i)	-1.45 (i)
dppe	+1.11 (i) +1.33 (i) +1.82 (i)	-0.63 (qr) -1.57 (i)
$P(p\text{-}tol)_3$	+1.19 (qr) +1.61 (i)	-1.57 (i)
PMe_2Ph	+1.02 (r) +1.39 (i)	-1.60 (i)
PMe_3	+0.99 (qr) +1.24 (i)	-1.69 (i)
PEt_3	+1.00 (qr) +1.46 (i)	-1.64 (i)

Potentials are quoted versus a Ag/AgCl reference electrode at which the fc/fc^+ couple occurs at +0.56V (see chapter 5).
r= reversible electron transfer step
qr= quasi-reversible electron transfer step
i= irreversible electron transfer step
(Reversibility criteria are outlined in chapter 5.)

3.23). There is no apparent trend in the oxidation potential so it is not possible to suggest its nature. However, if the first oxidation is Pt^{2+}/Pt^{3+} then further oxidation to Pt^{4+} may be possible.

The irreversible reductive process of all complexes, apart from the dppe-containing species, appears to become more difficult with increasing donor properties of the phosphorus ligand, although this trend is not particularly pronounced (see figure 3.24). This process may conceivably be primarily metal-based, involving the Pt^{2+}/Pt^{1+} couple, although from the available data this cannot be reliably concluded. In the reductive range the dppe complex behaves anomalously, exhibiting a quasi-reversible reduction at -0.63V as well as an irreversible reduction at -1.57V (corresponding to that observed for the other complexes). It can be concluded that in this complex there may be more scope for ligand-based redox processes.

Figure 3.22 Cyclic Voltammogram showing First oxidation of 1.

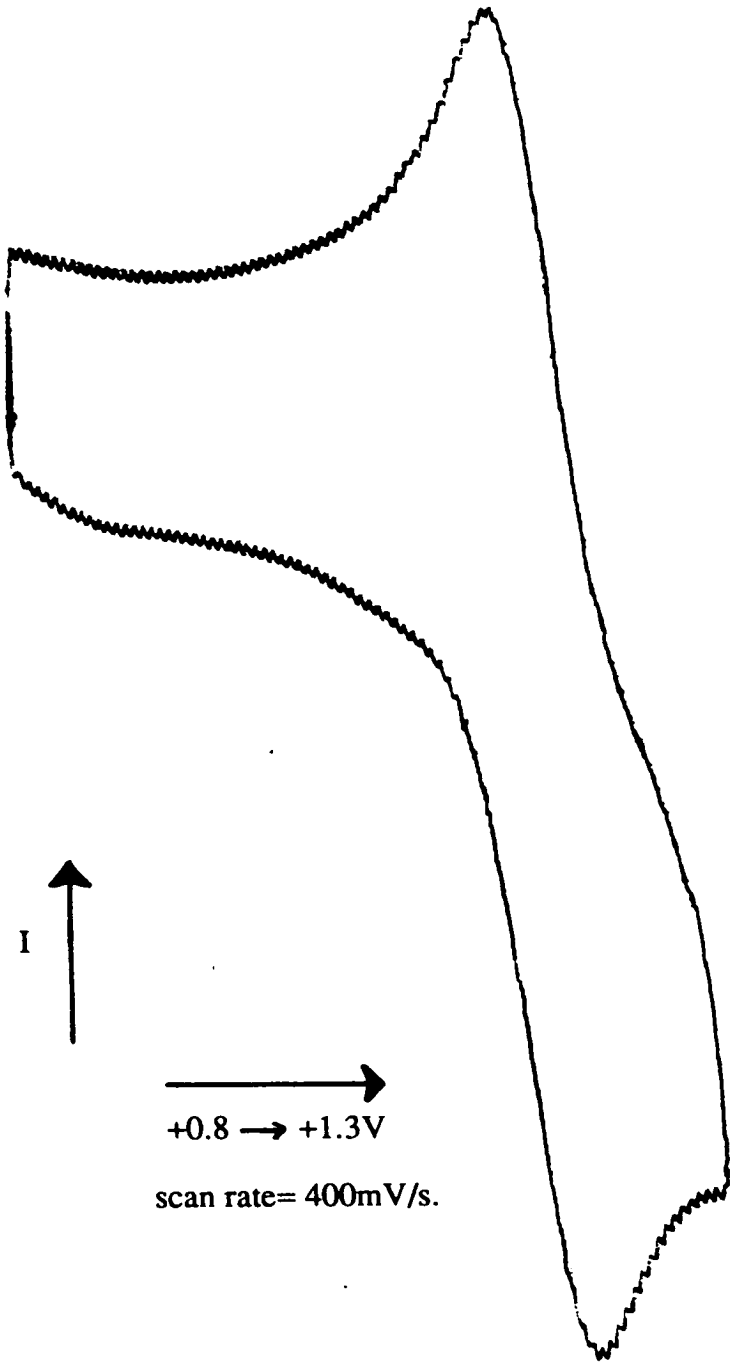

Figure 3.23 Cyclic Voltammogram showing Oxidations of 1.

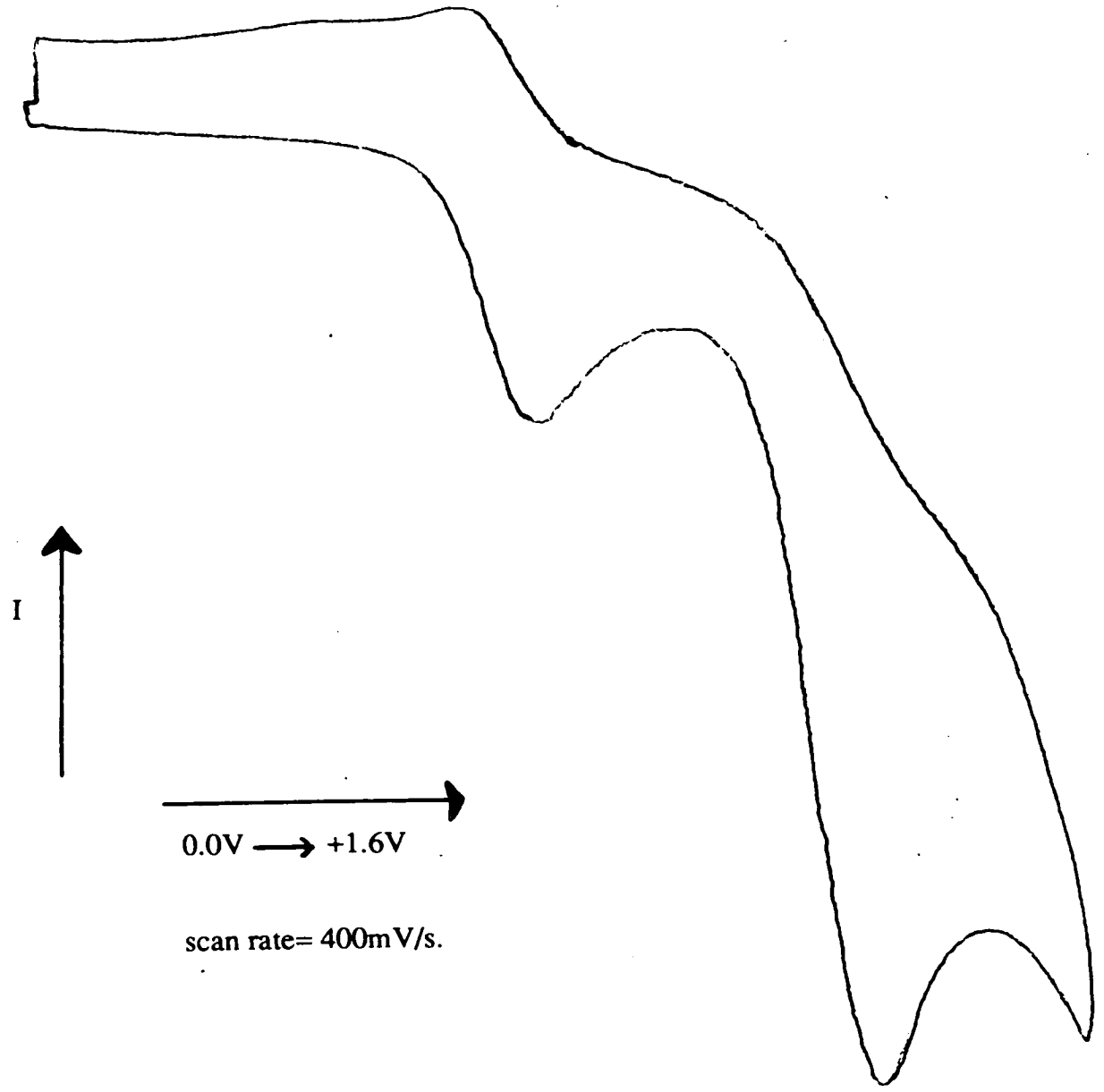

Figure 3.24 **Cyclic Voltammogram showing Reduction of 10.**

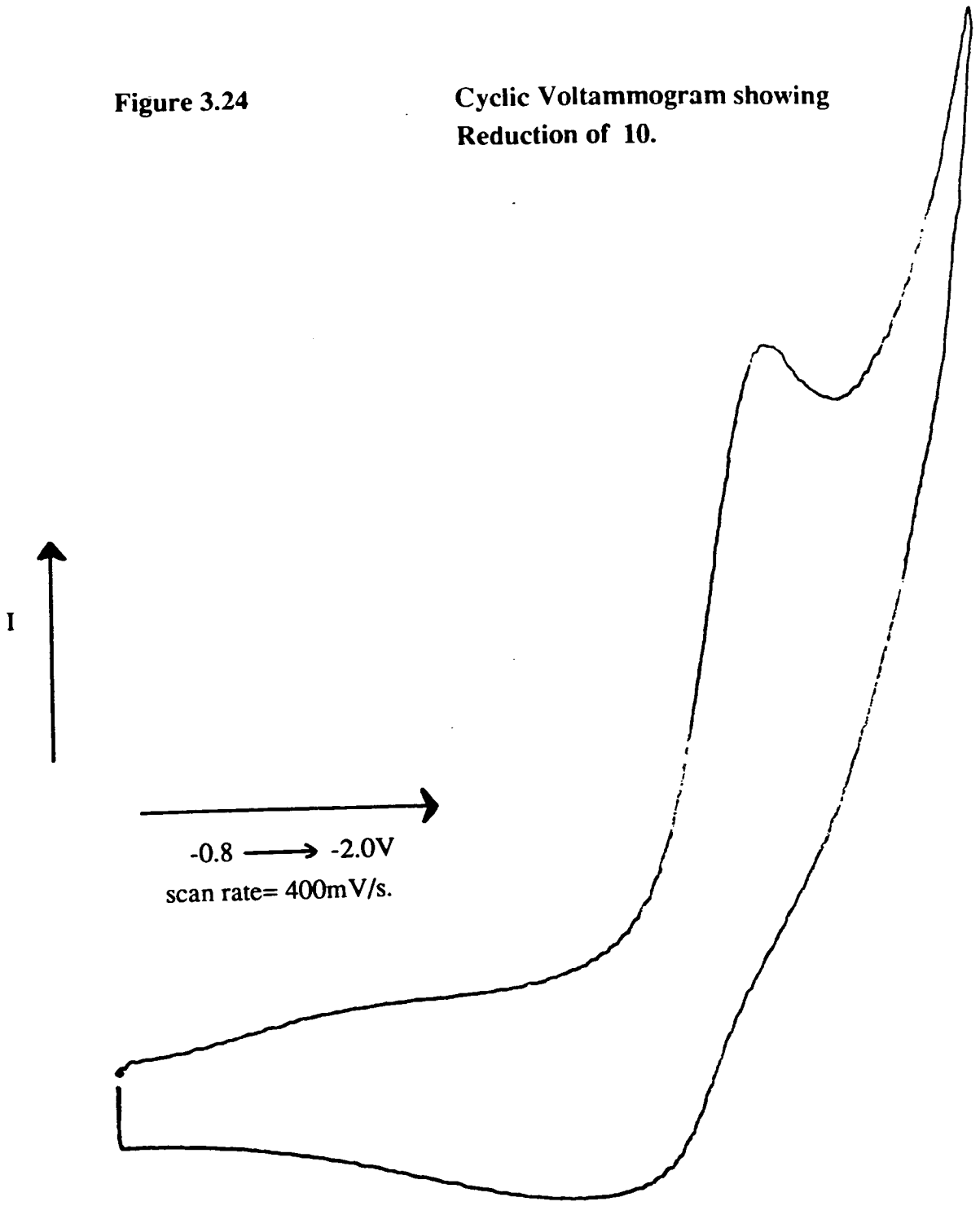

Similar cyclic voltammetry experiments were carried out on the range of complexes of the type [1,11-Ph_2-3,3-P_2-3,1,11-$PtC_2B_9H_9$] and the results are presented in table 3.6.

Table 3.6. Redox Processes for 1,11-Ph_2-3,3-P_2-3,1,11-$PtC_2B_9H_9$ Complexes.

Phosphorus Ligand	$E_{1/2}$/V(Oxid. Range)	$E_{1/2}$/V(Red. Range)
$P(OMe)_3$	+1.13 (i) +1.40 (i)	(obscured by adsorption onto electrode)
PPh_3	+1.09 (i) +1.27 (i) +1.58 (i)	-1.14 (i)
dppe	+1.12 (i) +1.38 (i)	-0.82 (i)
$P(p\text{-}tol)_3$	+1.11 (i) +1.42 (i)	-1.45 (i)
PMe_2Ph	+1.01 (i) +1.45 (i)	-1.25 (i)
PMe_3	+1.04 (i) +1.41 (i)	-1.24 (i)
PEt_3	+0.98 (i) +1.50 (i)	-1.50 (i)

Again, these species show two oxidations and one reduction (the first oxidation of **4** is shown in figure figure 3.25).

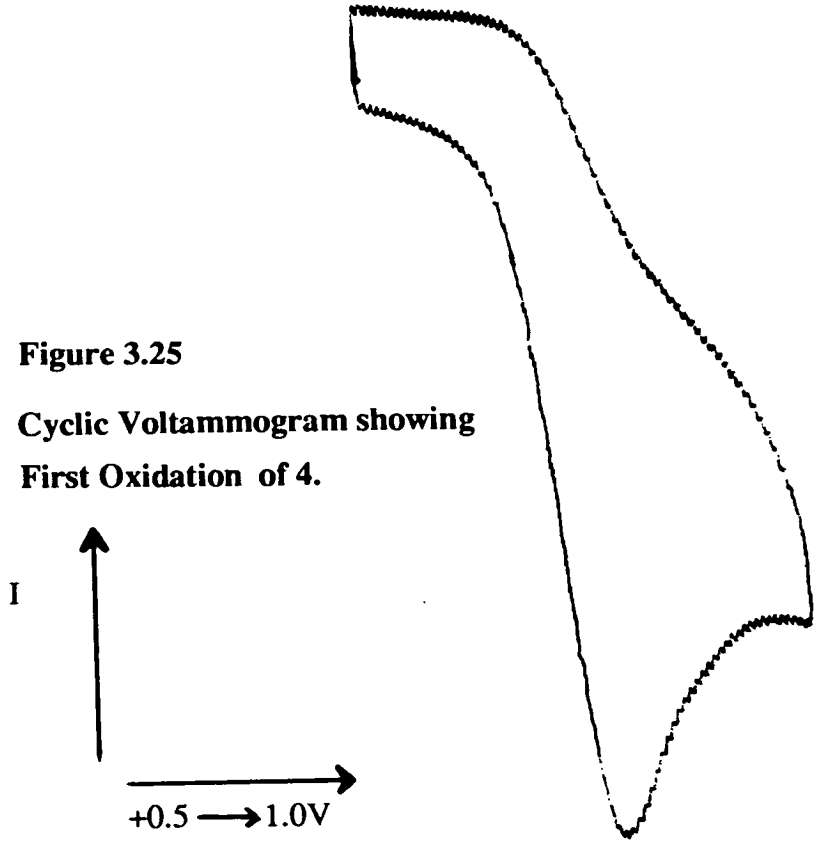

Figure 3.25

Cyclic Voltammogram showing First Oxidation of 4.

scan rate= 400mV/s.

In addition, the complex incorporating the $\{Pt(P(ptol)_3)_2\}$ fragment exhibits a third irreversible oxidation at +1.58V (see figure 3.26). The first oxidation becomes easier with increasing donor properties of the phosphorus ligands. This process can be tentatively assigned as a metal-based oxidation, possibly Pt^{2+}/Pt^{3+}. Comparison of the electrode potentials of these oxidations with those for the first oxidation of the analogous $[(P_2Pt)C_2B_9H_{10}Ph]$ species, indicates the former to be easier. This provides further evidence for the process being metal- based, as a metal bonded to a CB_4 face would have more available electron density and so be easier to oxidise than one bound to a C_2B_3 face[109]. The second oxidation processes in the $[1,11\text{-}Ph_2\text{-}3,3\text{-}P_2\text{-}3,1,11\text{-}PtC_2B_9H_9]$ complexes are irreversible under all experimental conditions and must be assigned to redox-active products arising from the decomposition of the starting complex following initial electron-transfer. They exhibit no discernible trend in the variation of electrode potential with phosphorus ligand. The potential of the reductive process also appears to be independent of the donor-properties of the phosphorus ligand. However, these are generally more facile than the reductive processes involving the mono-phenylcarbaborane analogues, consistent with addition of a second electron-withdrawing substituent resulting in the species becoming more prone to reduction.

From these preliminary experiments it appears that the carbaplatinaborane complexes studied exhibit a rich electrochemistry. Although, there is insufficient evidence from which to draw meaningful conclusions it has been shown that these complexes merit further study.

Figure 3.26

Cyclic Voltammogram showing
Oxidations of 13.

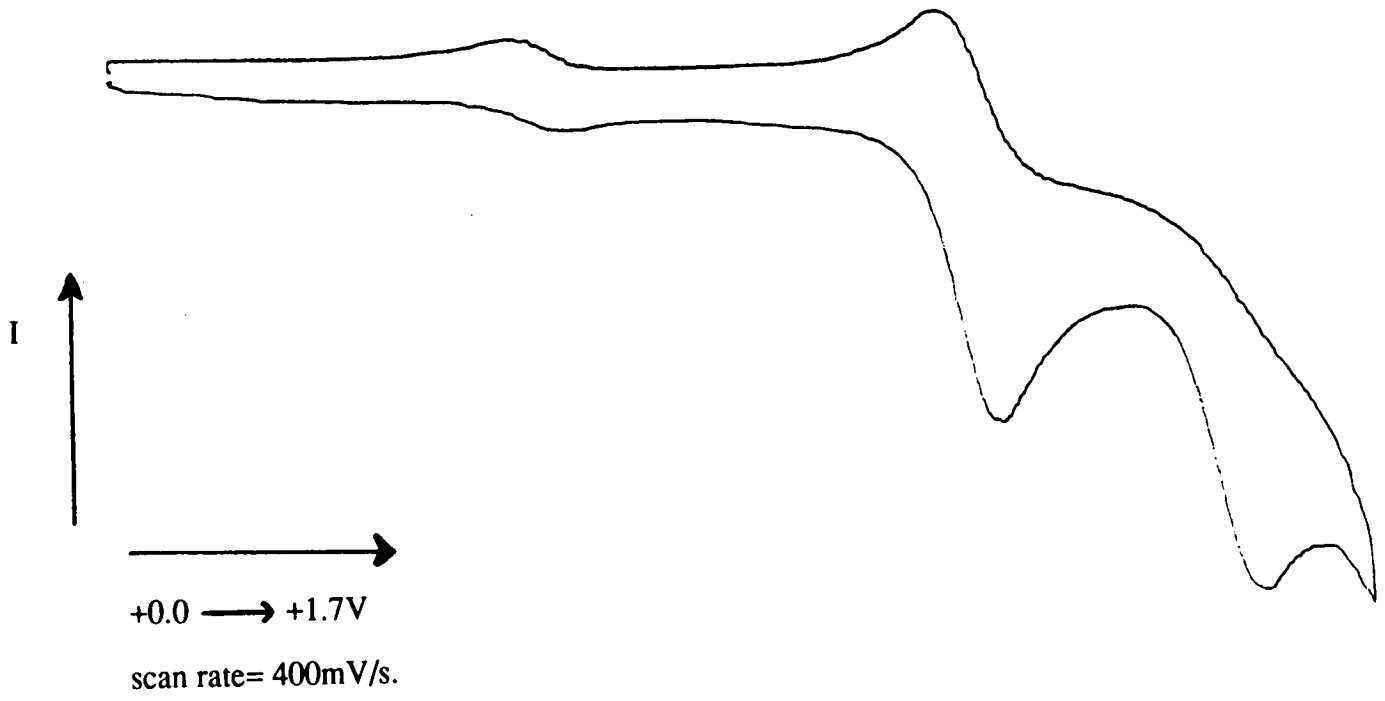

3.16 Conclusions: Complexes of the Type 1-Ph-3,3-P_2-3,1,2-$PtC_2B_9H_{10}$.

Complexes of the general form [1-Ph-3,3-P_2-3,1,2-$PtC_2B_9H_{10}$] are readily formed incorporating all the metal fragments employed except {$Pt(PCy_3)_2$}. As this fragment is the most bulky it is assumed that the steric bulk prohibits co-ordination to the carbaborane *nido*-face. All the species produced were believed to be of the 3,1,2-isomeric form, and proved stable to isomerisation at room temperature, even when the metal fragment was the bulky {$Pt(PPh_3)_2$} or {$Pt(P(p\text{-}tol)_3)_2$}. However, all the 3,1,2-species are found to undergo a thermally induced isomerisation to produce one or two 3,1,11-isomers. Even the smallest of the phosphorus ligands employed gives rise to a 3,1,2-carbaplatinaborane which is readily isomerised. In this example, **5**, the decreased size of the metal fragment may be compensated for by reduced slippage of the metal fragment, due to the π-acceptor properties of the phosphite ligand, so the steric interaction of the metal fragment may be greater than would be predicted solely on the grounds of ligand cone angle. This is to some extent confirmed by the presence, in the ^{11}B n.m.r. spectrum of **5**, of a high frequency boron resonance at the lowest chemical shift of all those observed, indicating a smaller slippage of the metal fragment in this case. The isomerisation of the dppe complex, **9**, proceeds in a similar manner to those of the {PtP_2} complexes, and if it is assumed that all these rearrangements take place via the same mechanism, this precludes the cleavage of a M-P bond on the reaction pathway.

While all the 3,1,2-isomers undergo isomerisation, some give rise to two products while others give only one. This can largely be attributed to the steric bulk of the metal fragment. The complex with the smallest fragment {$Pt(P(OMe)_3)_2$}, **5**, gives rise to two 3,1,11-isomers in the ratio 2:1, however **1** produces two isomers in the ratio 4:1 and the complex of the even larger {$Pt(PEt_3)_2$}, **10**, forms two isomers in the

The isolation of **22** as the 3,1,11-skeletal isomer indicates that the rearrangement which leads to its formation does not involve the breaking of a metal-phosphorus bond.

Chapter 4

Phenyl-substituted Carbapalladaboranes and Related Complexes.

4.1 Introduction.

This chapter discusses the effect of substituting Pd^{2+} for Pt^{2+} in mono- and di-phenyl C-substituted carbaborane complexes incorporating an $\{ML_2\}^{2+}$ fragment. The effect of varying the nature of the ligand(s) on the metal fragment is also outlined. For this purpose the *pseudo*-ML_2 fragment, $\{Pd(1,5\text{-COD})\}^{2+}$ was treated with each of the phenyl-carbaborane anions and the resulting carbapalladaboranes were characterised. In the case of the diphenyl substituted carbaborane complex an X-ray crystallographic study was undertaken. Each of the {Pd(1,5-COD)} complexes differs significantly from the $\{PtP_2\}$ complexes discussed in the previous chapters with regard to the stability of the carbaborane skeletal isomers. In order to determine if this resulted from the nature of the metal centre or the COD ligand, complexes incorporating the {Pt(1,5-COD)} fragment were also studied.

4.2 Carbaborane Complexes Containing the $\{Pd(PMe_2Ph)_2\}$ Fragment.

The reaction between $Tl_2C_2B_9H_{10}Ph$ and *cis*-$PdCl_2(PMe_2Ph)_2$, in CH_2Cl_2, produced a red soluble species, and insoluble TlCl. Column chromatography (alumina/CH_2Cl_2) yielded a purple complex in good yield, as the sole product. Microanalysis is consistent with the composition of the target complex, $C_{24}H_{37}B_9P_2Pd$. The solution i.r. spectrum of the product, **16**, confirms the presence of borane (νB-H= 2540cm^{-1}) and co-ordinated phosphine (ν = 1490 and 1450cm^{-1}).

The n.m.r. spectra of **16** are consistent with the formation of a *closo*-carbametallaborane. The $^{11}B\{^1H\}$ n.m.r. spectrum (64.210MHz.) contains 5 resonances in the ratio 1:1:2:2:3, including a relatively high frequency signal at δ +9.75p.p.m., which is indicative of a slipped structure[60]. The other resonances occur at δ= -0.99, -6.26, -14.05 and -16.00p.p.m. Each signal is a doublet in the proton coupled spectrum, with ^{1}JB-H in the range 130 - 147Hz., suggesting coupling to terminal hydrogen atoms. The ^{11}B n.m.r. spectra at higher field (115.546MHz.) are better resolved and are shown in figure 4.1. The position of the high frequency boron resonance can be compared with that observed for **1**. In the palladium species this boron nucleus resonates at δ= 9.75p.p.m. compared with δ= 11.00p.p.m. in the platinum analogue. This difference would be expected if the palladium species was less distorted. However, it is at variance with the other reported[60] comparison of a carbapalladaborane and a carbaplatinaborane. In this case the high frequency boron resonance in 3-dppe-3,1,2-$PdC_2B_9H_{11}$ resonates at δ= 12.77 p.p.m. while that of the platinum analogue occurs at δ= 10.32 p.p.m. Once again, this illustrates the danger in attempting to relate spectroscopic and structural features. While the chemical shifts in **16** and **1** agree with what would be predicted, this may simply be fortuitous.

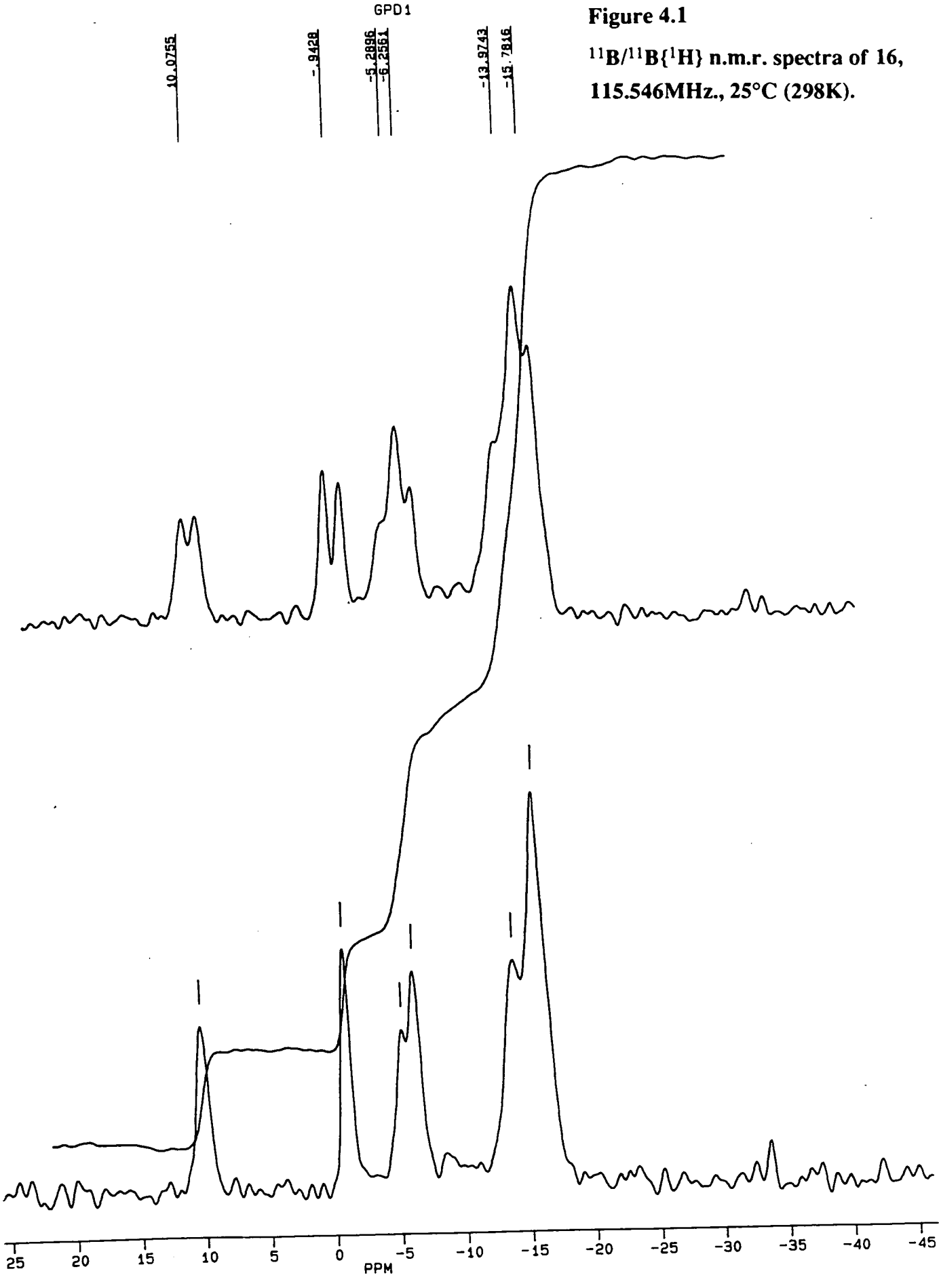

Figure 4.1

$^{11}B/^{11}B\{^{1}H\}$ n.m.r. spectra of 16, 115.546MHz., 25°C (298K).

The $^{31}P\{^{1}H\}$ spectrum of **16** consists of a broad envelope centred on δ -4.65p.p.m (see figure 4.2), indicating that the phosphorus environments in the molecule are nearly equivalent (probably by rotation about the M-cage bonding). In addition, there is a singlet at δ= +35.00p.p.m. corresponding to the phosphorus nucleus of the phosphine oxide ($Me_2PhP{=}O$) (not shown in figure). When the sample is cooled to approximately -55°C (218K), the spectrum of **16** is two doublets, centred on δ= +4.09p.p.m. and -9.77p.p.m., which show mutual P-P coupling of $^{2}JP\text{-}P$= 52.9Hz. (see figure 4.3). This is consistent with the two phosphorus nuclei being in a *cis*-arrangement at a square-planar Pd centre[41]. The increase in ^{2}JPP on replacement of Pt^{2+} with Pd^{2+} has been described[110] previously (the value of ^{2}JPP in **1** is <10Hz.). The signal indicating the presence of phosphine oxide is also present.

The $^{11}B\{^{1}H\}$ n.m.r. spectrum at this temperature is broad and structureless, in the range δ +5 to -35p.p.m., and also has two sharp peaks at δ= -37.22p.p.m. and -38.25p.p.m. (see figure 4.4). The proton spectrum at -55°C is dominated by the phosphine oxide signal[111]; a doublet at δ= +1.77p.p.m. ($^{2}JP\text{-}H$= 13.0Hz.) and 2 multiplets in the phenyl region of the spectrum (centred on δ= 7.53p.p.m. and 7.73p.p.m.) There are also resonances which can be assigned[112] to free PMe_2Ph (at δ= 0.8p.p.m.) and the *closo*- species described above (C-H at δ= 3.25p.p.m., Ph-H at δ= 7.22p.p.m. (multiplet) and two doublets corresponding to the methyl protons at δ 1.06p.p.m. (^{2}JPH= 10Hz) and 1.59p.p.m. (^{2}JPH= 11Hz.).

At elevated temperature (+55°C, 328K) the $^{31}P\{^{1}H\}$ spectrum contains a singlet at δ= -4.45p.p.m. indicating that the phosphorus environments have become equivalent, on the n.m.r. timescale (in addition to the phosphine oxide signal). The room temperature proton spectrum of **16** is second order for the phosphino-methyl protons, showing apparent triplets at δ= 1.16 and 1.46p.p.m. with a $|^{2}JPH + {}^{4}JPH|$ coupling of 9.8Hz. (see figure 4.5).

Figure 4.2

$^{31}P\{^{1}H\}$ n.m.r. spectrum of 16, 81.020MHz., 25°C, (298K).

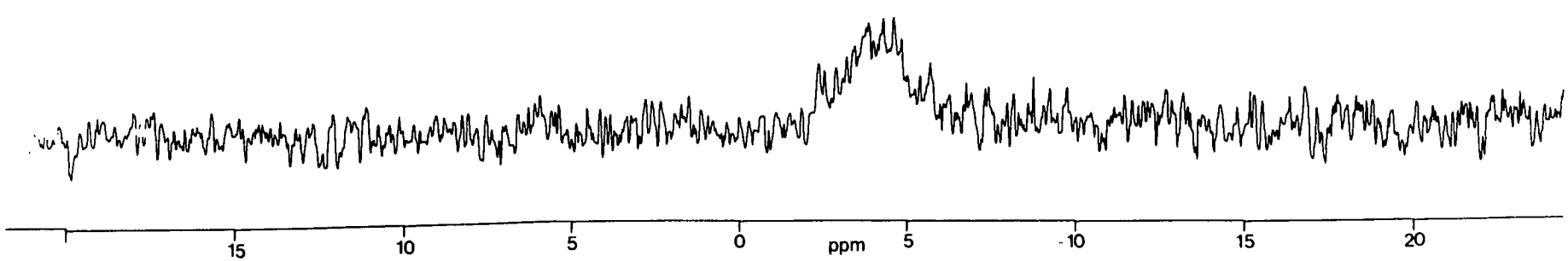

Figure 4.3

$^{31}P\{^{1}H\}$ n.m.r. spectrum of 16, 81.020MHz., -55°C (218K).

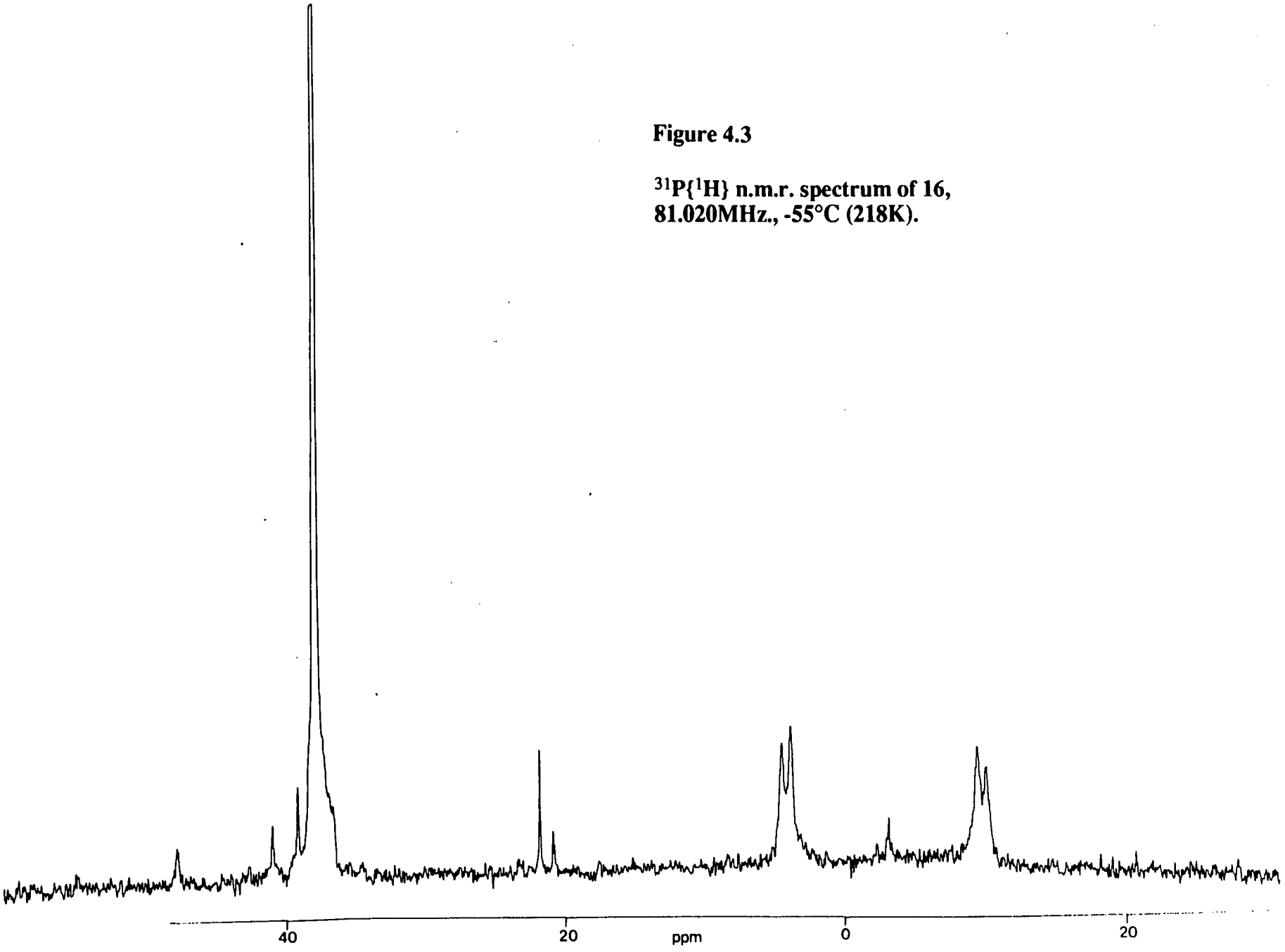

Figure 4.4

$^{11}B\{^{1}H\}$ n.m.r. spectrum of 16, 64.210MHz., -55°C, (218K).

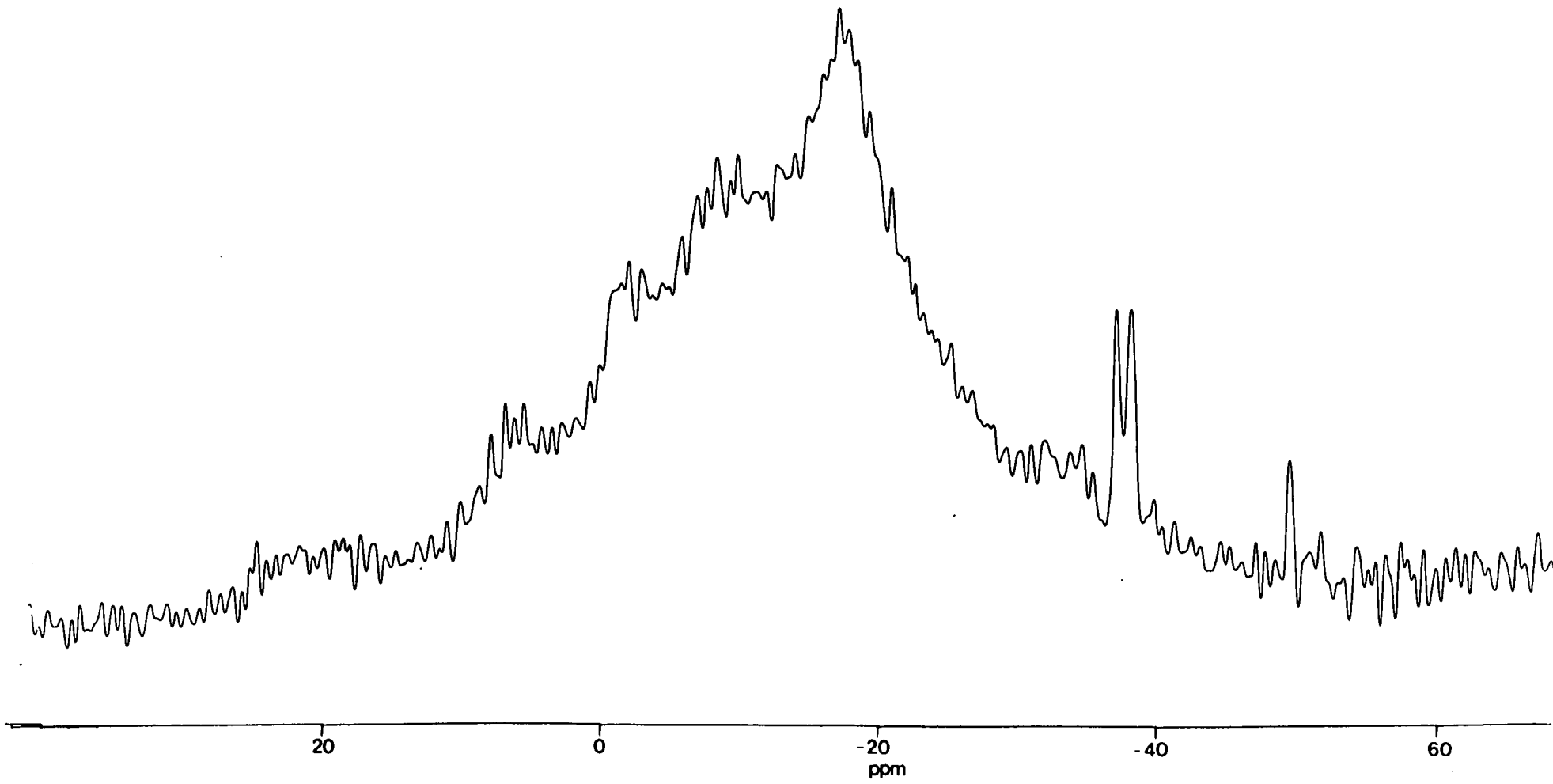

Figure 4.5

^{1}H n.m.r. spectrum of 16, 200.130MHz., 25°C (298K).

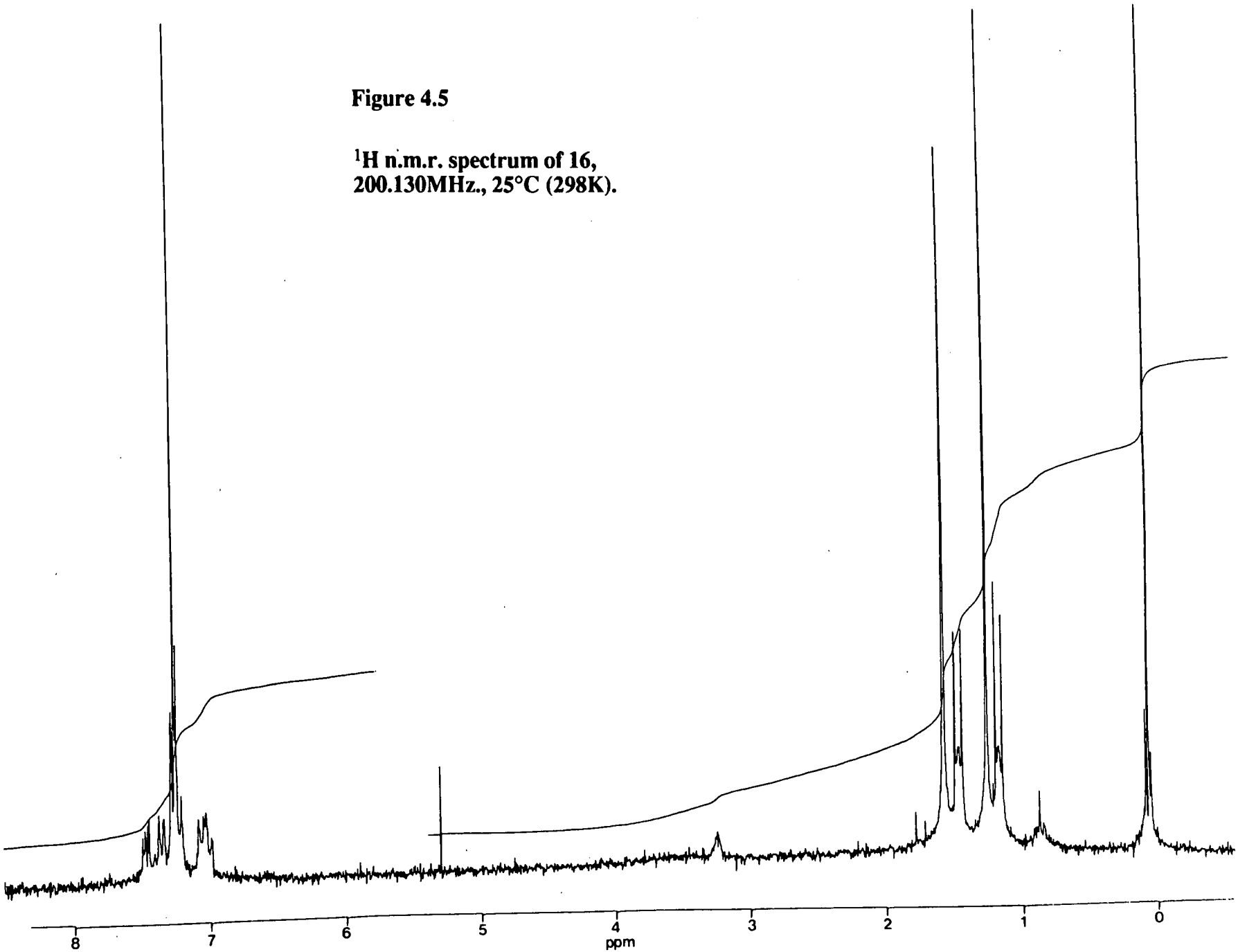

Each of these signals integrates for 3 protons. The observed pattern is consistent with a *cis*- arrangement of the phosphine ligands at the metal centre[113]. The single cage C-H resonates at δ= 3.24p.p.m. and there are 3 multiplets arising from the phenyl protons, centred on δ= 7.07, 7.24 and 7.47p.p.m., and a doublet at δ= 7.35p.p.m. with a coupling constant of 7.1Hz. The combined integral of the signals in the phenyl region confirms that there are 10 phenyl protons. The signals corresponding to the free phosphine and phosphine oxide are also observed.

Crystals suitable for an X-ray diffraction study were obtained by slow diffusion of n-hexane into a CH_2Cl_2 solution of **16**, at -30°C (243K). Two distinct types of crystals formed; red hexagons and purple needles. Each of these gave the same lattice parameters and data were collected for one of the purple crystals. This was found to be isomorphous to **1**, so only the positions of the non-hydrogen atoms were determined, to enable comparative calculations to be carried out. These suggest that the structure of **16** is less distorted, from an idealised icosahedral one, than that of **1**.

The slippage parameter, Δ, of **16** is 0.30Å (towards B(8)), appreciably less than that of **1** (= 0.39Å). This is consistent with the idea[60] that the lower d-p promotion energy[61] in the Pd-complex than in the Pt-analogue lessens the unfavourable 4-electron anti-bonding interaction (involving filled metal xy orbitals and cage $5e^1$ (a^1) orbitals) and, hence, allows a more closed structure to be adopted. The direction of the slippage makes an angle of 51.2° with the centroid to B(8) vector (= σ). The value of σ in **1** is 35.7°. The related folding parameters are also lower for **16**, at 6.15 and 1.97°, for φ and θ, respectively (compared with 7.25 and 2.76° in **1**). The two species are folded about the same axis, which passes through B(4) and C(2). Similarly, the rotation of the $\{P_2Pd\}$ fragment about the cage mirror plane is comparable with that observed in **1** (37.1 ° and 37.2 °, respectively). The lateral movement of the C_2B_3 face with respect to the B_5 belt in **16** is 0.07Å, similar to the value observed in **1** (= 0.09Å).

The metal-cage connectivities are generally shorter in the palladium complex: M-C(1)= 2.530(11) vs. 2.596(10)Å, M-C(2)= 2.308(12) vs. 2.326(10)Å, M-B(4)= 2.282(13) vs. 2.313(12)Å, however, M-B(8)= 2.277(14) vs. 2.239(12)Å. This latter variation may result from the smaller slippage away from B(8) in the palladium complex (as may the other observed changes). However, a lengthening of M-ligand distances has been previously observed[114], on substitution of Pd^{II} for Pt^{II}. The M-B(7) connectivities are within one standard deviation of each other: Pd-B(7)= 2.269(13)Å, Pt-B(7)= 2.257(12)Å.

The spectroscopic and crystallographic data presented up to this point are consistent with **16** being the species 1-Ph-3,3-$(PMe_2Ph)_2$-3,1,2-$PdC_2B_9H_{10}$. However, the other available data suggest that formation of this complex does not occur in a straightforward manner, and the *closo*-carbametallaborane may itself be unstable under certain conditions.

Firstly, it was mentioned that the reaction mixture was dark red whereas the chromatographically isolated product was purple. The reaction was repeated and the red species isolated by filtration, under an atmosphere of N_2. The n.m.r. spectra were recorded and the data indicated the presence of more than one compound. The $^{11}B\{^1H\}$ n.m.r. spectrum contained 16 resonances (see figure 4.6). Some of these may be due to **16** (at δ (p.p.m.)= 9.43, -1.22, -6.60, -14.89 and -16.45). These become doublets on retention of proton coupling, with ^{1}JB-H in the range 120-145Hz., except for the signal at δ= -6.60p.p.m. which is apparently unperturbed (in contrast to the corresponding signal in the spectrum of **16**). There are, in addition, two more resonances, which arise from boron atoms apparently not bound to protons, occurring at δ= +8.18p.p.m. and +5.98p.p.m. The other 9 signals all show proton coupling. These appear at δ (p.p.m.)= -8.44, -9.59, -12.87, -17.92, -20.05, -21.93, -32.01, -34.54 and -35.01. The ^{1}JB-H values lie in the range 130-150Hz., except for the coupling to the boron atom which resonates at δ= -32.01p.p.m. which shows a

proton coupling of only 68Hz. This magnitude of coupling suggests that this proton may occupy an *endo* or bridging position. Due to the complexity of the spectrum it is not possible to obtain relative integrals.

The $^{31}P\{^{1}H\}$ spectrum (see figure 4.7) contains the phosphine oxide resonance at δ= +35.16p.p.m. In addition, there is a complex, weak pattern at just below 0p.p.m. This consists of 2 doublets at δ= -1.55p.p.m. and -6.53p.p.m. which possess mutual P-P coupling of 65.1Hz. This is consistent with *cis*- PP coupling at a square-planar Pd centre[41]. There is also a sharp singlet at δ= -4.84p.p.m. and several other weaker signals. The ^{1}H n.m.r. spectrum of the red material (see figure 4.8) shows evidence for the presence of **16** in small quantity- C-H δ= 3.25p.p.m., Me-H δ= 1.16p.p.m. and 1.44p.p.m. (^{2}JP-H= 10.0Hz.). There is a more intense doublet at δ= 1.73p.p.m. (^{2}JP-H= 13.0Hz), which probably corresponds to the methyl protons in free phosphine oxide. The presence of another carbaborane complex, which gives rise to a C-H resonance at δ= 2.75p.p.m., is also apparent. The phenyl region of the spectrum contains 4 broad multiplets centred on δ(p.p.m.) = 7.10, 7.23, 7.51 and 7.70. Finally, there is a signal of low intensity, arising from free PMe_2Ph (Me-H), at around δ= 0.8p.p.m.

From this spectroscopic evidence, it was not possible to determine the composition of the red product mixture with any certainty. However, it appears to contain **16** and another carbaborane complex, as well as free phosphine oxide and a little un-coordinated phosphine. The presence of phosphine oxide in the sample is not easy to explain, especially given that only a trace of free phosphine is present and that this phosphine is not rapidly oxidised under normal conditions. In solution the mixture turns purple with time and even in the solid state, under an atmosphere of dry N_2, the purple colouration slowly appears. It seems most likely that the red species is a reaction intermediate.

Figure 4.6

$^{11}B/^{11}B\{^1H\}$ n.m.r. spectra of red reaction mixture, 64.210MHz., 25°C (298K).

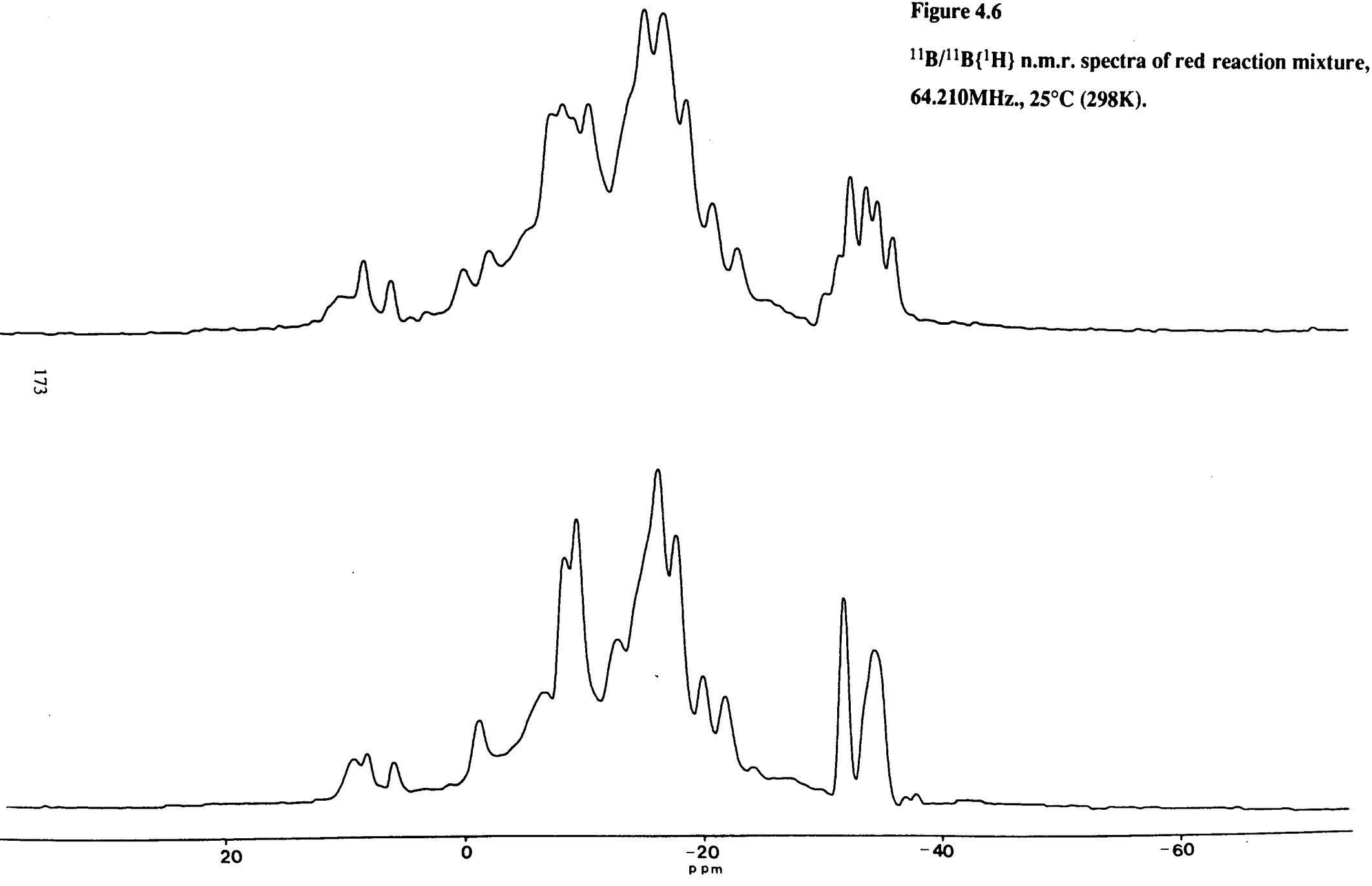

Figure 4.7

$^{31}P\{^{1}H\}$ n.m.r. spectrum of red reaction mixture, 81.020MHz., 25°C (298K).

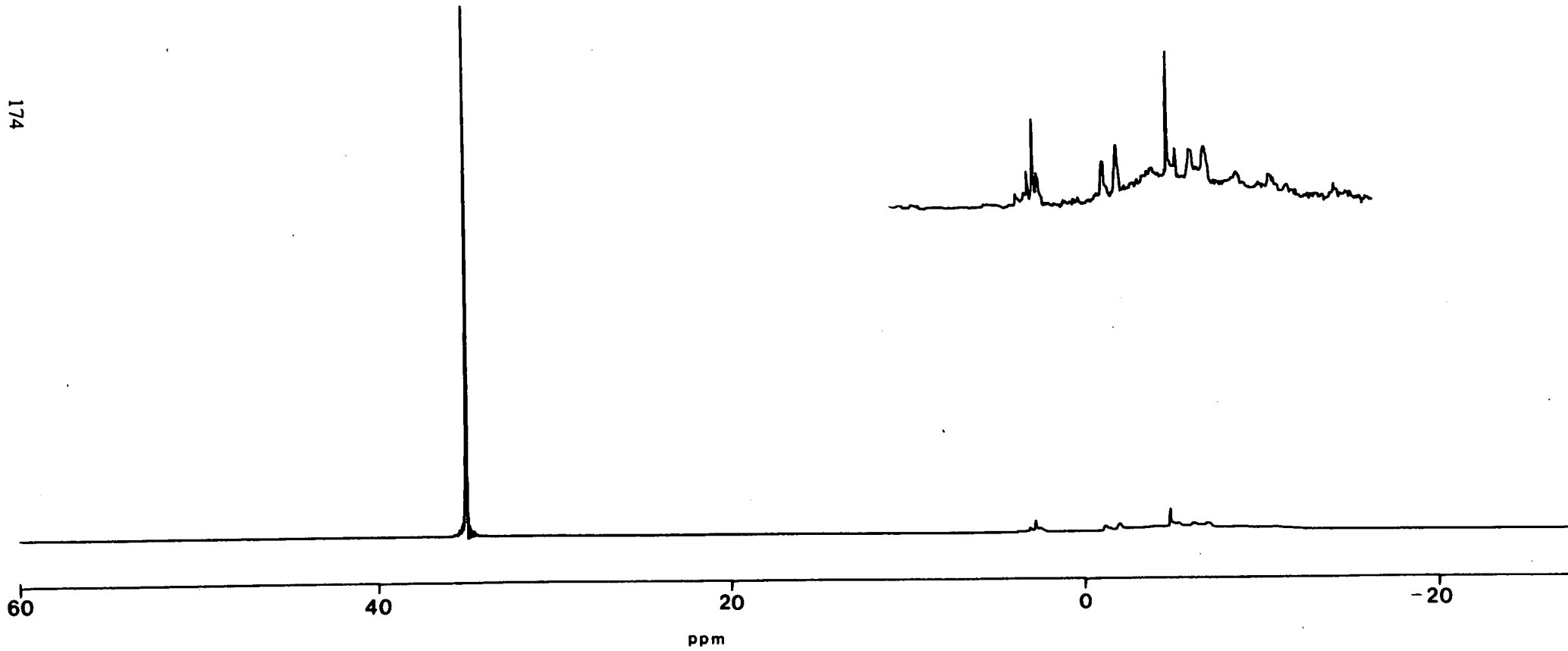

Figure 4.8

^{1}H n.m.r. spectrum of red reaction mixture, 200.130MHz., 25°C (298K).

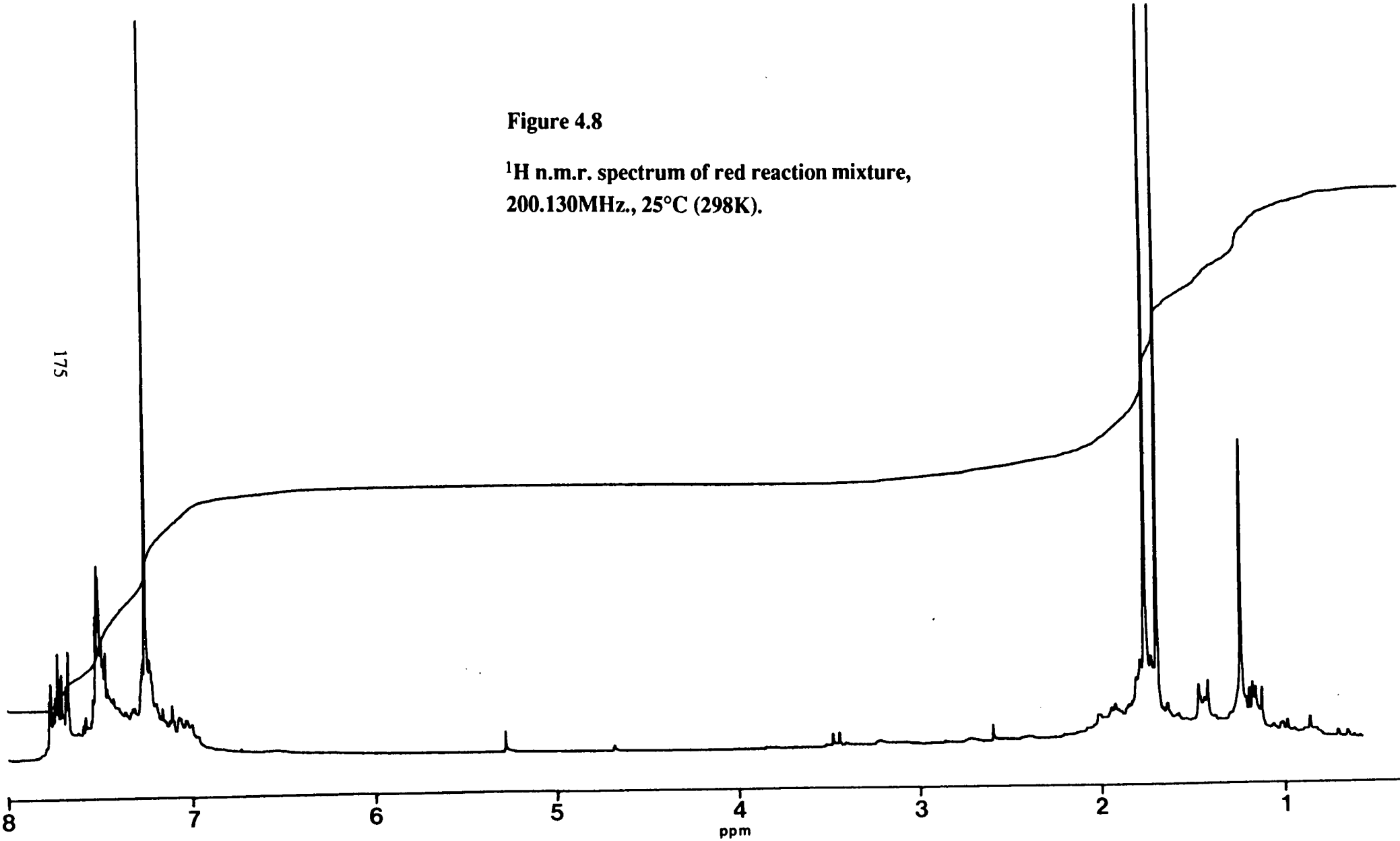

The reaction was repeated on a number of occasions, but consistent n.m.r. data of the product of column chromatography could not be obtained. Often the resonances denoting **16** were dominated by another set of peaks and sometimes they were not present at all. The $^{11}B\{^1H\}$ spectrum of this other product contains 7 resonances in the ratio 2:1:2:1:1:1:1, at δ (p.p.m.)= -9.33, -14.45, -16.49, -20.00, -32.07, -33.64 and -34.33 (see figure 4.9). The 4 resonances to high frequency show "normal" coupling to terminal protons[38] in the proton coupled spectrum with ^1JBH in the range 125 - 155Hz. However, the 3 signals to low frequency give only 4 lines on retention of proton coupling. This can be explained if only one of these boron atoms (the one which resonates at δ= -33.64p.p.m.) is coupled to a terminal proton with ^1JBH= 145Hz. The other 2 boron atoms could then be coupled only to *endo* or bridging hydrogen atoms (^1JBH= 64.2Hz., 63.9Hz.). One line from each of these doublets overlapping with the other doublet would give rise to the observed pattern and intensities.

The $^{31}P\{^1H\}$ n.m.r. spectrum of this species (81.020MHz.) consists of 2 overlapping doublets (in the ratio 1:1), at δ= -6.55p.p.m. and -8.85p.p.m., with mutual coupling of ^2JPP= 291.1Hz. (see figure 4.10). That this was a genuine coupling was confirmed from the spectrum at higher field (145.836MHz.) in which the couplings were retained. This magnitude of coupling suggests that there has been a change in the ligand arrangement at the metal centre. The coupling is approximately midway between that expected for a *cis*- palladium bis-phosphine species (^2JPP *circa* 8-80Hz.) and that for the *trans*- analogue (^2JPP *circa* 500-800Hz.)[41].

The proton spectrum (see figure 4.11) contains a doublet of doublets representing the methyl protons at δ= 1.77p.p.m. with ^2JPH =12.3Hz. and ^4JPH= 3.9Hz., integrating for 6 protons.

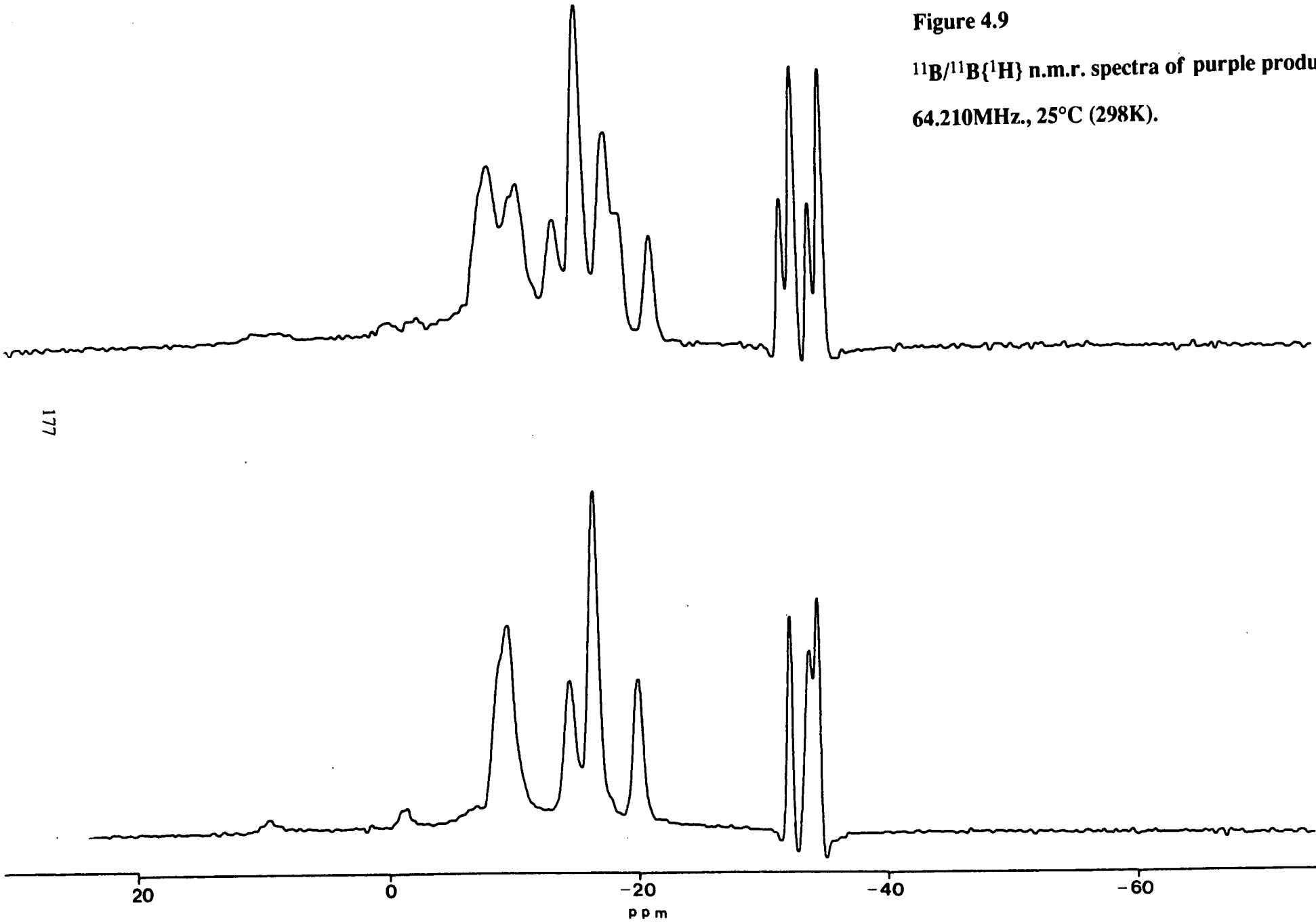

Figure 4.9

$^{11}B/^{11}B\{^{1}H\}$ n.m.r. spectra of purple product, 64.210MHz., 25°C (298K).

Figure 4.10

$^{31}P\{^{1}H\}$ n.m.r. spectrum of purple product, 81.020MHz., 25°C (298K).

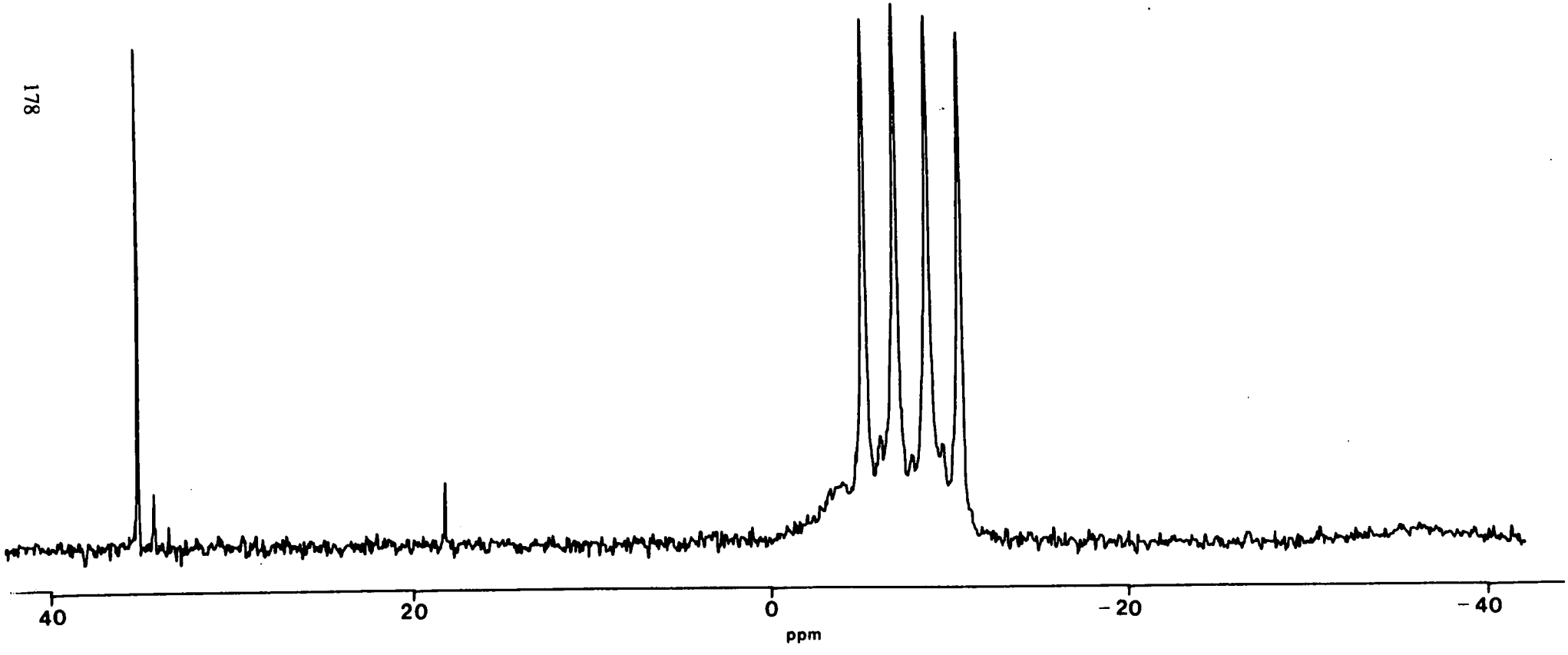

Figure 4.11

^{1}H n.m.r. spectrum of purple product, 200.130MHz., 25°C (298K).

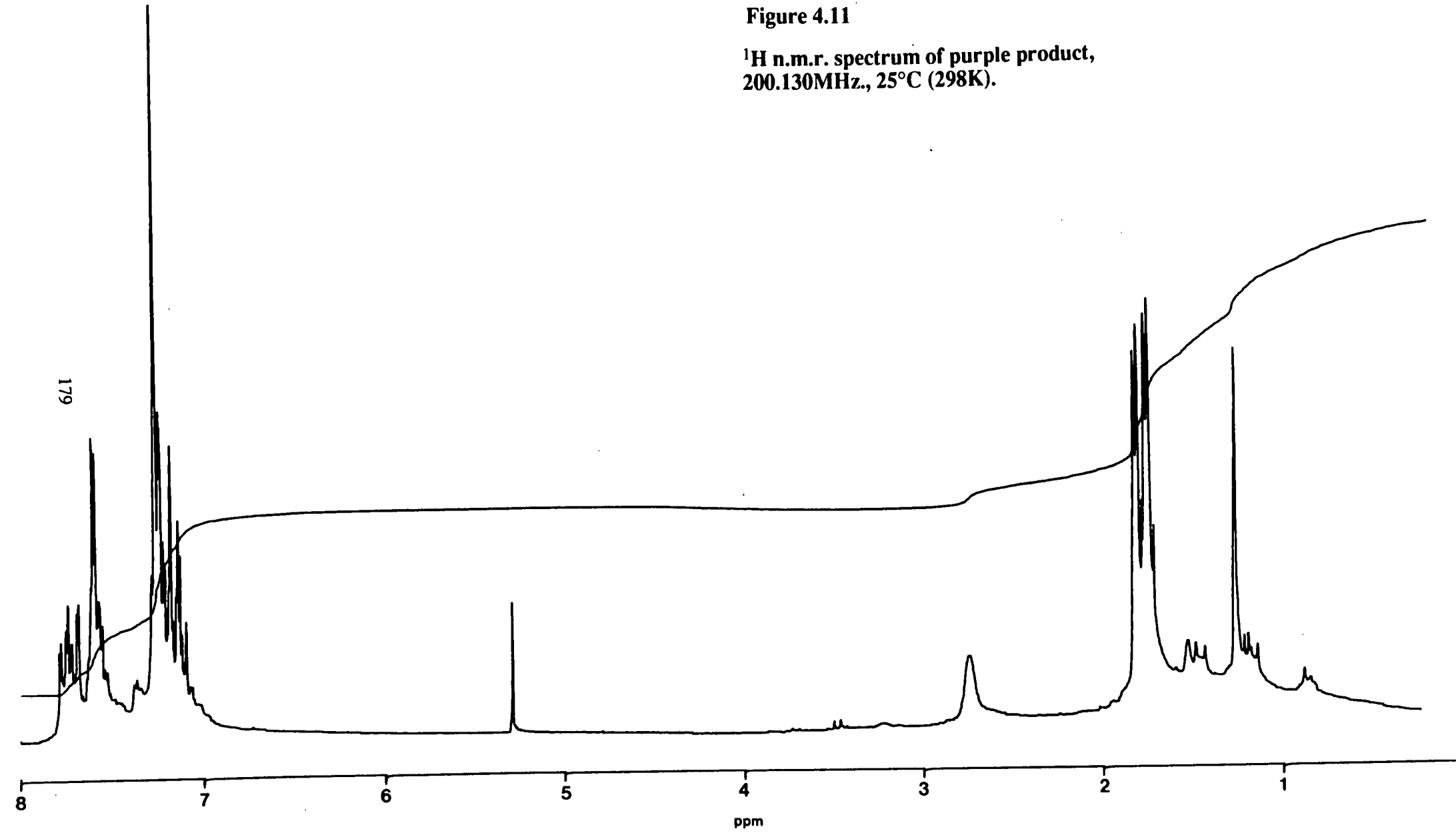

The C-H proton resonates at δ= 2.74p.p.m. The phenyl region contains 4 multiplets centred on δ= 7.12p.p.m., 7.17p.p.m., 7.23p.p.m. and 7.60p.p.m. In addition there are two overlapping doublets of doublets at δ= 7.76p.p.m. with couplings of 12.1Hz. and 1.6Hz., and at δ= 7.71p.p.m. with couplings of 12.1Hz. and 2.2Hz. The total relative integral of the signals in this region suggests that there are 10 phenyl protons.

Although the ^{11}B n.m.r. spectra of this species show no evidence for the presence of a high frequency boron resonance, the complex is not believed to be simply the 3,1,11-isomer of **16**. This is implied from the low frequency region of the spectrum, in which there are two boron resonances which do not couple to a terminal proton, but, in each case, couple only to a bridging or *endo* hydrogen. Further, the phosphorus spectrum is not consistent with a *cis* square-planar palladium centre (as the PP coupling constant is too large).

Attempts to devise a plausible structure, consistent with the observed data, proved largely unsuccessful. The metal fragment may contain a third ligand, causing the 2 phosphines to adopt a more transoid arrangement. There is no evidence for the presence of a metal-hydride bond (from ^{1}H n.m.r. or infra-red spectroscopies) leaving the most likely candidate to be Cl^-, which could conceivably have been picked up from the solvent. Alternatively, the metal-centre may be 3 co-ordinate (Pd^0), with the concomitant increase in s-character of the bonding causing the observed increase in P-P coupling[115]. Reduction of the M^{2+} could be related to the appearance of $O{=}PMe_2Ph$ in the sample. The nature of the co-ordination of the metal fragment to the cage is not clear. There is no evidence for bridging B-H-Pd linkages, which may suggest Pd-B σ bonding. It may be helpful if the conditions which favour the formation of this species, rather than **16**, could be determined. However, other than a possible concentration effect, in which **16** is favoured at high concentrations, no such conditions were apparent. Indeed, from sample to sample it was not possible to predict the nature of the dominant product.

Warming a sample (in which this latter species was thought to be the major one) in toluene, for 30 minutes leads to a change in the colour of the solution (purple to yellow) and some deposition to a black material. The n.m.r. spectra of the isolated yellow species indicates that it is essentially similar to the starting complex. The ^{11}B and proton spectra are identical to those of an un-thermolysed sample. However, the $^{31}P\{^{1}H\}$ spectrum, as well as containing the signals previously observed, also contains an additional singlet at δ +6.86p.p.m. It was concluded that thermolysis does not lead to isomerisation. With the complication of the presence of more than one carbametallaborane, it is not possible to determine if the failure to isolate a 3,1,11-carbametallaborane, in this case, provides any important data on the factors which facilitate low temperature isomerisations in carbaplatinaboranes.

$Tl_2C_2B_9H_9Ph_2$ and *cis*-$PdCl_2(PMe_2Ph)_2$ were mixed in CH_2Cl_2 and stirred for two hours. The solution turned orange and TlCl was precipitated. The soluble product was separated by column chromatography and the orange mobile band further purified by t.l.c. (silica plates, CH_2Cl_2 eluent). There were several mobile bands but only was one of sufficient intensity to merit collection- a yellow band at R_f= 0.9. This band was removed from the plates with CH_2Cl_2 and yielded a yellow solid, **17**, on removal of solvent *in vacuo*.

The i.r. spectrum confirms the presence of borane (νB-H= 2550cm^{-1}). There are 8 resonances in the $^{11}B\{^{1}H\}$ n.m.r. spectrum of **17**, in the range δ= -1.89 to -25.70p.p.m. in the ratio 1:1:1:1:1:1:2:1 (see figure 4.12).

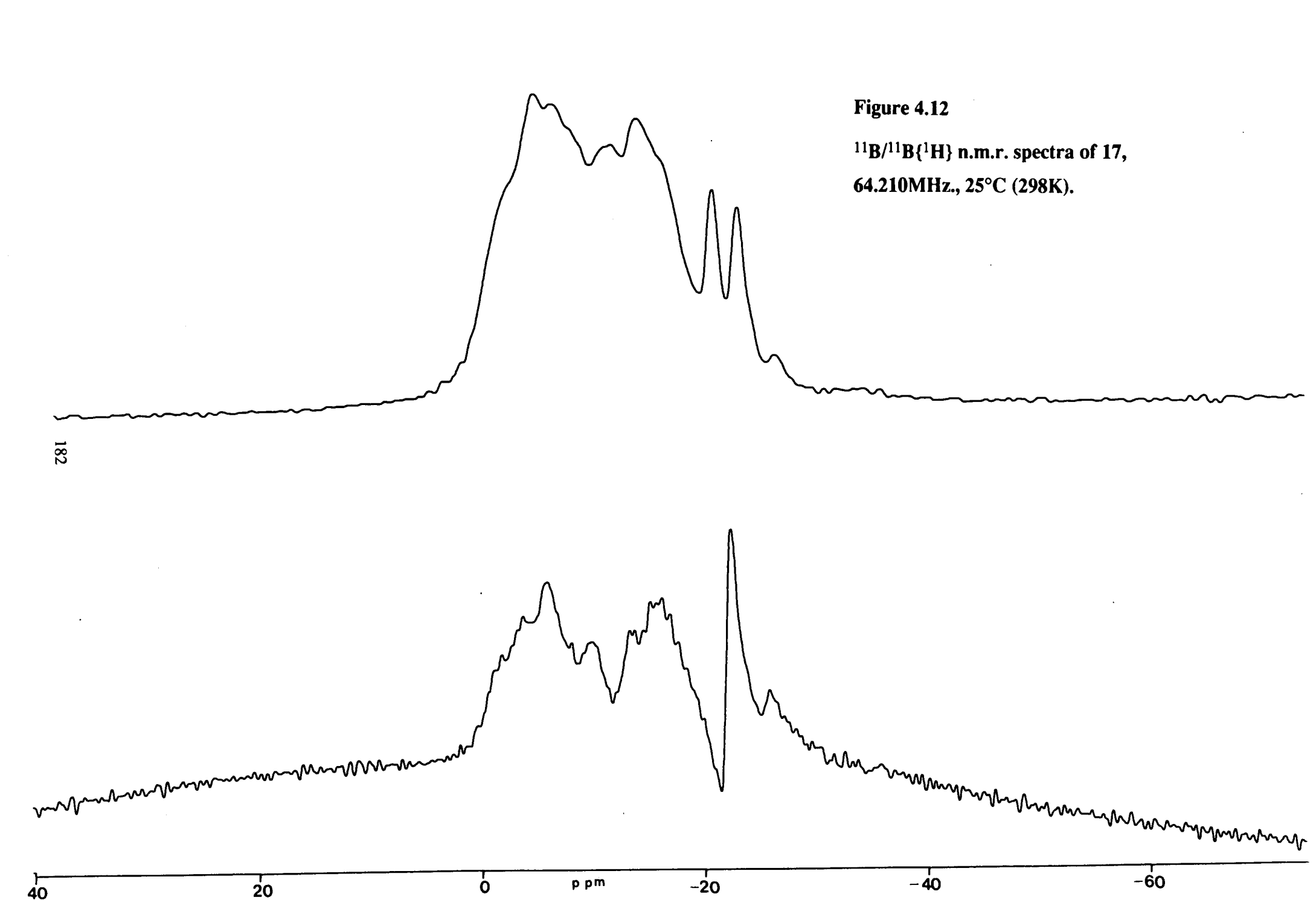

Figure 4.12

$^{11}B/^{11}B\{^{1}H\}$ n.m.r. spectra of 17, 64.210MHz., 25°C (298K).

Each of these signals becomes a doublet in the proton coupled spectrum, with ^{1}JB-H in the range 125-160Hz. The $^{31}P\{^{1}H\}$ spectrum shows that there are two phosphorus environments. These give rise to resonances at δ= -8.31 and -11.61p.p.m. and possess mutual P-P coupling of 52.7Hz. (see figure 4.13). This indicates that two types of nuclei are present in one molecule. The ^{1}H n.m.r. spectrum of a sample of **17** contains one broad multiplet representing the methyl protons. There are 5 additional signals corresponding to phenyl protons. Four of these are multiplets (centred on δ= 7.16p.p.m., 7.29p.p.m., 7.48p.p.m. and 7.83p.p.m.(weak)), while the fifth is a doublet of doublets at δ= 7.03p.p.m. with couplings of 8.2 and 1.2Hz.

The absence of a high frequency boron resonance in the ^{11}B n.m.r. spectra indicates that the metal-bonded face is not of the C_2B_3 type, and the complexity of the phenyl region of the proton spectrum, suggests that the carbaborane is asymmetric. It is reasonable to assume that the nature of the carbaborane is the same as in the analogous platinum species (**4**) and, therefore, **17** can be formulated as 1,11-Ph_2-3,3-$(PMe_2Ph)_2$-3,1,11-$PdC_2B_9H_9$.

The cyclic voltammetry of the purple species from the previous reaction, and of **17** were studied. The former is oxidised quasi-reversibly (at 1.16V). This process becomes more reversible with increasing scan rate and decreasing temperature. There are two further oxidations which are both irreversible, at 1.61V and 1.75V. In the reductive range there are two redox processes (see figure 4.14). The one occurring at -1.45V is quasi-reversible, whereas the other one, at -1.85V, gives rise to a daughter product which is re-oxidised at -0.48V. **17** exhibits two oxidations at 1.23V and 1.78V. The former of these is quasi-reversible, becoming more reversible at low temperature, whereas the latter is irreversible. Comparison of this behaviour with that of **4** shows that both exhibit two oxidations but both of these are more facile in the platinum-species. No reductions are observed for the purple complex, whereas **17** has a single irreversible process.

Figure 4.13

$^{31}P\{^{1}H\}$ n.m.r. spectrum of 17, 81.020MHz., 25°C (298K).

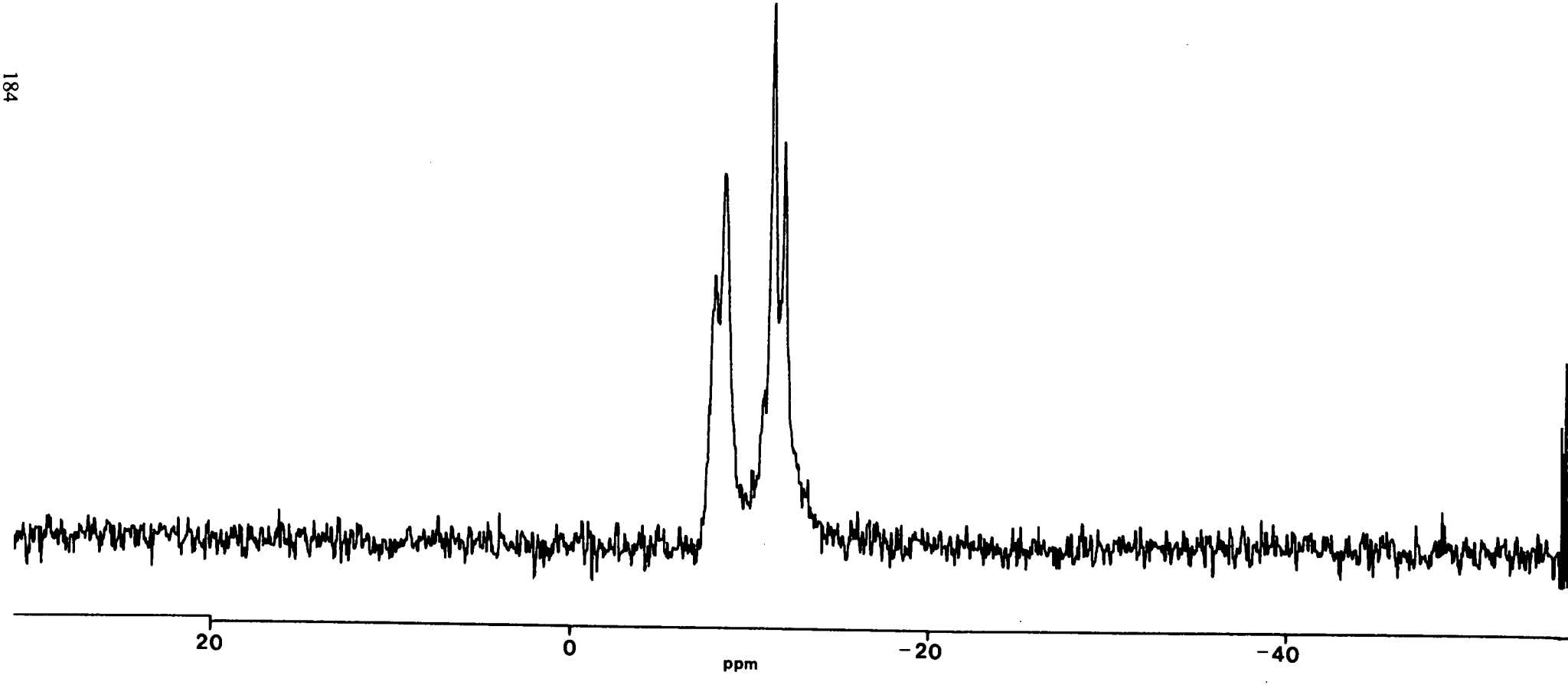

Figure 4.14

Cyclic voltammogram showing reduction of purple product.

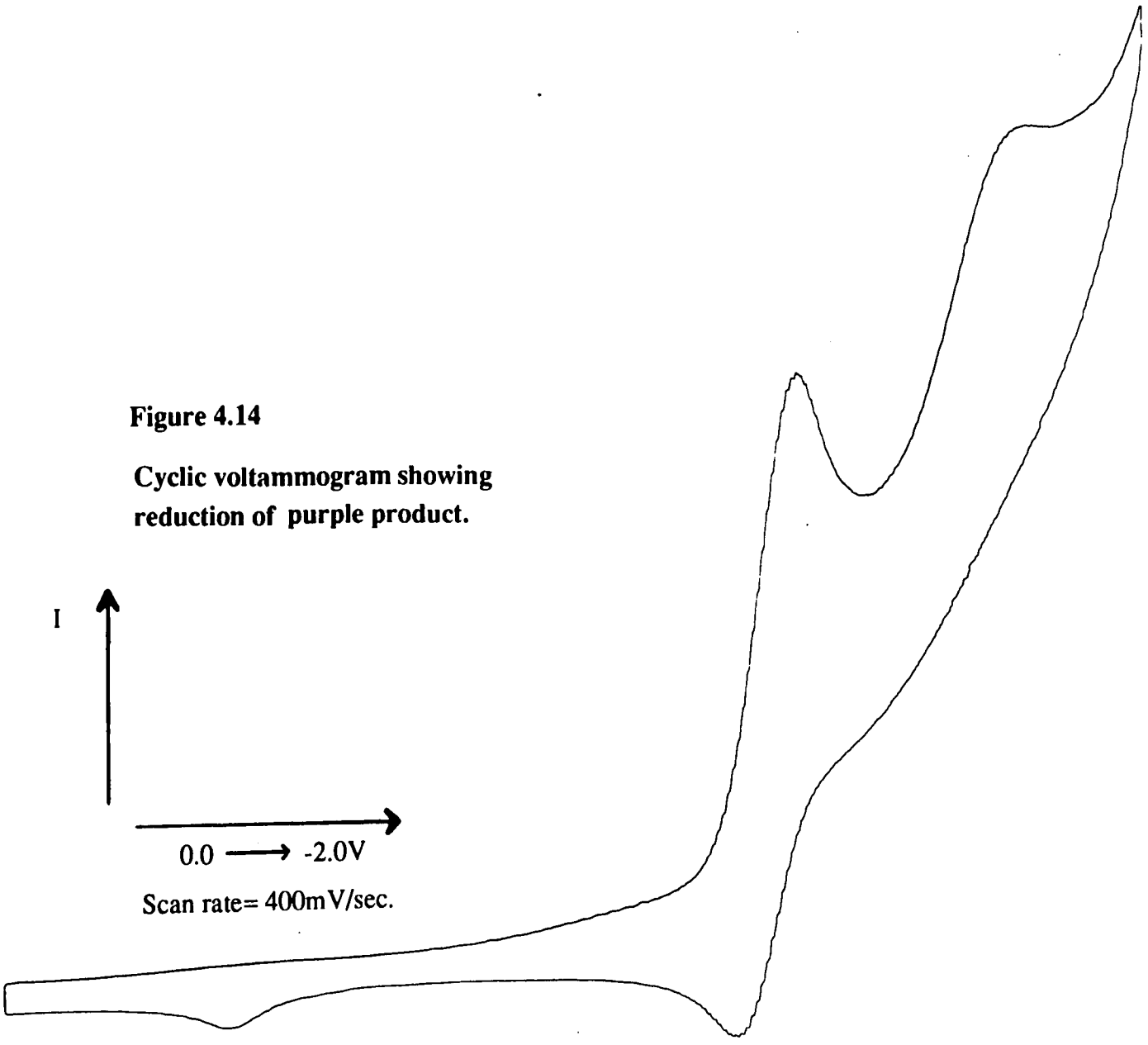

Whereas **17** is analogous to **4** it is clear that **16** behaves differently to **1**. Even discounting the failure of **16** to form a 3,1,11-isomer, the presence of another accessible carbametallaborane alone represents a significant change in its behaviour. As the nature of this other carbametallaborane could not be ascertained, it was not clear which factors were important in its formation. The effect of varying the nature of the non-carbaborane ligand was now studied via the synthesis of complexes incorporating the {Pd(1,5-COD)} fragment.

4.3 Carbaborane Complexes Containing the {Pd(1,5-COD)} Fragment.

When $Tl_2C_2B_9H_{10}Ph$ and $PdCl_2$(1,5-COD) were reacted in CH_2Cl_2, a dark red soluble product was obtained. After separation from the reaction mixture, this was found to consist of a number of species, although microanalysis figures were reasonable for the expected composition, $C_{16}H_{27}B_9Pd$. The constituents were separated by t.l.c. (silica plates, 1:1 CH_2Cl_2/n-hexane eluent). This revealed 6 mobile bands and an immobile one. All the mobile bands were collected although only the most intense of these (band A, purple, R_f= 0.5) was in sufficient quantity to permit satisfactory characterisation. This is described later, but first the minor products and the limited spectroscopic data available for them are discussed.

Band B is dark red with an R_f of 0.6 and shows a B-H stretching band in the i.r. spectrum at ν= 2530cm^{-1}, as well as a C-H band at 2860cm^{-1}. The $^{11}B\{^1H\}$ n.m.r. spectrum is extremely complex and shows evidence of decomposition during spectral accumulation. There are 8 principal resonances in the range δ +20.25 to -16.15p.p.m. and also a number of peaks of lower intensity. This decomposition prevented the recording of a proton coupled spectrum. The ^1H spectrum is poorly resolved. There are 3 signals attributable to the COD-C$\underline{H}_2$ protons (δ= 2.13, 2.30 and 2.55p.p.m.) which are all multiplets. In addition, there is a resonance at δ= 5.75p.p.m.

corresponding to the COD-C<u>H</u> protons. In the phenyl region of the spectrum there are 2 multiplets centred on δ= 7.30 and 7.60p.p.m. The appearance of a high frequency boron resonance, coupled with the multiplicity of the COD signals in the proton spectrum, implies that the metal fragment is bound to an asymmetric cage face.

At slightly higher R_f value there is a red/green band (band C). There are two C-H bands in the i.r. spectrum of this species, at ν= 2900 and 2840cm^{-1}, and also a B-H band at ν= 2530cm^{-1}. The $^{11}B\{^1H\}$ n.m.r. spectrum contains 9 resonances in the range δ= +20.40 to -14.97p.p.m. Each of these becomes a doublet on retention of proton coupling (^{1}JB-H in the range 135-160Hz.), except for the signal at δ= +6.73p.p.m., which is unperturbed. The ^{1}H n.m.r. spectrum contains a broad resonance and a multiplet representing COD-C<u>H</u>$_2$ protons. There are 2 broad multiplets corresponding to COD-C<u>H</u> protons centred on δ= 5.60 and 5.75p.p.m., while the phenyl region contains 2 multiplets. The cage C-<u>H</u> resonates at δ 4.92p.p.m. From this data it seems that a 3,1,2-framework may be maintained. However, the nature of this species is not clear, in view of the fact that one of the boron atoms appears not to be bonded to a hydrogen atom.

Band D has a slightly higher R_f value still (0.7). This purple species has 8 signals in its $^{11}B\{^1H\}$ n.m.r. spectrum in the range δ= +20.39 to -17.00p.p.m. (see figure 4.15). All of these signals become doublets in the proton coupled spectrum (^{1}JB-H in the range 130 to 160Hz.) except the one at around δ= 6.7p.p.m. (as observed in the spectra of band C). The i.r. spectrum contains bands at ν= 2910cm^{-1} (C-H) and 2520cm^{-1} (B-H).

Figure 4.15

^{11}B n.m.r. spectrum of band D, 64.210MHz., 25°C (298K).

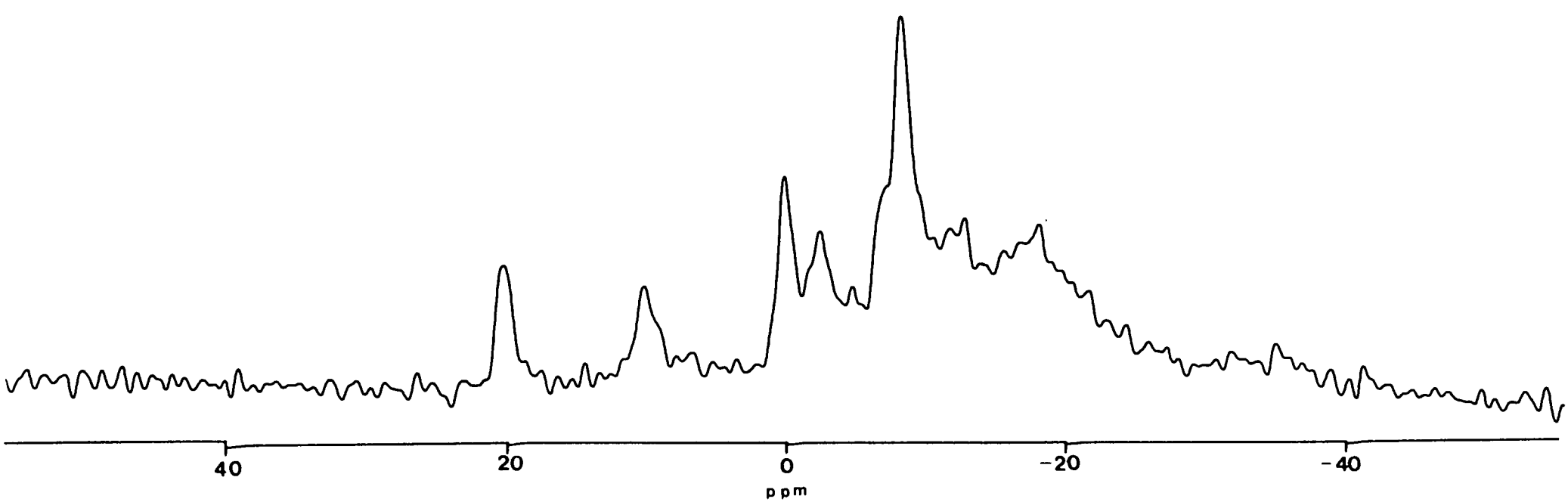

Band E has an R_f value of 0.74 and is yellow, with a B-H band in the i.r spectrum at ν= 2560cm^{-1}. The $^{11}B\{^1H\}$ n.m.r. spectrum is poorly resolved. However, 5 resonances can be distinguished in the range δ= +20.18 to -16.93 and in the ratio 1:1:3:3:1 (see figure 4.16). It was not possible to obtain a proton coupled spectrum nor a ^1H spectrum for this species and hence no conclusions can be drawn as to its nature.

Band F is yellow and has an R_f value of 0.83. The i.r. spectrum contains bands at ν= 2920cm^{-1} (C-H) and 2570cm^{-1} (B-H). There are 9 major resonances in the complicated $^{11}B\{^1H\}$ spectrum, in the range δ= +26.20 to -12.07 and in the ratio 1:1:1:1:1:1:2:2:1. Each of these shows coupling to a terminal hydrogen atom in the proton coupled spectrum (^{1}JB-H in the range 140 to 180Hz.). The proton spectrum shows no evidence for the presence of COD, but does confirm the presence of cage C-H (δ= 3.12p.p.m.) and phenyl protons (2 multiplets centred on δ= 7.36 and 7.70p.p.m.). Bis-carbaborane palladium sandwich complexes, of the type $[Pd(C_2B_9H_{11})_2]$, which contain unsubstituted carbaboranes are well documented[106]. It is possible that this band corresponds to a phenyl- substituted analogue of this type (*e.g.* $Pd(C_2B_9H_{10}Ph)_2$).

Figure 4.16

^{11}B n.m.r. spectrum of band E, 64.210MHz., 25°C (298K).

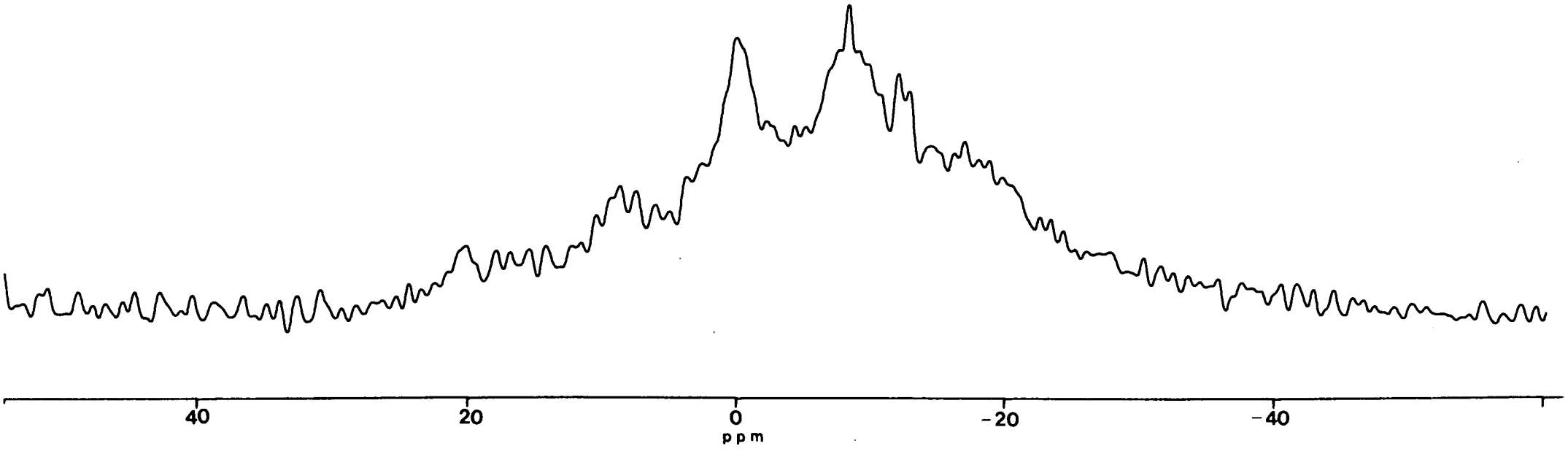

The major band (A) shows 7 resonances in the $^{11}B\{^1H\}$ n.m.r. spectrum in the ratio 1:1:1:1:3:1:1 (see figure 4.17). The one at highest frequency, δ +20.06p.p.m., can tentatively be assigned to B(8). All the resonances are doublets in the proton coupled spectrum with $^1JB\text{-}H$ in the range 135-160Hz., indicating that each boron atom is bound to a terminal hydrogen atom. The ^1H n.m.r. spectrum (see figure 4.18) contains 3 multiplets, centred on δ 2.09, 2.30 and 2.54p.p.m., arising from the COD-$C\underline{H}_2$ protons. The COD-C<u>H</u> protons are denoted by 2 multiplets centred on δ 4.93 and 5.81p.p.m. The presence of multiple signals corresponding to the COD protons suggests that the metal fragment is associated with an asymmetric carbaborane. The spectrum also contains a signal which denotes the cage C-<u>H</u>, at δ 4.73p.p.m. Finally, there are two resonances in the phenyl region of the spectrum; a multiplet centred on δ 7.32p.p.m. corresponding to 3 hydrogen atoms, and a doublet of doublets, centred on δ= 7.58p.p.m., integrating for 2 protons, with couplings of 7.8Hz. and 1.4Hz. The i.r. spectrum (CH_2Cl_2) contains a B-H stretching band at 2515cm^{-1}. The spectroscopic evidence is consistent with the expected species, namely 1-Ph-3-(1,5-COD)-3,1,2-$PdC_2B_9H_{10}$.

A sample of **18** was suspended in toluene and the mixture warmed at 50°C for 1 hour. There was no apparent colour change so the temperature was increased and the mixture stirred at reflux temperature for a further 30 mins. During this time some decomposition was observed. However, the colour of the remainder of the sample was unchanged. The solvent was removed *in vacuo* to yield a purple/black residue. The $^{11}B\{^1H\}$ spectrum is almost identical to that of **18** except for the appearance of 2 new signals, at δ= -10.26 and -12.15p.p.m. These additional resonances perhaps indicate some decomposition has occurred. Crucially, however, the high frequency resonance, at *circa* δ= +20p.p.m. is still present, suggesting that the nature of the metal-bonded face has not changed. The proton spectrum is identical to that of **18** confirming that no isomerisation has occurred.

Figure 4.17

$^{11}B/^{11}B\{^1H\}$ n.m.r. spectra of band A (18), 64.210MHz., 25°C (298K).

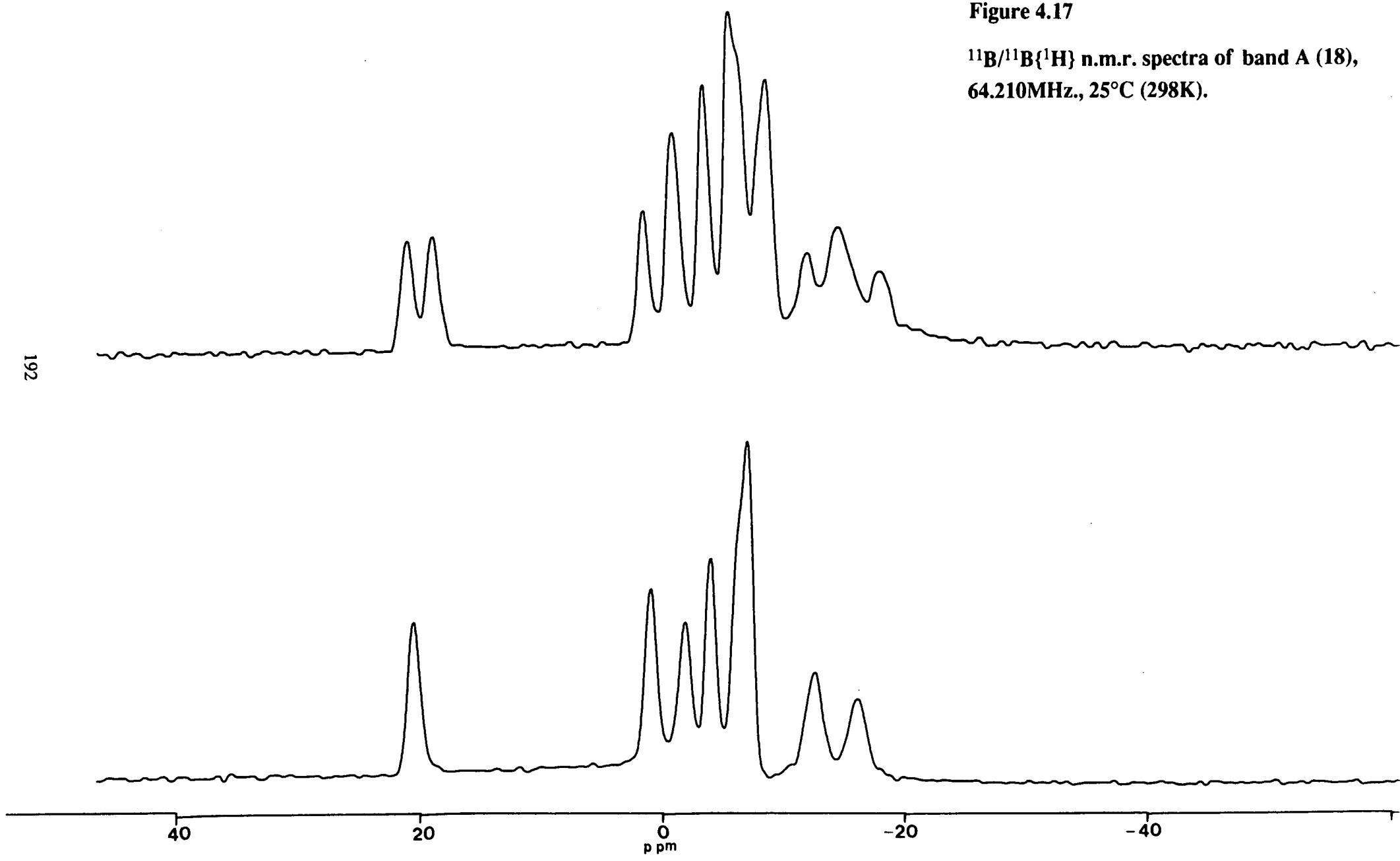

Figure 4.18

^{1}H n.m.r. spectrum of band A (18), 200.130MHz., 25°C (298K).

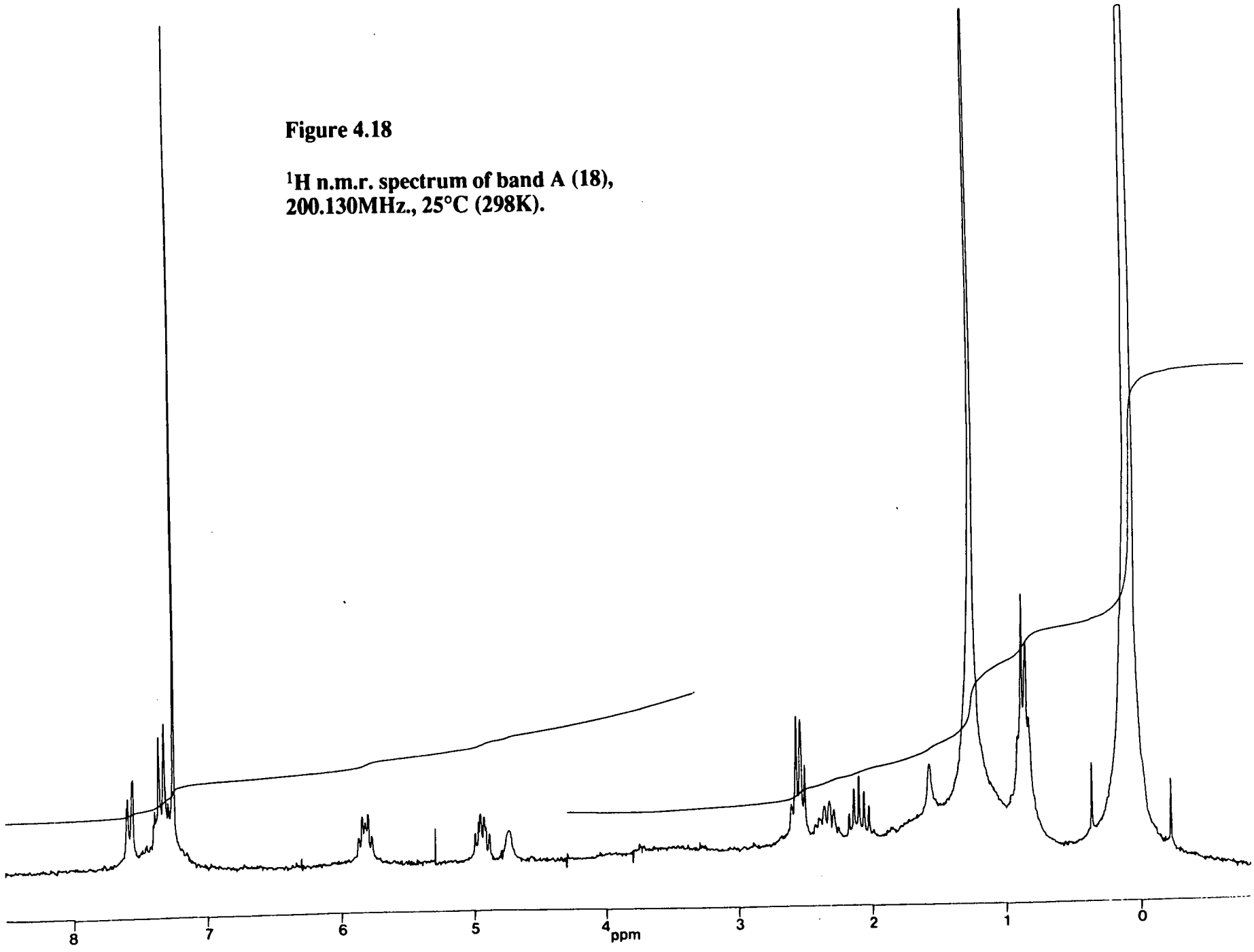

When $Tl_2C_2B_9H_9Ph_2$ was reacted with $PdCl_2$(1,5-COD) in CH_2Cl_2 a purple soluble product formed. This was separated from the reaction mixture by filtration. Microanalysis figures were reasonable for the predicted formulation, $C_{22}H_{31}B_9Pd$, however, t.l.c. indicated the presence of several components. The crude product was chromatographed (silica plates/CH_2Cl_2 eluent) to yield 7 bands. Six of these were mobile and were recovered while the seventh immobile band was not. The red band (band 1), with lowest R_f (0.51), was the most abundant and full characterisation was possible (see later).

The next band (band 2, orange, R_f= 0.56) has 7 resonances in its $^{11}B\{^1H\}$ spectrum (see figure 4.19). One of these is at relatively high frequency (δ +14.98p.p.m.). Each of these signals becomes a doublet in the proton coupled spectrum with ^{1}JB-H in the range 130 to 160Hz. The signals corresponding to the COD protons in the ^{1}H n.m.r. spectrum are broad, occurring at δ 2.55p.p.m. for the 8 $C\underline{H}_2$ protons and δ 5.58p.p.m. for the 4 C<u>H</u> protons (see figure 4.20). The phenyl region of the spectrum contains 2 signals- a multiplet at δ 7.16p.p.m. representing 6 protons and a doublet of doublets at 7.41p.p.m. (J= 6.5 and 1.0Hz.) integrating for 4 protons. The i.r. spectrum contains a band at ν= 2515cm^{-1} (B-H).

Band 3 is yellow with an R_f value of 0.66. In the i.r. spectrum there is a band at ν 2565cm^{-1} (B-H). The $^{11}B\{^1H\}$ n.m.r. spectrum is complicated, containing 5 bands in the range δ= -4.22 to -14.99p.p.m. as well as a number of less intense resonances. The major signals all show coupling to a terminal proton, in the proton coupled spectrum, with ^{1}JB-H in the range 120 to 160Hz., but for a number of the minor bands there is no resolved coupling. The ^{1}H spectrum is poorly resolved. While the signals corresponding to the phenyl protons are present (multiplets centred on δ= 7.15 and 7.38p.p.m.) there is no conclusive evidence for the presence of COD. There does appear to be some structure on the baseline in the relevant regions of the spectrum, however.

Figure 4.19

$^{11}B/^{11}B\{^1H\}$ n.m.r. spectra of band 2, 64.210MHz., 25°C (298K).

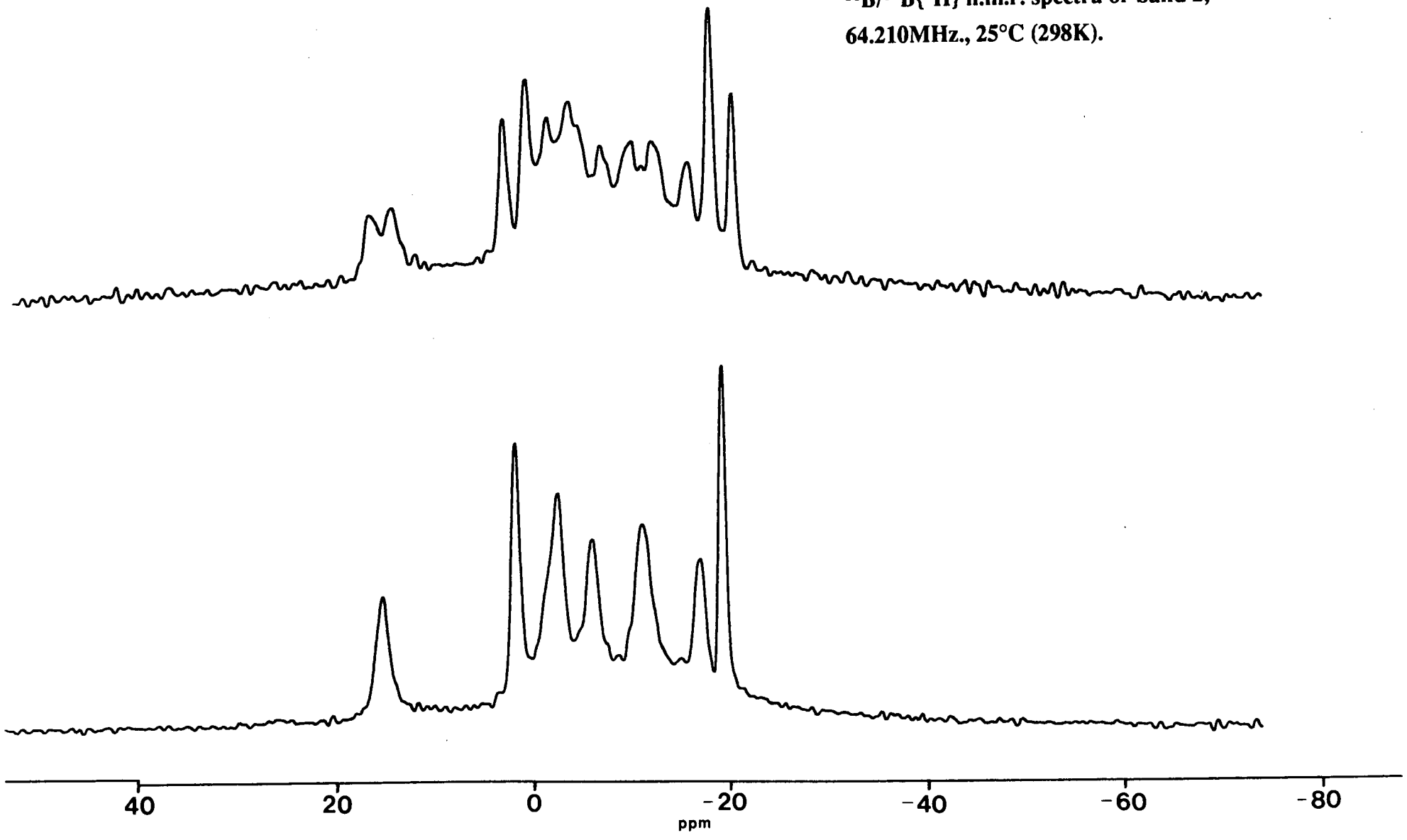

Figure 4.20

^{1}H n.m.r. spectrum of band 2, 200.130MHz., 25°C (298K).

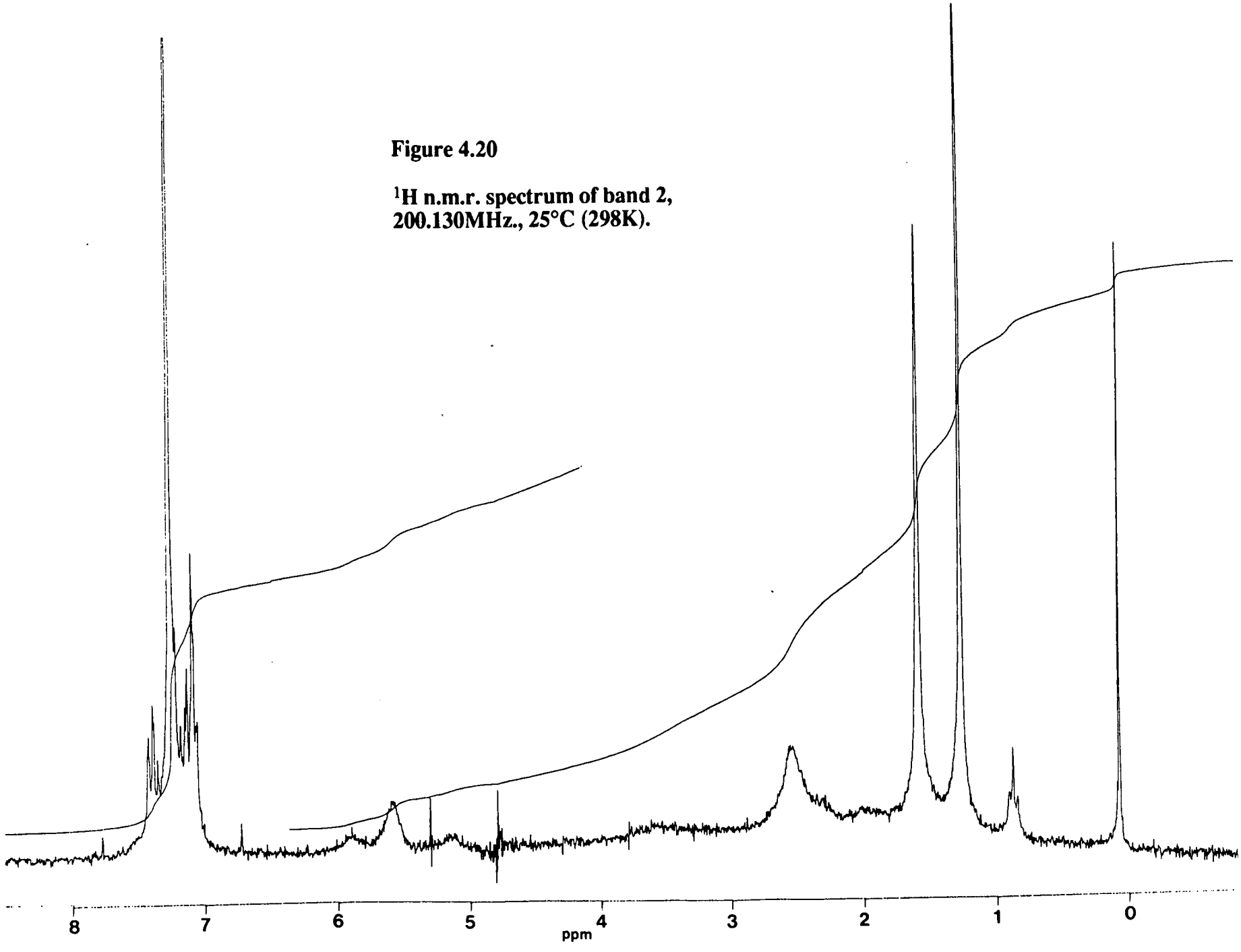

At slightly higher R_f value (0.7) a weak red band (band 4) was observed. The i.r. spectrum contains a band corresponding the B-H stretch (at 2560cm^{-1}). The $^{11}B\{^1H\}$ spectrum comprises 8 resonances in the range δ +25.76 to -27.23p.p.m. (see figure 4.21). As for the previous band, the spectrum is complicated by the presence of several lower intensity signals. More information can be obtained from the ^1H n.m.r. spectrum (see figure 4.22). This consists of 2 broad resonances arising from the COD protons, at δ 2.52p.p.m. for the 8 $C\underline{H}_2$ protons and at δ 5.52p.p.m. for the 4 $C\underline{H}$ protons. In addition there are 2 multiplets in the phenyl region of the spectrum- occurring at δ 7.17p.p.m. corresponding to 4 protons and at δ= 7.55p.p.m. integrating for 6 protons. The appearance of this spectrum suggests that the carbaborane ligand is symmetric.

Band 5 is orange with an R_f value of 0.78. The i.r. spectrum contains a bands at 2540cm^{-1} (B-H). The $^{11}B\{^1H\}$ spectrum of this species is poorly resolved, but 5 principal resonances can be distinguished, including a relatively high frequency one at δ= +15.56p.p.m. The ^1H n.m.r. spectrum contains signals attributable to the COD protons, at δ= 2.55p.p.m. and 5.56p.p.m. for the CH_2 and CH protons, respectively. There are also two multiplets which denote the phenyl protons, centred on δ= 7.20 and 7.40p.p.m. Again, these spectra are consistent with the presence of a symmetric carbaborane ligand.

The final minor band collected is pale yellow with an R_f value of 0.89. It has bands at ν= 2910cm^{-1} and 2855cm^{-1} (C-H) and 2570cm^{-1} (B-H) in its i.r. spectrum. The $^{11}B\{^1H\}$ spectrum contains 3 resonances in the ratio 2:4:4, at δ= -1.76, -8.43 and -9.73p.p.m., respectively (see figure 4.23). This corresponds to the spectrum of 1,2-Ph_2-*closo*-1,2-$C_2B_{10}H_{10}$. The ^1H spectrum of band 6 comprises two multiplets only, arising from the phenyl protons. The origin of the *closo*-carbaborane is not clear. It may be present as an impurity in the $Tl_2C_2B_9H_9Ph_2$ or as a by-product of reaction.

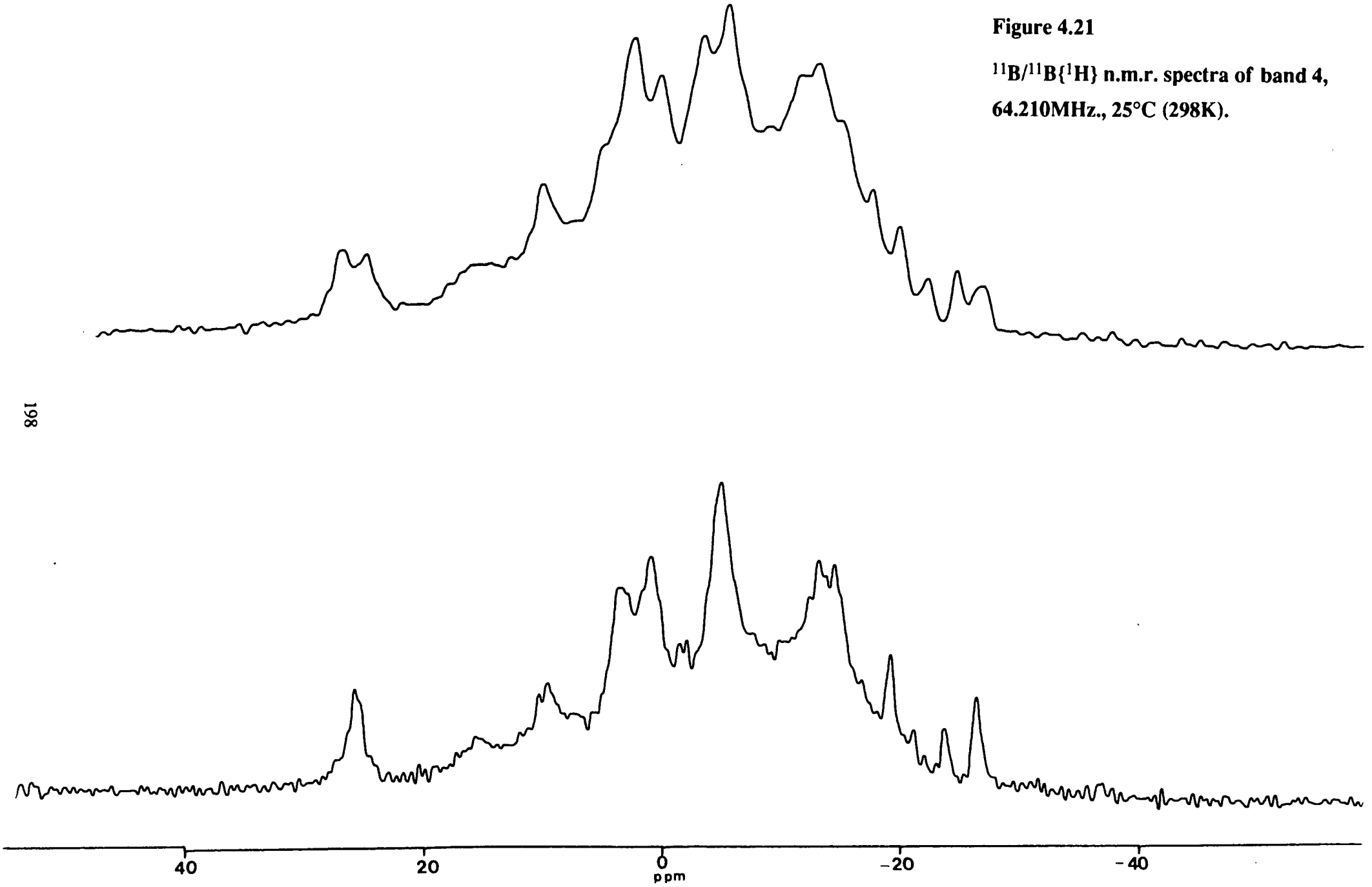

Figure 4.21

$^{11}B/^{11}B\{^{1}H\}$ n.m.r. spectra of band 4, 64.210MHz., 25°C (298K).

Figure 4.22

^{1}H n.m.r. spectrum of band 4, 200.130MHz., 25°C (298K).

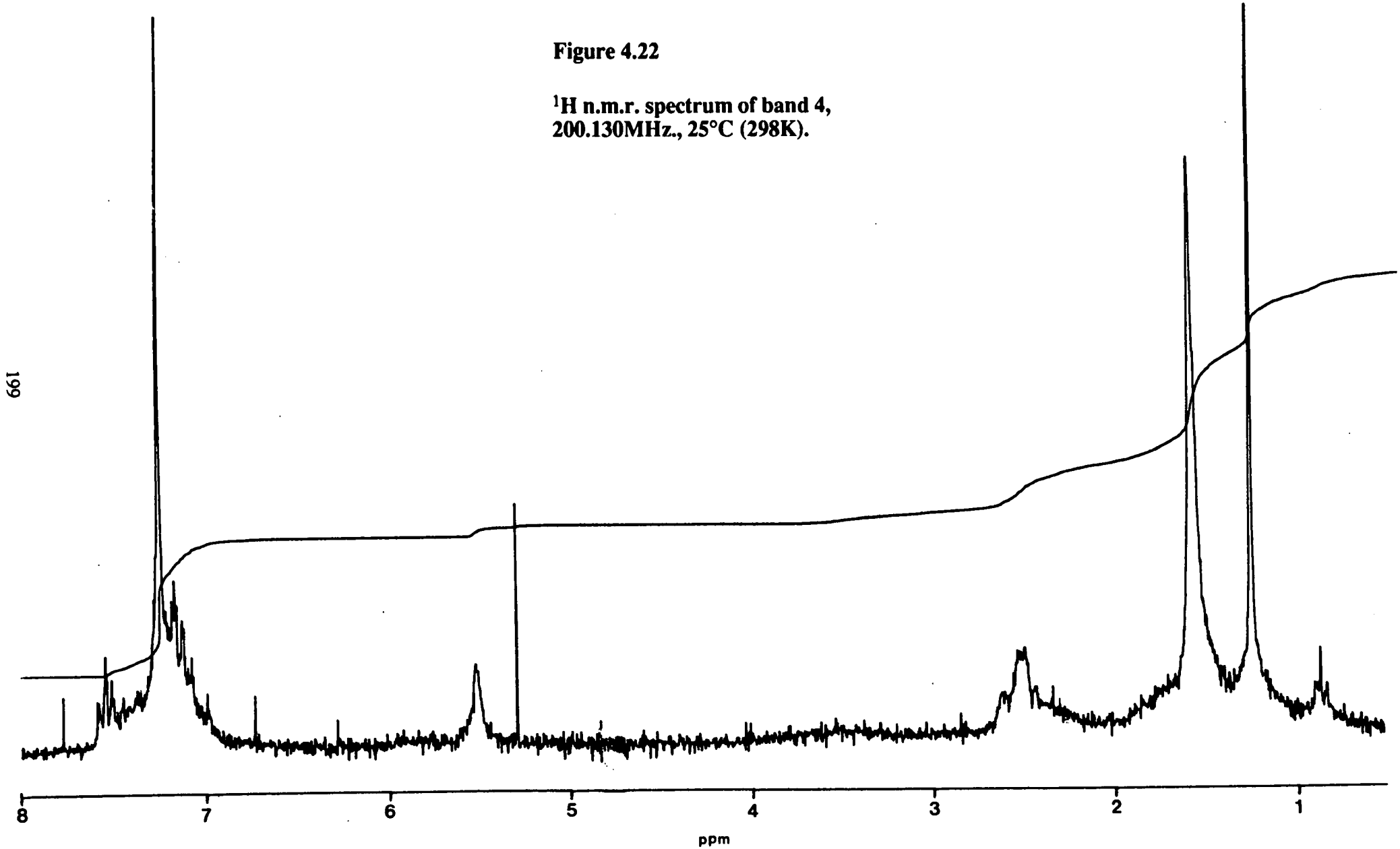

Figure 4.23

$^{11}B/^{11}B\{^{1}H\}$ n.m.r. spectra of band 6, 64.210MHz., 25°C (298K).

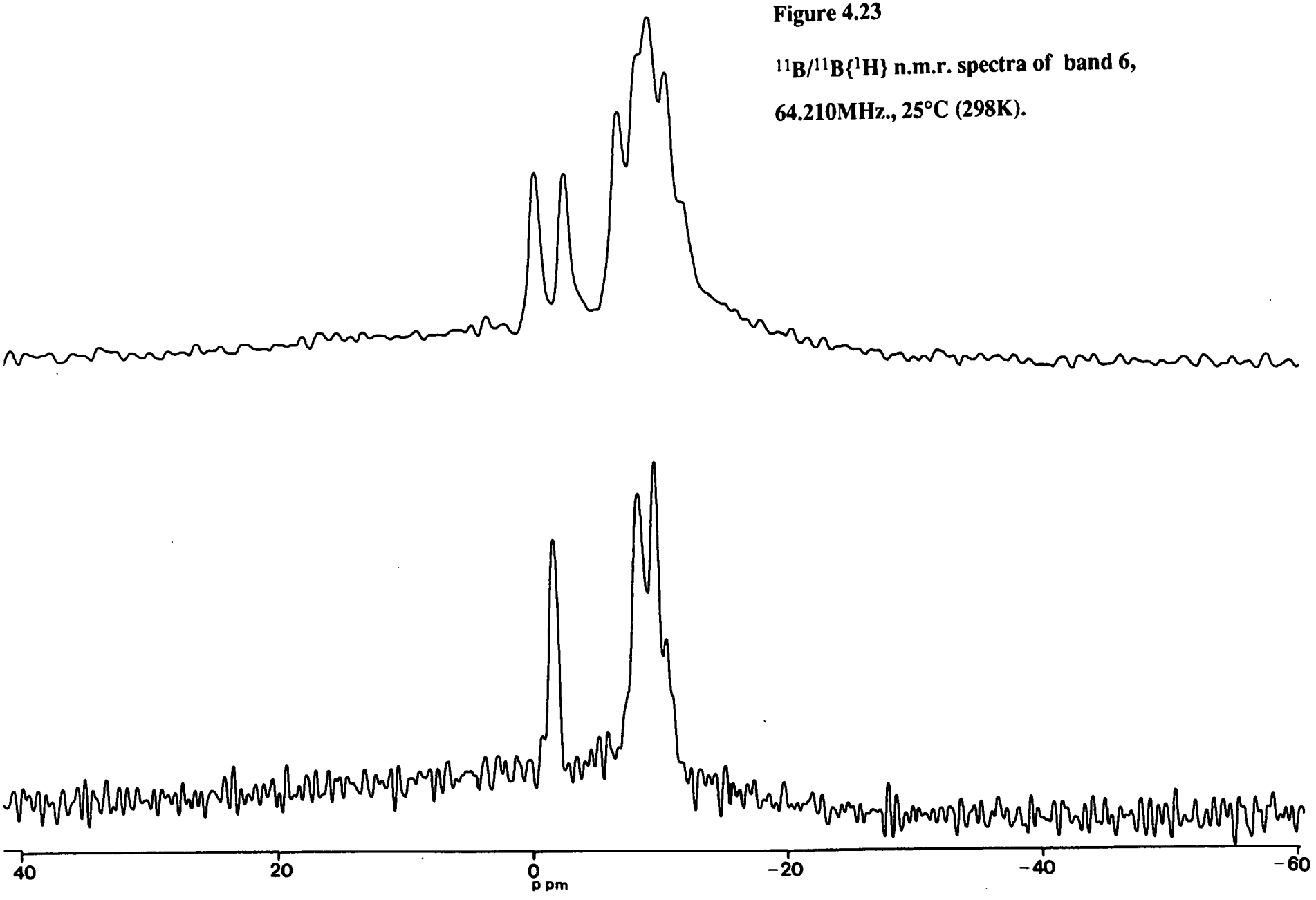

The major product (band 1) has a band in the i.r. spectrum (CH_2Cl_2) at 2515cm^{-1} (B-H). There are 5 environments in the $^{11}B\{^1H\}$ spectrum in the ratio 1:2:2:3:1 (see figure 4.24). One of these is at high frequency (δ= 25.21p.p.m.), suggesting the presence of a C_2B_3 metal-bonded face. Further evidence for the 3,1,2-framework is provided by the presence of only 5 peaks. Whereas a symmetrically substituted carbametallaborane would be expected to possess 6 resonances (in the ratio 1:2:2:2:1:1) when arranged in the 3,1,2-form, as the cage becomes asymmetric (as in a 3,1,11-carbametallaborane) 9 would be expected (although coincidences may reduce the number actually observed). These two observations provide compelling evidence that, in this case, a complex of the 3,1,2-skeletal isomer has been generated. The proton coupled spectrum consists of 5 doublets with ^{1}JB-H in the range 125 to 155Hz. The proton spectrum of **19** contains a multiplet at δ 2.52p.p.m. corresponding to the 8 COD-C$\underline{H}_2$ hydrogen atoms (see figure 4.25). The 4 COD-C$\underline{H}$ protons resonate at δ= 5.58p.p.m. and there are two signals in the phenyl region of the spectrum. The first of these is a multiplet centred on δ 7.16p.p.m. and represents 6 protons while the other is a doublet of doublets at δ 7.57p.p.m., integrating for 4 protons, with coupling constants of 8.1 and 1.1Hz. The presence of only two signals in this region suggests that the two phenyl groups are equivalent and hence provides further evidence that **19** exists in the 3,1,2-isomeric form.

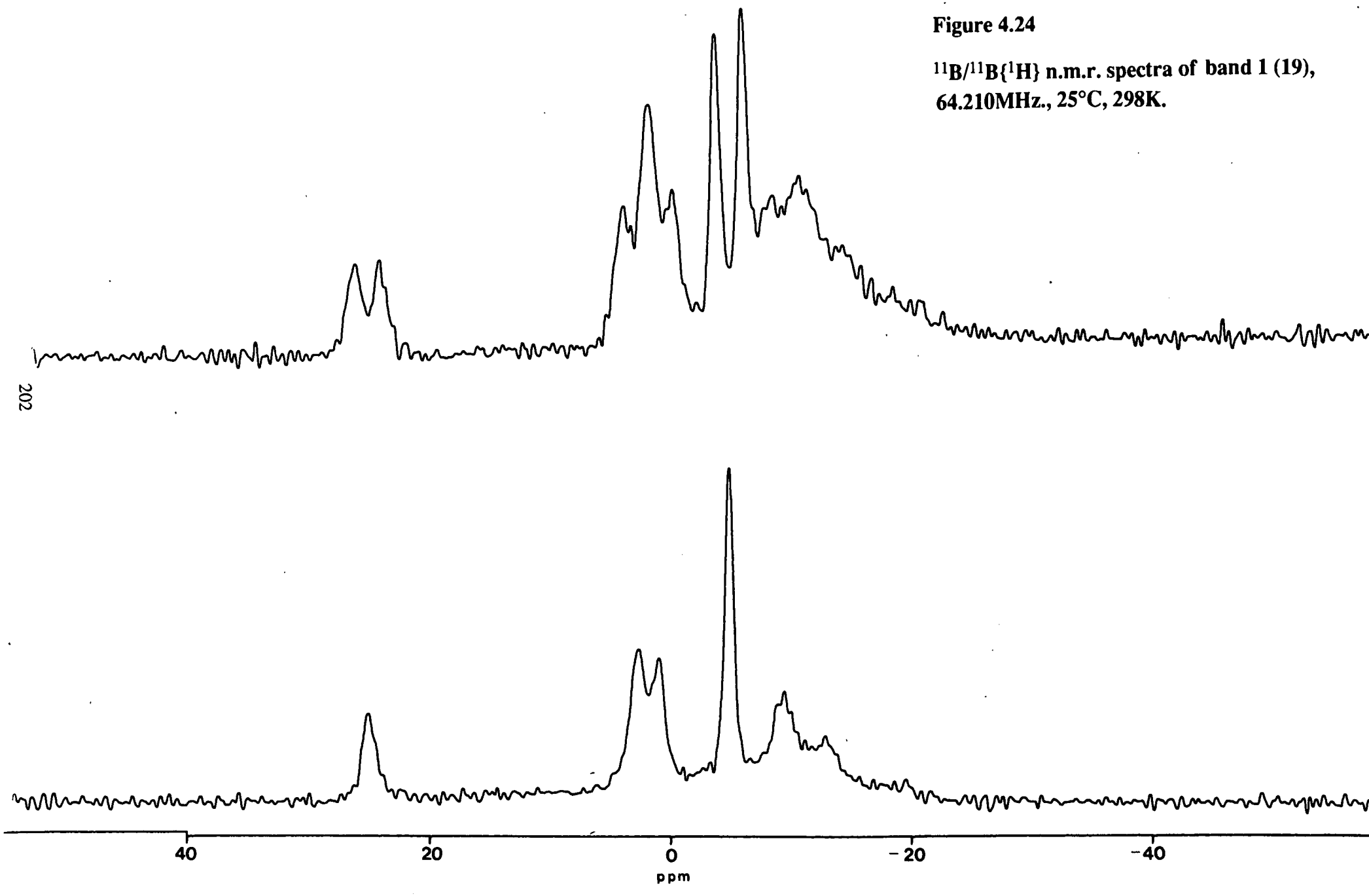

Figure 4.24

$^{11}B/^{11}B\{^{1}H\}$ n.m.r. spectra of band 1 (19), 64.210MHz., 25°C, 298K.

Figure 4.25

^{1}H n.m.r. spectrum of band 1 (19), 200.130MHz., 25°C (298K).

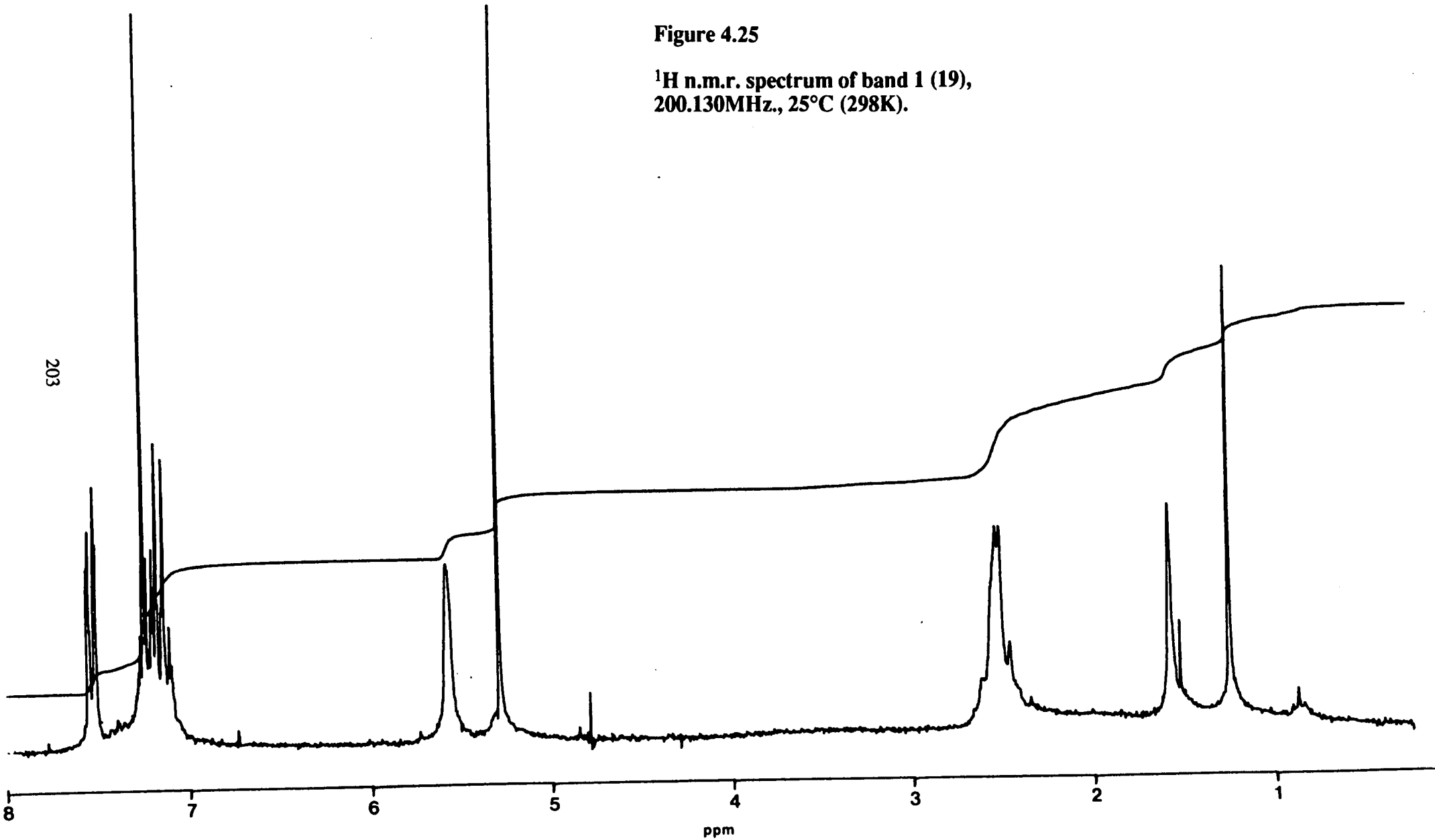

4.4 Crystal Structure Determination of 19.

In order to confirm the structure of **19** an X-ray crystallographic study was undertaken. Single, dark red crystals were obtained by slow diffusion of Et_2O into a solution of **19** in CH_2Cl_2, at -30°C (243K). Details of data collection and structure refinement can be found in chapter 5. **19** forms discrete, neutral, monomeric molecules with no imposed symmetry. Selected bond distances and angles are given in tables 4.1 and 4.2, respectively. A perspective view of a single molecule is depicted in figure 4.26. This confirms the 3,1,2-architecture of **19**.

Table 4.1 Selected Bond Lengths in 19, Å, with Standard Deviations.

C(1) - C(2)	1.521(4)	B(7) -B(12)	1.821(5)
C(1) -Pd(3)	2.710(3)	B(8) - B(9)	1.740(5)
C(1) - B(4)	1.846(4)	B(8) -B(12)	1.754(5)
C(1) - B(5)	1.648(4)	B(9) -B(10)	1.760(6)
C(1) - B(6)	1.704(4)	B(9) -B(12)	1.749(6)
C(1) -C(11)	1.490(4)	B(10) -B(11)	1.806(5)
C(2) -Pd(3)	2.669(3)	B(10) -B(12)	1.751(6)
C(2) - B(6)	1.752(4)	B(11) -B(12)	1.791(5)
C(2) - B(7)	1.821(4)	C(12) -C(13)	1.395(4)
C(2) -B(11)	1.671(4)	C(12) -C(11)	1.389(4)
C(2) -C(21)	1.508(4)	C(13) -C(14)	1.377(5)
Pd(3) - B(4)	2.177(4)	C(14) -C(15)	1.381(5)
Pd(3) - B(7)	2.230(3)	C(15) -C(16)	1.388(5)
Pd(3) - B(8)	2.229(4)	C(16) -C(11)	1.393(4)
Pd(3) -C(101)	2.302(4)	C(22) -C(23)	1.379(4)
Pd(3) -C(104)	2.315(4)	C(22) -C(21)	1.396(4)
Pd(3) -C(105)	2.295(4)	C(23) -C(24)	1.384(5)
Pd(3) -C(108)	2.229(4)	C(24) -C(25)	1.371(5)
B(4) - B(5)	1.830(5)	C(25) -C(26)	1.396(4)
B(4) - B(8)	1.810(5)	C(26) -C(21)	1.393(4)
B(4) - B(9)	1.823(5)	C(101)-C(102)	1.504(5)
B(5) - B(6)	1.727(5)	C(101)-C(108)	1.355(5)
B(5) - B(9)	1.798(6)	C(102)-C(103)	1.515(6)
B(5) -B(10)	1.770(6)	C(103)-C(104)	1.514(5)
B(6) -B(10)	1.753(5)	C(104)-C(105)	1.355(5)
B(6) -B(11)	1.790(5)	C(105)-C(106)	1.506(6)
B(7) - B(8)	1.786(5)	C(106)-C(107)	1.508(7)
B(7) -B(11)	1.801(5)	C(107)-C(108)	1.510(6)

Table 4.2 Selected Angles, in 19, °, with Standard Deviations.

C(2) - C(1) - B(6)	65.50(19)	B(4) - B(8) - B(9)	61.76(21)
C(2) - C(1) -C(11)	121.56(22)	B(7) - B(8) -B(12)	61.93(20)
Pd(3) - C(1) - C(2)	72.08(14)	B(9) - B(8) -B(12)	60.07(22)
Pd(3) - C(1) - B(4)	53.04(13)	B(4) - B(9) - B(5)	60.70(21)
Pd(3) - C(1) -C(11)	104.95(16)	B(4) - B(9) - B(8)	61.01(21)
B(4) - C(1) - B(5)	62.85(19)	B(5) - B(9) -B(10)	59.65(23)
B(4) - C(1) -C(11)	117.02(21)	B(8) - B(9) -B(12)	60.37(22)
B(5) - C(1) - B(6)	62.01(20)	B(10) - B(9) -B(12)	59.86(23)
B(5) - C(1) -C(11)	121.21(23)	B(5) -B(10) - B(6)	58.70(22)
B(6) - C(1) -C(11)	121.69(22)	B(5) -B(10) - B(9)	61.25(23)
C(1) - C(2) -Pd(3)	75.07(14)	B(6) -B(10) -B(11)	60.38(21)
C(1) - C(2) - B(4)	40.79(14)	B(9) -B(10) -B(12)	59.76(23)
C(1) - C(2) - B(6)	62.28(18)	B(11) -B(10) -B(12)	60.45(22)
C(1) - C(2) -C(21)	121.51(22)	C(2) -B(11) - B(6)	60.67(19)
Pd(3) - C(2) -C(21)	110.64(16)	C(2) -B(11) - B(7)	63.12(18)
B(6) - C(2) -B(11)	63.02(19)	B(6) -B(11) -B(10)	58.36(21)
B(6) - C(2) -C(21)	115.98(22)	B(7) -B(11) -B(12)	60.95(20)
B(7) - C(2) -B(11)	61.90(18)	B(10) -B(11) -B(12)	58.25(22)
B(7) - C(2) -C(21)	119.51(21)	B(7) -B(12) - B(8)	59.89(20)
B(11) - C(2) -C(21)	115.55(22)	B(7) -B(12) -B(11)	59.79(20)
C(1) -Pd(3) - C(2)	32.84(8)	B(8) -B(12) - B(9)	59.56(22)
C(1) -Pd(3) - B(4)	42.68(11)	B(9) -B(12) -B(10)	60.39(23)
C(2) -Pd(3) - B(7)	42.46(10)	B(10) -B(12) -B(11)	61.30(22)
B(4) -Pd(3) - B(8)	48.48(13)	C(13) -C(12) -C(11)	120.5(3)
B(7) -Pd(3) - B(8)	47.21(12)	C(12) -C(13) -C(14)	120.9(3)
C(101)-Pd(3) -C(104)	77.64(12)	C(13) -C(14) -C(15)	119.2(3)
C(101)-Pd(3) -C(108)	34.75(13)	C(14) -C(15) -C(16)	120.1(3)
C(104)-Pd(3) -C(105)	34.19(13)	C(15) -C(16) -C(11)	121.4(3)
C(105)-Pd(3) -C(108)	80.65(14)	C(1) -C(11) -C(12)	121.64(24)
C(1) - B(4) -Pd(3)	84.28(16)	C(1) -C(11) -C(16)	120.45(24)
C(1) - B(4) - B(5)	53.27(17)	C(12) -C(11) -C(16)	117.9(3)
Pd(3) - B(4) - B(8)	67.29(16)	C(23) -C(22) -C(21)	121.0(3)
B(5) - B(4) - B(9)	58.99(21)	C(22) -C(23) -C(24)	120.3(3)
B(8) - B(4) - B(9)	57.24(20)	C(23) -C(24) -C(25)	119.8(3)
C(1) - B(5) - B(4)	63.88(19)	C(24) -C(25) -C(26)	120.2(3)
C(1) - B(5) - B(6)	60.58(20)	C(25) -C(26) -C(21)	120.7(3)
B(4) - B(5) - B(9)	60.31(21)	C(2) -C(21) -C(22)	121.63(24)
B(6) - B(5) -B(10)	60.17(22)	C(2) -C(21) -C(26)	120.18(23)
B(9) - B(5) -B(10)	59.10(22)	C(22) -C(21) -C(26)	118.01(25)
C(1) - B(6) - C(2)	52.22(16)	Pd(3) -C(101)-C(108)	69.67(21)
C(1) - B(6) - B(5)	57.41(19)	C(102)-C(101)-C(108)	125.6(3)
C(2) - B(6) -B(11)	56.30(18)	C(101)-C(102)-C(103)	115.2(3)
B(5) - B(6) -B(10)	61.13(22)	C(102)-C(103)-C(104)	115.7(3)
B(10) - B(6) -B(11)	61.25(21)	Pd(3) -C(104)-C(105)	72.10(22)
C(2) - B(7) -Pd(3)	81.75(15)	C(103)-C(104)-C(105)	126.5(3)
C(2) - B(7) -B(11)	54.97(17)	Pd(3) -C(105)-C(104)	73.72(22)
Pd(3) - B(7) - B(8)	66.37(16)	C(104)-C(105)-C(106)	123.6(4)
B(8) - B(7) -B(12)	58.18(20)	C(105)-C(106)-C(107)	116.2(4)
B(11) - B(7) -B(12)	59.26(20)	C(106)-C(107)-C(108)	115.1(4)
Pd(3) - B(8) - B(4)	64.23(16)	Pd(3) -C(108)-C(101)	75.58(22)
Pd(3) - B(8) - B(7)	66.42(16)	C(101)-C(108)-C(107)	126.9(3)

Figure 4.26

A Perspective View of 19.

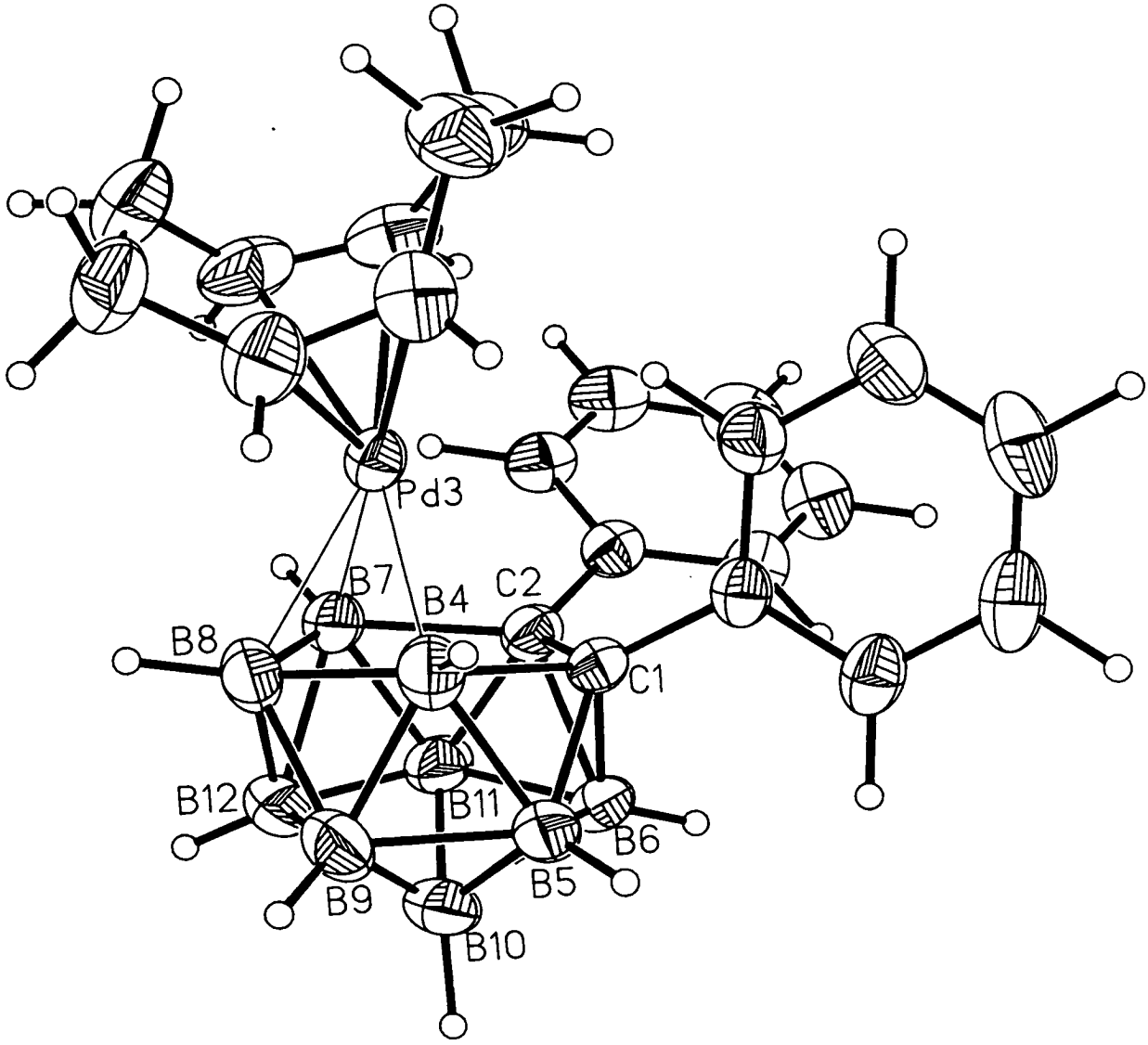

The palladium atom and the carbaborane cage define a distorted icosahedron. The metal vertex is slipped away from the centre of the C_2B_3 face towards B(8) (positive slippage), by 0.56Å, at an angle of 3.0° to the face centroid to B(8) vector (= σ). The magnitude of slippage (Δ) is considerably greater than that observed in the analogous complex 3-(1,5-COD)-3,1,2-$PdC_2B_9H_{11}$[65] (Δ= +0.24Å). In addition, the metal bonded face is folded about an axis passing through B(4) and B(7) making folding angles of 8.32 and 5.22° for ϕ and θ, respectively. Again, these distortion parameters are larger than those exhibited by the unsubstituted analogue, which has values of 5.9 and 4.9°, for ϕ and θ.

Related to the metal fragment slippage is a disparity in the bonding of the C_2B_3 face to the metal atom. The Pd-B distances are similar (Pd-B(4)= 2.177(4), Pd-B(7)= 2.230(3) and Pd-B(8)= 2.229(4)Å) and comparable to those in 3-(1,5-COD)-3,1,2-$PdC_2B_9H_{11}$[65] in which the average metal - boron distance is 2.230Å. However, the palladium- carbon distances are significantly longer than those in the unsubstituted analogue, with a Pd-C(1) distance of 2.710(3)Å and a Pd-C(2) distance of 2.669(3)Å compared with 2.432(3) and 2.377(3)Å. In fact, the Pd-C interactions in **19** can be considered to be essentially non-bonding. The distortions described up to this point can be attributed to the presence of the two bulky phenyl substituents on the cage carbon atoms in **19**. This can also account for lengthening of the cage C-C distance from 1.495(4)Å in 3-(1,5-COD)-3,1,2-$PdC_2B_9H_{11}$ to 1.521(4)Å in **19**.

A means of describing the conformation of the phenyl substituents in a carbaborane was described in section 1.4. To recap θ_{phenyl} can be defined as the average deviation from a 90° torsion about the C(1)-C(11) (and C(2)-C(21)) bonds. In **19** the values of θ_{phenyl} are 42.5 and 56.7° for the C11-C16 ring and the C21-C26 ring, respectively, with rotation occurring in a conrotatory manner, as shown in figure 4.27.

Figure 4.27

Alternative view of 19.

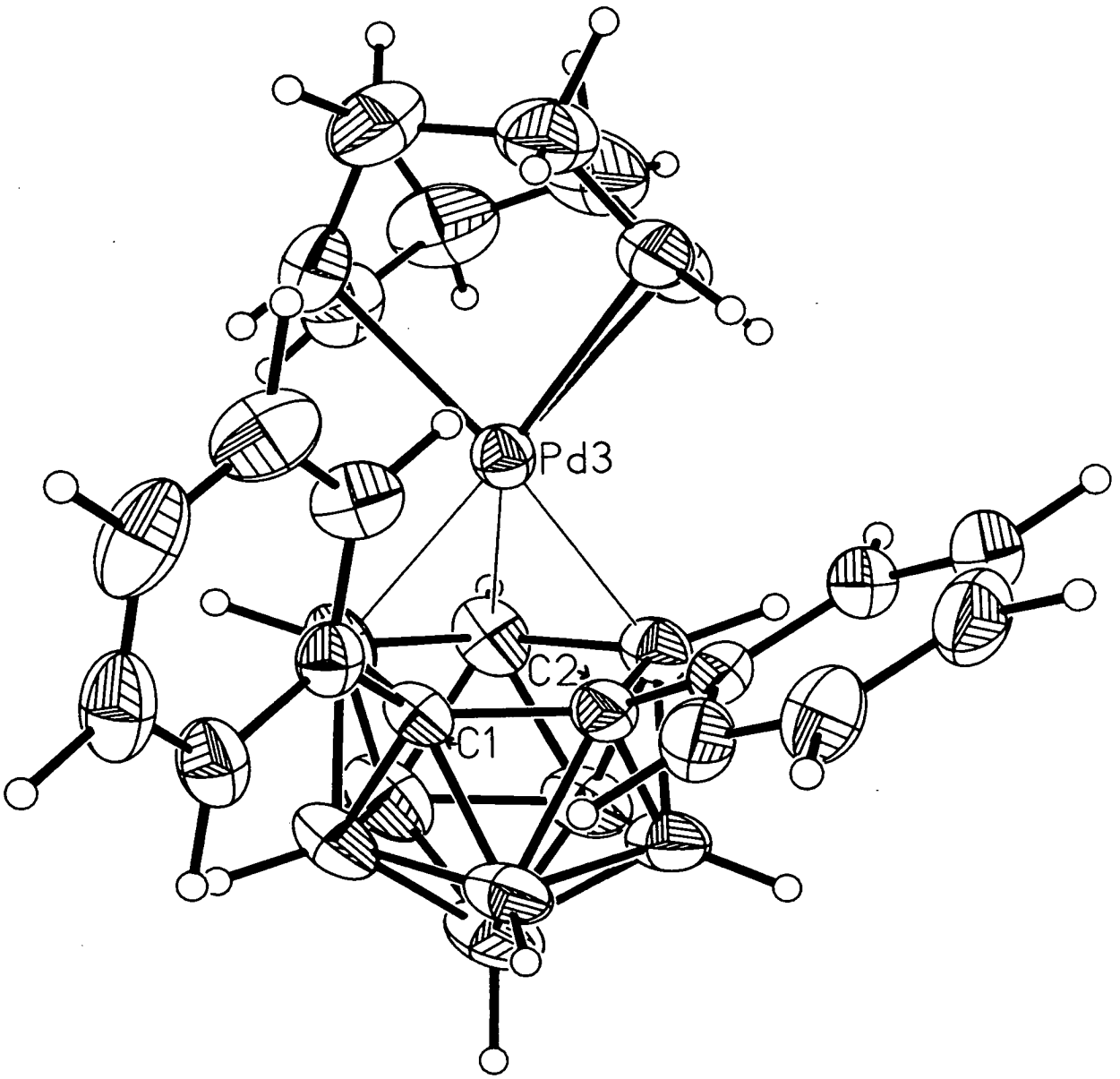

The average θ_{phenyl} value (49.6°) is close to the optimum[43] value at which the overall energy in a *closo* diphenyl-carbaborane complex is at a minimum (as the phenyl substituents are as close to parallel to the C_{cage}-C_{cage} bond as they can be without steric interference causing destabilisation). Thus, the C_{cage}-C_{cage} bond length is the shortest so far observed in a diphenyl-substituted carbametallaborane.

The average substituent elevation angle (χ) for the C_2B_3 face of **19** is 20.7°, indicating bending of the substituents away from the metal centre. One final cage distortion can be measured; lateral slippage of the C_2B_3 face over the B_5 one (Q). This has a value of 0.09Å, in the same direction as Δ,leading to a slight over-estimate of the slippage parameter.

Co-ordination of an unconjugated diene such as 1,5-COD, to a metal atom can be considered as equivalent to co-ordination of the two isolated alkenes.

The metal-alkene bonds can be described[116] in terms of a σ and a π component. The σ interaction involves a filled alkene π orbital and an empty metal hybrid orbital. The π "back donation" occurs between a filled metal hybrid orbital and a π^* alkene orbital. This bonding scheme, known as the Dewar-Chatt-Duncanson model, requires the alkene to be perpendicular to the plane of the metal centre and the other ligands. Confirmation of the validity of this scheme was provided by a neutron diffraction determination of the structure of Zeise's salt, $[PtCl_3(C_2H_4)]^-K^+$[117]. This illustrates that, as well as having the alkene at right angles to the plane through the platinum atom and the 3 chloride ligands, the alkene is also situated symmetrically about this plane (as required for the suggested bonding scheme).

Back donation into the π^* alkene orbitals leads to an increase in the C-C bond length, in comparison with that observed in the free alkene. In addition, the alkene substituents are bent back from the metal[118]. This can be thought of as arising from a change in hybridisation at the carbon atoms, from sp_2 towards sp_3.

In **19**, the 1,5-COD ligand adopts a twist boat (tub) configuration, similar to that observed in $PdCl_2$(1,5-COD)[119] and 3-(1,5-COD)-3,1,2-$PdC_2B_9H_{11}$[65] and to the lowest energy configuration of the free diene in the gas phase[120]. The COD "bite angle" is defined[119] as the Z1-Pd-Z2 angle, where Z1 is the mid-point of the C(101)-C(108) bond and Z2 the mid-point of the C(104)-C(105) bond. In **19** the bite angle is 83.6°, similar to that measured in $PdCl_2$(1,5-COD) (= 86.3°). Hence, the geometry at the metal centre can be regarded as pseudo-square planar. The metal-COD distances (Pd-Z1= 2.162 and Pd-Z2= 2.203Å) are significantly longer than those observed in $PdCl_2$(1,5-COD) (2.092 and 2.097Å), but similar to those found in 3-(1,5-COD)-3,1,2-$PdC_2B_9H_{11}$. This can be rationalised by consideration of the donor properties of the non-COD ligands. Whereas Cl^- is a weak π-donor, the carbaborane ligands are considered to be weak π-acceptor ligands and hence will be in competition with the diene for back-donation[65]. This leads to shortening in the carbon-carbon double bonds in the carbaborane complexes (1.355(5) and 1.360(5)Å for 3-(1,5-COD)-3,1,2-$C_2B_9H_{11}$ and 1.355(5) for both the double bonds in **19**) compared with 1.38, 1.39Å for $PdCl_2$(1,5-COD).

A number of other parameters have been suggested[118,119] which quantify the distortions of the COD ligand arising from co-ordination to a metal. These have been calculated for **19** and are tabulated along with the reported values for $PdCl_2$(1,5-COD)[119] and 3-(1,5-COD)-3,1,2-$PdC_2B_9H_{11}$[65]. α is the angle between the planes defined by each alkenic carbon atom and its two substituents. For example, for the C(101)-C(108) bond α= [C(101), C(102), H(101)] plane versus [C(108), C(107), H(108)] plane. An undistorted olefin will have a value of 0° for α. β is the angle subtended by the C-C vector and the plane containing an alkenic carbon atom and its substituents, and decreases from 90° with bending back of substituents from the metal centre.

Three other parameters have been described[119]. However, these have not been

rigorously defined so comparisons of calculated and literature values may not be valid. Nevertheless, the values have been calculated for **19** and are quoted here for completeness. The "twist" distortion is described as the deviation from perpendicular of the best plane through the alkene and the metal-alkene mid-point vector via rotation about the C-C double bond. This is calculated as 90- {[C(101), C(102), H(101), C(108), C(107), H(101)] plane versus [Pd, Z1, Z2] plane}°, where Z1 and Z2 are defined as above. The "torque" is described as rotation of the C-C bond about the M-alkene mid-point vector, from the normal perpendicular orientation towards the "in-plane" orientation. For the C(101)-C(108) bond this was calculated as: {90-[Pd-Z1-Z2] plane versus [C(101)-C(108)] vector}. The "tilt" is described as the deviation from perpendicularity of the C-C bond and the M-alkene mid-point vector. This was calculated for the C101-C108 bond as the deviation of the angle Pd-Z1-C(101) (or Pd-Z1-C(108)) from 90°.

Table 4.3 Distortion Parameters for Pd(1,5-COD)-Complexes.

Non-COD ligand	α^a	β^b	Twist[a]	Torque[a]	Tilt[a]
2x Cl	26,40	79,75; 71,69	2,3	6,5	0,0
$[C_2B_9H_{11}]$	19,19	79,79; 79,82	11,12	7,4	1,0
$[C_2B_9H_9Ph_2]$	25,18	76,77; 82,80	4,1	8,3	3,1

N.B. All parameters quoted in °.

[a] bond 1, bond 2. [b] alkenic carbons in increasing order of numbering.

From the above table it can be observed that the C101-C108 alkene is more distorted than the C104-C105 alkene. This can be readily observed by inspection of figure 4.27,and is best quantified by considering the heights of the 8 COD carbon atoms above the best plane through the B_5 girdle, which is assumed to be planar. These heights are given in table 4.4.

Table 4.4 Heights of COD Carbon Atoms With Respect to B_5 Plane.

Carbon Atom	Vertical Height (arbitrary scale)
101	4.95
102	6.28
103	6.28
104	5.23
105	4.94
106	5.64
107	5.78
108	4.45

It can be noted that the COD carbon atoms nearest the carbon atoms of the ligating face (C(101)-C(104)) are elevated relative to those nearest the boron atoms. Deviation of the C-C double bonds from the parallel to the B_5 belt can be calculated. The C(101)-C(108) bond is at an angle of 21.6° from the parallel while the C(104)-C(105) bond is at an angle of 12.4°. This difference can be related to the orientation of the closest cage phenyl substituent. The larger twist is observed for the double bond closest to C(1) which bears a phenyl group which is closer to the "normal" *i.e.* closer to perpendicular to the B_5 plane and hence that for which a greater steric interaction with the COD ligand would be expected. The *ortho* hydrogen atom in this group (H(116)) is in close contact with one of the COD-H atoms (H(103)) (see figure 4.28).

Their separation of 2.197Å can be compared with the sum of the van der Waals radii (2 x 1.2Å)[64]. The substituent on C(2) is twisted away from the COD ligand by another *circa* 14° and this can be correlated with the smaller deviation from the predicted orientation of the C(104)-C(105) bond. The closest H...H contact involving this ring is between H(216) and H(104) at a distance of 2.320Å *i.e* further apart than the closest contact involving the C(11)-(16) ring but still within the sum of the van der Waals radii.

Figure 4.28 **Interactions of Phenyl-Hs with COD-Hs in 19.**

Cage BHs removed for clarity.

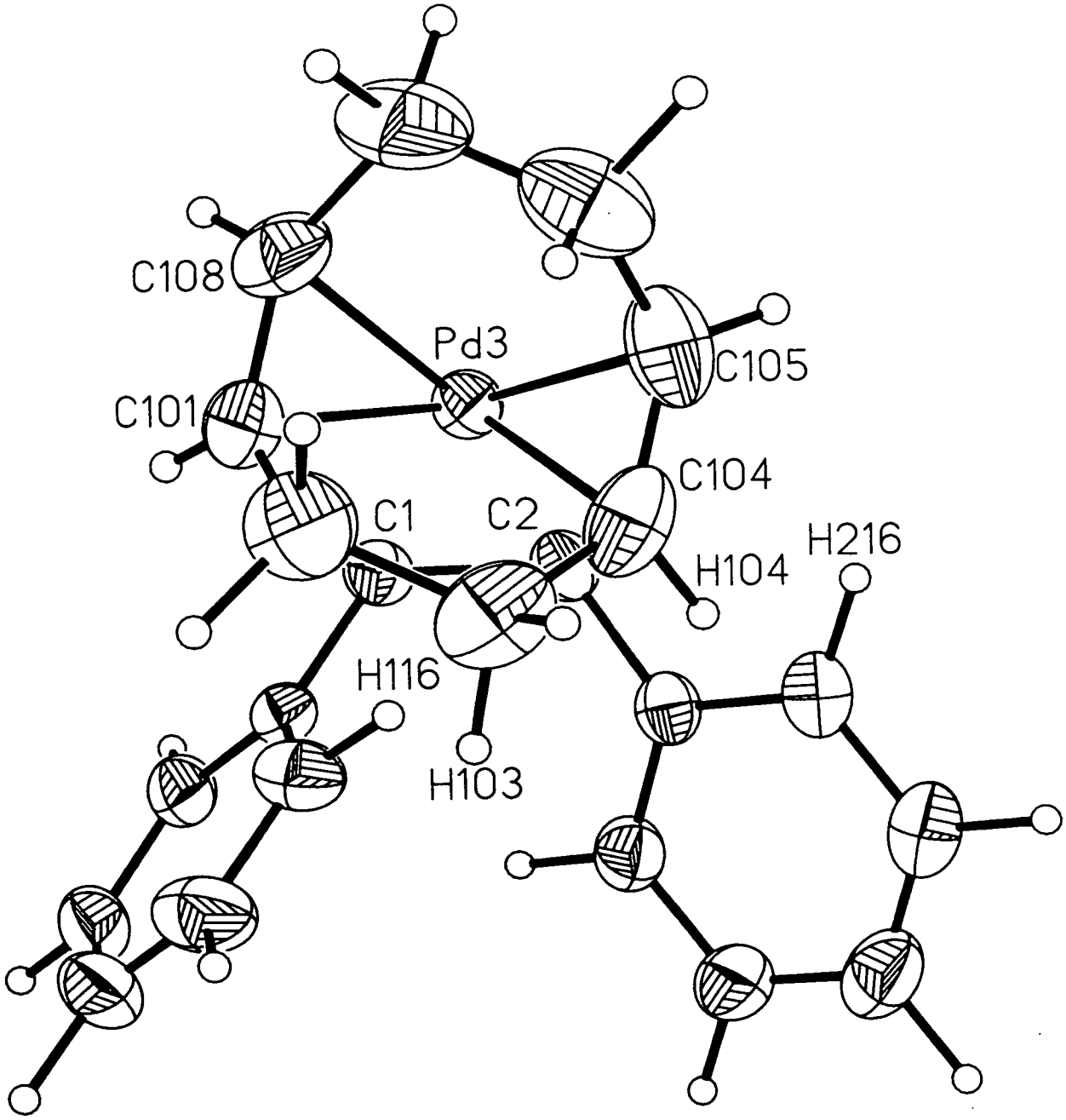

The effect of changing the conformation of the phenyl substituent on the COD ligand is further demonstrated by the calculated Pd-Z distances. The Pd-Z1 distance of 2.710(3)Å is significantly longer than the Pd-Z2 distance of 2.669(3)Å, which can be correlated with the greater twist and hence lesser steric interaction with the COD ligand, involving the phenyl group closest to the latter double bond (*i.e.* C(21)-C(26) lying closer to C(104)-C(105)).

One final distortion requires comment. The plane through the metal fragment (Z1-Pd-Z2) lies at an angle of 74.9° to the cage mirror plane (through B(6) B(8) B(10)). A value of 90° would be predicted from E.H.M.O. calculations (see section 1.4). This magnitude of deviation from the calculated orientation is commonly found- *e.g.* for $1,1\text{-}(PMe_2Ph)_2\text{-}2,4\text{-}Me_2\text{-}1,2,4\text{-}PtC_2C_2B_9H_9$ (= 10.1°)[72] and $3,3\text{-}(PEt_3)_2\text{-}3,1,2\text{-}PtC_2B_9H_{11}$ (= 13.9°)[27]. The formation of **19** with a 3,1,2-architecture may be related to the ability of the metal fragment to adopt an orientation close to the predicted one. This seems to be a direct result of the nature of the COD ligand, which can distort in order to permit the two phenyl-bearing cage carbon atoms to be accommodated on the metal-bonded face. This is apparently not possible when the COD ligand is replaced by two phosphorus ligands and hence the 3,1,11-form is favoured.

A sample of **19** was suspended in toluene and warmed to *circa* 50°C (223K). After 1 hour there was no colouration of the solution so the temperature was raised to reflux. The mixture was stirred for 30 minutes, at this temperature, during which time the solution turned pale yellow and some black material was deposited. This was removed by filtration and the solvent removed from the filtrate *in vacuo* . The $^{11}B\{^1H\}$ n.m.r. spectrum of the yellow residue consists of 3 resonances in the ratio 1:4:5 at δ= +1.07, -5.86 and -14.98p.p.m. (see figure 4.29). There is no longer a high frequency resonance present indicating that there has been a change in the nature of the metal-bonded face. The proton coupled spectrum consists of 3 doublets with

$^1J_{B-H}$ in the range 140 to 155Hz., indicating that each boron atom is bonded to a terminal hydrogen atom. The proton spectrum (see figure 4.30) is more complex than that of **19**. There are 3 multiplets corresponding to the COD-C$\underline{H}_2$ protons, centred on δ= 2.07, 2.34 and 2.63p.p.m. in the ratio 4:2:2. In addition, there are two signals denoting the COD-C$\underline{H}$ protons in the ratio 2:2. The phenyl region of the spectrum contains 2 signals; a multiplet centred on δ= 7.21p.p.m. and integrating for 6 protons and a doublet of doublets at δ= 7.40p.p.m. integrating for 4 hydrogen atoms (J= 8.2, 1.4Hz.). The multiplicity of the signals corresponding to the COD protons provides further evidence that the carbaborane has become asymmetric. If it is assumed that any isomerisation would be of a similar nature to that discussed in the previous chapters then the thermolysis product can tentatively be formulated 1,11-Ph_2-3-(1,5-COD)-3,1,11-$PdC_2B_9H_9$.

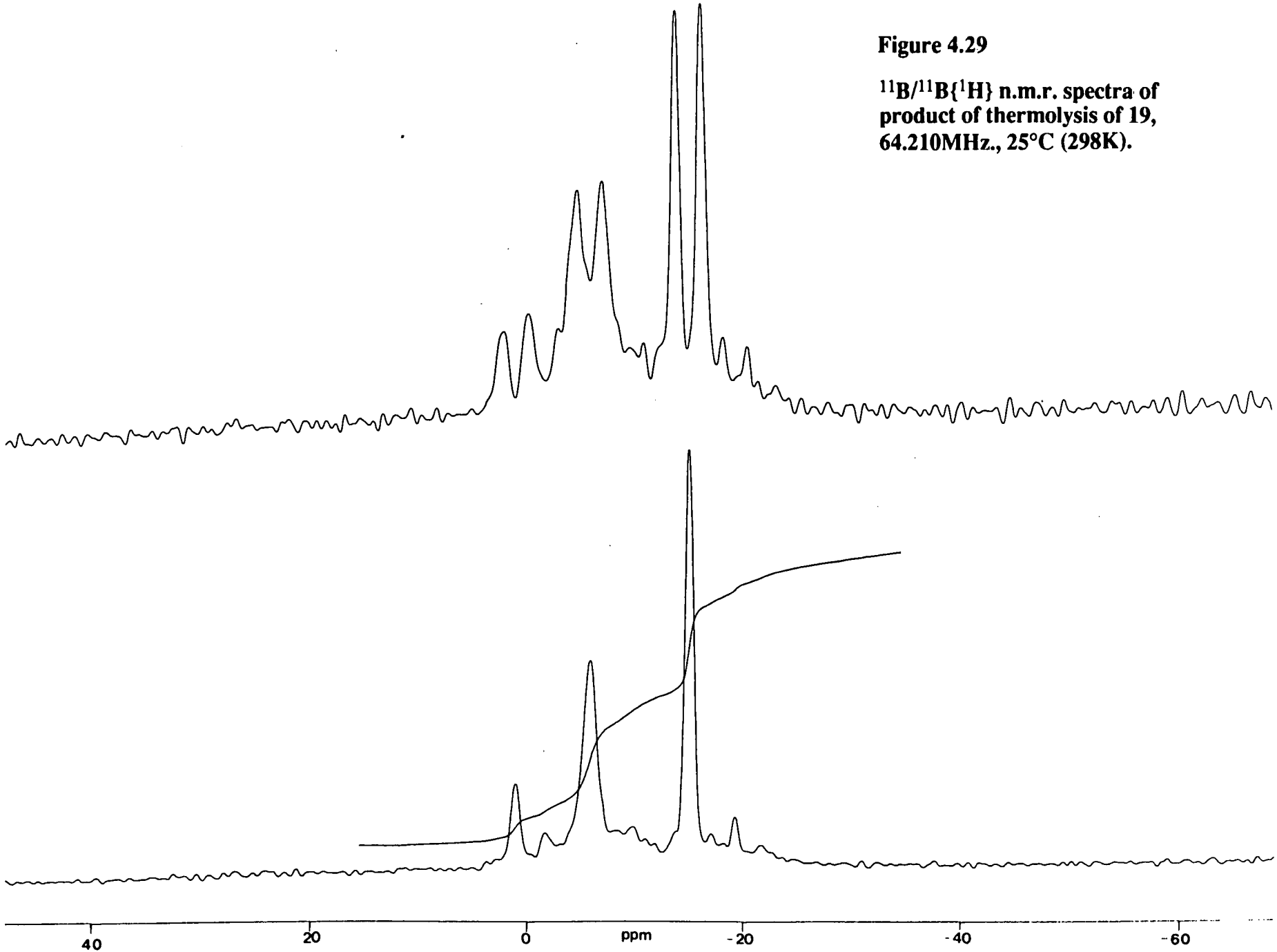

Figure 4.29

$^{11}B/^{11}B\{^{1}H\}$ n.m.r. spectra of product of thermolysis of 19, 64.210MHz., 25°C (298K).

Figure 4.30

^{1}H n.m.r. spectrum of product of thermolysis of 19, 200.130MHz., 25°C (298K).

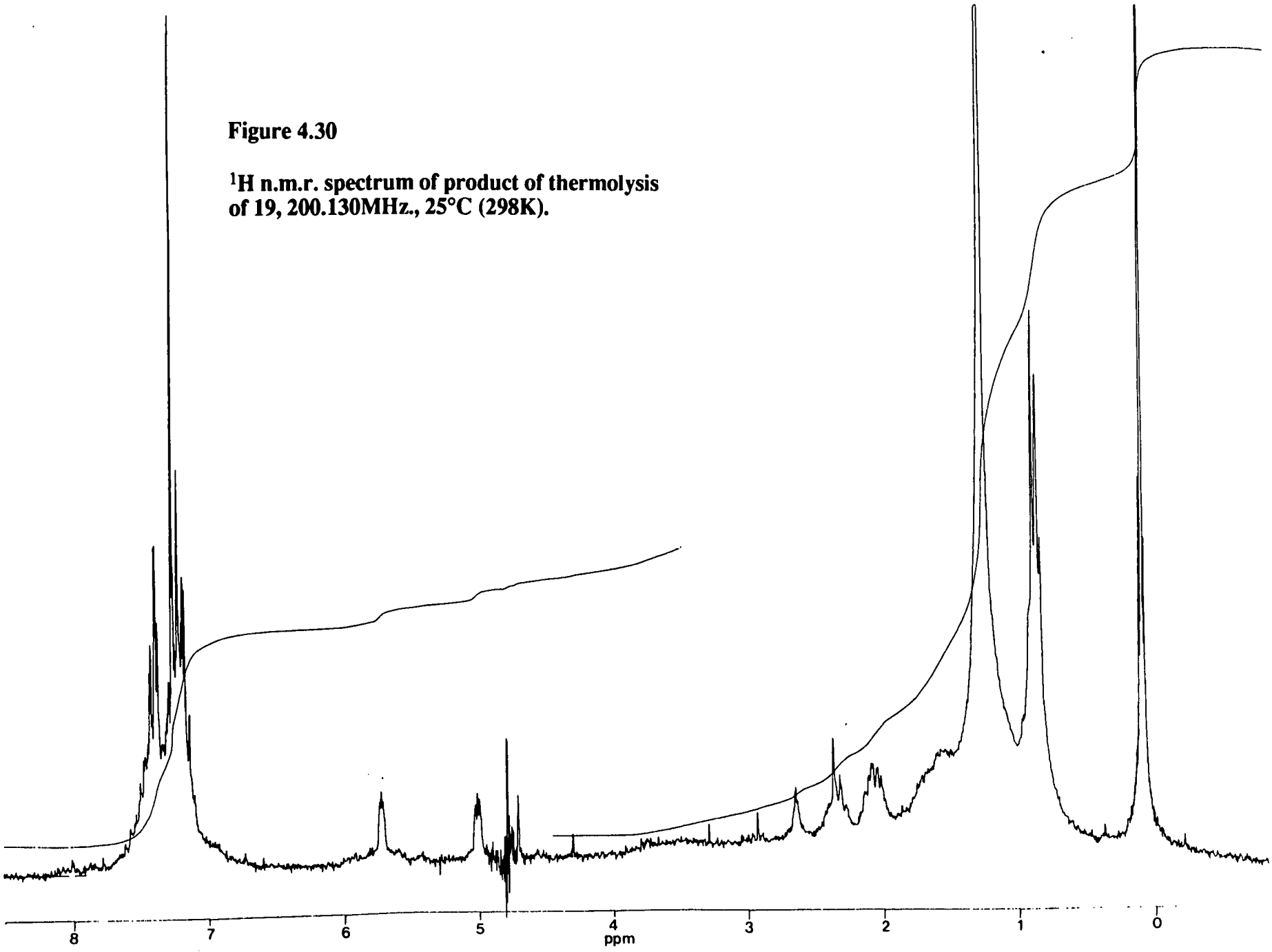

4.5 Carbaborane Complexes Containing the {Pt(1,5-COD)} Fragment.

The behaviour of the complexes containing the {Pd(1,5-COD)} fragment is unique amongst the ML_2-complexes so far discussed. Of particular interest is the failure of **18** to isomerise at elevated temperatures and also the formation of **19** with a 3,1,2-framework. It may be that these apparent anomalies result from the ability of the COD ligand to distort and hence permit a stable orientation of the metal fragment with respect to the ligated carbaborane cage. However, the nature of the metal may also be important. Although Pd^{2+} and Pt^{2+} have approximately the same radius, bonding at palladium involves 4d orbitals whereas that involving platinum involves 5d orbitals[17]. This may be significant in stabilising the palladium species. To probe this, the carbaborane complexes incorporating the {Pt(1,5-COD)} fragment were prepared in order to compare their behaviour with the palladium analogues.

$Tl_2C_2B_9H_{10}Ph$ and $PtCl_2$(1,5-COD) were mixed in CH_2Cl_2 and stirred at room temperature. After two hours a soluble red product and TlCl had been formed. The latter was removed by filtration and the solvent removed from the filtrate *in vacuo* to yield a red/brown residue. This was chromatographed (silica plates, 2:1 CH_2Cl_2/n-hexane eluent). There were several mobile bands, but only two were of sufficient intensity to merit collection. The less intense of these was a rust-coloured band at R_f= 0.95. The $^{11}B\{^1H\}$ n.m.r. spectrum of this species contains 6 bands in the ratio 1:2:2:1:1:2, and includes a high frequency resonance at δ +12.90p.p.m. Each one becomes a doublet in the proton coupled spectrum (^{1}JB-H in the range 135 to 165p.p.m.) indicating that there is a terminal hydrogen atom bound to every boron atom. There are also several less intense signals present. There is tentative evidence for the presence of co-ordinated COD in the ^1H n.m.r. spectrum. This takes the form of some structure on the baseline at approximately δ= 2.1, 2.4, 4.5 and 5.3p.p.m. The phenyl protons give rise to two multiplets centred on δ= 7.17 and 7.40p.p.m.

The major band separated by chromatography was yellow with an R_f value of 0.85. The $^{11}B\{^1H\}$ n.m.r. spectrum consists of 8 resonances (see figure 4.31). The one at highest frequency, at δ= +10.26p.p.m., integrates for 1 boron atom and displays coupling to the platinum nucleus ($^1J^{195}Pt$-P= 300Hz.). The chemical shift of this resonance can be compared with that of the corresponding resonance in the palladium analogue (**18**) (δ= 20.06p.p.m.). This is contrary to what would be predicted if the correlation between chemical shift of the high frequency boron resonance and slippage of the metal fragment is considered (see section 3.13). The other signals arising from **20** are in the range δ= -1.62 to -16.44p.p.m. and in the ratio 1:1:2:1:1:1:1:1. The proton coupled spectrum contains 8 doublets with ^{1}JB-H in the range 140 to 175Hz. The ^1H spectrum (see figure 4.32) contains 2 multiplets corresponding to COD-C<u>H</u>$_2$ protons (centred on δ 2.11 and 2.53p.p.m.) which have a total integral of 8 protons. The 4 COD-C<u>H</u> protons give rise to two multiplets which appear at δ 4.58 and 5.42p.p.m. There are also two multiplets in the phenyl region of the spectrum (centred on δ 7.23 and 7.34p.p.m.) corresponding to 5 protons. The n.m.r. data strongly suggest that this species is the desired product; namely 1-Ph-3-(1,5-COD)-3,1,2-$PtC_2B_9H_{10}$, **20**. The identity of the other species is unclear but the complexity of the ^{11}B spectra suggests that it may be prone to decomposition. In addition, the absence of any resolved Pt-B coupling implies that it is not a slipped carbametallaborane.

Figure 4.31

$^{11}B/^{11}B\{^1H\}$ n.m.r. spectra of 20, 64.210MHz., 25°C (298K).

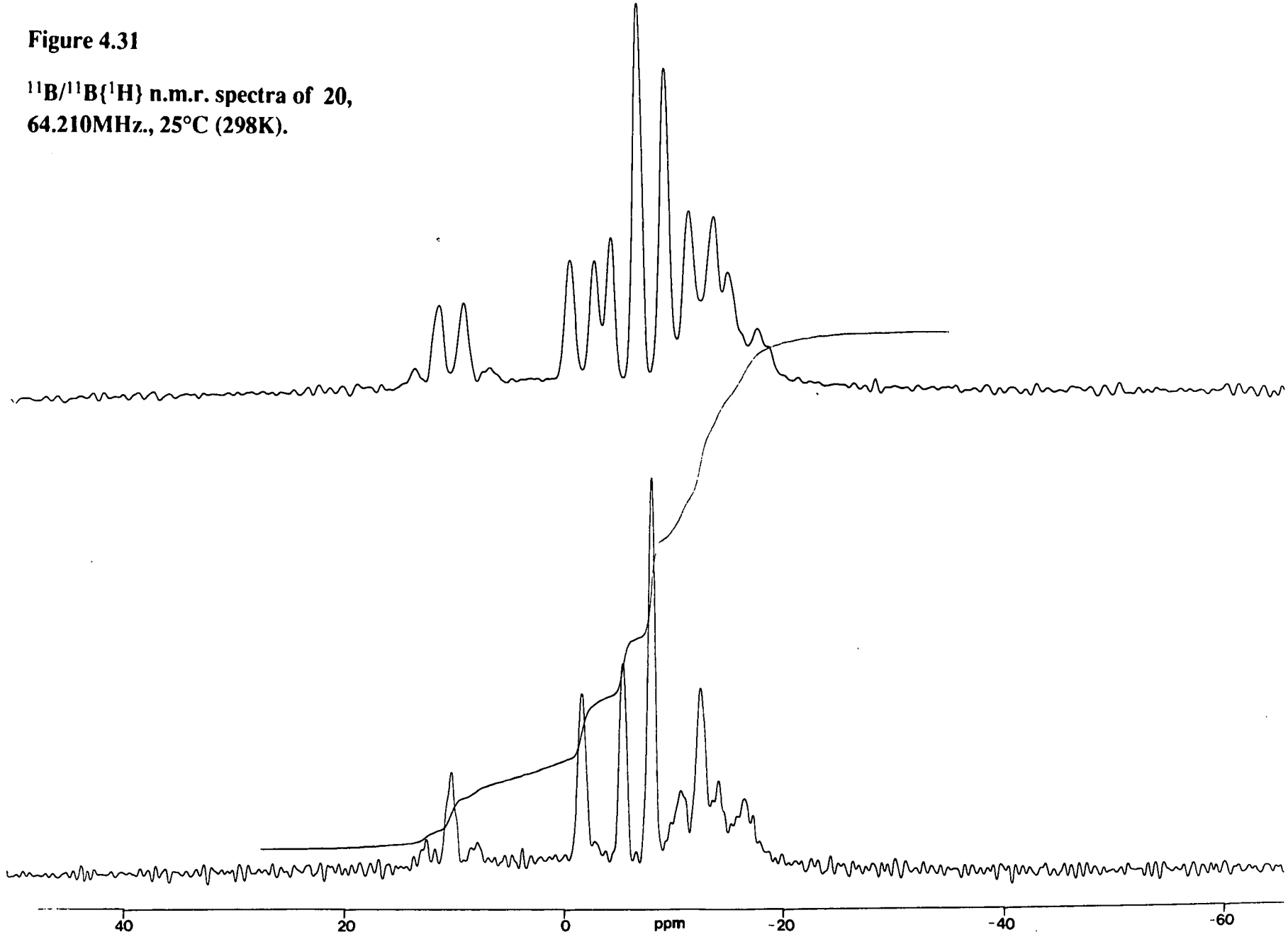

Figure 4.32

^{1}H n.m.r. spectrum of 20, 200.130MHz., 25°C (298K).

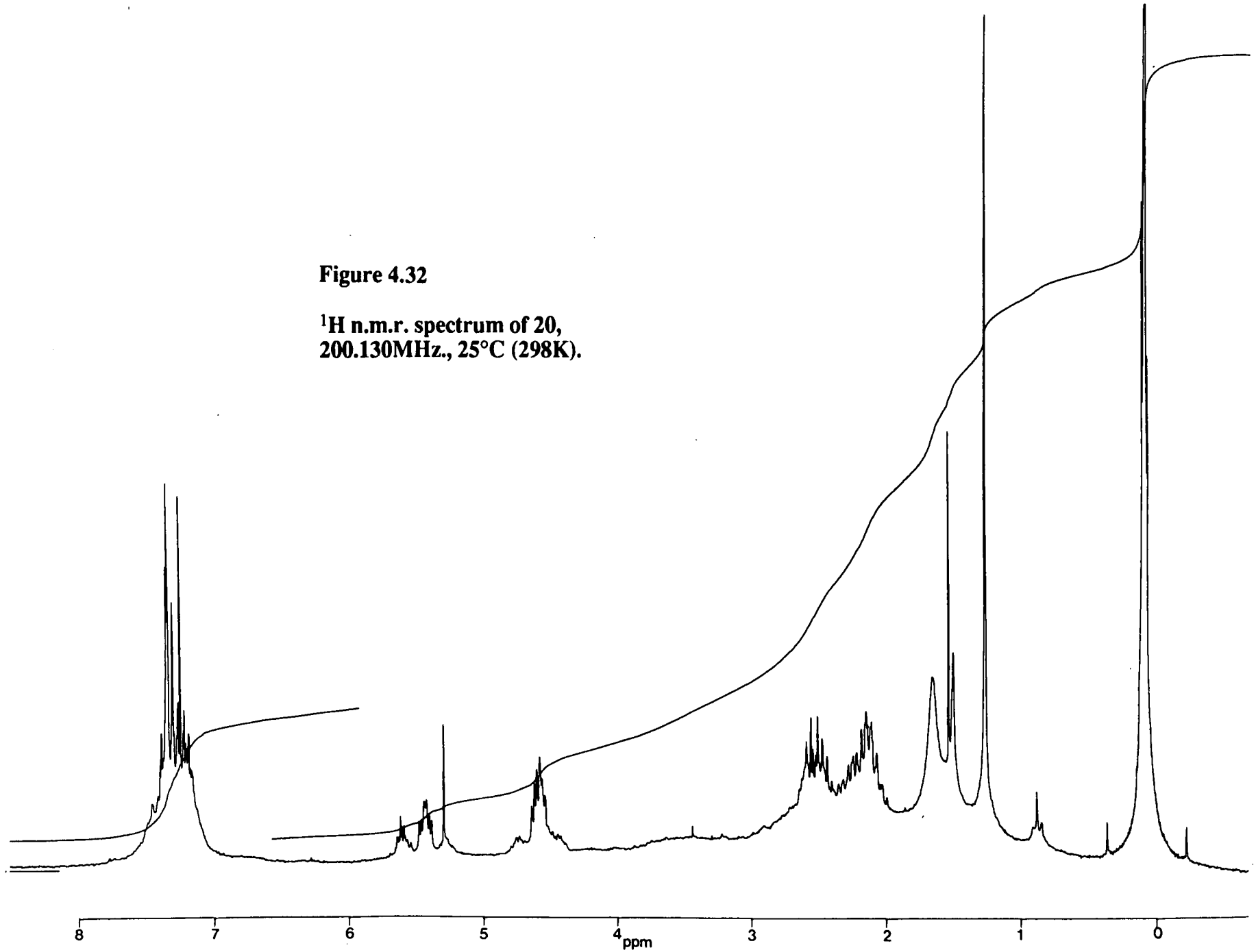

A sample of **20** was suspended in toluene and stirred at reflux temperature for 30 minutes. There was no apparent colour change and removal of the solvent *in vacuo* yielded a yellow residue. The $^{11}B\{^1H\}$ n.m.r. spectrum contains 8 resonances which can be attributed to **20**, including a high frequency signal at δ 10.34p.p.m. which shows coupling to the ^{195}Pt nucleus. There are also several other resonances, at δ= -3.56, -6.37, -15.20, -17.54 and -19.62p.p.m., which are not associated with **20**. All the signals become doublets in the proton coupled spectrum with $^1JB\text{-}H$ in the range 130 to 160Hz. The proton spectrum contains 6 multiplets centred on δ= 2.73, 3.27, 4.59, 5.40, 7.18 and 7.35p.p.m. It was concluded that thermolysis of **20** did not lead to isomerisation, but rather to a degree of decomposition.

$Tl_2C_2B_9H_9Ph_2$ and $PtCl_2$(1,5-COD) were mixed in CH_2Cl_2 and stirred together for two hours. The solution was passed through a column (alumina/CH_2Cl_2) and the orange, mobile band collected. The solvent was removed *in vacuo* to yield an orange solid, **21**. The $^{11}B\{^1H\}$ n.m.r. spectrum of this species contains 9 resonances in the range δ= -1.72 to -17.80p.p.m. each of which integrates for one boron atom. The proton coupled spectrum has 9 doublets with $^1JB\text{-}H$ in the range 135 to 160Hz., indicating that each boron atom is bound to a terminal hydrogen atom. The ^1H n.m.r. spectrum contains 2 multiplets denoting the COD-C$\underline{H}_2$ protons (centred on δ 2.21 and 2.60p.p.m.) and 3 corresponding to the COD-C$\underline{H}$ protons, centred on δ 5.02, 5.16 and 5.26p.p.m. There are 2 signals in the phenyl region of the spectrum; two multiplets centred on δ 7.24 and 7.50p.p.m., and a doublet of doublets at δ= 7.38p.p.m. with couplings of 8.1 and 1.4Hz. The complexity of this spectrum indicates that the carbaborane is no longer symmetric. Coupled to this, the absence of a high frequency resonance in the ^{11}B n.m.r. spectrum suggests that a polytopal rearrangement has occurred. Assuming that this is of a similar nature to those previously observed, then **21** can be formulated 1,11-Ph_2-3-(1,5-COD)-3,1,11-$PtC_2B_9H_9$.

The formation of **21** with a 3,1,11-framework while **19** is stable in the 3,1,2-form

and requires heat to force isomerisation is consistent with previous observations that second row transition metal carbaborane complexes are more stable to rearrangement than their third row analogues. Thus, the complex[87] $[N(PPh_3)_2][1,2\text{-}Me_2\text{-}3\text{-}(\eta^3\text{-}C_3H_5)\text{-}3,3\text{-}(CO)_2\text{-}3,1,2\text{-}WC_2B_9H_9]$ reacts with aqueous HI and CO to form the 2,1,8 species $[N(PPh_3)_2][1,8\text{-}Me_2\text{-}2\text{-}I\text{-}2,2,2\text{-}(CO)_3\text{-}2,1,8\text{-}WC_2B_9H_9]$, in quantitative yield at room temperature. However, the Mo-2,1,8 analogue is formed only after prolonged reflux of the 3,1,2-$\{Mo(CO)_4I\}$ carbaborane, in CH_2Cl_2. In third row complexes the bonding interactions involve metal 5d orbitals, compared with metal 4d orbitals in second row complexes. It may be that the better energy match of the 4d orbitals with the cage orbitals leads to the formation of a more closed icosahedral structure. In the case of d^8 metal complexes the unfavourable 4-electron interaction between the metal xz and cage $5e^1$ orbitals may be the dominant effect. The d-p transition is of lower energy for second than for third row metals[61] and d-p mixing allows a more closed structure to be adopted.

However, previously it was suggested that the facile isomerisations observed were the result of unfavourable steric interactions involving the metal fragment and cage substituents. On this basis, carbapalladaboranes, with relatively more closed structures and hence more steric crowding at the metal-bonded face, would be predicted to isomerise more readily than their platinum analogues. These two apparently contradictory ideas can be reconciled as follows. Given that, for whatever reason, second-row transition-metal carbametallaboranes are more stable to polytopal isomerisation than their third-row analogues, then, even if the palladium carbaborane complex is destabilised to a greater extent, by interaction of the metal-fragment and the cage-phenyl groups, then the barrier to isomerisation may *still* be higher than that experienced by the platinum anologue.

The electrochemistries of **18-21** have been studied and the results are tabulated below.

Redox Properties of 18, 19, 20 and 21.

Compound	$E_{1/2}$/V(Oxid. Range)	$E_{1/2}$/V(Red. Range)
18	+1.67(i)	-0.98(qr) -1.70(i)
19	+1.66(i)	-0.89(qr) -1.57(i)
20	+1.78(i) +1.97(i)	-1.59(i) -1.99(i)
21	+1.69(qr) (r.w. at +1.39)	-0.63(qr) -1.55(qr) (r.w. at -1.20)

i=irreversible, qr= quasi-reversible (reversibility criteria are outlined in chapter 5). r.w.= return wave. All voltammograms are recorded in CH_2Cl_2/0.5M$[Bu_4N]^+[BF_4]^-$, at 298K, versus Ag/AgCl.

Firstly, comparing **18** with **19**, each shows a single irreversible oxidation at similar potential. In addition, there are two reductions of each species, those for **19** being easier than those for **18**. This is consistent with the expected effect of the addition of a second electron-withdrawing phenyl-substituent in **19**. Similarly, **20** and **21** each show 2 reductions with those of the diphenyl-substituted analogue easier. **20** has 2 oxidations while **21** shows only one. If the Pt and Pd-analogues are compared all the redox processes are more facile in **18** than in **20**. In contrast, the oxidative process and the second reductive process occur at similar potential in **19** and **21**. However, the first reduction of **21** is easier than the corresponding process in **19**. Unfortunately, there is insufficient data available for the nature of these processes to be ascertained.

4.6 Conclusions.

The bis-(phoshine) carbapalladaboranes, **16** and **17**, form in an analogous manner to their platinum equivalents. The structure of **16** is less distorted than that of **1** as would be predicted. However, there is another stable carbametallaborane, related to **16**, which is readily formed. This does not appear to be the 3,1,11-isomer of **16**, however, although it is stable to thermolysis. **17** is isolated only in the 3,1,11-form, similar to **4**.

The mono-phenyl carbaborane complex incorporating the {Pd(1,5-COD)} fragment is formed as the 3,1,2-skeletal isomer but is stable to rearrangement up to 110°C. The Pt analogue is also stable to isomerisation and is isolated only in the 3,1,2-form. Similarly, the di-phenyl carbaborane complex exists in this form and, thereby, provides the only reported example of an $\{ML_2\}$ complex in which the carbaborane contains two cage carbon atoms which are adjacent on the polytopal surface. The structure of this species, **19**, shows that the COD ligand distorts to allow the $\{ML_2\}$ fragment to adopt close to its lowest energy orientation with respect to the ligated carbaborane face, in spite of the presence of 2 phenyl substituents on the cage face. At elevated temperature the 3,1,11-form is generated. The Pt analogue exists only as the isomerised form, indicating that the nature of the metal atom is also important in determining the stability of the skeletal isomers.

The ability of the COD ligand to distort appears to stabilise the carbametallaboranes described. Thus, **18** and **20** are stable to isomerisation whereas no complex incorporating an angular (less flexible) $\{MP_2\}$ (P= alkyl and/or aryl phosphine) is formed under similar conditions. **19** is stable in the 3,1,2-form (although steric crowding between the cage phenyl groups and the metal fragment leads to rearrangement at 110°C) while the Pt analogue, **21** is not, illustrating the general enhanced stability of second row transition metal carbaborane complexes, to skeletal isomerisation, relative to their third row analogues.

Chapter 5.

Experimental.

Introduction.

This chapter outlines the experimental procedures employed in the work described in chapters 2-4. Section A details the syntheses of the complexes and the analytical data obtained. In section B the crystallographic techniques utilised in the determination of the structures of compounds **1**, **4** and **19** are described along with the partial determination of the structure of **16**. Section C covers the methodology of E.H.M.O. calculations and includes tables of the atomic co-ordinates used in the calculations discussed in chapter 2. In section D the basic electrochemical techniques which were used are outlined.

Section A Synthesis and Analysis.

5.1 General Methods and Starting Materials.

All the reactions described were carried out under an atmosphere of dry oxygen-free nitrogen, using standard Schlenk techniques. Some subsequent manipulations were carried out in air. Preparations involving Tl-salts were carried out in foil-covered vessels. Dichloromethane was pre-treated with KOH pellets and n-hexane with Na wire. These were then distilled over CaH_2 and Na wire, respectively, under N_2, immediately prior to use. Diethyl-ether was dried with Na wire. Microanalyses were carried out by the departmental service (when available). Infra-red spectra were recorded as solutions, in CaF_2 cells, on a Perkin-Elmer 598

double-beam spectrophotometer. A reference cell containing the relevant solvent was placed in the second beam and the difference spectrum recorded. N.m.r. spectra were recorded using the following spectrometers: Varian VXR-600 (^{11}B, $^{11}B\{^1H\}$), Bruker WH-360 (^{11}B, $^{11}B\{^1H\}$), Bruker WP-200 (^{11}B, $^{11}B\{^1H\}$, $^{31}P\{^1H\}$ and ^1H) and Jeol FX-90 ($^{31}P\{^1H\}$). Chemical shifts are quoted relative to external standards: $BF_3.OEt_2$ (^{11}B), 85% H_3PO_4 (^{31}P) and $SiMe_4$ (^1H), with positive shifts to high frequency. FAB mass spectra (described in text) were recorded of samples suspended in a liquid matrix (of 3-NOBA) by the departmental service.

The complexes $Tl_2C_2B_9H_{10}Ph$ and $Tl_2C_9H_9Ph_2$ were prepared by the methods developed by the author's research group[44,49]. *cis*-$PtCl_2(PMe_2Ph)_2$[73], *cis*-$PtCl_2(PEt_3)_2$[122], *cis*-$PtCl_2(PPh_3)_2$[123], *cis*-$PtCl_2(P(p\text{-}tol)_3)_2$[124], *trans*-$PtCl_2(PCy_3)_2$[125], $PtCl_2$(1,5-COD)[8] and $PdCl_2$(1,5-COD)[126] were prepared using literature methods and their identities confirmed by ^{31}P n.m.r. spectroscopy[124,128,129] and microanalysis. The complexes *cis*-$PtCl_2(PMe_3)_2$ & *cis*-$PtCl_2(P(OMe)_3)_2$ were prepared by displacement of (1,5-COD) from the complex $PtCl_2$(1,5-COD), in an appropriate solvent. These were readily identified by ^{31}P n.m.r. spectroscopy. Attempts to prepare $PtCl_2$dppe by the method of Cavinato and Toniolo[1130], from H_2PtCl_6, gave a species with an anomalously low value of ^1JPt-P[131]. The microanalysis figures obtained were consistent with the expected formulation, however, it was believed that the Magnus salt[132] ($[PtCl_4]^{2-}[Pt(dppe)_2]^{2+}$) may have been formed. This was heated at reflux temperature in 1:1 EtOH/2M HCl for approximately 1 hour. The white precipitate which formed on cooling the solution was isolated by filtration and thoroughly washed with water, EtOH and Et_2O. A $^{31}P\{^1H\}$ n.m.r. spectrum confirmed this to be the molecular species. The complex *cis*-$PdCl_2(PMe_2Ph)_2$ was prepared from $PdCl_2$(1,5-COD) and its identity established by n.m.r. spectroscopy.

5.2
1-Ph-3,3-$(PMe_2Ph)_2$-3,1,2-$PtC_2B_9H_{10}$, 1.

$Tl_2C_9B_9H_{10}Ph$ (0.50g, 0.81mmol.) and *cis*-$Pt(PMe_2Ph)_2Cl_2$ (0.33g, 0.60mmol.) were mixed in de-gassed CH_2Cl_2($15cm^3$), in a foil covered vessel, at -196°C (77K). The mixture was allowed to warm to room temperature and stirred for 2 hours. During this time the solution turned orange and TlCl was precipitated. This was allowed to settle and the supernatant removed by pipette. It was concentrated to *circa* $5cm^3$ and chromatographed on an alumina column (Brockman activity 2, pre-washed, CH_2Cl_2 eluent). A fast moving orange band was collected and this afforded an orange-red solid on removal of solvent *in vacuo*. Recrystallisation from CH_2Cl_2/Et_2O, at -30°C (243K), yielded orange-red crystals of 1-Ph-3,3-$(PMe_2Ph)_2$-3,1,2-$PtC_2B_9H_{10}$ (0.27g, 65%).

Microanalysis: Calc. for $C_{24}H_{37}B_9P_2Pt$, m.wt. 679.9, 42.4%C 5.44%H. Found 41.6%C 5.52%H.

I.r.(CH_2Cl_2): ν= 2530cm^{-1}(B-H), 1490cm^{-1}(broad, PMe_2Ph).

N.m.r.($CDCl_3$): $^{11}B\{^1H\}$ δ(p.p.m.)= +11.00 (1B, $^1J^{195}Pt$-B= 225Hz), -2.46 (1B), -4.36 (1B), -7.01 (1B), -14.82 (3B), -18.51 (1B) and -20.35 (1B).

$^{31}P\{^1H\}$ δ= -12.09p.p.m.($^1J^{195}Pt$-P= 3280Hz.)

^1H δ(p.p.m.)= 1.71p.p.m. (broad, Me-H), 3.60 (broad, cage C-H), 7.20 and 7.50 (complex multiplets, Ph-H).

5.3 Thermolysis of (1)- Method (a).

A sealed n.m.r. tube containing a sample of **1**, in $CDCl_3$, was placed in a flask of water maintained at +55°C (328K), for 15 days. During this time the sample became pale yellow and the small amount of suspended **1** dissolved.

N.m.r.($CDCl_3$): $^{11}B\{^1H\}$ δ(p.p.m.)= -6.21 (1B), -8.48 (1B), -17.60 (1B), -20.00 (1B), -21.87 (3B), -24.12 (1B), -25.49 (1B).

$^{31}P\{^1H\}$ δ= -14.47p.p.m ($^1J^{195}Pt$-P= 3327Hz., major product) and -15.30p.p.m., $^1J^{195}Pt$-P= 3228Hz., minor product).

^1H (major product (2) first) δ(p.p.m.)= 2.74, 2.20 (broad, cage C-H), 7.05, 7.38 and 7.18, 7.52 (complex multiplets, Ph-H), 1.70p.p.m (broad, Me-H).

5.4 Thermolysis of 1- Method (b).

A sample of **1** (0.25g, 0.04mmol.) was dissolved in toluene ($15cm^3$) and stirred at reflux temperature for 30 minutes. During this time the solution lightened. The solvent was removed *in vacuo* to yield a pale yellow residue which was dissolved in CH_2Cl_2 ($5cm^3$) and chromatographed on silica plates (pre-washed, CH_2Cl_2 eluent). The yellow band at highest R_f(= 0.85) was collected using CH_2Cl_2 and afforded a pale yellow solid on removal of solvent *in vacuo*.

I.r. (CH_2Cl_2): ν= 2905cm^{-1} and 2845cm^{-1} (C-H) 2555cm^{-1} (B-H) and 1450cm^{-1} (broad, PMe_2Ph).

N.m.r. ($CDCl_3$): $^{31}P\{^1H\}$ -14.53p.p.m. ($^1J^{195}Pt$-P= 3327Hz., **2**) and -15.37p.p.m. ($^1J^{195}Pt$-P= 3255Hz., **3**).

^1H δ (p.p.m.) 2.68 (broad, cage C-H), 7.51, 7.37, 7.18 and 7.13 (complex multiplets, Ph-H), 1.68 (broad multiplet, Me-H) and 0.86 (Me-H, free PMe_2Ph).

5.5 Thermolysis of (1)- Method (c).

A sample of **1** (0.25g, 0.04mmol) was dissolved in decalin (decahydranaphthalene) ($15cm^3$), and stirred at reflux temperature for 30 minutes, during which time the solution lightened and a dark orange solid precipitated. The mixture was allowed to cool and was filtered. The solvent was removed from the filtrate yielding a yellow residue (X). The precipitate was washed with Et_2O and dried *in vacuo*, to yield an orange solid (Y).

I.r.(CH_2Cl_2): (X) ν= 2920cm^{-1} and 2845cm^{-1} (C-H), 2560cm^{-1} (B-H) and 1450cm^{-1} (broad, PMe_2Ph).

(Y) ν= 2910cm^{-1} and 2850cm^{-1} (C-H), 2550cm^{-1} (B-H), 1450cm^{-1} (broad, PMe_2Ph).

N.m.r.($CDCl_3$): (X) $^{11}B\{^1H\}$ Broad structureless envelope in range δ= -0.68 to -28.14p.p.m.

$^{31}P\{^1H\}$ +35.15p.p.m. (=O<u>P</u>Me_2Ph).

^1H δ (p.p.m.)= 7.70 (multiplet, Ph-H), 7.52 (broad, Ph-H) and 1.97 (broad, Me-H).

(Y) $^{11}B\{^1H\}$ Broad envelope in which 10 signals distinguishable at δ(p.p.m.) -4.57, -7.03, -9.30, -9.97, -14.07, -15.23, -18.80, -20.63, -23.00 and -24.34.

$^{31}P\{^1H\}$ -15.44p.p.m. ($^1J^{195}Pt$-P= 3219Hz., **3**), -14.53 ($^1J^{195}Pt$-P= 3316Hz., **2**) and +35.53p.p.m. (O=<u>P</u>Me_2Ph).

^1H δ (p.p.m.)= 2.70 (broad, cage C-H), 1.70 (broad, Me-H), 7.20, 7.37 and 7.70

(multiplets, Ph-H).

5.6
1,11-Ph_2-3,3-$(PMe_2Ph)_2$-3,1,11-$PtC_2B_9H_9$, 4.

$Tl_2C_2B_9H_9Ph_2$ (0.50g, 0.72mmol.) and *cis*-$Pt(PMe_2Ph)_2Cl_2$ (0.30g, 0.55mmol.) were mixed in degassed CH_2Cl_2 (15cm^3), at -196° (77K). The mixture was allowed to warm to room temperature and was stirred for 2 hours. During this time the solution turned orange and TlCl was precipitated. This was allowed to settle and the supernatant was removed by pipette, concentrated to *circa* 5cm^3, and chromatographed (alumina column, Brockman activity 2, pre-washed, CH_2Cl_2 eluent). A fast moving yellow band was collected and afforded a yellow solid on removal of solvent *in vacuo*. On some occasions, further chromatographic purification was required in the form of preparative t.l.c. (silica plates, prewashed, CH_2Cl_2 eluent). The yellow band with highest R_f(= 0.9) was collected using CH_2Cl_2 and this afforded a yellow solid on removal of solvent *in vacuo*. Two further bands at lower R_f values were also present but these were not collected. Recrystallisation of the yellow product at -30°C (243K), from CH_2Cl_2/n-hexane, yielded yellow crystals (0.23g, 55%).

Microanalysis: Calc. for $C_{30}H_{41}B_9P_2Pt$, m.wt.= 756.0, 47.7%C 5.42%H. Found 47.0%C 5.81%H.

I.r.(CH_2Cl_2): ν= 2550cm^{-1} (B-H) and 1480cm^{-1} (broad, PMe_2Ph).

N.m.r.($CDCl_3$): $^{11}B\{^1H\}$ (Varian VXR-600, 192.630MHz.) δ(p.p.m.)= -3.81 (2B), -6.52 (1B), -8.41 (1B), -12.43 (1B), -13.16 (1B), -14.69 (1B), -17.55 (1B) and -22.48 (1B).

$^{31}P\{^1H\}$ δ= -14.94p.p.m. ($^1J^{195}Pt$-P= 3257Hz.).

^1H δ(p.p.m.)= 7.50 (complex multiplet, Ph-H), 7.10 (complex multiplet, Ph-H) and 1.60 (broad complex multiplet, Me-H).

5.7 1-Ph-3,3-$(P(OMe)_3)_2$-3,1,2-$PtC_2B_9H_{10}$, 5.

In a similar manner to the synthesis of **1**, $Tl_2C_2B_9H_{10}Ph$ (0.50g, 0.81mmol.) was allowed to warm together with *cis*-$PtCl_2(P(OMe)_3)_2$ (0.31g, 0.60mmol.), in degassed CH_2Cl_2 ($15cm^{-3}$). The mixture was stirred for 2 hours at room temperature, during which time the solution became yellow and TlCl was precipitated. Column chromatography (alumina/CH_2Cl_2) and collection of the mobile yellow band yielded a yellow solid on removal of solvent *in vacuo* (0.20g, 55%).

I.r.(CH_2Cl_2): ν= 2540cm^{-1} (B-H), 1175cm^{-1} and 1040cm^{-1} ($P(OMe)_3$).

N.m.r.($CDCl_3$): $^{11}B\{^1H\}$ δ(p.p.m.)= 8.97 (1B, $^1J^{195}Pt$-P= 260Hz.), -3.25 (1B), -5.40 (2B), -12.81 (2B), -13.75 (1B), -18.89 (1B) and -21.61 (1B).

$^{31}P\{^1H\}$ δ= 104.95p.p.m. ($^1J^{195}Pt$-P= 5478Hz.)

^1H δ (p.p.m.)= 3.53 (OMe-H, second order pattern- apparent triplet ^3JP-H= 12.6Hz., 18H), 4.21 (cage C-H, broad, 1H), 7.48 (Ph-H, doublet, ^3JH-H = 6.6Hz., 2H), 7.15 (Ph-H, multiplet, 3H).

5.8 Thermolysis of 5.

A sample of **5** (0.10g, 0.28mmol.) was heated in toluene ($15cm^3$) at reflux temperature, for 30 minutes. During this time the solution lightened. Removal of the solvent *in vacuo* yielded a pale yellow residue.

N.m.r.($CDCl_3$): $^{11}B\{^1H\}$ δ(p.p.m.)= -5.65 (3B), -9.80 (1B), -16.22 (1B), -19.28 (2B) and -20.53 (2B).

$^{31}P\{^{1}H\}$ δ= 114.99p.p.m. ($^{1}J^{195}Pt$-P= 5388.6Hz.)

^{1}H Two sets of peaks-in approximate ratio 2:1. Major isomer first. δ(p.p.m.)= 3.71 (second order signal- apparent triplet, OMe-H, ^{3}JP-H= 12.6Hz.), 3.15 (second order signal- apparent triplet, OMe-H, ^{3}JP-H= 17.0Hz.), 2.82 and 1.83 (broad, cage C-H), (7.41 and 7.13) and (7.44 and 7.21) (multiplets, Ph-H). There are also 2 6-line signals in the ratio 1:1, at 1.40 (J= 7.2Hz) and 1.59 (J= 7.3Hz.) and a triplet at 0.98 (J= 7.1Hz) which were not assigned.

5.9
1,11-Ph_2-3,3-$(P(OMe)_3)_2$-3,1,11-$PtC_2B_9H_9$, 6.

$Tl_2C_2B_9H_9Ph_2$ (0.50g, 0.72mmol.) and *cis*-$PtCl_2(P(OMe)_3)_2$ (0.29g, 0.56mmol.) were allowed to react in a similar manner to that described above. An orange soluble product was formed along with TlCl. Purification was effected by column chromatography (alumina, pre-washed, CH_2Cl_2 eluent). An orange mobile band was collected and this yielded an orange solid residue on removal of solvent *in vacuo* (0.16g, 48%). Subsequent spot t.l.c. of this residue indicated that it either contained more than one species or was unstable in the solvents employed. However, a solvent mixture, which could satisfactorily effect separation of the constituents, could not be found and, hence, the spectra of the crude product, **6**, were recorded.

I.r.(CH_2Cl_2): ν= 2535cm^{-1} (B-H), 1170cm^{-1}, 1110cm^{-1} and 1010cm^{-1} (all $P(OMe)_3$).

N.m.r.($CDCl_3$): $^{11}B\{^{1}H\}$ δ(p.p.m.)= -5.70, -7.80, -9.60, -14.31, -16.03, -18.03, -20.85, -32.59 and -35.05 (each 1B).

$^{31}P\{^{1}H\}$ δ(p.p.m.)= 114.54 ($^{1}J^{195}Pt$-P= 5331.1Hz.) and 114.22 ($^{1}J^{195}Pt$-P= 5320.1Hz., ^{2}JP-P= 26.3Hz.).

^{1}H δ(p.p.m.)= 3.75 (complex second order pattern, OMe-H), 3.54 (doublet of doublets, ^{3}JP-H= 18.3Hz., ^{4}J^{195}Pt-H= 6Hz.), 6.91, 7.04 and 7.20 (all multiplets, Ph-H), 7.46 (doublet of doublets, ^{3}JH-H= 8.2Hz., ^{4}JH-H= 1.7Hz., Ph-H) and 7.55 (second order signal, Ph-H).

5.10 1-Ph-3,3-$(PMe_3)_2$-3,1,2-$PtC_2B_9H_{10}$, 7.

Similarly, $Tl_2C_2B_9H_{10}Ph$ (0.50g, 0.81mmol.) was mixed with *cis*-$PtCl_2(PMe_3)_2$ (0.25g, 0.6mmol.) in CH_2Cl_2 at -196°C. The mixture was allowed to warm to room temperature and stirred for two hours, during which time the solution became orange/red and grey insoluble TlCl formed. The solution was concentrated to *circa* 5cm^3 and chromatographed (alumina/CH_2Cl_2). A dark orange mobile band was collected which afforded a rust/orange coloured solid on removal of solvent *in vacuo*. Spot t.l.c. of this residue indicated that it contained more than one component, so the bulk was re-chromatographed (alumina/75:25 CH_2Cl_2/n-hexane). Two bands were collected- a fast moving yellow band and a rust coloured band. The latter of these was found to contain at least 5 constituents, but in amounts too small to permit isolation. The yellow band yielded a yellow solid which afforded yellow crystals from CH_2Cl_2/Et_2O (0.13g, 40%).

I.r.(CH_2Cl_2): ν= 3850cm^{-1} (C-H), 2510cm^{-1} (B-H), 1450cm^{-1} and 1375cm^{-1} (both PMe_3).

N.m.r.($CDCl_3$): ^{11}B{^{1}H} δ(p.p.m)= +11.51 (1B, ^{1}J^{195}Pt-P= 270Hz.), -2.90 (1B), -4.97 (1B), -7.87 (1B), -14.61 (3B), -18.37 (1B) and -21.66 (1B).

^{31}P{^{1}H} δ= -42.79p.p.m. (^{1}J^{195}Pt-P= 3240.3Hz.).

^{1}H δ(p.p.m.)= 2.16 (broad, 18H , Me-H), 3.77 (broad, 1H, cage C-H), 7.16 (multiplet, 2H, Ph-H) and 7.54 (multiplet, 3H, Ph-H).

5.11 Thermolysis of 7.

A sample of 7 (0.10g, 0.18mmol.) was dissolved in toluene and stirred at reflux temperature for 30 minutes, during which time the solution lightened. The solvent was removed *in vacuo* to yield a pale yellow residue.

N.m.r.($CDCl_3$): $^{11}B\{^1H\}$ δ (p.p.m.)= -4.99 (1B), -7.67 (1B), -9.77 (1B), -11.46 (1B), -15.57 (1B), -18.96 (2B), -23.47 (1B) and -24.34 (1B).

$^{31}P\{^1H\}$ δ= -19.98p.p.m. ($^1J^{195}PtP$= 3278.7Hz.)

^1H δ(p.p.m.)= 1.58 (complex multiplet, Me-H), 1.73 (second order signal- apparent triplet, $|^2JP\text{-}H + {}^4JP\text{-}H|$= 9.6Hz.), 3.15 (weak, second order- apparent triplet, $|^2JP\text{-}H + {}^4JP\text{-}H|$≈15Hz.), 2.53 (broad, cage C-H) and 7.04, 7.10 and 7.42 (multiplets, Ph-H).

5.12
$1,11\text{-}Ph_2\text{-}3,3\text{-}(PMe_3)_2\text{-}3,1,11\text{-}PtC_2B_9H_9$, 8.

$Tl_2C_2B_9H_9Ph_2$ (0.50g, 0.73mmol.) and *cis*-$PtCl_2(PMe_3)_2$ (0,23g, 0.55mmol.) were reacted in a similar manner to that described above, to give an orange/brown soluble product (and TlCl). Chromatographing this solution (alumina/CH_2Cl_2) afforded a brown mobile band which yielded a brown solid on removal of solvent *in vacuo* (0.16g, 45%).

I.r.(CH_2Cl_2): ν=2530cm^{-1} and 1430cm^{-1} (broad, PMe_3).

N.m.r.($CDCl_3$): $^{11}B\{^1H\}$ Broad envelope in which 7 signals could be distinguished at δ(p.p.m.)= -5.30, -6.91, -9.65, -13.44, -15.34, -17.83 and -23.67.

$^{31}P\{^1H\}$ δ= -26.22p.p.m. ($^1J^{195}Pt\text{-}P$= 3225.0Hz.) and -27.12p.p.m. ($^1J^{195}Pt\text{-}P$=

3210.9Hz., ^{2}JP-P<10Hz.).

^{1}H δ (p.p.m.)= 1.59 (multiplet {possibly doublet of doublets of doublets}, Me-H), 7.30 and 7.51 (multiplets, Ph-H).

5.13 1-Ph-3-(dppe)-3,1,2-$PtC_2B_9H_{10}$, 9.

$Tl_2C_2B_9H_{10}Ph$ (0.50g, 0.81mmol.) and $PtCl_2$(dppe) (0.31g, 0.60mmol.) were stirred in CH_2Cl_2 (15cm^3), for 2 hours, during which time a yellow soluble product and TlCl formed. The solution was concentrated to *circa* 5cm^3, and chromatographed (alumina/CH_2Cl_2). A pale yellow mobile band was collected which afforded a yellow crystalline solid on removal of solvent *in vacuo* (0.16g, 41%).

Microanalysis: Calculated for $C_{34}H_{39}B_9P_2Pt$, m.wt.= 801.7, 50.9%C 4.86%H. Found 48.9%C 5.23%H.

I.r.(CH_2Cl_2): ν=2920cm^{-1} and 2850cm^{-1} (C-H), 2510cm^{-1} (B-H) and 1370cm^{-1} (dppe).

N.m.r. ($CDCl_3$): ^{11}B{^{1}H} δ(p.p.m.) +14.18 (1B, $^1J^{195}$PtP= 300Hz.), -3.97 (2B), -7.31 (1B), -12.51 (3B), -17.02 (1B) and -21.08 (1B).

^{31}P{^{1}} δ= 48.21p.p.m. ($^1J^{195}$PtP= 3286.8Hz.)

^{1}H δ (p.p.m.)= 2.20 (broad second order signal, (dppe-C<u>H</u>$_2$), 3.20 (broad, cage C-<u>H</u>), 6.61 (5 line pattern, Ph-<u>H</u>), 7.26 (multiplet, Ph-<u>H</u>), 7.51 (multiplet, Ph-<u>H</u>) and 7.72 (multiplet, Ph-<u>H</u>).

5.14 Thermolysis of 9.

A sample of **9** (0.10g, 0.15mmol.) was dissolved in toluene ($15cm^3$) and heated at reflux temperature for 30 minutes, during which time the solution lightened. The solvent was removed *in vacuo* to yield a pale yellow residue.

N.m.r. ($CDCl_3$): $^{11}B\{^1H\}$ δ(p.p.m.)= -7.26 and -8.19 (total 4B), -15.33 (1B), -20.00 and -21.25 (total 4B).

$^{31}P\{^1H\}$ δ= 46.52p.p.m. ($^1J^{195}PtP$= 3377.6Hz.)

^1H δ (p.p.m.)= 2.63 (broad), 3.27 (multiplet), 7.25 (broad, Ph-H), 7.53 (12.3Hz. doublet, Ph-H) and 7.75 (broad, Ph-H).

5.15 1,11-Ph_2-3-(dppe)-3,1,11-$PtC_2B_9H_9$, 22.

$Tl_2C_2B_9H_9Ph_2$ (0.50g, 0.72mmol.) and $PtCl_2$(dppe) (0.25g, 0.50mmol.) were mixed in CH_2Cl_2 ($15cm^3$) and allowed to react in a similar manner as described previously. After 2 hours, the solution was yellow and TlCl had been precipitated. The product was separated chromatographically (alumina/CH_2Cl_2). A deep yellow mobile band was collected which yielded a yellow residue on removal of solvent *in vacuo*.

I.r. (CH_2Cl_2: νB-H= $2540cm^{-1}$, ν= $1410cm^{-1}$ (broad, dppe).

N.m.r.($CDCl_3$): $^{11}B\{^1H\}$ δ(p.p.m.)= -1.78 (1B), -8.42 (1B), -9.76 (1B), -13.25 (1B), -15.86 (2B), -22.05 (1B), -32.26 (1B) and -34.98 (1B).

$^{31}P\{^1H\}$ δ= 44.55p.p.m. ($^1J^{195}Pt$-P= 3296.6Hz.) and 46.17p.p.m. ($^1J^{195}Pt$-P= 3268.6Hz.). Also, 47.95p.p.m. ($^1J^{195}Pt$-P= 2305.7Hz. $[PtCl_4]^{2-}[Pt(dppe)_2]^{2+}$) and

47.24p.p.m. ($^1J^{195}$Pt-P= 2104.3Hz.)

^{1}H δ (p.p.m.)= 2.3 (broad, low intensity, dppe-C<u>H</u>$_2$), 6.90, 7.05, 7.19, 7.41, 7.47 and 7.71 (all multiplets, Ph protons).

5.16 1-Ph-3,3-$(PEt_3)_2$-3,1,2-$PtC_2B_9H_{10}$, 10.

$Tl_2B_9H_{10}Ph$ (0.50g, 0.81mmol) and *cis*-$PtCl_2(PEt_3)_2$ (0.30g, 0.60mmol) were mixed in CH_2Cl_2 (20cm^{-1}) and stirred for two hours at room temperature, in a similar manner to that described previously. During this time a soluble orange product formed, together with insoluble TlCl. The solution was concentrated to *circa* 5cm^{-1} and chromatographed (alumina/CH_2Cl_2). A mobile orange band was collected which yielded an orange solid on removal of solvent *in vacuo*. Recrystallisation from CH_2Cl_2/n-hexane, at -30°C (243K) afforded orange/red crystals (0.26g, 67%).

Microanalysis: Calculated for $C_{20}H_{45}B_9P_2Pt$, m.wt. 639.6, 37.6%C 7.04%H. Found 35.3%C 6.98%H.

I.r. (CH_2Cl_2): ν= 2530cm^{-1} (B-H), 2970cm^{-1} (C-H).

N.m.r.($CDCl_3$): ^{11}B{^{1}H} δ(p.p.m.)= 13.87 ($^1J^{195}$Pt-B= 254Hz., 1B), -1.98 (1B), -3.11 (1B), -7.69 (1B), -13.62 (1B), -14.67 (2B), -19.35 (1B) and -22.19 (1B).

^{31}P{^{1}H} δ= +13.68p.p.m. ($^1J^{195}$Pt-P= 3038.5Hz.) and +8.59p.p.m. ($^1J^{195}$Pt-P= 3388.8Hz., ^{2}JP-P= 10Hz.)

^{1}H δ (p.p.m.)= 0.83 and 1.12 (broad second-order signals, C<u>H</u>$_3$), 1.80, 1.93 (broad, second-order signals,C<u>H</u>$_2$), 3.89p.p.m. (broad, cage C-<u>H</u>), 7.49p.p.m. (doublet of doublets, J= 9Hz. and 1.5Hz., 2H, Ph-<u>H</u>), 7.13p.p.m. (multiplet, 3H, Ph-<u>H</u>).

5.17 Thermolysis of 10.

A sample of **10** (0.1g, 0.16mmol.) was dissolved in toluene ($15cm^3$) and heated at reflux temperature for 30 minutes, during which time the solution lightened. The solvent was removed *in vacuo* to yield a pale yellow residue.

I.r. (CH_2Cl_2): ν= $2930cm^{-1}$ and $2875cm^{-1}$ (C-H), $2550cm^{-1}$ (B-H), $1485cm^{-1}$, $1430cm^{-1}$ (broad) and $1375cm^{-1}$ (all PEt_3).

N.m.r. ($CDCl_3$): $^{11}B\{^1H\}$ δ(p.p.m.) -4.73 (2B), -8.39 (1B), -9.81 (1B), -15.35 (1B), -18.95 (3B) and -23.63 (1B).

$^{31}P\{^1H\}$ δ= +7.82p.p.m. ($^1J^{195}Pt$-P= 3257.0Hz.) and +6.56p.p.m. ($^1J^{195}Pt$-P= 3288.3Hz., ^2JP-P <10Hz., major product). +4.51p.p.m.($^1J^{195}Pt$-P= 3200.2Hz., minor product).

^1H δ(p.p.m.)= 1.94 (broad, C<u>H</u>$_3$, 18H), 1.11 (doublet of triplets, C<u>H</u>$_2$, 12H, ^2JP-H= 14.2Hz., $^3JCH_3$-H= 7.5Hz.), 2.60 (broad, cage C-<u>H</u>, 1H), 7.13 (multiplet, 2H, Ph-<u>H</u>), 7.45 (multiplet, 3H, Ph-<u>H</u>).

5.18
1,11-Ph_2-3,3-$(PEt_3)_2$-3,1,2-$PtC_2B_9H_9$, 11.

$Tl_2C_2B_9H_9Ph_2$ (0.50g, 0.73mmol.) and *cis*-$PtCl_2(PEt_3)_2$ (0.28g, 0.55mmol.) were mixed in CH_2Cl_2 ($15cm^3$) and stirred for two hours. During this time an orange soluble product formed in addition to TlCl. The solution was chromatographed (alumina/CH_2Cl_2) and a yellow, mobile band collected. This afforded a pale orange solid on removal of solvent *in vacuo*, which was recrystallised from CH_2Cl_2/Et_2O, to yield yellow crystals (0.24g, 61%).

Microanalysis: Calculated for $C_{26}H_{49}B_9P_2Pt$, m.wt. 714.6, 43.7%C 6.86%H. Found 43.3%C 7.71%H.

I.r.(CH_2Cl_2): ν= 2540cm^{-1} (B-H) and 2900cm^{-1} (C-H).

N.m.r.($CDCl_3$): $^{11}B\{^1H\}$ δ(p.p.m.)= -1.74 (1B), -4.36 (1B), -8.51 (3B), -9.56 (1B), -13.78 (1B), -18.70 (1B) and -24.41 (1B).

$^{31}P\{^1H\}$ δ= +5.76p.p.m. ($^1J^{195}$Pt-P= 3206.2Hz.) and +4.58p.p.m. ($^1J^{195}$Pt-P= 3173Hz., ^{2}JP-P= 10Hz.).

^1H δ(p.p.m.)= 0.89 (doublet of triplets of doublets, C$\underline{H}_3$, 18H, ^{3}JP-H= 11Hz., ^{3}JCH$_2$-H= 7.5Hz, $^4J^{195}$Pt-P= 2.6Hz.), 1.93 (complex pattern (possibly doublet of quartets of doublets), C$\underline{H}_2$, 12H), 7.04 (multiplet, Ph-$\underline{H}$, 3H), 7.16 (multiplet, Ph, 3H), 7.44 (doublet of doublets, Ph-$\underline{H}$, 2H, ^{3}JH-H= 7.8Hz. and ^{4}JH-H = 1.6Hz.) and 7.56 (doublet of doublets, Ph-$\underline{H}$, 2H, ^{3}JH-H= 10.3Hz. and ^{4}JH-H = 1.7Hz.).

5.19 1-Ph-3,3-$(PPh_3)_2$-3,1,2-$PtC_2B_9H_{10}$, 12.

$Tl_2C_2B_9H_{10}Ph$ (0.50g, 0.81mmol) and *cis*-$PtCl_2(PPh_3)_2$ (0.53g, 0.67mmol.) were mixed in CH_2Cl_2 (15cm^3), at -196°C (77K) and allowed to react as described previously. The orange crude product yielded a yellow mobile band when chromatographed (alumina/ CH_2Cl_2). This afforded a yellow solid on removal of solvent *in vacuo*, which was further purified by recrystallisation (CH_2Cl_2/n-hexane), giving an orange crystalline solid (0.31g, 50%).

Microanalysis: Calculated for $C_{44}H_{45}B_9P_2Pt$, m.wt. 927.8, 57.0%C 4.85%H. Found 52.8%C 4.79%H.

I.r. (CH_2Cl_2): ν= 2540cm^{-1} (B-H), 1480cm^{-1} and 1330cm^{-1} (both PPh_3).

N.m.r. ($CDCl_3$): $^{11}B\{^1H\}\delta$(p.p.m.)= +21.11 ($^1J^{195}Pt$-P= 270Hz., 1B), +2.46 (1B), -4.32 (3B), -10.00 (2B), -14.80 (1B) and -23.04 (1B).

$^{31}P\{^1H\}$ δP_1= 26.20p.p.m. ($^1J^{195}Pt$-P= 3032.4Hz.), δP_2= 22.25p.p.m. ($^1J^{195}Pt$-P= 3438.8Hz. and $^2JP_1$-P_2= 20Hz.)

^1H δ (p.p.m.)= 2.85 (cage C-H, broad), 6.95 and 7.20 (broad multiplets, Ph-H).

5.20 Thermolysis of 12.

A sample of **12** (0.15g, 0.16 mmol), was stirred in toluene, at reflux temperature for 30 minutes. This yielded a pale yellow solid on removal of solvent *in vacuo*.

N.m.r. ($CDCl_3$): $^{11}B\{^1H\}$ Broad envelope in the range δ= 0 to -23p.p.m. consisting of three distinguishable resonances at δ (p.p.m.)= -4.2, -18.1 and -22.2.

$^{31}P\{^1H\}$ δ= 21.87p.p.m.(poorly resolved AB pattern, $^1J^{195}Pt$-P= 3409Hz., $^2JP_1P_2$= 22Hz.)

^1H δ (p.p.m.)= 1.57 (broad, C-H), 7.22 (complex multiplet, Ph-H), 7.45 (broad, Ph-H).

5.21
1,11-Ph_2-3,3-$(PPh_3)_2$-3,1,2-$PtC_2B_9H_9$, 13.

$Tl_2C_2B_9H_9Ph_2$ (0.50g, 0.73mmol.) and *cis*-$PtCl_2(PPh_3)_2$ (0.40g, 0.55mmol.) were mixed in degassed CH_2Cl_2, at -196°C (77K). The mixture was allowed to warm to room temperature and stirred for 2 hours, during which time the solution became orange and TlCl was formed. Column chromatography of the crude product (alumina/ CH_2Cl_2) afforded a fast moving yellow band, which was collected. This yielded a yellow crystalline solid, on removal of solvent *in vacuo* (0.27g, 49%).

Microanalysis: Calculated for $C_{50}H_{49}B_9P_2Pt$, m.wt. 1003.8, 59.82%C 4.88%H. Found 52.4%C 5.39%H.

I.r. (CH_2Cl_2): ν_{B-H}= 2540cm^{-1}.

N.m.r. ($CDCl_3$): $^{11}B\{^1H\}$ δ(p.p.m.)= +9.30, +2.77, -1.65, -4.05, -9.56, -10.59, -12.23, -22.57, -25.74 (each 1B).

$^{31}P\{^1H\}$ νP_1= 24.32p.p.m. ($^1J^{195}$Pt-P= 3209Hz., νP_2= 22.22p.p.m. ($^1J^{195}$Pt-P= 3306Hz., poorly resolved AB pattern, $^2JP_1$-P_2= 18.2Hz.).

^1H δ(p.p.m.)= 6.94, 7.05, 7.14, 7.19, 7.40 and 7.50 (complex multiplets, Ph-H).

5.22 1-Ph-3,3-(P(p-tol)$_3$)$_2$-3,1,2-PtC$_2$B$_9$H$_{10}$, 14.

$Tl_2C_2B_9H_{10}Ph$ (0.50g, 0.81mmol.) was mixed with *cis*-$PtCl_2(P(p\text{-}tol)_3)_2$ (0.52g, 0.62mmol.), in CH_2Cl_2(15cm^3) and the mixture treated as before. This gave rise to a soluble orange product and TlCl. Purification was effected by column chromatography (alumina/CH_2Cl_2). The mobile orange band which was collected afforded an orange solid on removal of solvent *in vacuo* (0.36g, 56%).

I.r. (CH_2Cl_2): ν_{B-H}= 2540cm^{-1},$\nu P(p\text{-}tol)_3$= 1490cm^{-1} and 1450cm^{-1}.

N.m.r. ($CDCl_3$): $^{11}B\{^1H\}$ δ(p.p.m.)= +20.19 (1B, $^1J^{195}$Pt-B= 280Hz.), 2.18 (1B), -4.71 (3B) , -10.43 (2B), -21.91 (1B), -24.08 (1B).

$^{31}P\{^1H\}$ δ_{P_1}= 24.33p.p.m. ($^1J^{195}$Pt-P= 3055.6Hz.) and δ_{P_2}= 20.33p.p.m. ($^1J^{195}$Pt-P= 3439.3Hz., $^2JP_1P_2$= 27.0Hz.)

^1H δ(p.p.m.)= 2.95 (broad, 1H, cage C-H,), 2.34 and 2.32 (singlets, total 18H, Me-H), 7.50, 7.32, 7.10 and 6.91 (multiplets, total 29H, Ph-H).

5.23 Thermolysis of 14.

A sample of **14** (0.10g, 0.13mmol.) in toluene was heated at reflux temperature for 30 minutes, during which time the solution lightened. The solvent was removed *in vacuo* to yield a pale orange residue.

N.m.r. ($CDCl_3$): $^{11}B\{^1H\}$ Broad envelope within which 3 resonances could be distinguished at δ (p.p.m.)= -5.87, -18.68 and -22.24.

$^{31}P\{^1H\}$ δ= 20.02p.p.m. (poorly resolved AB pattern, $^1J^{195}Pt$-P= 3404.9Hz., ^2JP-P= 26.3Hz.).

^1H δ (p.p.m.)= 3.05 (broad, cage C-H), 2.32 and 2.37 (2 singlets, Me-H), 7.24, 6.91 and 6.74 (multiplets, Ph-H).

5.24
$1,11\text{-}Ph_2\text{-}3,3\text{-}(P(p\text{-}tol)_3)_2\text{-}3,1,11\text{-}PtC_2B_9H_9$, 15.

$Tl_2B_9H_9Ph_2$ (0.50g, 0.73mmol.) was mixed with *cis*-$PtCl_2(P(p\text{-}tol)_3)_2$ (0.52g, 0.51mmol.) in CH_2Cl_2 ($15cm^{-1}$). After stirring for 2 hours at room temperature, an orange soluble product, together with TlCl, had been formed. The solution was chromatographed (alumina/CH_2Cl_2) and a fast moving orange band was collected. This was further chromatographed (fluorosil/75:25 CH_2Cl_2/n-hexane). A mobile pale red band was collected and on removal of solvent *in vacuo* this yielded an orange/red solid (0.23g, 45%).

I.r. (CH_2Cl_2): ν=2540cm^{-1} (B-H), 1500cm^{-1} and 1450cm^{-1} ($P(p\text{-}tol)_3$).

N.m.r. ($CDCl_3$): $^{11}B\{^1H\}$ δ(p.p.m.)= +8.41 (1B), +2.36 (2B), -4.67 (2B), -9.58 (3B) and -26.09 (1B).

$^{31}P\{^{1}H\}$ δP_1= 20.05p.p.m. ($^{1}J^{195}$Pt-P= 3323.1Hz.), δP_2= 22.65p.p.m. ($^{1}J^{195}$Pt-P= 3228.2Hz, $^{2}JP_1$-P_2= 20.4Hz.)

^{1}H δ (p.p.m.)= 2.25 and 2.37 (singlets, Me-H), 7.24, 6.91 and 6.74 (multiplets, Ph-H).

5.25 Reaction of $Tl_2C_2B_9H_{10}Ph$ with t-$PtCl_2(PCy_3)_2$.

$Tl_2C_2B_9H_{10}Ph$ (0.50g,0.81mmol.) and *trans*-$PtCl_2(PCy_3)_2$ were mixed in degassed CH_2Cl_2, at -196°C (77K). After stirring for 20 hours, at room temperature, no reaction was apparent. The solvent was removed *in vacuo* and a $^{31}P\{^{1}H\}$ n.m.r. spectrum of the residue recorded.

N.m.r. ($CDCl_3$): $^{31}P\{_{1}H\}$ δ= 16.83p.p.m. (singlet, $^{1}J^{195}$Pt-P= 2392.5Hz., *t*-$PtCl_2(PCy_3)_2$)

The residue was re-dissolved in CH_2Cl_2 and stirred at reflux temperature for 3 hours, during which time no colour change was visible. The solvent was removed *in vacuo* and an n.m.r. spectrum of the residue recorded.

N.m.r. ($CDCl_3$): $^{31}P\{^{1}H\}$ 16.83p.p.m. ($^{1}J^{195}$Pt-P= 2397.5Hz., *t*-$PtCl_2(PCy_3)_2$).

The residue was dissolved in toluene and heated to reflux temperature for 1 hour. The solution turned pale yellow, but the yellow insoluble $Tl_2C_2B_9H_{10}Ph$ was still present. The solvent was removed *in vacuo* to yield a pale yellow residue.

I.r. (CH_2Cl_2): ν= 2540cm^{-1} (B-H).

N.m.r. ($CDCl_3$): $^{11}B\{_{1}H\}$ Broad envelope in the range -3.9 to -35.6p.p.m. (decomposition?).

$^{31}P\{^{1}H\}$ δ= 16.83p.p.m. ($^{1}J^{195}Pt$-P= 2397.5Hz.). Also, 51.15p.p.m. (singlet, decomposition?).

5.26 1-Ph-3,3-$(PMe_2Ph)_2$-3,1,2-$PdC_2B_9H_{10}$, 16.

$Tl_2C_2B_9H_{10}Ph$ (0.50g, 0.81mmol.) and *cis*-$PdCl_2(PMe_2Ph)_2$ (0.26, 0.61mmol.) were mixed in CH_2Cl_2 ($15cm^3$) and stirred for 2 hours. During this time the solution became dark red and grey insoluble TlCl was precipitated. The solution was chromatographed (alumina/ CH_2Cl_2) and the mobile purple band collected. This yielded a purple solid on removal of solvent *in vacuo* (0.24g, 67%).

Microanalysis: Calculated for $C_{24}H_{37}B_9P_2Pd$, m.wt. 590.9, 48.78%C 6.26%H. Found 49.18%C 6.14%H.

I.r. (CH_2Cl_2): ν= 2540cm^{-1} (B-H), 1490 and 1450cm^{-1} (PMe_2Ph).

N.m.r. ($CDCl_3$): (**16**) $^{11}B\{^{1}H\}$ δ (p.p.m.)= +9.75 (1B), -0.99 (1B), -6.26 (2B), -14.05 (2B) and -16.00 (3B).

^{31}P δ= +35.00p.p.m. (singlet, O=$\underline{P}Me_2Ph$) and -4.65p.p.m. (broad).

^{1}H δ (p.p.m.)= 1.16, 1.46 (doublets, Me-$\underline{H}$, $|^{2}JPH + {}^{4}JPH|$= 9.8Hz., Me-$\underline{H}$, 3H + 3H), 3.24 (cage C-$\underline{H}$, 1H), 7.07, 7.24, 7.47 (multiplets, Ph-$\underline{H}$), 7.35 (doublet, Ph-$\underline{H}$, J= 7.1Hz.), 0.8 (Me-$\underline{H}$, PMe_2Ph) and 1.73 (doublet, Me-$\underline{H}$, O=PMe_2Ph, ^{2}JPH= 13Hz.).

Crude product (un-chromatographed)

$^{11}B\{^{1}H\}$ Very complex. δ (p.p.m.)= 9.48, 8.18, 5.98, -1.23, -6.60, -8.44, -9.59, -12.87, -14.89, -16.45, -17.92, -20.05, -21.93, -32.01, -34.70 and -35.01.

$^{31}P\{^{1}H\}$ δ (p.p.m.)= 35.00 (singlet, O=$\underline{P}Me_2Ph$). Also, some very weak structure

on the baseline at *circa* 0p.p.m. including -1.55 (doublet) and -6.53 (doublet, ^{2}JPP= 65.1Hz.), -4.84 (singlet).

^{1}H δ (p.p.m.)= 0.8 (Me-H, PMe_2Ph), 1.16 and 1.44 (doublets, ^{2}JPH= 10Hz., Me-H, **16**), 3.25 (cage C-H, **16**), 1.73 (doublet, ^{2}JP-H= 13.0Hz., Me-H), 7.10, 7.22, 7.51 and 7.72 (all multiplets, Ph-H).

"Other Carbapalladaborane"

N.m.r. ($CDCl_3$): $^{11}B\{^1H\}$ δ(p.p.m.)= -9.33 (2B), -14.45 (1B), -16.49 (2B), -20.00 (1B), -32.07 (1B), -33.64 (1B) and -34.33 (1B).

$^{31}P\{^1H\}$ (Bruker WP-200, 81.020MHz.) δ (p.p.m.)= -6.55, -8.85 (doublets, ^{2}JPP= 291.1Hz.).

$^{31}P\{^1H\}$ (Bruker WH-360, 145.836MHz.) δ (p.p.m.)= -10.32 and -11.33 (doublets, ^{2}JPP= 295.0Hz.).

^{1}H δ (p.p.m.)= 1.77 (doublet of doublets, ^{2}JP-H= 12.3Hz., ^{4}JP-H= 3.9Hz., 6H, Me-H), 2.74 (broad, cage C-H, 1H), 7.12, 7.17, 7.23, 7.60 (all multiplets, Ph-H) and 7.76, 7.71 (both doublets of doublets, Ph-H, J= 12.1Hz., 1.6Hz.; 12.1Hz., 2.2Hz.)(Total relative integral for Ph protons= 10H).

This reaction was repeated on a number of occasions giving products with spectra made up of differing combinations of the above resonances.

5.27 Thermolysis of Purple Complex.

A sample of the purple species described in the previous section (0.12g) was warmed in toluene (15cm^3) at reflux temperature for 30 minutes. There was some evidence for decomposition (formation of a black precipitate) and the solution

became pale yellow. The precipitate was removed by filtration, the filtrate collected and the solvent removed *in vacuo* This yielded a small amount of a yellow residue.

N.m.r. ($CDCl_3$): $^{11}B\{^1H\}$ δ (p.p.m.)= -9.41, -14.59, -16.52, -20.15, -32.23, -33.74 and -34.45.

$^{31}P\{^1H\}$ δ (p.p.m.)= 34.15, 5.85, -6.55 and -8.85 (doublets, $^2JP\text{-}P$= 292.4Hz.). The spectrum of a sample of the product of a similar reaction also contained an additional resonance at +6.86p.p.m.

^1H δ (p.p.m.)= 1.73 (doublet, $^2JP\text{-}H$= 13Hz., Me-H), 7.15, 7.52, 7.58 and 7.74 (multiplets, Ph-H).

5.28
$1,11\text{-}Ph_2\text{-}3,3\text{-}(PMe_2Ph)_2\text{-}3,1,2\text{-}PdC_2B_9H_9$, 17.

$Tl_2C_2B_9Ph_2$ (0.50g, 0.73mmol.) and *cis*-$PdCl_2(PMe_2Ph)_2$ (0.24g, 0.57mmol.) were allowed to warm together in CH_2Cl_2 ($15cm^3$) and stirred for 2 hours. The resulting orange soluble product was separated and purified by column chromatography (fluorosil, CH_2Cl_2). A mobile orange band was collected and further purified by t.l.c. (silica plates, pre-washed, 3:2 CH_2Cl_2/n-hexane eluent). This yielded a major yellow band (at R_f= 0.9) and at least 4 weak bands which were not collected. The major band was removed using CH_2Cl_2 and afforded a yellow solid on removal of solvent *in vacuo* (0.22g, 61%).

I.r. (CH_2Cl_2): ν= 2550cm^{-1} (B-H).

N.m.r. ($CDCl_3$): $^{11}B\{^1H\}$ δ (p.p.m.)= -1.89 (1B), -3.80 (1B), -5.85 (1B), -9.76 (1B), -13.25 (1B), -15.13 (1B), -22.30 (2B) and -25.70 (1B).

$^{31}P\{^1H\}$ δ (p.p.m.)= -8.31 and -11.61 ($^2JP\text{-}P$= 52.7Hz.).

^1H δ (p.p.m.)= 1.32 (multiplet, Me-H), 7.03 (doublet (8.2Hz.) of doublets (1.2Hz.), Ph-H), 7.16, 7.29 and 7.48 (multiplets, Ph-H) and 7.83 (weak multiplet, Ph-H).

5.29 1-Ph-3-(1,5-COD)-3,1,2-$PdC_2B_9H_{10}$, 18.

$Tl_2C_2B_9H_{10}Ph$ (0.5g, 0.83mmol.) and $PdCl_2$(1,5-COD) (0.18g, 0.63mmol.) were stirred in CH_2Cl_2 (15cm^3) for 2 hours. During this time the solution turned brown/red and TlCl was precipitated. The solution was passed down a column (fluorosil, pre-washed, CH_2Cl_2 eluent) and a mobile, dark red band collected. This yielded a dark red residue on removal of solvent *in vacuo* (0.18g, 68%).

Microanalysis: Calculated for $C_{16}H_{27}B_9Pd$, m.wt= 422.8, 45.4%C 6.39%H. Found 43.6%C 6.96%H.

The crude product was purified by t.l.c. (silica plates, 1:1 CH_2Cl_2/n-hexane). The 6 mobile bands were collected, but an immobile brown band was not. The bands recovered were A - purple, R_f= 0.5, major band; B - dark red, R_f 0.6; C red/green, R_f 0.65; D - purple, R_f 0.7; E - yellow, R_f 0.74 and F - yellow, R_f= 0.83.

I.r. (CH_2Cl_2): Band A ν= 2515cm^{-1} (B-H). Band B ν= 2860cm^{-1} (C-H), 2530cm^{-1} (B-H). Band C ν= 2900 and 2840cm^{-1} (C-H) and 2530cm^{-1} (B-H). Band D ν= 2910cm^{-1} (C-H) and 2520cm^{-1} (B-H). Band E ν= 2560cm^{-1} (B-H). Band F ν= 2920cm^{-1} (C-H) and 2570cm^{-1} (B-H).

N.m.r. ($CDCl_3$): Band A $^{11}B\{^1H\}$ δ(p.p.m.)= 20.06 (1B), 0.42 (1B), -2.41 (1B), -4.51 (1B), -7.67 (3B), -13.14 (1B) and -16.66 (1B).

^1H δ(p.p.m.)= 2.09, 2.30 and 2.54 (all multiplets, total 8H, CH_2), 4.93 and 5.81 (multiplets, total 4H, CH), 4.73 (broad, cage C-H), 7.32 (multiplet, 3H, Ph-H) and

7.58 (doublet (7.8Hz.) of doublets (1.4Hz.), 2H, Ph-H).

Band B $^{11}B\{^1H\}$ δ (p.p.m.)= 20.25, 8.10, -0.02, -1.35, -4.56, -6.83, -12.35 and -16.15, evidence of decomposition during spectral accumulation.

^1H δ(p.p.m.)= 7.6, 7.3 (multiplets, Ph-H), 5.75 (multiplet, COD-CH), 2.55, 2.30 and 2.13 (multiplets, CH_2).

Band C $^{11}B\{^1H\}$ δ (p.p.m.)= 20.40, 17.45, 6.73, 0.39, -2.41, -5.00, -6.77, -10.25 and -14.97.

^1H (p.p.m.)= 7.59 and 7.36 (multiplets, Ph-H), 5.75, 5.6 and (broad, CH), 2.50 (multiplet, CH_2) and 2.25 (broad, CH_2), 4.92 (broad, cage C-H).

Band D $^{11}B\{^1H\}$ δ (p.p.m.)= 20.35 (1B), 10.20 (1B), 0.11 (1B), -2.40 (1B), -7.16 (1B), -8.31 (2B), -12.40 (1B) and -17.00 (1B).

^1H (very weak solution) δ(p.p.m.)= 7.6, 5.7 and 2.52 (multiplets).

Band E $^{11}B\{^1H\}$ δ (p.p.m.)= 20.18 (1B), 8.69 (1B), 0.06 (3B), -8.36 (3B) and -16.93 (1B).

Band F $^{11}B\{^1H\}$δ(p.p.m.)= 26.20 (1B), 15.67 (1B), 2.85 (1B), 1.64 (1B), -1.31 (1B), -3.64 (1B), -8.21 (2B), -10.21 (2B) and -12.07 (1B).

^1H δ(p.p.m.)= 7.70 and 7.36 (multiplets, Ph-H) and 3.12 (broad, cage C-H).

5.30 Thermolysis of 18.

18 (band A, 0.08g, 0.19mmol.) was suspended in degassed toluene and stirred for 1 hour at +55°C (328K). There was no apparent reaction so the mixture was stirred at reflux temperature for a further 1 hour, during which time there was some

decomposition but no colour change. The solvent was removed *in vacuo* and the spectra of the residue were recorded.

N.m.r. ($CDCl_3$): $^{11}B\{^1H\}$ δ(p.p.m.)= 20.03 (1B), 0.38 (1B), -2.40 (1B), -4.54 (1B), -7.76 (2B) and (-10.26, -12.15, -13.18 and -16.65) (total 3B).

^1H δ(p.p.m.)= 2.10, 2.30 and 2.53 (broad multiplets, $C\underline{H}_2$), 4.74 (cage C-$\underline{H}$), 4.93 and 5.82 (multiplets, COD-C-$\underline{H}$), 7.33 (multiplet, Ph-$\underline{H}$) and 7.57 (doublet (6.4Hz.) of doublets (2.0Hz.), Ph-$\underline{H}$).

5.31
1,2-Ph_2-3-(1,5-COD)-3,1,2-$PdC_2B_9H_9Ph_2$, 19.

$Tl_2C_2B_9H_9Ph_2$ (0.5g, 0.73mmol.) and $PdCl_2$(1,5-COD) (0.15g, 0.53mmol.) were stirred in CH_2Cl_2 (15cm^3) for 2 hours. During this time the solution became brown and TlCl was precipitated. The solution was passed down a column (fluorosil, pre-washed, CH_2Cl_2 eluent) and the mobile, dark red band collected. This yielded a dark red residue on removal of solvent *in vacuo* (0.15g, 57%).

Microanalysis: Calculated for $C_{21}H_{31}B_9Pd$, m.wt. 498.5, 53.0%C 6.21%H. Found 51.9%C 6.79%H.

The crude product was purified by t.l.c. (silica plates, pre-washed, 60:40 CH_2Cl_2/n-hexane. There were 6 mobile bands, which were all collected and an immobile brown band which was not. The bands were 1 (dark red, R_f= 0.51), 2 (orange, R_f= 0.56), 3 (yellow, R_f= 0.66), 4 (red, R_f= 0.70), 5 (orange, R_f= 0.78) and 6 (yellow, R_f= 0.89).

I.r. (CH_2Cl_2): Band 1 ν= 2900cm^{-1} (C-H) and 2515cm^{-1} (B-H). Band 2 ν= 3020 and 2960cm^{-1} (C-H) and 2515cm^{-1} (B-H). Band 3 ν= 2900cm^{-1} (C-H) and 2565cm^{-1} (B-H). Band 4 ν= 2900 and 2850cm^{-1} (C-H) and 2560cm^{-1} (B-H). Band 5 ν=

2900cm^{-1} (C-H) and 2540cm^{-1} (B-H). Band 5 ν= 2910 and 2855cm^{-1} (C-H) and 2570cm^{-1} (B-H).

N.m.r. ($CDCl_3$): Band 1 $^{11}B\{^1H\}$ δ(p.p.m.)= 25.21 (1B), 2.85 (2B), 0.85 (2B), -4.86 (3B) and -9.50 (1B).

^1H δ(p.p.m.)= 2.52 (broad, second order, 8H, C$\underline{H}_2$), 5.58 (broad, second order, 4H, C$\underline{H}$), 7.16 (multiplet, 6H, Ph-$\underline{H}$) and 7.57 (doublet (8.1Hz.) of doublets (1.1Hz.), 4H, Ph-$\underline{H}$).

Band 2 $^{11}B\{^1H\}$ δ(p.p.m.)= 14.98 (1B), 1.48 (1B), -2.79 (2B), -6.25 (1B), -11.31 (2B), -17.25 (1B) and -19.57 (1B).

^1H δ(p.p.m.)= 2.55 (broad multiplet, C$\underline{H}_2$), 5.58 (broad multiplet, C-$\underline{H}$), 7.16 (multiplet, 6H, Ph-$\underline{H}$) and 7.41 (doublet (6.5Hz.) of doublets (1.0Hz.), 4H, Ph-$\underline{H}$).

Band 3 $^{11}B\{^1H\}$ δ (p.p.m.)= 7.26, 3.52, -4.22 (2B), -5.88 (1B), -12.11 (2B), -13.12, -13.31 (1B) and -14.99 (3B).

^1H δ(p.p.m.)= 7.38 and 7.15 (multiplets, Ph-$\underline{H}$).

Band 4 $^{11}B\{^1H\}$ δ (p.p.m.)= 25.76 (1B), 3.53 (1B), 0.75 (1B), -5.14 (2B), -13.33 (1B), -14.67 (1B), -19.32 (1B) and -27.23 (1B).

^1H δ(p.p.m.)= 2.52 (multiplet, 8H, C$\underline{H}_2$), 5.52 (multiplet, 4H, C-$\underline{H}$) and 7.17 and 7.55 (multiplets, 4H, 6H, respectively, Ph-$\underline{H}$).

Band 5 $^{11}B\{^1H\}$ δ (p.p.m.)= 15.46, -1.86, -6.39, -14.73 and 19.58.

^1H δ(p.p.m.)= 2.55 (broad, C$\underline{H}_2$), 5.56 (broad, C$\underline{H}$) and 7.20 and 7.40 (multiplets, Ph-$\underline{H}$).

Band 6 $^{11}B\{^1H)\}$ δ (p.p.m.)= -1.76 (2B), -8.43 (4B) and -9.73 (4B)

($C_2B_{10}H_{10}Ph_2$).

^1H δ (p.p.m.)= 7.19 and 7.41 (multiplets, Ph-H).

5.32 Thermolysis of 19.

19 (0.08g, 0.16mmol.) was suspended in degassed toluene and stirred at +55°C (328K) for 1 hour. There was no apparent reaction so the temperature was raised to 110°C (383K) and the mixture stirred for a further 30 minutes. During this time the solution turned yellow and there was some evidence of decomposition (precipitation of some black material). The solution was filtered and the solvent removed from the filtrate to yield a yellow residue.

N.m.r. ($CDCl_3$): $^{11}B\{^1H\}$ δ (p.p.m.)= +1.07 (1B), -5.86 (4B) and -14.98 (5B).

^1H δ= 2.07, 2.34 and 2.63 (multiplets, 4H, 2H, 2H, all CH_2), 5.01 and 5.72 (multiplets, 2H, 2H, CH), 7.21 (multiplet, 6H, Ph-H) and 7.40 (doublet (8.2Hz.) of doublets (1.4Hz.), 4H, Ph-H).

5.33 1-Ph-3-(1,5-COD)-3,1,2-$PtC_2B_9H_{10}$, 20.

$Tl_2C_2B_9H_{10}Ph$ (0.50g, 0.81mmol.) and $PtCl_2$(1,5-COD) (0.23g, 0.61mmol.) were mixed in CH_2Cl_2 (15cm^3), at -196°C (77K) and stirred at room temperature for 2 hours. The resulting red solution was concentrated and purified by preparative t.l.c. (silica plates, pre-washed, 2:1 CH_2Cl_2/n-hexane). There were several bands but only two of sufficient intensity to merit collection- a rust coloured band at R_f= 0.95 and a yellow band at R_f= 0.85. These were removed using CH_2Cl_2 and afforded solids on removal of solvent *in vacuo* (yield of yellow band= 0.13g, 42%).

N.m.r. ($CDCl_3$): $^{11}B\{^1H\}$ Rust coloured band δ (p.p.m.)= 12.90 (1B), -1.30 (2B),

-2.79 (2B), -5.21 (1B), -7.98 (1B) and -12.18 (2B). Also lower intensity signals at 23.31 and 10.15.

Yellow band δ (p.p.m.)= +10.26 (1B, $^1J^{195}$Pt-B= 300Hz.), -1.62 (1B), -5.32 (1B), -7.94 (2B), -10.60 (1B), -12.42 (1B), -14.07 (1B) and -16.44 (1B).

^{1}H Rust coloured band δ (p.p.m.)= 7.17 and 7.40 (multiplets, Ph-H) and some structure on baseline at approx. 2.1, 2.4, 4.5 and 5.3.

Yellow band δ (p.p.m.)= 2.11 and 2.53 (multiplets, 8H, CH_2), 4.58 and 5.42 (multiplets, 4H, COD-CH) and 7.23 and 7.34 (multiplets, 5H, Ph-H).

5.34 Thermolysis of 20.

A sample of **20** (0.1g, 0.2mmol) was suspended in toluene and stirred at reflux temperature for 30 minutes. There was no apparent reaction, but the solvent was removed *in vacuo* and the n.m.r. data of the residue recorded.

N.m.r.($CDCl_3$): ^{11}B{^{1}H} δ(p.p.m.)= 10.33, -1.60, -5.29, -7.93, -10.38, -12.48, -13.77 and -17.54. Also additional resonances (not seen for **20**) at -3.56, -6.37, -15.20 and -19.62.

^{1}H δ(p.p.m.)= 2.73 and 3.27 (multiplets, CH_2), 4.59 and 5.40 (multiplets,COD-CH) and 7.18 and 7.35 (multiplets, Ph-H).

5.35 1,11-Ph_2-3-(1,5-COD)-$PtC_2B_9H_9$, 21.

$Tl_2C_2B_9H_9PH_2$ (0.50g, 0.73mmol.) and $PtCl_2$(1,5-COD) (0.21g, 0.56mmol.) were allowed to warm together, in CH_2Cl_2 (15cm^3), and stirred for 2 hours. The resulting orange solution was chromatographed (alumina/CH_2Cl_2) and a mobile orange band collected. This yielded an orange solid, **21**, on removal of solvent *in vacuo* (0.19g,

58%).

N.m.r. ($CDCl_3$): $^{11}B\{^1H\}$ δ (p.p.m.)= -1.72, -4.11, -6.88, -8.39, -9.62, -13.15, -15.23, -16.94 and -17.80 (each 1B).

^1H δ (p.p.m.)= 2.21 and 2.60 (broad multiplets, $C\underline{H}_2$), 5.02, 5.16 and 5.26 (multiplets, C<u>H</u>), 7.24 and 7.50 (multiplets, Ph-<u>H</u>) and 7.38 (doublet (8.1Hz.) of doublets (1.4Hz.), Ph-<u>H</u>).

Section B Crystal Structure Determinations.

This section describes the procedures employed in the collection of data and subsequent structure solution and refinement, for the crystallographic determinations discussed in this thesis. In addition, supplementary crystallographic data are tabulated.

All data were collected, at ambient temperature, on an Enraf-Nonius CAD4 diffractometer, using graphite monochromated Mo-K_α X-radiation, with λ= 0.71069Å.

Unit cell parameters and orientation matrices for data collection were established by least-squares refinements of setting angles of 25 strong, high angle reflections. No decay or movement was noted during data collection for any of the compounds studied. Only data for which $F>2.0\sigma(F)$ were retained for structure solution and refinement. Data were corrected for Lorentz and polarisation effects (CADABS[133]).

Metal atoms were located by inspection of a Patterson map (SHELX76[67]). All other non-hydrogen atoms were found by ΔF syntheses and iterative least-squares refinement on F. The positions of the cage-carbon atoms were established by a combination of refined (as B) thermal parameters and interatomic distances. The cage H atoms were refined from positions located on the ΔF map, whereas other H atoms were set in idealised positions, depending on their bound carbon atom.

Scattering factors for C, H, B and P atoms were inlaid in the programs, while those for Pt and Pd atoms were taken from *International Tables for X-Ray Crystallography*[134]. After isotropic convergence, data were corrected empirically for absorption (DIFABS[68]) and thereafter, all non-H atoms were allowed anisotropic thermal motion. Before the end of the refinement process, data were weighted,

according to $w^{-1}= [\sigma^2(F)= g(F)^2]$ (where g is a variable) and refined to convergence by full-matrix least-squares.

Geometrical calculations were carried out using CALC[135] and figures were produced using SHELXTL[136].

The isotropic thermal parameter takes the form $\exp[-8\pi^2U(\sin^2\Theta/\lambda^2]$.

For anisotropic thermal parameters $U_{ij}= \exp[-2\pi(U11a^{*2}h^2+ U22b^{*22}k^2+ U33c^{*2}l^2+ 2U23b^*c^*kl+ 2U13a^*c^*hl+ 2U12a^*b^*hk)]$.

The equivalent isotropic thermal parameter is defined as $U_{eq}= \{\Sigma_i\Sigma_jU_{ij}a_i^*a_j^*a_j\}/3$

1-Ph-3,3-$(PMe_2Ph)_2$-3,1,2-$PtC_2B_9H_{10}$, (1).

Crystal data.

$C_{24}H_{37}B_9P_2Pt$, M= 689.89, monoclinic, space group $P2_1/c$, a=10.381(3), b=25.706(4), c= 10.880(7)Å, β= 104.57(4)°, V= 2810.0Å^3 from the least squares refinement of 25 centred reflections ($12<\theta<14$), Z=4, D_{calc}= 1.607gcm^{-1}, $\mu_{MoK\alpha}$= 51.71cm^{-1}, F(000)= 1336.

Data collection and processing.

ω-2θ scans in 96 steps, with ω scan width 0.8 + 0.34tanθ. Variable scan speeds between 0.92 and 2.35°min^{-1}. 3901 independent reflections were measured of which 3310 (with $F>2\sigma(F)$, h: 0 to 11, k: 0 to 28 and l: ± 11, $1<\theta<23°$) were retained for structure solution.

Structure solution.

The Pt atom was located from a Patterson map. The cage-H atoms, along with all other non-H atoms were located from full-matrix least squares refinement/ΔF syntheses. The phenyl-H atoms were set in fixed positions with C-H= 1.08Å. The methyl groups were treated as rigid groups with the same C-H distance. All H atoms were assigned a common thermal parameter (U_H= 0.061(54)Å^2 at convergence). An empirical absorption correction was applied whereafter all non-H atoms were allowed anisotropic thermal motion. R= 0.0476, R_W= 0.0416, S= 1.035, g= 0.000063. Maximum and minimum residues in the final ΔF map were +0.94 and -1.50eÅ^{-3}.

Crystallographic numbering scheme.

C(n01-n06) refers to the phenyl carbon atoms in the ring bound to the cage atom Cn, with Cn01 bonded to Cn. The phenyl rings bound to the phosphorus atoms are labelled C(n11-n16) for Pn. The phosphino-methyl carbons are Cn17 and Cn18. H

atoms are labelled according to their bound carbon atom. The methyl protons bound to Cn are labelled Hn, Hn+1 and Hn+2.

Table 5.1 Fractional Coordinates of Non-H Atoms with Standard Deviations.

Atom	x	y	z	Ueq
Pt(3)	0.17930(4)	0.15165(1)	0.02634(3)	0.0274(2)
C(1)	-0.0493(10)	0.1358(3)	0.0764(9)	0.034(6)
C(2)	-0.0064(9)	0.1944(4)	0.0597(9)	0.036(6)
B(4)	-0.0129(11)	0.1036(5)	-0.0480(10)	0.033(7)
B(5)	-0.1813(13)	0.1171(4)	-0.0392(12)	0.041(7)
B(6)	-0.1777(11)	0.1771(5)	0.0364(13)	0.040(7)
B(7)	0.0352(12)	0.2114(5)	-0.0814(11)	0.037(7)
B(8)	0.0273(11)	0.1498(5)	-0.1606(10)	0.036(7)
B(9)	-0.1356(12)	0.1262(6)	-0.1824(12)	0.043(8)
B(10	-0.2361(12)	0.1739(5)	-0.1271(12)	0.044(8)
B(11)	-0.1212(12)	0.2233(5)	-0.0576(12)	0.041(8)
B(12)	-0.1067(12)	0.1937(5)	-0.1985(12)	0.045(8)
C(101)	-0.0199(9)	0.1116(4)	0.2070(9)	0.033(6)
C(102)	-0.0314(10)	0.1427(4)	0.3122(10)	0.048(8)
C(103)	-0.0006(12)	0.1206(6)	0.4329(11)	0.066(9)
C(104)	0.0421(12)	0.0710(6)	0.4513(12)	0.067(10)
C(105)	0.0534(12)	0.0409(5)	0.3532(12)	0.058(8)
C(106)	0.0226(9)	0.0618(4)	0.2306(10)	0.045(7)
P(1)	0.33893(25)	0.20045(10)	0.16053(25)	0.0334(16)
C(111)	0.4190(9)	0.1733(4)	0.3159(9)	0.036(6)
C(112)	0.3408(11)	0.1449(5)	0.3773(10)	0.058(8)
C(113)	0.3919(12)	0.1259(5)	0.4983(11)	0.064(9)
C(114)	0.5241(14)	0.1346(4)	0.5573(11)	0.060(8)
C(115)	0.6022(11)	0.1610(5)	0.4974(11)	0.057(8)
C(116)	0.5494(10)	0.1815(4)	0.3772(10)	0.051(7)
C(121)	0.2735(10)	0.2624(4)	0.2015(10)	0.047(7)
C(131)	0.4749(10)	0.2230(4)	0.0960(11)	0.050(8)
P(2)	0.3195(3)	0.08800(10)	0.00181(24)	0.0373(16)
C(211)	0.4378(10)	0.0612(4)	0.1411(10)	0.038(6)
C(212)	0.3880(12)	0.0254(5)	0.2132(12)	0.064(9)
C(213)	0.4737(16)	0.0042(5)	0.3211(13)	0.081(11)
C(214)	0.6077(17)	0.0214(6)	0.3573(13)	0.085(12)
C(215)	0.6526(12)	0.0563(5)	0.2860(12)	0.065(9)
C(316)	0.5682(11)	0.0758(4)	0.1774(11)	0.055(8)
C(221)	0.4179(11)	0.1060(5)	-0.1067(10)	0.058(8)
C(231)	0.2401(11)	0.0295(4)	-0.0765(12)	0.060(8)

Table 5.2 Fractional Coordinates of Hydrogen Atoms.

Atom	x	y	z
H(2)	0.024(9)	0.218(4)	0.150(8)
H(4)	0.008(10)	0.063(3)	-0.042(9)
H(5)	-0.250(9)	0.085(3)	-0.032(9)
H(6)	-0.207(10)	0.187(4)	0.112(8)
H(7)	0.086(9)	0.250(3)	-0.085(9)
H(8)	0.084(9)	0.133(4)	-0.227(8)
H(9)	-0.162(10)	0.100(3)	-0.252(8)
H(10)	-0.349(8)	0.190(4)	-0.177(8)
H(11)	-0.156(9)	0.263(3)	-0.038(9)
H(12)	-0.108(10)	0.208(4)	-0.284(7)
H(102)	-0.0636	0.1827	0.2984
H(103)	-0.0110	0.1435	0.5130
H(104)	0.0678	0.0552	0.5462
H(105)	0.0860	0.0010	0.3692
H(106)	0.0329	0.0376	0.1525
H(112)	0.2380	0.1374	0.3297
H(113)	0.3292	0.1046	0.5463
H(114)	0.5652	0.1201	0.6523
H(115)	0.7065	0.1662	0.5430
H(116)	0.6120	0.2042	0.3319
H(121)	0.3509	0.2858	0.2611
H(123)	0.2002	0.2527	0.2528
H(122)	0.2265	0.2840	0.1169
H(133)	0.5395	0.1914	0.0847
H(131)	0.5342	0.2550	0.1440
H(132)	0.4177	0.2357	0.0037
H(216)	0.2844	0.0142	0.1861
H(215)	0.4386	-0.0249	0.3764
H(214)	0.6741	0.0063	0.4427
H(213)	0.7549	0.0691	0.3140
H(212)	0.6059	0.1031	0.1197
H(222)	0.4777	0.1339	-0.0428
H(223)	0.3602	0.1259	-0.1899
H(221)	0.4820	0.0777	-0.1347
H(231)	0.2995	0.0012	-0.1110
H(232)	0.1716	0.0477	-0.1561
H(233)	0.1850	0.0103	-0.0176

Table 5.3 Anisotropic Thermal Parameters for Non-H Atoms, Å^2.

Atom	U11	U22	U33	U23	U13	U12
Pt(3)	0.0271(2)	0.0265(2)	0.0266(2)	-0.0006(2)	0.0066(1)	0.0020(2)
C(1)	0.033(6)	0.030(6)	0.037(6)	0.002(4)	0.005(5)	-0.002(4)
C(2)	0.035(6)	0.035(6)	0.038(6)	0.005(5)	0.016(5)	0.007(5)
B(4)	0.023(6)	0.042(8)	0.031(7)	-0.012(6)	0.002(5)	0.002(5)
B(5)	0.038(7)	0.032(7)	0.051(8)	-0.001(7)	0.014(6)	-0.021(6)
B(6)	0.025(6)	0.040(7)	0.053(8)	0.009(6)	0.015(6)	0.008(5)
B(7)	0.032(7)	0.041(8)	0.034(7)	0.009(6)	0.006(5)	0.001(6)
B(8)	0.034(6)	0.043(7)	0.028(6)	-0.012(6)	0.005(5)	-0.001(6)
B(9)	0.024(7)	0.062(9)	0.036(7)	-0.013(6)	-0.007(6)	0.004(6)
B(10)	0.035(7)	0.048(8)	0.044(7)	-0.004(6)	-0.004(6)	-0.004(6)
B(11)	0.036(7)	0.039(8)	0.042(7)	0.002(6)	0.002(6)	-0.001(6)
B(12)	0.039(7)	0.054(9)	0.040(8)	0.020(6)	0.009(6)	0.003(6)
C(101)	0.039(6)	0.026(6)	0.032(6)	-0.005(4)	0.010(5)	-0.017(5)
C(102)	0.048(7)	0.041(8)	0.053(7)	0.001(6)	0.012(6)	-0.006(5)
C(103)	0.071(9)	0.083(10)	0.041(7)	-0.004(7)	0.019(7)	-0.013(8)
C(104)	0.058(8)	0.090(11)	0.049(8)	0.038(8)	0.013(7)	-0.012(8)
C(105)	0.064(8)	0.050(8)	0.055(8)	0.020(7)	0.014(7)	-0.012(6)
C(106)	0.032(6)	0.045(7)	0.055(7)	0.008(6)	0.014(5)	-0.004(5)
P(1)	0.030(1)	0.031(2)	0.037(2)	-0.003(1)	0.008(1)	-0.001(1)
C(111)	0.035(6)	0.029(6)	0.038(6)	-0.007(5)	0.000(5)	-0.003(5)
C(112)	0.043(6)	0.078(10)	0.044(7)	0.008(6)	-0.008(5)	-0.024(7)
C(113)	0.066(8)	0.064(8)	0.051(8)	0.024(6)	-0.007(7)	-0.016(7)
C(114)	0.090(10)	0.040(7)	0.037(7)	-0.002(5)	-0.016(7)	0.000(7)
C(115)	0.041(7)	0.065(9)	0.054(7)	-0.008(7)	-0.017(6)	0.004(7)
C(116)	0.042(7)	0.051(7)	0.054(7)	-0.012(6)	0.005(6)	-0.008(6)
C(121)	0.049(7)	0.032(7)	0.056(7)	-0.017(5)	0.007(6)	0.003(5)
C(131)	0.038(7)	0.043(7)	0.067(8)	-0.003(6)	0.021(6)	-0.003(5)
P(2)	0.037(1)	0.034(2)	0.039(2)	-0.003(1)	0.014(1)	0.007(1)
C(211)	0.034(6)	0.033(6)	0.046(6)	-0.003(5)	0.016(5)	0.007(5)
C(212)	0.053(8)	0.064(9)	0.070(9)	0.013(7)	0.012(7)	0.003(7)
C(213)	0.097(12)	0.072(10)	0.072(10)	0.034(8)	0.040(9)	0.028(9)
C(214)	0.107(13)	0.094(12)	0.047(8)	0.000(8)	0.014(9)	0.051(10)
C(215)	0.051(8)	0.078(10)	0.056(8)	-0.006(7)	-0.007(7)	0.019(7)
C(216)	0.047(7)	0.049(8)	0.067(8)	-0.020(6)	0.017(6)	0.001(6)
C(221)	0.056(8)	0.077(10)	0.040(7)	-0.003(6)	0.018(6)	0.010(7)
C(231)	0.055(8)	0.034(7)	0.083(9)	-0.029(6)	0.009(7)	0.004(6)

1,11-Ph_2-3,3-$(PMe_2Ph)_2$-3,1,11-$PtC_2B_9H_9$, 4.

Crystal data.

$C_{30}H_{41}B_9P_2Pt$, M= 755.99, triclinic, space group Pbar1, a= 11.060(4), b= 12.997(4), c= 13.293(3), α= 79.703(24)°, β= 80.314(24)°, γ= 65.14(3)°, V=1695.5Å^3 by a least squares refinement of 25 centred reflections ($14<\theta<17°$), Z= 2, D_{calc}= 1.480gcm^{-1}, $\mu_{MoK\alpha}$= 42.90cm^{-1}, F(000)= 748.

Data collection and processing.

ω- 2θ scans in 96 steps, with ω scan width 0.8= 0.34tanθ. Variable scan speeds 0.92 to 2.35°min^{-1}. 5492 independent reflections of which 5482 retained (with $F>2\sigma F$, h: 0 to +13, k: ±15, l:±15, $1<\theta<25°$).

Structure solution.

Pt atom position from Patterson map. Cage-H atoms and all other non-H atoms from least-squares refinement/ΔF syntheses. Phenyl groups were refined as rigid planar rings with C-C= 1.395Å and C-H= 1.08Å. Methyl groups were refined as rigid groups with C-H= 1.08Å. An empirical absorption correction was applied after isotropic convergence and thereafter all non-H atoms were allowed anisotropic thermal motion. All H atoms were assigned a common equivalent thermal parameter (U_{eq}= 0.079(30)Å^2 , at convergence). R= 0.0298, R_w= 0.0353, S= 1.025, g= 0.000459. Max. and min. residues in final ΔF map= +0.81 and -0.76eÅ^{-3}.

Crystallographic numbering scheme.

As for **1**.

Table 5.4 Fractional Coordinates of Non-H Atoms with Standard Deviations.

Atom	x	y	z	Ueq
Pt(3)	-0.36575(2)	-0.14206(1)	-0.19978(1)	0.0333(1)
P(2)	-0.22556(13)	-0.05912(11)	-0.28504(10)	0.0469(8)
P(1)	-0.20080(12)	-0.31001(11)	-0.13976(10)	0.0427(7)
C(1)	-0.5439(4)	-0.1714(3)	-0.2841(3)	0.036(3)
B(2)	-0.5165(5)	-0.2180(4)	-0.1587(6)	0.033(3)
B(4)	-0.5372(5)	-0.0411(4)	-0.3009(4)	0.039(3)
B(5)	-0.6902(5)	-0.0600(5)	-0.3030(4)	0.043(3)
B(6)	-0.6769(5)	-0.1762(4)	-0.2096(4)	0.038(3)
B(7)	-0.5385(5)	-0.1030(4)	-0.0816(4)	0.039(3)
B(8)	-0.5508(6)	0.0162(4)	-0.1780(4)	0.042(3)
B(9)	-0.6945(6)	0.0522(4)	-0.2408(5)	0.044(3)
B(10)	-0.7790(5)	-0.0367(4)	-0.1818(4)	0.042(3)
C(11)	-0.6714(4)	-0.1353(4)	-0.0956(3)	0.036(3)
B(12)	-0.6977(5)	0.0076(4)	-0.1070(5)	0.043(3)
C(106)	-0.4358(4)	-0.21859(22)	-0.46199(23)	0.055(4)
C(105)	-0.3794(4)	-0.29484(22)	-0.53545(23)	0.078(5)
C(104)	-0.3684(4)	-0.40711(22)	-0.51033(23)	0.082(5)
C(103)	-0.4138(4)	-0.44314(22)	-0.41173(23)	0.078(5)
C(102)	-0.4702(4)	-0.36689(22)	-0.33827(23)	0.056(4)
C(101)	-0.4812(4)	-0.25462(22)	-0.36340(23)	0.040(3)
C(202)	-0.64031(22)	-0.2678(3)	0.07047(24)	0.050(3)
C(203)	-0.69027(22)	-0.3183(3)	0.15961(24)	0.060(4)
C(204)	-0.82725(22)	-0.2925(3)	0.17864(24)	0.060(4)
C(205)	-0.91426(22)	-0.2163(3)	0.10853(24)	0.061(4)
C(206)	-0.86430(22)	-0.1658(3)	0.01939(24)	0.050(3)
C(201)	-0.72732(22)	-0.1916(3)	0.00036(24)	0.039(3)
C(212)	0.0465(4)	-0.1637(4)	-0.3637(3)	0.071(4)
C(213)	0.1482(4)	-0.2293(4)	-0.4322(3)	0.088(6)
C(214)	0.1169(4)	-0.2747(4)	-0.5067(3)	0.109(7)
C(215)	-0.0161(4)	-0.2544(4)	-0.5128(3)	0.143(10)
C(216)	-0.1178(4)	-0.1889(4)	-0.4444(3)	0.096(6)
C(211)	-0.0865(4)	-0.1435(4)	-0.3698(3)	0.055(4)
C(221)	-0.1541(6)	-0.0118(5)	-0.1978(5)	0.071(5)
C(231)	-0.3020(7)	0.0735(5)	-0.3689(5)	0.075(5)
C(112)	-0.2598(4)	-0.32197(24)	0.07143(25)	0.059(4)
C(113)	-0.2952(4)	-0.36853(24)	0.16889(25)	0.073(5)
C(114)	-0.3199(4)	-0.46698(24)	0.18014(25)	0.067(4)
C(115)	-0.3092(4)	-0.51887(24)	0.09393(25)	0.059(4)
C(116)	-0.2738(4)	-0.47231(24)	-0.00353(25)	0.053(3)
C(111)	-0.2491(4)	-0.37386(24)	-0.01478(25)	0.041(3)
C(121)	-0.1487(7)	-0.4197(5)	-0.2251(5)	0.071(4)
C(131)	-0.0407(6)	-0.3135(6)	-0.1172(6)	0.081(5)

Table 5.5 Fractional Co-ordinates of Hydrogen Atoms.

Atom	x	y	z
H(2)	-0.476(6)	-0.301(5)	-0.129(5)
H(4)	-0.494(6)	-0.008(5)	-0.377(5)
H(5)	-0.725(6)	-0.045(5)	-0.372(5)
H(6)	-0.712(6)	-0.238(5)	-0.211(5)
H(7)	-0.512(6)	-0.115(5)	0.004(5)
H(8)	-0.514(6)	0.082(5)	-0.180(5)
H(9)	-0.744(6)	0.140(5)	-0.270(5)
H(10)	-0.874(7)	0.001(5)	-0.169(5)
H(12)	-0.768(7)	0.054(5)	-0.045(5)
H(106)	-0.4442	-0.13167	-0.48144
H(105)	-0.3442	-0.26695	-0.61178
H(104)	-0.3247	-0.46614	-0.56720
H(103)	-0.4053	-0.53006	-0.39228
H(102)	-0.5053	-0.39478	-0.26194
H(202)	-0.53426	-0.2877	0.05574
H(203)	-0.62290	-0.3772	0.21389
H(204)	-0.86593	-0.3316	0.24765
H(205)	-1.02031	-0.1964	0.12326
H(206)	-0.93166	-0.1069	-0.03489
H(212)	0.0708	-0.1286	-0.3060
H(213)	0.2511	-0.2449	-0.4274
H(214)	0.1956	-0.3254	-0.5597
H(215)	-0.0404	-0.2895	-0.5706
H(216)	-0.2207	-0.1732	-0.4491
H(222)	-0.1042	-0.0828	-0.1423
H(223)	-0.2331	0.0552	-0.1583
H(221)	-0.0827	0.0203	-0.2411
H(231)	-0.2421	0.1228	-0.3778
H(232)	-0.4017	0.1223	-0.3352
H(233)	-0.3074	0.0540	-0.4432
H(112)	-0.2407	-0.24574	0.06273
H(113)	-0.3035	-0.32835	0.23564
H(114)	-0.3473	-0.50303	0.25559
H(115)	-0.3283	-0.59510	0.10263
H(116)	-0.2655	-0.51249	-0.07028
H(121)	-0.2361	-0.4261	-0.2445
H(122)	-0.0853	-0.5008	-0.1869
H(123)	-0.0938	-0.3972	-0.2944
H(133)	0.0018	-0.2775	-0.1861
H(131)	0.0271	-0.4008	-0.0968
H(132)	-0.0563	-0.2643	-0.0552

Table 5.6 Anisotropic Vibration Parameters of Non-H Atoms with Standard Deviations, Å^2.

Atom	U11	U22	U33	U23	U13	U12
Pt(3)	0.0307(1)	0.0307(1)	0.0308(1)	-0.0036(1)	-0.0038(1)	-0.0120(1)
P(2)	0.0437(7)	0.0470(7)	0.0421(7)	-0.0027(5)	-0.0051(6)	-0.0254(6)
P(1)	0.0313(6)	0.0396(6)	0.0433(7)	0.0006(5)	-0.0029(5)	-0.0075(5)
C(1)	0.040(2)	0.031(2)	0.030(2)	-0.005(2)	-0.006(2)	-0.016(2)
B(2)	0.031(2)	0.027(2)	0.034(3)	-0.006(2)	-0.004(2)	-0.012(2)
B(4)	0.038(3)	0.033(3)	0.036(3)	-0.003(2)	-0.010(2)	-0.013(2)
B(5)	0.039(3)	0.040(3)	0.042(3)	0.003(2)	-0.015(2)	-0.017(2)
B(6)	0.034(3)	0.034(3)	0.038(3)	-0.005(2)	-0.004(2)	-0.013(2)
B(7)	0.039(3)	0.036(3)	0.032(3)	-0.010(2)	-0.005(2)	-0.014(2)
B(8)	0.043(3)	0.029(2)	0.047(3)	-0.009(2)	-0.005(2)	-0.014(2)
B(9)	0.039(3)	0.030(3)	0.050(3)	0.000(2)	-0.009(2)	-0.009(2)
B(10)	0.035(3)	0.033(3)	0.047(3)	-0.003(2)	-0.010(2)	-0.007(2)
C(11)	0.031(2)	0.032(2)	0.036(2)	-0.006(2)	-0.004(2)	-0.009(2)
B(12)	0.038(3)	0.030(3)	0.047(3)	-0.014(2)	-0.002(2)	-0.005(2)
C(106)	0.065(3)	0.051(3)	0.036(3)	-0.007(2)	-0.006(2)	-0.025(3)
C(105)	0.107(5)	0.071(4)	0.035(3)	-0.018(3)	0.010(3)	-0.038(4)
C(104)	0.113(6)	0.064(4)	0.049(4)	-0.029(3)	0.007(4)	-0.034(4)
C(103)	0.111(6)	0.047(3)	0.056(4)	-0.017(3)	0.005(4)	-0.031(3)
C(102)	0.069(4)	0.041(3)	0.046(3)	-0.012(2)	0.006(3)	-0.025(3)
C(101)	0.042(2)	0.038(2)	0.030(2)	-0.005(2)	-0.009(2)	-0.017(2)
C(202)	0.044(3)	0.045(3)	0.047(3)	-0.001(2)	0.002(2)	-0.015(2)
C(203)	0.062(4)	0.055(3)	0.043(3)	0.002(2)	0.001(3)	-0.018(3)
C(204)	0.064(4)	0.049(3)	0.051(3)	-0.016(3)	0.015(3)	-0.026(3)
C(205)	0.051(3)	0.054(3)	0.066(4)	-0.024(3)	0.021(3)	-0.027(3)
C(206)	0.043(3)	0.045(3)	0.051(3)	-0.014(2)	0.007(2)	-0.019(2)
C(201)	0.037(2)	0.031(2)	0.037(2)	-0.010(2)	0.001(2)	-0.011(2)
C(212)	0.049(3)	0.085(4)	0.062(4)	-0.005(3)	0.003(3)	-0.032(3)
C(213)	0.061(4)	0.099(5)	0.075(5)	-0.003(4)	0.014(4)	-0.026(4)
C(214)	0.087(6)	0.110(7)	0.097(6)	-0.044(5)	0.033(5)	-0.028(5)
C(215)	0.114(7)	0.180(10)	0.110(7)	-0.099(7)	0.039(6)	-0.070(7)
C(216)	0.075(5)	0.129(7)	0.068(4)	-0.041(4)	0.004(4)	-0.051(5)
C(211)	0.049(3)	0.061(3)	0.045(3)	-0.007(2)	0.000(2)	-0.031(3)
C(221)	0.070(4)	0.073(4)	0.065(4)	-0.021(3)	-0.007(3)	-0.044(3)
C(231)	0.074(4)	0.059(4)	0.075(4)	0.023(3)	-0.018(3)	-0.034(3)
C(112)	0.070(4)	0.046(3)	0.048(3)	-0.007(2)	-0.009(3)	-0.026(3)
C(113)	0.085(4)	0.072(4)	0.045(3)	-0.011(3)	-0.006(3)	-0.035(4)
C(114)	0.061(4)	0.067(4)	0.051(3)	0.009(3)	-0.001(3)	-0.023(3)
C(115)	0.056(3)	0.041(3)	0.064(4)	0.008(3)	-0.009(3)	-0.018(2)
C(116)	0.048(3)	0.035(3)	0.062(3)	-0.002(2)	-0.013(3)	-0.012(2)
C(111)	0.033(2)	0.032(2)	0.045(3)	0.000(2)	-0.010(2)	-0.003(2)
C(121)	0.075(4)	0.049(3)	0.059(4)	-0.012(3)	0.007(3)	-0.004(3)
C(131)	0.038(3)	0.088(5)	0.093(5)	0.030(4)	-0.020(3)	-0.026(3)

1-Ph-3,3-$(PMe_2Ph)_2$-3,1,2-$PdC_2B_9H_{10}$, 16.

Crystal Data.

$C_{24}H_{37}B_9P_2Pd$, M= 591.20, monoclinic, space group $P2_1/c$, a= 10.339(3), b= 25.813(5), c= 10.879(1)Å, β= 104.161(22)°, V= 2815.2Å^3, from least-squares refinements of 25 centred reflections ($12<\theta<14°$), Z= 4, $D_{calc.}$= 1.395gcm^{-3}, $\mu_{MoK\alpha}$= 7.76cm^{-1}, F(000)= 1208.

Data Collection and Processing.

ω- 2θ scans in 96 steps with ω scan width 0.8 = 0.34tanθ. Variable scan speeds between 0.55 and 2.35°min.$^{-1}$. 5220 reflections measured in the range $1<\theta<22°$ (h 0-15, k 0-29, l ±18), of which 3882 retained for structure elucidation ($F>2\sigma(F)$).

Structure Elucidation.

Atomic co-ordinates from **1** were used as the starting point for refinement, with individual thermal parameters for all atoms (no H-atoms included). The 11 non-M cage atoms were refined as boron atoms. After 4 full-matrix least-squares refinement cycles R= 0.0854. From the refined thermal parameters and interatomic distances, the cage carbon atoms were unambiguously assigned to sites 1 and 2, confirming **16** as isostructural to **1**. Further refinement was not undertaken.

Crystallographic Numbering Scheme.

As for **1**.

Table 5.7 Selected Bond Lengths, Å, with Standard Deviations.

Pd(3)	- C(1)	2.530(11)	B(9)	-B(12)	1.803(20)
Pd(3)	- C(2)	2.308(12)	B(10)	-B(11)	1.812(20)
Pd(3)	- B(4)	2.282(13)	B(10)	-B(12)	1.779(20)
Pd(3)	- B(7)	2.269(13)	B(11)	-B(12)	1.778(20)
Pd(3)	- B(8)	2.276(14)	C(101)	-C(102)	1.408(18)
Pd(3)	- P(1)	2.318(3)	C(101)	-C(106)	1.419(17)
Pd(3)	- P(2)	2.272(3)	C(102)	-C(103)	1.424(20)
C(1)	- C(2)	1.574(16)	C(103)	-C(104)	1.396(22)
C(1)	- B(4)	1.717(17)	C(104)	-C(105)	1.342(22)
C(1)	- B(5)	1.699(18)	C(105)	-C(106)	1.418(20)
C(1)	- B(6)	1.694(18)	P(1)	-C(111)	1.802(12)
C(1)	-C(101)	1.490(16)	P(1)	-C(121)	1.812(13)
C(2)	- B(6)	1.773(18)	P(1)	-C(131)	1.825(13)
C(2)	- B(7)	1.757(17)	C(111)	-C(112)	1.380(18)
C(2)	-B(11)	1.765(18)	C(111)	-C(116)	1.414(17)
B(4)	- B(5)	1.837(19)	C(112)	-C(113)	1.421(22)
B(4)	- B(8)	1.822(20)	C(113)	-C(114)	1.443(23)
B(4)	- B(9)	1.780(20)	C(114)	-C(115)	1.368(21)
B(5)	- B(6)	1.731(20)	C(115)	-C(116)	1.390(20)
B(5)	- B(9)	1.809(20)	P(2)	-C(211)	1.804(13)
B(5)	-B(10)	1.775(20)	P(2)	-C(221)	1.820(14)
B(6)	-B(10)	1.762(20)	P(2)	-C(231)	1.861(17)
B(6)	-B(11)	1.835(20)	C(211)	-C(216)	1.411(20)
B(7)	- B(8)	1.788(19)	C(211)	-C(212)	1.399(18)
B(7)	-B(11)	1.744(19)	C(216)	-C(215)	1.43(3)
B(7)	-B(12)	1.785(19)	C(215)	-C(214)	1.41(3)
B(8)	- B(9)	1.768(20)	C(214)	-C(213)	1.378(24)
B(8)	-B(12)	1.782(20)	C(213)	-C(212)	1.417(21)
B(9)	-B(10)	1.799(21)			

Table 5.8 Selected Angles, °, with Standard Deviations.

C(1)	-Pd(3)	- C(2)	37.6(4)	B(5)	-B(10)	- B(6)	58.6(8)
C(1)	-Pd(3)	- B(4)	41.4(4)	B(5)	-B(10)	- B(9)	60.8(8)
C(2)	-Pd(3)	- B(7)	45.1(4)	B(6)	-B(10)	-B(11)	61.8(8)
B(4)	-Pd(3)	- B(8)	47.1(5)	B(9)	-B(10)	-B(12)	60.5(8)
B(7)	-Pd(3)	- B(8)	46.3(5)	B(11)	-B(10)	-B(12)	59.4(8)
P(1)	-Pd(3)	- P(2)	95.95(11)	C(2)	-B(11)	- B(6)	59.0(7)
Pd(3)	- C(1)	- C(2)	63.5(6)	C(2)	-B(11)	- B(7)	60.1(7)
Pd(3)	- C(1)	- B(4)	61.5(6)	B(6)	-B(11)	-B(10)	57.8(8)
Pd(3)	- C(1)	-C(101)	106.1(7)	B(7)	-B(11)	-B(12)	60.9(8)
C(2)	- C(1)	- B(6)	65.6(8)	B(10)	-B(11)	-B(12)	59.4(8)
C(2)	- C(1)	-C(101)	119.7(9)	B(7)	-B(12)	- B(8)	60.2(8)
B(4)	- C(1)	- B(5)	65.1(8)	B(7)	-B(12)	-B(11)	58.6(7)
B(4)	- C(1)	-C(101)	122.8(9)	B(8)	-B(12)	- B(9)	59.1(8)
B(5)	- C(1)	- B(6)	61.4(8)	B(9)	-B(12)	-B(10)	60.3(8)
B(5)	- C(1)	-C(101)	120.6(10)	B(10)	-B(12)	-B(11)	61.2(8)
B(6)	- C(1)	-C(101)	117.1(9)	C(1)	-C(101)	-C(102)	119.8(10)
Pd(3)	- C(2)	- C(1)	78.9(6)	C(1)	-C(101)	-C(106)	120.3(10)
Pd(3)	- C(2)	- B(7)	66.3(6)	C(102)	-C(101)	-C(106)	119.9(11)
C(1)	- C(2)	- B(6)	60.5(7)	C(101)	-C(102)	-C(103)	119.2(12)
B(6)	- C(2)	-B(11)	62.5(7)	C(102)	-C(103)	-C(104)	119.9(13)
B(7)	- C(2)	-B(11)	59.4(7)	C(103)	-C(104)	-C(105)	120.7(15)
Pd(3)	- B(4)	- C(1)	77.1(6)	C(104)	-C(105)	-C(106)	122.2(14)
Pd(3)	- B(4)	- B(8)	66.3(6)	C(101)	-C(106)	-C(105)	118.2(12)
C(1)	- B(4)	- B(5)	57.0(7)	Pd(3)	- P(1)	-C(111)	117.1(4)
B(5)	- B(4)	- B(9)	60.0(8)	Pd(3)	- P(1)	-C(121)	112.8(4)
B(8)	- B(4)	- B(9)	58.8(8)	Pd(3)	- P(1)	-C(131)	114.9(4)
C(1)	- B(5)	- B(4)	57.9(7)	C(111)	- P(1)	-C(121)	102.4(6)
C(1)	- B(5)	- B(6)	59.2(8)	C(111)	- P(1)	-C(131)	106.4(6)
B(4)	- B(5)	- B(9)	58.4(8)	C(121)	- P(1)	-C(131)	101.4(6)
B(6)	- B(5)	-B(10)	60.3(8)	P(1)	-C(111)	-C(112)	118.2(9)
B(9)	- B(5)	-B(10)	60.3(8)	P(1)	-C(111)	-C(116)	122.4(9)
C(1)	- B(6)	- C(2)	54.0(7)	C(112)	-C(111)	-C(116)	119.4(11)
C(1)	- B(6)	- B(5)	59.5(8)	C(111)	-C(112)	-C(113)	121.6(13)
C(2)	- B(6)	-B(11)	58.5(7)	C(112)	-C(113)	-C(114)	117.8(14)
B(5)	- B(6)	-B(10)	61.0(8)	C(113)	-C(114)	-C(115)	119.1(14)
B(10)	- B(6)	-B(11)	60.5(8)	C(114)	-C(115)	-C(116)	122.5(13)
Pd(3)	- B(7)	- C(2)	68.6(6)	C(111)	-C(116)	-C(115)	119.4(12)
Pd(3)	- B(7)	- B(8)	67.1(6)	Pd(3)	- P(2)	-C(211)	119.1(4)
C(2)	- B(7)	-B(11)	60.5(7)	Pd(3)	- P(2)	-C(221)	111.7(5)
B(8)	- B(7)	-B(12)	59.8(8)	Pd(3)	- P(2)	-C(231)	116.1(5)
B(11)	- B(7)	-B(12)	60.5(8)	C(211)	- P(2)	-C(221)	106.6(6)
Pd(3)	- B(8)	- B(4)	66.6(6)	C(211)	- P(2)	-C(231)	101.9(7)
Pd(3)	- B(8)	- B(7)	66.6(6)	C(221)	- P(2)	-C(231)	99.1(7)
B(4)	- B(8)	- B(9)	59.4(8)	P(2)	-C(211)	-C(216)	117.9(10)
B(7)	- B(8)	-B(12)	60.0(8)	P(2)	-C(211)	-C(212)	121.3(10)
B(9)	- B(8)	-B(12)	61.0(8)	C(216)	-C(211)	-C(212)	120.6(12)
B(4)	- B(9)	- B(5)	61.6(8)	C(211)	-C(216)	-C(215)	118.8(15)
B(4)	- B(9)	- B(8)	61.8(8)	C(216)	-C(215)	-C(214)	118.1(17)
B(5)	- B(9)	-B(10)	58.9(8)	C(215)	-C(214)	-C(213)	123.8(17)
B(8)	- B(9)	-B(12)	59.8(8)	C(214)	-C(213)	-C(212)	117.2(15)
B(10)	- B(9)	-B(12)	59.2(8)	C(211)	-C(212)	-C(213)	121.4(13)

Table 5.9 Fractional Coordinates of Non-H Atoms with Standard Deviations.

Atom	x	y	z	Ueq
Pd(3)	0.17872(8)	0.15094(3)	0.03220(8)	0.0247(2)
C(1)	-0.0459(11)	0.1362(4)	0.0799(11)	0.0211(23)
C(2)	-0.0065(11)	0.1941(4)	0.0625(11)	0.0249(24)
B(4)	-0.0113(13)	0.1045(5)	-0.0470(13)	0.033(3)
B(5)	-0.1820(14)	0.1175(5)	-0.0336(14)	0.037(3)
B(6)	-0.1770(13)	0.1774(5)	0.0391(13)	0.036(3)
B(7)	0.0361(12)	0.2107(5)	-0.0793(12)	0.029(3)
B(8)	0.0292(13)	0.1500(6)	-0.1601(13)	0.040(3)
B(9)	-0.1348(14)	0.1258(5)	-0.1820(14)	0.039(3)
B(10)	-0.2343(14)	0.1735(6)	-0.1271(14)	0.041(3)
B(11)	-0.1223(13)	0.2259(5)	-0.0605(13)	0.036(3)
B(12)	-0.1075(13)	0.1940(5)	-0.2013(13)	0.035(3)
C(101)	-0.0179(11)	0.1133(4)	0.2094(11)	0.0337(25)
C(102)	-0.0311(12)	0.1439(5)	0.3127(12)	0.047(3)
C(103)	0.0002(14)	0.1220(6)	0.4366(14)	0.058(4)
C(104)	0.0413(15)	0.0704(6)	0.4539(15)	0.061(4)
C(105)	0.0545(15)	0.0415(6)	0.3552(15)	0.063(4)
C(106)	0.0247(12)	0.0610(5)	0.2296(12)	0.042(3)
P(1)	0.3407(3)	0.20114(11)	0.1644(3)	0.0305(6)
C(111)	0.4188(11)	0.1748(4)	0.3180(11)	0.0335(25)
C(112)	0.3417(12)	0.1456(5)	0.3791(12)	0.048(3)
C(113)	0.3945(16)	0.1251(7)	0.5025(16)	0.071(5)
C(114)	0.5329(14)	0.1352(6)	0.5622(14)	0.057(4)
C(115)	0.6082(14)	0.1625(6)	0.4971(14)	0.056(4)
C(116)	0.5545(12)	0.1838(5)	0.3781(12)	0.045(3)
C(121)	0.2766(12)	0.2625(5)	0.2044(12)	0.043(3)
C(131)	0.4756(12)	0.2225(5)	0.0951(12)	0.045(3)
P(2)	0.3191(3)	0.08681(12)	0.0036(3)	0.0346(7)
C(211)	0.4349(12)	0.0598(5)	0.1400(12)	0.040(3)
C(216)	0.3861(15)	0.0231(6)	0.2135(15)	0.063(4)
C(215)	0.4752(19)	0.0023(8)	0.3241(19)	0.086(6)
C(214)	0.6072(18)	0.0213(7)	0.3576(18)	0.078(5)
C(213)	0.6558(15)	0.0581(6)	0.2888(15)	0.061(4)
C(212)	0.5667(13)	0.0774(5)	0.1779(13)	0.049(3)
C(221)	0.4166(14)	0.1059(5)	-0.1073(13)	0.052(3)
C(231)	0.2387(16)	0.0276(6)	-0.0786(16)	0.066(4)

1,2-Ph_2-3-(1,5-COD)-3,1,2-$PdC_2B_9H_9$, 19.

Crystal Data.

$C_{22}H_{31}B_9Pd$, M= 499.18, monoclinic, $P2_1/n$, a= 10.946(2), b= 12.077(3), c= 17.680(3)Å, β= 91.2340(14)°, V= 2336.6Å^3, from least squares refinement of 25 centred reflections (11<θ<12°), Z= 4, $D_{calc.}$= 1.419gcm^{-1}, $\mu_{MoK\alpha}$= 7.92cm^{-1}.

Data Collection and Processing.

ω- 2θ scans in 96 steps with ω scan width 0.8+ 0.34tanθ. Variable scan speeds between 0.82 and 2.35°min.$^{-1}$. 6778 independent reflections of which 5412 retained with F>2σ(F) (1<θ<30, h: ±15, k:0 to 17 and l: 0 to 24).

Structure Solution and Refinement.

Pd atom position from Patterson map; B, C, cage H-atoms and COD C-H atoms from full matrix least-squares refinement/ΔF syntheses. Phenyl H-atoms set in fixed positions with C-H= 1.08Å. COD CH_2 H-atoms set in idealised positions with C-H= 1.08Å. H atoms refined with a common thermal parameter (U_{eq}= 0.0684(21) at convergence). R= 0.0422, R_w= 0.0478, S= 0.914, g= 0.00815. Max. and min. residues in final ΔF map +0.47 and -0.72eÅ^{-3}.

Crystallographic numbering scheme.

C(n1-6) refer to the phenyl carbon atoms in the ring attached to Cn. C101-108 refer to the COD carbon atoms. All H-atoms are numbered according to their bound carbon atom except for the COD-CH_2 protons. These are labelled H(n0m) and H(n9m) when bound to C(n0m).

Table 5.10 Fractional Coordinates of Non-H Atoms with Standard Deviations.

Atom	x	y	z	Ueq
C(1)	0.50568(25)	0.25437(21)	0.20781(14)	0.0329(13)
C(2)	0.56589(25)	0.17889(20)	0.15069(15)	0.0343(12)
Pd(3)	0.33036(2)	0.18371(2)	0.10855(1)	0.0330(1)
B(4)	0.3581(3)	0.1898(3)	0.23075(19)	0.0430(17)
B(5)	0.4953(4)	0.1958(3)	0.29163(19)	0.0466(18)
B(6)	0.6292(4)	0.1834(3)	0.24246(19)	0.0440(17)
B(7)	0.4734(3)	0.05612(25)	0.13230(18)	0.0387(16)
B(8)	0.3477(4)	0.0497(3)	0.19486(20)	0.0450(18)
B(9)	0.4082(4)	0.0697(3)	0.28563(21)	0.0562(22)
B(10)	0.5690(4)	0.0657(3)	0.28612(22)	0.0571(22)
B(11)	0.6127(3)	0.0588(3)	0.18834(20)	0.0453(18)
B(12)	0.4842(4)	-0.0164(3)	0.22252(22)	0.0518(21)
C(12)	0.5552(3)	0.44550(24)	0.25581(17)	0.0429(15)
C(13)	0.5549(3)	0.5603(3)	0.24665(21)	0.0534(18)
C(14)	0.5056(3)	0.6082(3)	0.18220(24)	0.0608(21)
C(15)	0.4581(3)	0.5410(3)	0.12558(22)	0.0561(20)
C(16)	0.4605(3)	0.42674(24)	0.13379(18)	0.0443(16)
C(11)	0.50729(23)	0.37709(21)	0.19936(15)	0.0333(13)
C(22)	0.7290(3)	0.30909(23)	0.10309(18)	0.0427(15)
C(23)	0.8071(3)	0.3440(3)	0.04776(20)	0.0504(18)
C(24)	0.8022(3)	0.2962(3)	-0.02338(21)	0.0551(19)
C(25)	0.7191(3)	0.2139(3)	-0.03885(18)	0.0509(17)
C(26)	0.6407(3)	0.17723(23)	0.01718(16)	0.0414(14)
C(21)	0.64443(23)	0.22464(21)	0.08899(15)	0.0336(12)
C(101)	0.1741(3)	0.3109(3)	0.09941(22)	0.0494(17)
C(102)	0.1643(4)	0.3651(3)	0.0229(3)	0.0646(23)
C(103)	0.2670(4)	0.3387(4)	-0.03019(22)	0.0629(22)
C(104)	0.3273(3)	0.2269(3)	-0.01905(18)	0.0532(19)
C(105)	0.2697(4)	0.1285(3)	-0.01066(19)	0.0592(21)
C(106)	0.1328(4)	0.1156(4)	-0.0117(3)	0.077(3)
C(107)	0.0716(4)	0.1268(3)	0.0635(3)	0.072(3)
C(108)	0.1296(3)	0.2097(3)	0.11717(24)	0.0554(20)

Table 5.11 Fractional Coordinates of Hydrogen Atoms.

Atom	x	y	z
H(4)	0.290(3)	0.250(3)	0.2548(21)
H(5)	0.488(3)	0.254(4)	0.3372(21)
H(6)	0.710(4)	0.224(3)	0.2470(22)
H(7)	0.490(3)	0.011(3)	0.0785(20)
H(8)	0.268(3)	-0.006(3)	0.1895(20)
H(9)	0.353(4)	0.046(3)	0.3297(21)
H(10)	0.630(3)	0.029(3)	0.3344(21)
H(11)	0.692(4)	0.018(3)	0.1642(20)
H(12)	0.490(3)	-0.105(3)	0.2224(21)
H(112)	0.5929(3)	0.40959(24)	0.30716(17)
H(113)	0.5938(3)	0.6122(3)	0.29067(21)
H(114)	0.5041(3)	0.6971(3)	0.17601(24)
H(115)	0.4190(3)	0.5775(3)	0.07481(22)
H(116)	0.4253(3)	0.37522(24)	0.08838(18)
H(212)	0.7333(3)	0.34769(23)	0.15818(18)
H(213)	0.8724(3)	0.4089(3)	0.06001(20)
H(214)	0.8635(3)	0.3237(3)	-0.06656(21)
H(215)	0.7142(3)	0.1772(3)	-0.09455(18)
H(216)	0.5765(3)	0.11146(23)	0.00469(16)
H(101)	0.197(4)	0.347(4)	0.1391(24)
H(102)	0.0814(4)	0.3380(3)	-0.0056(3)
H(192)	0.1578(4)	0.4525(3)	0.0354(3)
H(103)	0.3380(4)	0.4002(4)	-0.02319(22)
H(193)	0.2340(4)	0.3388(4)	-0.08820(22)
H(104)	0.421(4)	0.234(3)	-0.0283(22)
H(105)	0.320(4)	0.057(3)	-0.0135(21)
H(106)	0.0977(4)	0.1771(4)	-0.0508(3)
H(196)	0.1248(4)	0.0345(4)	-0.0370(3)
H(107)	-0.0254(4)	0.1348(3)	0.0523(3)
H(197)	0.0904(4)	0.0468(3)	0.0885(3)
H(108)	0.118(4)	0.201(3)	0.1694(24)

Table 5.12 Anisotropic Vibration Parameters of Non-H Atoms with Standard Deviations, Å^2.

Atom	U11	U22	U33	U23	U13	U12
C(1)	0.040(1)	0.034(1)	0.025(1)	-0.002(1)	-0.002(1)	-0.004(1)
C(2)	0.038(1)	0.033(1)	0.032(1)	-0.003(1)	-0.004(1)	0.002(1)
Pd(3)	0.0333(1)	0.0333(1)	0.0324(1)	-0.0034(1)	0.0008(1)	-0.0021(1)
B(4)	0.055(2)	0.042(2)	0.032(1)	-0.004(1)	0.009(1)	-0.013(2)
B(5)	0.072(2)	0.039(2)	0.029(1)	0.001(1)	-0.005(1)	-0.012(2)
B(6)	0.055(2)	0.040(2)	0.037(2)	-0.001(1)	-0.018(1)	-0.002(2)
B(7)	0.049(2)	0.030(1)	0.037(2)	-0.003(1)	-0.006(1)	-0.001(1)
B(8)	0.059(2)	0.036(1)	0.041(2)	0.000(1)	0.005(2)	-0.015(1)
B(9)	0.088(3)	0.043(2)	0.037(2)	0.007(1)	0.004(2)	-0.019(2)
B(10)	0.089(3)	0.041(2)	0.041(2)	0.010(1)	-0.019(2)	-0.003(2)
B(11)	0.056(2)	0.035(1)	0.045(2)	-0.001(1)	-0.019(2)	0.005(1)
B(12)	0.077(3)	0.033(1)	0.045(2)	0.008(1)	-0.013(2)	-0.005(2)
C(12)	0.044(2)	0.043(1)	0.042(2)	-0.013(1)	0.007(1)	-0.007(1)
C(13)	0.050(2)	0.043(2)	0.068(2)	-0.021(2)	0.015(2)	-0.008(1)
C(14)	0.055(2)	0.031(1)	0.096(3)	-0.002(2)	0.019(2)	0.002(1)
C(15)	0.050(2)	0.043(2)	0.075(2)	0.015(2)	0.001(2)	-0.001(1)
C(16)	0.040(2)	0.040(1)	0.053(2)	0.005(1)	-0.003(1)	-0.006(1)
C(11)	0.029(1)	0.034(1)	0.037(1)	-0.003(1)	0.006(1)	-0.004(1)
C(22)	0.038(1)	0.044(1)	0.046(2)	-0.007(1)	0.004(1)	0.000(1)
C(23)	0.041(2)	0.049(2)	0.062(2)	0.000(1)	0.013(1)	0.000(1)
C(24)	0.049(2)	0.061(2)	0.056(2)	0.007(2)	0.018(2)	0.012(2)
C(25)	0.053(2)	0.060(2)	0.040(2)	-0.004(1)	0.006(1)	0.011(2)
C(26)	0.044(2)	0.044(1)	0.036(1)	-0.005(1)	-0.001(1)	0.009(1)
C(21)	0.031(1)	0.034(1)	0.036(1)	-0.002(1)	-0.001(1)	0.007(1)
C(101)	0.040(2)	0.047(2)	0.062(2)	-0.006(1)	0.012(1)	0.004(1)
C(102)	0.059(2)	0.057(2)	0.078(3)	0.012(2)	0.001(2)	0.014(2)
C(103)	0.059(2)	0.078(2)	0.051(2)	0.019(2)	-0.002(2)	0.004(2)
C(104)	0.044(2)	0.080(2)	0.035(2)	0.001(2)	0.000(1)	0.012(2)
C(105)	0.071(2)	0.065(2)	0.041(2)	-0.016(2)	-0.016(2)	0.016(2)
C(106)	0.083(3)	0.072(3)	0.077(3)	-0.013(2)	-0.029(2)	-0.020(2)
C(107)	0.051(2)	0.068(2)	0.097(3)	0.002(2)	-0.019(2)	-0.019(2)
C(108)	0.035(2)	0.066(2)	0.065(2)	-0.002(2)	0.009(2)	-0.007(1)

Section C Extended Huckel Molecular Orbital Calculations.

E.H.M.O. calculations[137-139] have been widely used for probing structural problems in organometallic chemistry. The molecular orbital energies obtained from these calculations are often inaccurate, but are found to be of use qualitatively in predicting preferred conformations and rotational barriers. In order to carry out such a calculation a model of the molecule of interest, with co-ordinates in orthogonalised Angstrom space, as well as a basis set of atomic orbital parameters for all the atoms in the molecule, are required.

Molecular orbitals (MO's) are derived by the linear combination of atomic orbitals (LCAO) method. The mathematical function for an MO (Ψ) is obtained from the functions for the corresponding atomic orbitals (AO's), Ψ_i and Ψ_j, according to the following equation.

$$\Psi = c_i\Psi_i + c_j\Psi_j$$

where c_i and c_j are AO coefficients.

In practice[140-142], the AO wave functions are represented by normalised Slater-type orbitals (STO's) of the form

$$\Psi_{lmn} = r^{n-1}\exp^{-\zeta r}Y_{ml}(\theta,\phi)$$

n= effective quantum number (related to the principal quantum number)

$Y_{ml}(\theta, \phi)$ are spherical harmonics

ζ is the orbital exponent which defines the diffuseness of the STO's in physical terms and is related to the effective nuclear charge.

$\zeta = (Z - \sigma)/n$

where Z is the nuclear charge and σ is a screening constant.

To calculate orbital energies, a secular determinant is set up from equations of the type shown below, using evaluated 1-electron Hamiltonian operators (H_{ii} and H_{ij}) and overlap integrals (S_{ij}).

$\Sigma c_{ij}(H_{ij} - S_{ij}E) = 0$

where $H_{ii} = \int\psi_i H\psi_i = \int\psi_i H\psi_j = \int\psi_j H\psi_i$ and $S_{ij} = \psi_i\psi_j$

The H_{ii}'s used are valence shell ionisation energies (VSIE's).

The H_{ij}'s are calculated using the modified Wolfsberg-Helmholtz formula[143]:

$H_{ij} = K'S_{ij}(H_{ii}+H_{jj})/2$

where $K' = K + \Delta + \Delta^2 + \Delta^4(1-K)$

and $\Delta = (H_{ii} - H_{jj})/(H_{ii} + H_{jj})$.

The AO parameters used in the calculations discussed in this thesis are the following.

AO	H_{ii} (eV)	$\zeta_1{}^g$
H1s	-13.60	1.30
B2s	-15.20	1.30
B2p	-8.50	1.30
C2s	-21.40	1.625
C2p	-11.40	1.625

g= exponents

The calculations described in this work involved two idealised models. The first was the $\{C_2B_9H_{11}\}^{2-}$ fragment and the second the $\{C_2B_9H_{10}Ph)\}^{2-}$ fragment. These

determined the characteristics of the frontier molecular orbitals which were concentrated on the *nido*-C_2B_3 face. The bond distances used in the construction of the models were: B-B= 1.85Å, B-C= 1.7575Å, C_{cage}-C_{cage}= 1.65Å, C_{cage}-C_{phenyl}= 1.50Å= C_{phenyl}-C_{phenyl}= 1.395Å, B-H= C-H_{cage}= 1.15Å, C-H_{phenyl}= 1.08Å. The co-ordinates for the $\{C_2B_9H_{11}\}^{2-}$ fragment are given below, followed by the co-ordinates of the phenyl ring, which was substituted for H12 in the second model.

Co-ordinates for the Idealised Icosahedral Fragment, $\{C_2B_9H_{11}\}^{2-}$.

H1	-2.1054	1.5296	-1.3012
H2	-2.1054	-1.5296	-1.3012
H3	-2.6023	0.0000	1.3012
H4	-0.8041	2.4750	1.3012
H5	0.8041	2.4750	-1.3012
H6	0.0000	0.0000	-2.9095
H7	-0.8041	-2.4750	1.3012
H9	1.9678	1.4297	1.2162
H10	2.6023	0.0000	-1.3012
H11	0.8041	-2.4750	-1.3012
H12	1.9678	-1.4297	1.2162
B1	-1.2732	0.9250	-0.7868
B2	-1.2732	-0.9250	-0.7868
B3	-1.5737	0.0000	0.7869
B4	-0.4863	1.4967	0.7868
B5	0.4863	1.4967	-0.7868
B6	0.0000	0.0000	-1.7595
B7	-0.4863	-1.4967	0.7868
C9	1.1355	0.8250	0.7018
B10	1.5737	0.0000	-0.7869
B11	0.4863	-1.4967	-0.7868
C12	1.1355	-0.8250	0.7018

Co-ordinates for the Phenyl Substituent, Replacing H12, in the Above Model.

H22	3.5949	0.0374	1.4429
H23	5.3858	-1.2639	2.5497
H24	5.0212	-3.6485	3.1032
H25	2.8657	-4.7318	2.5499
H26	1.0748	-3.4305	1.4431
C21	2.2209	-1.6137	1.3726
C22	3.4358	-1.0031	1.6845
C23	4.4452	-1.7366	2.3083
C24	4.2397	-3.0806	2.6203
C25	3.0248	-3.6912	2.3084
C26	2.0154	-2.9578	1.6846

Section D Electrochemical Techniques.

This section describes the basic electrochemical techniques employed[144] during this work. All the results discussed were obtained using cyclic voltammetry and therefore only this method is discussed. However, it should be noted that there are a number of other electrochemical techniques *e.g.* stirred voltammetry and a.c. voltammetry[145].

Cyclic voltammetry is carried out using a standard 3-electrode system consisting of a working electrode (w.e.), a counter electrode (c.e.) and a reference electrode (r.e.). To be suitable for use as working and counter electrodes a material must be chemically inert and stable over a wide potential range. In practise, a Pt micro-electrode is used as the w.e. and a Pt rod as the c.e. The reference electrode is a half cell of known potential against which all other potentials can be measured. The reference reaction must be reversible and obey the Nernst equation as well as having a stable potential with time and a low temperature dependence. In this work a Ag/AgCl cell in dichloromethane provides the reference. The electrode is housed in a salt bridge and in contact with the bulk solution via a porous glass frit. The salt bridge contains some of the electrolyte solution. The reference electrode has a high internal resistance so virtually no current flows through it. The current flow in a three electrode system is between the w.e. and the c.e. and hence, the r.e. is stable and non-polarized.

The three electrodes are immersed in a solvent[146] containing a high concentration of an inert electrolyte. In this work 0.5M $[Bu_4N]^+[BF_4]^-$ in CH_2Cl_2 is the electrolyte/solvent system. The role of the electrolyte is to decrease the contribution of migration to mass transport of the electroactive species and hence to ensure that the current limiting step is diffusion controlled. Further, the presence of a high

concentration of electrolyte lowers the cell resistance. The electrolyte ions must be non-electroactive in the potential range of interest and must be suitably soluble in the solvent being used. The criteria for a suitable solvent are as follows: it must possess a high dielectric constant, have a low vapour pressure and be liquid over the required temperature range, it must be non-electroactive over the required potential range and finally be unlikely to co-ordinate to the species of interest. Obviously, it is crucial that the solvent does not contain any impurities which may interfere with the experiment. For this reason, dichloromethane was allowed to stand over KOH pellets for approx. 1 week then freshly distilled, from CaH_2, immediately prior to use.

The cell is such as to optimise electrode geometry to achieve a symmetric electrical field around the w.e. and is shown diagrammatically in figure 5.1. It must also include an inlet to allow purging of the system of oxygen. This is achieved by bubbling argon through the solution (for approx. 10 mins.) before the test species is added and maintaining an atmosphere of Ar throughout the experiment. The presence of oxygen in the system must be avoided as this may cause oxidation of the species of interest. The redox chemistry of O_2 is also avoided. The final component present in the cell is a magnetic stirrer bar. As well as assisting in the dissolution of the test species, the solution must be stirred frequently between the recording of voltammograms to ensure there is no build up of undesired species in the vicinity of the w.e. Typically *circa* 10-20mg of the test species is added to the de-gassed solution. After stirring to aid dissolution, the voltammograms are recorded, on quiet solutions. All the results discussed in this thesis were obtained at 298K.

The electrodes are connected to a potentiostat and waveform generator (Hi-Tek Instruments, England, Potentiostat Type DT2101 and Waveform Generator PPRI) and the output recorded on an x-y recorder with current being recorded in the y-direction and potential in the x-direction.

In cyclic voltammetry the potential is ramped linearly from an initial potential to a switching potential and back to the initial potential again. The rate at which the potential is altered can be varied. Typically scan rates (v) are set between $50mVs^{-1}$ and $500mVs^{-1}$. The solution is unstirred and hence the only means of mass transport of the test species is thermal diffusion.

The nature of the trace obtained depends on the type of processes occurring. The electron transfer involving an electroactive species is described in terms of the reversibility of the process as reversible, irreversible or quasi-reversible. For a reversible process the electron transfer is faster than the rate of diffusion to the electrode. In this work, the transfer is defined as being quasi-reversible if either the rate is similar to that of diffusion or a chemical reaction follows the electron transfer. An irreversible process is one for which the rate of electron transfer is similar to that of diffusion. The reversibility of a process is determined using the criteria outlined overleaf.

Figure 5.1

Experimental Set-up for Conventional Electrochemistry.

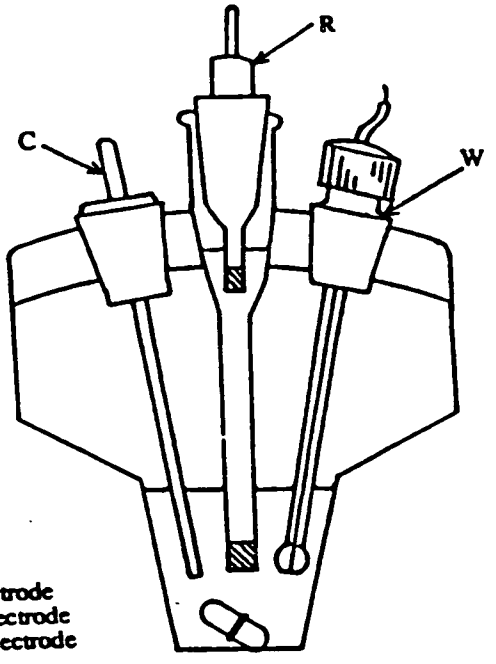

Key

C: Counter electrode
W: Working electrode
R: Reference electrode

Reversible process:	E is independent of ν
	$E^f - E^r = 59/n$ mV at 298K
	$E_{1/2}$ is independent of C
	$i/\nu^{1/2}$ is independent of ν
	$i^f/i^r = 1$ and is independent of ν
Quasi-reversible process:	E varies with ν
	$E^f - E$ varies with ν
	$i/\nu^{1/2}$ varies with ν
	i^f/i^r approx.= 1
Irreversible process:	E varies with ν
	$i/\nu^{1/2}$ varies with ν
	There is no peak i^r

A typical cyclic voltammogram for a reversible process is shown in figure 5.2 in which the variables used in determining the reversibility of an electron transfer step are defined. As the potential approaches that at which the redox process occurs the current begins to increase. The rate of increase rises rapidly as the material in the vicinity of the w.e. is consumed until it reaches a maximum. At this point the rate of diffusion of fresh material to the w.e. is equal to the rate of electron transfer. Beyond this potential the rate of diffusion becomes the limiting factor and the current drops to a diffusion controlled limit. When the potential is switched the same processes occur giving an inversion of the initial scan.

The nature of the return wave is used to determine the reversibility of the electron transfer reaction. For the ideal case which gives rise to the type of scan shown, there

is no gross chemical change occurring during the timescale of the experiment and the process is said to be chemically reversible. If there is no return wave this implies that a structural or chemical change follows the initial electron transfer step. If the return wave is asymmetric then there may be some degree of chemical reversibility and the process can be described as quasi-reversible.

Figure 5.2

Cyclic Voltammogram for a Fully Reversible Process.

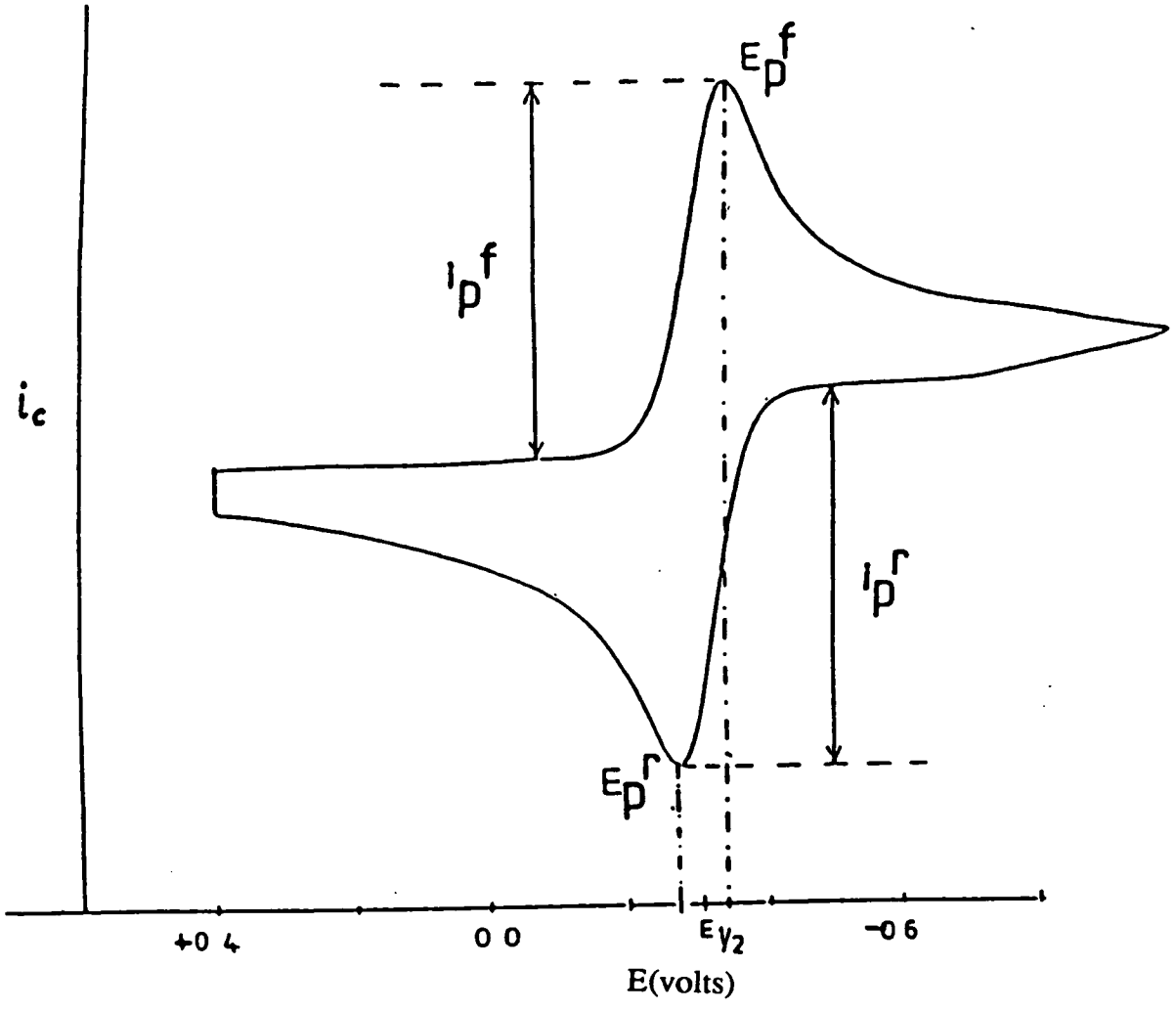

References.

1. A. Stock; *Hydrides of Boron and Silicon*, Cornell Univ. Press, Ithaca, New York, 1936.

2. W.N. Lipscomb; *Boron Hydrides*, Benjamin, New York, 1963.

3. W.N. Lipscomb; *Proc. Nat. Acad. Sci. U.S.*, 1961, 47, 1963.

4. C.D. Good, I Shapiro and R.E. Williams; *J. Amer, Chem. Soc.*, 1962, 84, 1791 and C.D. Good, B. Keilin, I. Shapiro and R.E. Williams; *J. Amer. Chem. Soc.*, 1963, 85, 3167.

5. T.L. Heyling, J.W. Ager Jr., S.L. Clark, D.J. Mangold, H.L. Goldstein, M. Hillman, R.J. Polak and J.W. Szymanski; *Inorg. Chem.*, 1963, 2, 1089.

6. E.J.M. Hamilton and A.J. Welch; *Polyhedron*, 1990, 9, 2407.

7. *e.g.* T.J. Kealy and P.L. Pauson; *Nature*, 1951, 168, 1039 and D.E. Crotty, E.R. Corey, T.J. Anderson, M.D. Glick and J.P. Oliver; *Inorg. Chem.*, 1977, 16, 920.

8. M.F. Hawthorne, P.A. Wegner and D.C. Young; *J. Amer. Chem. Soc.*, 1965, 87, 1818.

9. H. Hatanaka, K. Amano, H. Kanemitsu, I. Ikeuchi and T. Yoshikazi; in *B.N.C.T. for Tumours*, Ed. H. Hatanaka, Japan, 1985, Chap. 5.

10. R.F. Barth, R.G. Fairchild and A.H. Soloway; *Sci. Am.*, 1990, 263, 68.

11. J.H. Morris; *Chem. in Brit.*, 1991, 27, 331.

12. J. Plesek; *Chem. Rev.*, 1992, 92, 269 (and references therein).

13. R.N. Grimes; *Carboranes*, Academic Press Inc., New York, 1970, Chapter 8.

14. T.E. Paxson and M.F. Hawthorne; *J. Amer. Chem. Soc.*, 1974, 96, 4674.

15. P.E. Behnken, J.A. Belmont, D.C. Busby, M.S. Delaney, R.E. King III, C.W. Kreimendahl, T.B. Marder, J.J. Wilczynski and M.F. Hawthorne; *J. Amer. Chem. Soc.*, 1984, 106, 3011.

16. R.T. Baker, M.S. Delaney, R.E. King III, C.B. Knobler, J.A. Long, T.B. Marder, T.E. Paxson, R.G. Teller and M.F. Hawthorne; *J. Amer. Chem. Soc.*, 1984, 106, 2965.

17. J.D. Hewes, M. Thompson and M.F. Hawthorne; *Organometallics*, 1985, 4, 13.

18. H.C. Kang and M.F. Hawthorne; *Organometallics*; 1990, 9, 2327.

19. N.N. Greenwood and A. Earnshaw; *Chemistry of the Elements*; Pergamon Press, Oxford, 1982.

20. K. Wade; *J. Chem. Soc., Chem. Commun.*, 1971, 792.

21. K. Wade; *Adv. Inorg. Chem. Radiochem.*, 1976, 18, 1. and R.E. Williams; *ibid*, 1976, 18, 67.

22. J. Buchanan, E.J.M. Hamilton, D. Reed and A.J. Welch; *J. Chem. Soc., Dalton Trans.*, 1990, 677.

23. D.E. Smith and A.J. Welch; *Organometallics*, 1986, 5, 760.

24. A.J. Wynd and A.J. Welch; *J. Chem. Soc., Dalton Trans.*, 1990, 2803.

25. R.N. Grimes; *Carboranes*, Academic Press Inc., New York, 1970, Chapter 7.

26. R.K. Bohn and M.D. Bohn; *Inorg. Chem.*, 1971, 10, 350.

27. D.M.P. Mingos, M.I. Forsyth and A.J. Welch; *J. Chem. Soc., Dalton Trans.*, 1978, 1363.

28. H.M. Colquhoun, T.J. Greenhough and M.G.H. Wallbridge; *Acta Cryst., Section B*, 1978, 34, 2373.

29. D.M.P. Mingos; *J. Chem. Soc., Dalton Trans.*, 1977, 602.

30. H. Beall; in *Boron Hydride Chemistry*, Ed. E.L. Meutterties, Academic Press, New York, 1975.

31. R.N. Grimes; Carboranes, Academic Press Inc., New York, 1970, Chapter 6.

32. M.P. Garcia, M. Green, F.G.A. Stone, R.G. Somerville, A.J. Welch, C.E. Briant, D.N. Cox and D.M.P. Mingos; *J. Chem. Soc., Dalton Trans.*, 1985, 2343.

33. J.L. Spencer, M. Green and F.G.A. Stone; *J. Chem. Soc., Chem. Commun.*, 1972, 1178.

34. M.M. Fein, J. Bobinski, N. Mayes, N. Schwartz and M.S. Cohen; *Inorg. Chem.*, 1963, 2, 1111.

35. T. Onak; in *Comprehensive Organometallic Chemistry*, Eds. F.G.A. Stone and F.W. Abel, Pergammon Press, 1981, Section 5.4, p420.

36. R.A.W. Johnstone; *Mass Spectrometry for Organic Chemists*, Cambridge Univ. Press, 1972, pp49-56.

37. F. Teixidor, C. Vinas and R.W. Rudolph; *Inorg. Chem.*, 1986, 25, 3339.

38. D. Reed; *Chem. Soc. Rev.*, 1993, 109.

39. E.A.V. Ebsworth, D.W.H. Rankin and S. Cradock; *Structural Methods in Inorganic Chemistry*, Blackwell Scientific Publications, 1987, p54.

40. L.M. Venanzi; *Chem. in Brit.*, 1968, 4, 162.

41. E.G. Finer and R.K. Harris; in *Prog. in N.M.R. Spectroscopy*, Eds. J.W. Emsley, J. Feeney and L.H. Sutcliffe, Volume 6, 61 (and references therein).

42. D.J. Donohoe; Unpublished results.

43. Z.G. Lewis and A.J. Welch; *Acta Cryst., Section C*, 1993, 49, 705.

44. B.D. Reid; PhD. Thesis, University of Edinburgh, 1992.

45. T.D. McGrath; Unpublished results.

46. S. Bresadola, A. Frigo, B. Longato and G. Rigatti; *Inorg. Chem.*, 1973, 12, 2788.

47. J.A. Doi, E.A. Mizusawa, C.B. Knobler and M.F. Hawthorne; *Inorg. Chem.*, 1984, 23, 1482.

48. C.B. Knobler, T.B. Marder, E.A. Mizusawa, R.G. Teller, J.A. Long, P.E. Behnken and M.F. Hawthorne; *J. Amer. Chem. Soc.*, 1984, 106, 2990.

49. Z.G. Lewis; PhD. Thesis, University of Edinburgh, 1992.

50. D.E. Smith and A.J. Welch; *Organometallics*, 1986, 5, 760.

51. M. Bown, X.L.R. Fontaine, N.N. Greenwood, J.D. Kennedy, J. Plesek, B. Stibr and M. Thornton-Pett; *Acta Cryst., Section C*, 1990, 46, 995.

52. J. Cowie, D.J. Donohoe, N.L. Douek and A.J. Welch; *Acta Cryst. Section C*, 1993, 49, 710.

53. H.M. Colquhoun, T.J. Greenhough and M.G.H. Wallbridge; *J. Chem. Soc., Chem. Commun.*, 1977, 737.

54. Z.G. Lewis and A.J. Welch; *J. Organometal. Chem.*, 1992, 430, C45.

55. J. Cowie; Unpublished results.

56. M.J. Attfield, J.A.K. Howard, A.N. de M. Jelfs, C.M. Nunn and F.G.A. Stone; *J. Chem. Soc., Dalton Trans.*, 1987, 2219.

57. N.L. Douek; PhD. Thesis, University of Edinburgh, 1993.

58. J.A. Long, T.B. Marder, P.E. Behnken and M.F. Hawthorne; *J. Amer. Chem. Soc.*, 1984, 106, 2979.

59. N.W. Alcock, J.G. Taylor and M.G.H. Wallbridge; *J. Chem. Soc., Dalton Trans.*, 1987, 1805.

60. H.M. Colquhoun, T.J. Greenhough and M.G.H. Wallbridge; *J. Chem. Soc., Dalton Trans.*, 1985, 761.

61. G.A. Barclay, R.S. Nyholm and R.V. Parish; *J. Chem. Soc.*, 1961, 4433.

62. J.A. Walker, C.B. Knobler and M.F. Hawthorne; *Inorg. Chem.*, 1985, 24, 2688.

63. Z.G. Lewis, D. Reed and A.J. Welch; *J. Chem. Soc., Dalton Trans.*, 1992, 731.

64. F.A. Cotton and G. Wilkinson; *Basic Inorganic Chemistry*, International Edition, J. Wiley and Sons. Inc., 1976.

65. D.E. Smith and A.J. Welch; *Acta Cryst., Section C*, 1986, 42, 1717.

66. D.R. Baghurst, R.C.B. Copley, H. Fleischer, D.M.P. Mingos, G.O. Kyd, L.J.Yellowlees, A.J. Welch, T.R. Spalding and D.J. O'Connell; *J.Organometal. Chem.*, 1993, 447, C14.

67. G.M. Sheldrick; University of Gottingen, Germany, 1976.

68. N.G. Walker and D. Stuart; *Acta. Cryst.*, 1983, A39, 158.

69. K.F. Shaw; PhD. Thesis, Univ. of Edinburgh, 1992.

70. K.F. Shaw and A.J. Welch; *Polyhedron*, 1992, 11, 157.

71. L.A. Leites, L.E. Vinogradova, J.Belloc and A. Novak; *J. Molec. Struct.*, 1983, 100, 379.

72. A.J. Welch; *J. Chem. Soc., Dalton Trans.*, 1975, 1473.

73. J. M. Jenkins and B.L. Shaw; *J. Chem. Soc. (A)*, 1966, 770.

74. E.D. Becker; *High Resolution N.M.R.: Theory and Chemical Applications*, Academic Press, New York and London, 1972, pp135-38.

75. T.R. Spalding; Private communication in D.R. Baghurst, D.Phil Thesis, University of Oxford, 1992.

76. S.A. Macgregor, A.J. Wynd, N. Moulden, R.O. Gould, P. Taylor, L.J. Yellowlees and A.J. Welch; *J. Chem. Soc., Dalton Trans.*,1991, 3317.

77. D. Grafstein and J. Dvorak; *Inorg.Chem.*, 1963, 2, 1128.

78. S. Papetti and T.L. Heyling; *J.Amer.Chem.Soc.*,1964, 86, 2295.

79. R. Hoffmann and W.N. Lipscomb; *Inorg. Chem.*, 1963, 2, 231.

80. R.M. Salinger and C.L. Frye; *Inorg. Chem.*, 1965, 4, 1815.

81. R.N. Grimes; *Carboranes*, Academic Press, New York and London, 1970, pp159-60.

82. M.K. Kaloustian, R.J. Wiersema and M.F. Hawthorne; *J. Amer. Chem. Soc.*, 1972, 94, 6679.

83. R.R. Rietz, D.F. Dustin and M.F. Hawthorne; *Inorg. Chem.*, 1974, 13, 1580.

84. L.F. Warren Jr. and M.F. Hawthorne; *J.Amer.Chem.Soc.*, 1970, 92, 1157.

85. T.E. Paxson, M.K. Kaloustian, G.M. Tom, R.E. Wiersema and M.J. Hawthorne; *J. Amer. Chem. Soc.*, 1972, 94, 4882.

86a. S.A. Brew, J.C.Jeffery, M.U. Pilotti and F.G.A. Stone; *J. Amer. Chem. Soc.*, 1990, 112, 6148. b. S.A. Brew, N. Carr, J.C. Jeffery, M.U. Pilotti and F.G.A. Stone; *J. Amer. Chem. Soc.*, 1992, 114, 2203. c. S.A. Brew and F.G.A. Stone; *J. Chem. Soc. Dalton Trans.*, 1992, 867. d. J.C. Jeffrey, S. Li, D.W.I. Sams and F.G.A. Stone; *J. Chem. Soc. Dalton Trans.*, 1992, 877.

87. S. Li and F.G.A. Stone; *Polyhedron*, 1993, 12, 1689.

88. W.N. Lipscomb; *Science*, 1966, 153, 373.

89. H.D. Kaesz, R. Bau, H.A. Beall and W.N. Lipscomb; *J.Amer.Chem.Soc.*, 1967, 89, 4218.

90. H.S. Wong and M.N. Lipscomb; *Inorg. Chem.*, 1975, 14, 1350.

91. B.F.G. Johnson, Y.V. Roberts and E. Parisini; *Inorg. Chim. Acta.*, 1993, 211, 17.

92. D. Grafstein and J. Dvorak; *Inorg. Chem.*, 1962, 2, 1128.

93. E.L. Muetterties and W.N. Knoth; *Polyhedral Boranes*, Academic Press, New York, 1968, p70.

94. S. Wu and M. Jones Jr.; *J.Amer.Chem.Soc.*, 1989, 111, 5373.

95. G.M. Edvenson and D.F. Gaines; *Inorg. Chem.*,1990, 29, 1210.

96. *e.g.* B.M. Gimarc, D.S. Warren, J.J. Ott and C.Brown; *Inorg. Chem.*, 1991, 30, 1598. D.J. Wales and A.J. Stone; *Inorg. Chem.*, 1987, 26, 3845. D.J. Fuller and D.L. Kepert; *Inorg. Chem.*, 1982, 21, 163. D.J. Wales and D.M.P. Mingos; *Polyhedron*, 1989, 8, 1933. D.J. Wales; *J. Amer. Chem. Soc.*, 1993, 115, 1157.

97. C.A. Tolman; *J. Amer. Chem. Soc.*, 1970, 92, 2956.

98. C.A. Tolman; *J. Amer. Chem. Soc.*, 1970, 92, 2953.

99. C.A. Tolman; *Chem. Rev.*, 1977, 77, 313.

100. L.J. Guggenberger; *J. Organometal. Chem.*, 1974, 81, 271.

101a. N.S. Imyanitov; *Koord. Khim.*, 1985, 11, 1041. b. J.T. DeSanto, J.A. Mosbo, B.N. Storhoff, P.L. Bock and R.E. Bloss; *Inorg. Chem.*, 1980, 19, 3086.

102. W. Strohmeier and F-J. Muller, *Chem. Ber.*,100, 1967, 2812.

103. A. Pidcock and C.R. Waterhouse; *J.Chem. Soc. (A)*, 1970, 2080.

104. F.B. Ogilvie, J.M. Jenkins and J.G. Verkade; *J. Amer. Chem. Soc.*, 1970, 92, 1916.

105. E.A.V. Ebsworth, D.W.H. Rankin and S. Cradock; *Structural Methods in Inorganic Chemistry*, Blackwell Scientific Publications, 1987, pp57-8.

106. L.F. Warren Jr. and M.F. Hawthorne; *J. Amer. Chem. Soc.*, 1968, 90, 4823.

107. H.M. Colquhoun, T.J. Greenhough and M.G.H. Wallbridge; *J. Chem. Soc., Dalton Trans.*, 1979, 619.

108. J. Emsley and D. Hall; *The Chemistry of Phosphorus*, Harper and Row, London, 1976, pp 78-91 and 198-202.

109. D.E. Hyatt, J.L. Little, J.T. Moran, F.R. Scholer and L.J. Todd; *J. Amer. Chem. Soc.*, 1967, 89, 3342.

110. F.H. Allen, A. Pidcock and C.R. Waterhouse; *J. Chem. Soc. (A)*, 1970, 2087.

111. P. Haake, R.D. Cook and G.H. Hurst; *J. Amer. Chem. Soc.*, 1967, 89, 2650.

112. E.D. Kaplan and E.R. Thornton; *J. Amer. Chem. Soc.*, 1967, 89, 6644.

113. E.A.V. Ebsworth, D.W.H. Rankin and S. Cradock; *Structural Methods in Inorganic Chemistry*, p56.

114. L.L. Martin and R.A. Jacobson; *Inorg. Chem.*, 1971, 10, 1795.

115 D.H. Gerlach, A.R. Kane, G.W. Parshall, J.P. Jesson and E.L. Muetterties; *J. Amer. Chem. Soc.*, 1971, 93, 3543.

116a. M.J.S. Dewar; *Bull. Soc. Chim. France*, 1951, 18, C79. b. J. Chatt and L.A. Duncanson; *J. Chem. Soc.*, 1953, 2939.

117. R.A. Love, T.F. Koetzle, G.J.B. Williams, L.C. Andrews and R. Bau; *Inorg. Chem.*, 1975, 14, 2653.

118. S.D. Ittel and J.A. Ibers; *Adv. Organometal. Chem.*, 1976, 14, 33.

119. M.F. Rettig, R.M. Wing and G.R. Wiger; *J. Amer. Chem. Soc.*, 1981, 103, 2980.

120. L. Hedberg and J. Hedberg; *Abstracts, National Meeting of American Crystallographic Association*, 1964, Bozeman, MT.

121. F.A. Cotton and G. Wilkinson; *Advanced Inorganic Chemistry, A Comprehensive Text*, Fourth Edition, John Wiley & Sons, New York, 1980.

122. G.W. Parshall; *Inorg. Synth.*, Vol. 12, 26.

123. K.A. Jensen; *Z. Anorg. Chem.*, 1936, 229, 225.

124. R.G. Goel; *Inorg. Nucl. Chem. Lett.*, 1979, 15, 437.

125. P.G. Leviston and M.G.H. Wallbridge; *J. Organometal. Chem.*, 1976, 110, 271.

126. H.C. Clark and L.E. Manzer; *J. Organometal. Chem.*, 1973, 59, 411.

127. D. Drew and J.R. Doyle; *Inorg. Synth.*, Vol. 13, 47.

128. S.O. Grim, R.L. Keiter and W McFarlane; *Inorg. Chem.*, 1967, 6, 1133.

129. P.B. Hitchcock, B. Jacobson and A. Pidcock; *J. Chem. Soc., Dalton Trans.*, 1977, 2038.

130. G. Cavinato and L. Toriolo; *Inorg. Chim. Acta*, 1981, 52, 39.

131. T.G. Appleton, M.A. Bennett and I.B. Tomkins; *J. Chem. Soc., Dalton Trans.*, 1976, 439.

132. A.D. Westland; *J. Chem. Soc.*, 1965, 3060.

133. R.O. Gould and D.E. Smith; CADABS, University of Edinburgh, 1986.

134. International Tables for X-ray Crystallography, Kynoch Press, Birmingham, 1975, 4, 99.

135. R.O. Gould and P. Taylor; CALC, University of Edinburgh, 1986.

136. G.M. Sheldrick; SHELXTL, University of Gottingen, 1985.

137. J.K. Burdett; *Molecular Shapes*, Wiley, 1980.

138. R. Hoffmann and W.N. Lipscomb; *J. Chem. Phys.*, 1962, 36, 2179.

139. R. Hoffmann; *J. Chem. Phys.*, 1963, 39, 1397.

140. J.C. Slater; *Phys. Rev.*, 1930, 36, 57.

141. J. Howell, A. Rossi, D. Wallace, K. Haraki and R. Hoffmann; ICON, Quantum Chemistry Program Exchange, University of Indiana, 1977, No. 344.

142. J.H. Ammeter, H.-B. Burgi, J.C. Thibeault and R. Hoffmann; *J. Amer. Chem. Soc.*, 1982, 100, 3686.

143. M. Wolfsberg and L. Helmholtz; *J. Chem. Phys.*, 1952, 20, 837.

144. A.J. Fry; *Synthetic Organic Electrochemistry*, Harper and Row Publishers, New York, 1972.

145. A.J. Bard and L.R. Faulkner; *Electrochemical Methods*; John Wiley and Sons, New York, 1980.

146. C.K. Mann; *Elecroanal. Chem.*, 1969, 3, 57.

147. M. Buhl and P. von Rague Schleyer; *J. Amer. Chem. Soc.*, 1992, 114, 477.

148. H.V. Hart and W.N. Lipscomb; *Inorg. Chem.*, 1973, 12, 2644.

Appendix A.

Courses and Meetings Attended.

Inorganic Medicinal Chemistry by Drs. S.K. Chapman and A.J. Welch

E.P.R. Spectroscopy by Dr. R.E.P. Winpenny

Departmental Research Seminars and Colloquia

Inorganic Section Meetings

University of Strathclyde Inorganic Club (USIC) Meetings, 1991 and 1992.

R.S.C. Scottish Dalton Meeting, 1992.

Butler Electrochemistry Meeting, 1991-2

B.C.A. Intensive Residential Crystallography School, Aston University, 1991.

Intraboron X, XI and *XII*, Annual Meetings of United Kingdom Boron Chemists, 1990-92

Imeboron VII, International Meeting on Boron Chemistry, Torun, Poland, 1990.

Organosilicon IX, Edinburgh, 1990

Appendix B

Certain of the results presented in this thesis have been published. The reference for the relevant paper is:

D.R. Baghurst, R.C.B. Copley, H. Fleischer, D.M.P. Mingos, G.O. Kyd, L.J.Yellowlees, A.J. Welch, T.R. Spalding and D.J. O'Connell; *J.Organometal. Chem.*, 1993, 447, C14.

A reprint follows.

Journal of Organometallic Chemistry, 447 (1993) C14–C17

JOM 23412PC

Preliminary Communication

Sterically-induced low temperature polyhedral rearrangements of carbaplatinaboranes: synthesis and crystal structures of 1-Ph-3,3-$(PMe_2Ph)_2$-3,1,2-$PtC_2B_9H_{10}$, 1-Ph-3,3-$(PMe_2Ph)_2$-3,1,11-$PtC_2B_9H_{10}$, 11-Ph-3,3-$(PMe_2Ph)_2$-3,1,11-$PtC_2B_9H_{10}$ and 1,11-Ph_2-3,3-$(PMe_2Ph)_2$-3,1,11-$PtC_2B_9H_9$

David R. Baghurst [1], Royston C.B. Copley, Holm Fleischer and D. Michael P. Mingos [1]

Inorganic Chemistry Laboratory, University of Oxford, South Parks Road, Oxford OX1 3QR (UK)

Gwenda O. Kyd, Lesley J. Yellowlees and Alan J. Welch

Department of Chemistry, University of Edinburgh, West Mains Road, Edinburgh EH9 3JJ (UK)

Trevor R. Spalding and Donnacha O'Connell

Department of Chemistry, University College, Cork (Ireland)

(Received November 11, 1992)

Abstract

Reaction of *cis*-$Pt(PMe_2Ph)_2Cl_2$ with Tl_2[7-Ph-7,8-*nido*-$C_2B_9H_{10}$] affords 1-Ph-3,3-$(PMe_2Ph)_2$-3,1,2-$PtC_2B_9H_{10}$, mild thermolysis (55°C) of which yields 1-Ph-3,3-$(PMe_2Ph)_2$-3,1,11-$PtC_2B_9H_{10}$ and 11-Ph-3,3-$(PMe_2Ph)_2$-3,1,11-$PtC_2B_9H_{10}$. Both of the latter compounds are produced by the microwave irradiation of a mixture of *cis*-$Pt(PMe_2Ph)_2Cl_2$ and [$HNMe_3$][7-Ph-7,8-*nido*-$C_2B_9H_{11}$]. When *cis*-$Pt(PMe_2Ph)_2Cl_2$ is allowed to react with Tl_2[7,8-Ph_2-7,8-*nido*-$C_2B_9H_9$] at room temperature the only isolable species is 1,11-Ph_2-3,3-$(PMe_2Ph)_2$-3,1,11-$PtC_2B_9H_9$. The generation of rearranged products with 3,1,11-PtC_2B_9 architectures is inconsistent with a diamond-square-diamond mechanism for the isomerisation of icosahedral heteroboranes.

Correspondence to: Dr. A.J. Welch or Professor D.M.P. Mingos.

[1] Present address: Department of Chemistry, Imperial College of Science, Technology and Medicine, South Kensington, London SW7 2AY.

0022-328X/93/$6.00

The 1,2 → 1,7 → 1,12 isomerisation of *closo*-$C_2B_{10}H_{12}$ and its C-substituted analogues at elevated temperatures (*ca.* 470°C and 700°C, respectively, for the parent compound) has been known for many years [1], but the precise mechanism(s) of such rearrangement processes continue to be the subject of speculation [2]. With very few exceptions, [3], polyhedral rearrangements in carbametallaboranes also involve a high activation barrier [4]. Recently [5], we have found that severe molecular deformation in essentially icosahedral carbametallaboranes can be induced by the presence of bulky (phenyl) substituents at the cage carbon atoms, implying that transition metal derivatives of phenylcarbaboranes might undergo relatively facile rearrangement processes.

Reaction of *cis*-$Pt(PMe_2Ph)_2Cl_2$ with Tl_2[7-Ph-7,8-*nido*-$C_2B_9H_{10}$] [6] in CH_2Cl_2 at room temperature affords the expected product 1-Ph-3,3-$(PMe_2Ph)_2$-3,1,2-$PtC_2B_9H_{10}$ (**1**), characterised by microanalysis and multinuclear (^1H, ^{11}B, $^{11}B\{^1H\}$, ^{31}P) NMR spectrosopy. An X-ray diffraction study * reveals the molecular structure shown in Fig. 1. Pt(3) is between 2.24 and 2.33 Å from atoms C(2), B(7), B(8) and B(4), but 2.596(10) Å from C(1). The PtP_2 plane lies essentially orthogonal to the best plane through C(2)–B(4),

* *Crystal data*: All measurements were made at room temperature on CAD4 diffractometers (Edinburgh, compounds **1** and **4**; Oxford, compounds **2** and **3**) operating with graphite-monochromated Mo Kα X-radiation, $\lambda_{bar} = 0.71069$ Å.

Compound **1**, $C_{24}H_{37}B_9P_2Pt$, $M = 679.89$, monoclinic, space group $P2_1/c$, $a = 10.381(3)$, $b = 25.706(4)$, $c = 10.880(7)$ Å, $\beta = 104.57(4)°$, $V = 2810.0$ Å^3, $Z = 4$, $D_{calc} = 1.607$ g cm^{-3}, μ(Mo Kα) = 51.71 cm^{-1}, $F(000) = 1336$. $R = 0.048$ for 3310 reflections [$F \geq 2.0\sigma(F)$] measured in the range $1 \leq \theta \leq 23°$.

Compound **2**, $C_{24}H_{37}B_9P_2Pt$, $M = 679.89$, monoclinic, space group $P2_1/c$, $a = 10.408(3)$, $b = 25.847(5)$, $c = 10.993(3)$ Å, $\beta = 105.95(2)°$, $V = 2843.4$ Å^3, $Z = 4$, $D_{calc} = 1.588$ g cm^{-3}, μ(Mo Kα) = 51.10 cm^{-1}, $F(000) = 1336$. $R = 0.045$ for 3772 reflections [$F \geq 6.0\sigma(F)$] measured in the range $0 \leq \theta \leq 25°$.

Compound **3**, $C_{24}H_{37}B_9P_2Pt$. $M = 679.89$, triclinic, space group $P\bar{1}$, $a = 10.082(3)$, $b = 12.785(3)$, $c = 13.830(2)$ Å, $\alpha = 122.19(2)$, $\beta = 96.07(2)$, $\gamma = 94.23(2)°$, $V = 1479.0$ Å^3, $Z = 2$, $D_{calc} = 1.526$ g cm^{-3}, μ(Mo Kα) = 49.12 cm^{-1}, $F(000) = 668$. $R = 0.018$ for 4264 reflections [$F \geq 6.0\sigma(F)$] measured in the range $0 \leq \theta \leq 24.5°$.

Compound **4**, $C_{30}H_{41}B_9P_2Pt$, $M = 755.99$, triclinic, space group $P\bar{1}$, $a = 11.060(4)$, $b = 12.997(4)$, $c = 13.293(3)$ Å, $\alpha = 79.703(24)$, $\beta = 80.314(24)$, $\gamma = 65.14(3)°$, $V = 1696.5$ Å^3, $Z = 2$, $D_{calc} = 1.480$ g cm^{-3}, μ(Mo Kα) = 42.90 cm^{-1}, $F(000) = 748$. $R = 0.030$ for 5482 reflections [$F \geq 2.0\sigma(F)$] measured in the range $1 \leq \theta \leq 25°$.

but is orientated in such a way that it is almost perpendicular to a plane through C(1), B(10) and B(12), *i.e.* is twisted through *ca.* 36° from its idealised position in the analogous compound 3,3-$(PEt_3)_2$-3,1,2-$PtC_2B_9H_{11}$ [7].

The ^{31}P NMR spectrum of **1** in $CDCl_3$ at room temperature (singlet at −12.08 ppm with double satellites, *J*(PtP) 3227 Hz) is consistent with essentially free rotation of the $\{Pt(PMe_2Ph)_2\}$ fragment about the metal-cage axis. Increasing the temperature to 55°C (sealed tube) causes the colour of the solution to change slowly from orange to yellow, with the concommitant disappearance of the signal due to **1** and the growth of two new signals (−15.37 ppm *J*(PtP) 3258 Hz, compound **2**; −14.53 ppm, *J*(PtP) 3327 Hz, compound **3**), in the approximate ratio 1:4, respectively.

Compounds **2** and **3** are also formed, this time in approximately equal amounts, by the microwave irradiation (2450 MHz, 500w) [8] for 30 min of a mixture of *cis*-$Pt(PMe_2Ph)_2Cl_2$ and $[HNMe_3][7\text{-Ph-}7,8\text{-}nido\text{-}C_2B_9H_{11}]$ in EtOH at 10 atm. Following separation by TLC each compound was characterized by ^{11}B, $^{11}B\{^1H\}$ and ^{31}P NMR spectroscopies, mass spectrometry, and by X-ray crystallographic studies *. Compound **1** was not observed in the product mixture.

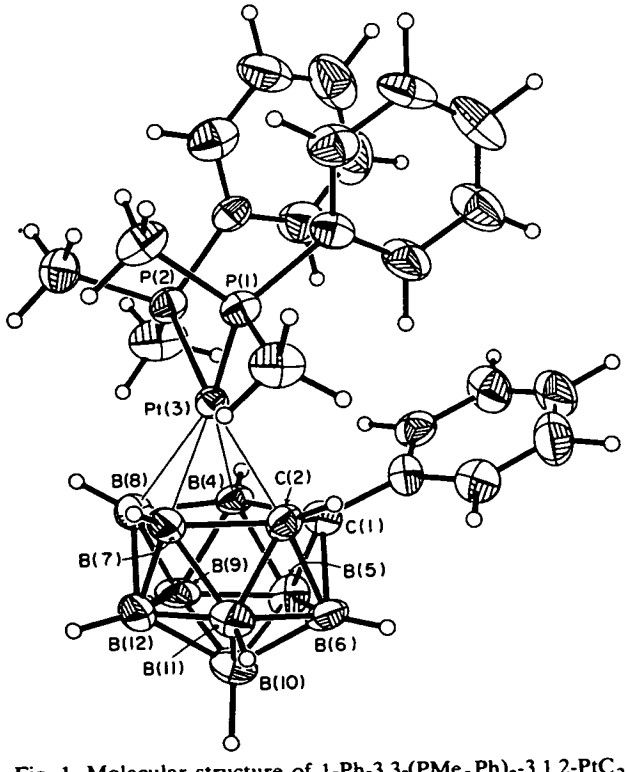

Fig. 1. Molecular structure of 1-Ph-3,3-$(PMe_2Ph)_2$-3,1,2-$PtC_2B_9H_{10}$ (**1**). Important molecular parameters (Å and °) Pt(3)–C(1) 2.596(10), Pt(3)–C(2) 2.326(10), Pt(3)–B(7) 2.257(12), Pt(3)–B(8) 2.239(12), Pt(3)–B(4) 2.313(12), Pt(3)–P(1) 2.288(3), Pt(3)–P(2) 2.250(3), C(1)–C(2) 1.594(14), P(1)–Pt(3)–P(2) 95.05(9).

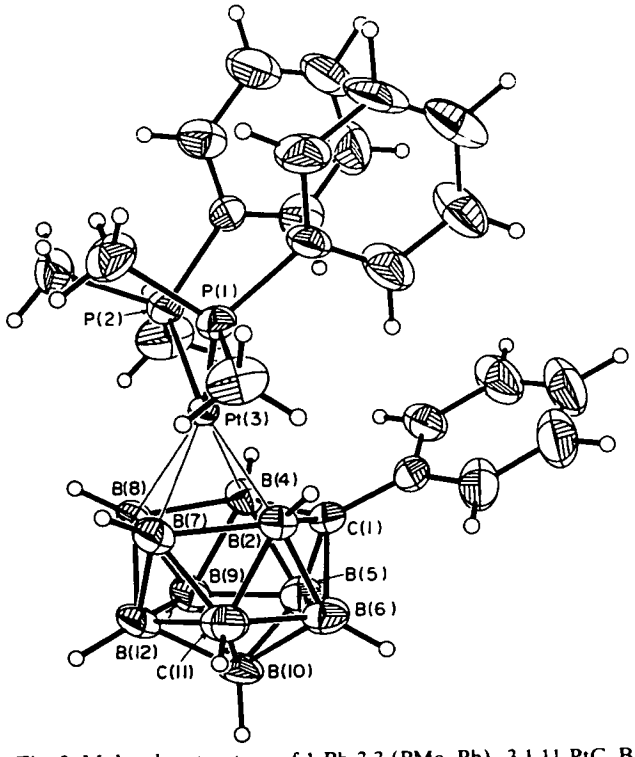

Fig. 2. Molecular structure of 1-Ph-3,3-$(PMe_2Ph)_2$-3,1,11-$PtC_2B_9H_{10}$ (**2**). Important molecular parameters (Å and °) Pt(3)–C(1) 2.622(8), Pt(3)–B(2) 2.237(8), Pt(3)–B(7) 2.211(9), Pt(3)–B(8) 2.212(9), Pt(3)–B(4) 2.275(8), Pt(3)–P(1) 2.2988(21), Pt(3)–P(2) 2.2963(22), P(1)–Pt(3)–P(2) 95.82(8).

The structure of **2** is shown in Fig. 2. It is isomorphous with **1** but it does not have the same structure. In fact, the compound is 1-Ph-3,3-$(PMe_2Ph)_2$-3,1,11-$PtC_2B_9H_{10}$, *i.e.* an isomer of **1** in which C(2) and B(11) of **1** are interchanged. This apart, the molecular geometries of **1** and **2** are practically superimposable, even down to fine details such as the slight twist of the phenyl ring attached to C(1) and the disposition of the PMe_2Ph ligands; indeed, an idealization calculation [9] on the entire molecules of **1** and **2** (excluding H atoms) yields an "r.m.s. misfit" of only 0.09 Å. In **2** Pt(3) to cage atom distances span 2.21–2.28 Å [B(2)–B(7)], with Pt(3)–C(1) again long at 2.622(8) Å. Thus compounds **1** and **2** represent a rare example of geometrical isomers of a compound that are isomorphous. Presumably this reflects the fact that the crystal packing of **1** and **2** is dictated by hydrocarbon contacts and is independent of the change in molecular dipole.

The molecular structure of compound **3**, 11-Ph-3,3-$(PMe_2Ph)_2$-3,1,11-$PtC_2B_9H_{10}$, is shown in Fig. 3. Thus **3** is yet another isomer of **1**, but now the {CPh} fragment is located in the lower pentagonal belt (cage

atoms 5, 6, 11, 12 and 9) with {CH} in the upper belt. Pt(3)–B distances again span the range 2.21–2.28 Å, and Pt(3)–C(1) is 2.581(4) Å. In both **2** and **3** the PtP_2 plane adopts an essentially perpendicular orientation to the C(1)B(10)B(12) plane, as is observed in the related species 1-NMe_3-3,3-(^{t}BuNC)$_2$-3,1-$PdCB_{10}H_{10}$ [10].

The isomerisations of **1** to **2** and **3** represent the two possible ways in which the cage carbon atoms can separate as they do in the 1,2 → 1,7 isomerization of *closo*-$C_2B_{10}H_{12}$, with the proviso that the ultimate metallabonded polyhedral face is B_4C and Pt is antipodal to boron.

As previously noted, the conformation of the PtP_2 plane in **1** is significantly distorted from that predicted to be of minimum energy for an $\{ML_2\}$ fragment above a B_3C_2(C-adjacent) face [7], presumably because of the steric influence of the phenyl substituent bound to C(1). The relatively low temperature at which **1** undergoes isomerisation is fully consistent with such *ground state destabilisation* of the 3,1,2-MC_2B_9 polyhedron. In both isomerised products the observed conformation of the $\{ML_2\}$ fragment is the predicted minimum energy one.

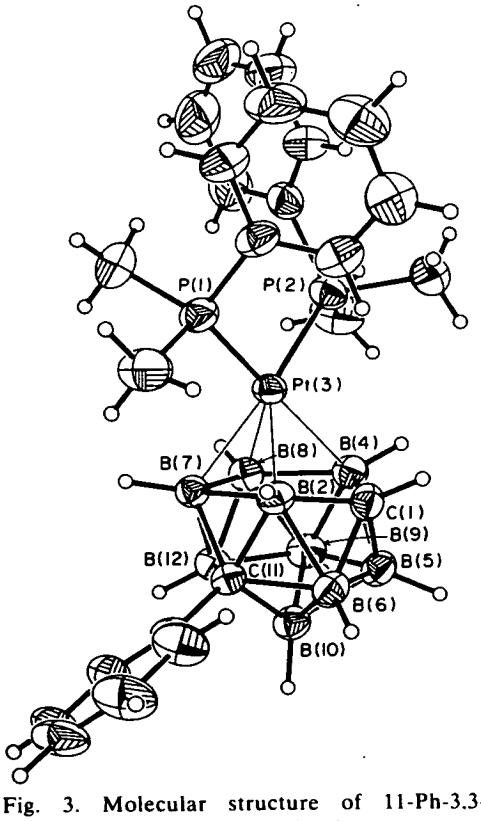

Fig. 3. Molecular structure of 11-Ph-3,3-(PMe_2Ph)$_2$-3,1,11-$PtC_2B_9H_{10}$ (**3**). Important molecular parameters (Å and °) Pt(3)–C(1) 2.581(4), Pt(3)–B(2) 2.233(5), Pt(3)–B(7) 2.211(4), Pt(3)–B(8) 2.246(5), Pt(3)–B(4) 2.281(5), Pt(3)–P(1) 2.2901(11), Pt(3)–P(2) 2.3037(11), P(1)–Pt(3)–P(2) 97.70(4).

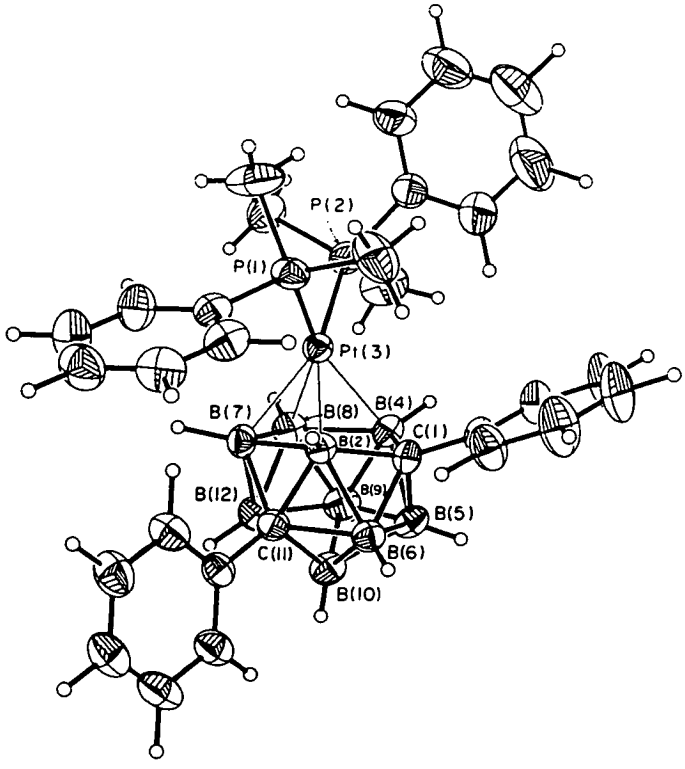

Fig. 4. Molecular structure of 1,11-Ph_2-3,3-(PMe_2Ph)$_2$-3,1,11-$PtC_2B_9H_9$ (**4**). Important molecular parameters (Å and °) Pt(3)–C(1) 2.610(5), Pt(3)–B(2) 2.222(6), Pt(3)–B(7) 2.199(6), Pt(3)–B(8) 2.231(6), Pt(3)–B(4) 2.293(6), Pt(3)–P(1) 2.2864(14), Pt(3)–P(2) 2.2909(14), P(1)–Pt(3)–P(2) 96.23(5).

A striking further example of sterically-induced low temperature polyhedral rearrangement is afforded by the fact that the only isolable product of the room temperature reaction between *cis*-$Pt(PMe_2Ph)_2Cl_2$ and the diphenylcarbaborane ligand [7,8-Ph_2-7,8-*nido*-$C_2B_9H_9]^{2-}$ [5] is the C-separated species 1,11-Ph_2-3,3-(PMe_2Ph)$_2$-3,1,11-$PtC_2B_9H_9$ (**4**), the structure of which * is shown in Fig. 4. In this case we assume that intramolecular crowding in the intermediate compound 1,2-Ph_2-3,3-(PMe_2Ph)$_2$-3,1,2-$PtC_2B_9H_9$ is so severe that it isomerizes to **4** without the need for even mild heating.

The isomerization of icosahedral heteroboranes with an initial 3,1,2-MC_2B_9 architecture by a diamond-square-diamond mechanism in which the C(1)–C(2) connectivity is broken in the transition state would initially afford a species with a 1,2,4-MC_2B_9 heteroatom pattern. Although it remains to be tested by experimentation, it is likely that the predicted conformation [7,11] of such species, in which one or even two phenyl groups are bound to cage carbon atoms, would be such that intramolecular crowding would not be critical, and therefore the non-observation of products of this type in the thermolysis reactions described

above argues against a diamond-square-diamond mechanism. Studies designed to probe further the precise mechanisms of these important reactions are being undertaken.

Acknowledgments

We thank the SERC (DRB, RCBC, GOK) and the British Council-EOLAS scheme (TRS) for support, the Callery Chemical Company for a generous gift of $B_{10}H_{14}$ and Johnson Matthey plc for a loan of platinum.

References

1 *e.g.* R. N. Grimes, *Carboranes*, Academic Press, New York, 1970.
2 *e.g.* G. M. Edvenson and D. F. Gaines, *Inorg. Chem., 29* (1990) 1210; B. M. Gimarc, D. S. Warren, J. J. Ott and C. Brown, *Inorg. Chem., 30* (1991) 1598; B. F. G. Johnson, Y. V. Roberts and E. Parisini, *J. Chem. Soc., Chem. Commun.*, (1992) in press.
3 *e.g.* L. F. Warren, Jr. and M. F. Hawthorne, *J. Am. Chem. Soc., 92* (1970) 1157; C. B. Knobler, T. B. Marder, E. A. Mizusawa, R. G. Teller, J. A. Long, P. E. Behnker and M. F. Hawthorne, *J. Am. Chem. Soc., 106* (1984) 2990; S. A. Brew, N. Carr, J. C. Jeffrey, M. U. Pilotti and F. G. A. Stone, *J. Am. Chem. Soc., 114* (1992) 2203.
4 *e.g.* M. K. Kaloustian, R. J. Wiersema and M. F. Hawthorne, *J. Am. Chem. Soc., 94* (1972) 6679.
5 Z. G. Lewis and A. J. Welch, *J. Organomet. Chem., 430* (1992) C45.
6 B. D. Reid and A. J. Welch, unpublished results.
7 D. M. P. Mingos, M. I. Forsyth and A. J. Welch, *J. Chem. Soc., Dalton Trans.*, (1978) 1363.
8 For experimental details see D. R. Baghurst and D. M. P. Mingos, *J. Chem. Soc., Dalton Trans.*, (1992) 1151.
9 S. A. Macgregor, A. J. Wynd, R. O. Gould, N. Moulden, P. Taylor, L. J. Yellowlees and A. J. Welch, *J. Chem. Soc., Dalton Trans.*, (1991) 3317.
10 W. E. Carroll, M. Green, F. G. A. Stone and A. J. Welch, *J. Chem. Soc., Dalton Trans.*, (1975) 2265.
11 M. Green, J. L. Spencer, F. G. A. Stone and A. J. Welch, *J. Chem. Soc., Dalton Trans.*, (1975) 179.